

MAGNETOM Flash

Issue Number 82 · 3/2022

RSNA Edition

siemens-healthineers.com/magnetom-world

Page 4

Editorial Comment

Susie Huang, Bruce Rosen, Daniel Paech

Page 26

High-resolution Accelerated Prostate TSE Axial Imaging with Deep Learning Reconstruction

Alain Luciani, et al.

Page 31

Improving Patients' Experience of MRI

Janika Madl, et al.

Page 38

Artificial Intelligence: Learning About the Future of Cardiovascular MR

Kerstin Hammernik, Thomas Küstner

Page 69

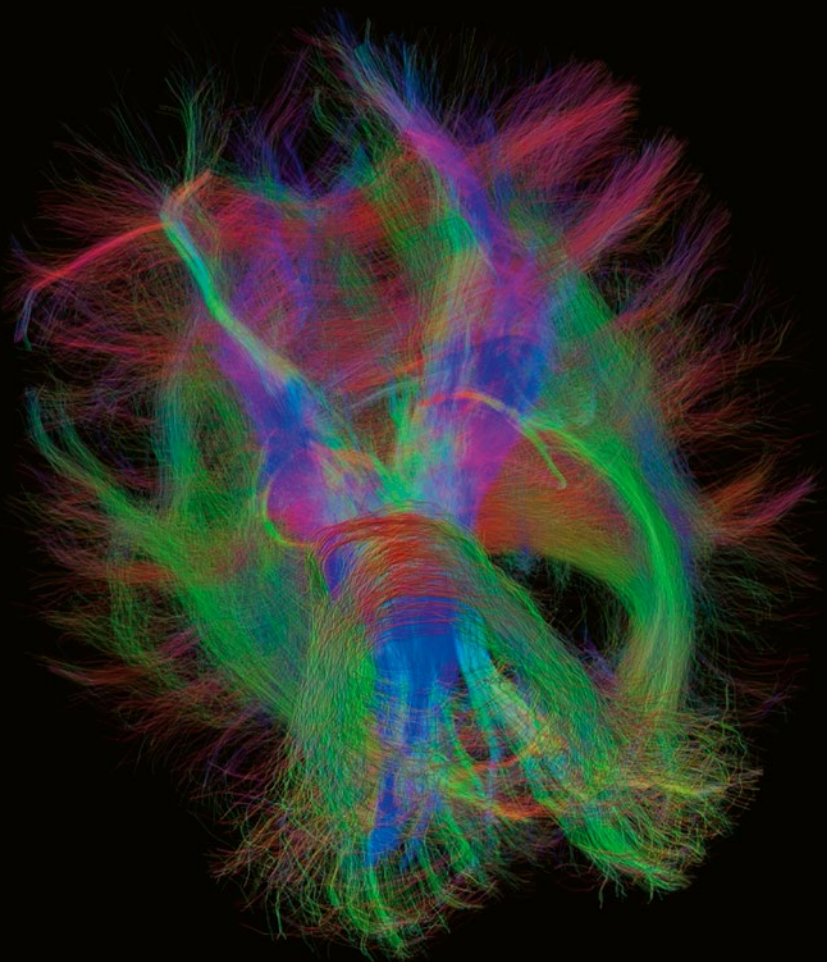
Musculoskeletal MRI in Children

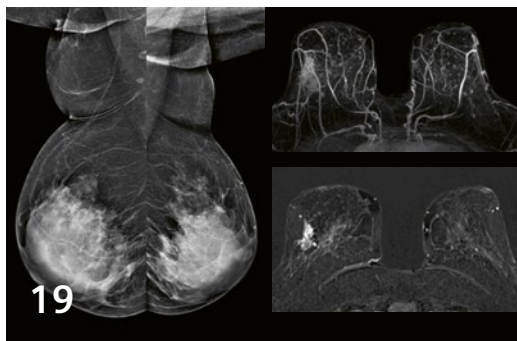
Dominik Świętoń, Małgorzata Grzywińska

Page 81

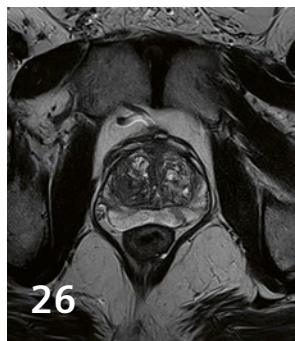
Clinical Benefits of MRF in Brain Tumors

Meiyun Wang, et al.

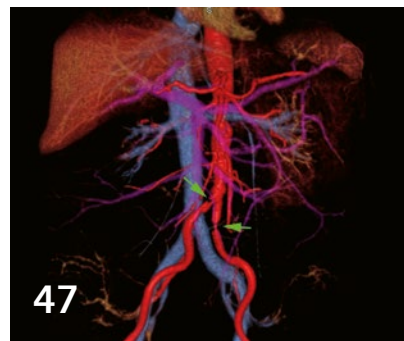




Breast MRI in India



DL TSE for prostate MRI



MRA with Ferumoxytol

Editorial Comment

4 Life at the edge – exploring the limits of our “fields”

Susie Huang, Bruce Rosen

Massachusetts General Hospital, Boston, MA, USA

Daniel Paech

University Hospital Bonn, Germany

Men's Health

26 High-Resolution Accelerated Prostate TSE Axial Imaging with Deep Learning Reconstruction at 3 Tesla

Alain Luciani, et al.

Hôpitaux Universitaires Henri Mondor, Créteil, France

Access to MRI

11 Building a Global Power of Experience in Diagnostic Imaging – Lessons from Africa's COVID-19 Response

Udunna Anazodo, et al.

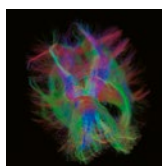
McGill University, Montreal, Quebec, Canada

19 Breast MRI in India: Practice and Challenges

Pratiksha Yadav

Dr. D. Y. Patil Medical College, Hospital and Research

Centre, Pune, India



Cover image: MAGNETOM Cima.X¹
Deep Resolve for EPI Diffusion
Tractography: 256 directions, b3000,
TA 18:53 min

Patient Experience

31 Improving Patients' Experience of MRI: Why and How Reducing Stress and Anxiety in Patients May Enhance Clinical Operations

Janika Madl, et al.

Universitätsklinikum Erlangen, Germany

Cardiovascular Imaging

38 Artificial Intelligence – Learning About the Future of Cardiovascular MR

Kerstin Hammernik

Technical University of Munich, Germany,

Thomas Küstner

University Hospital Tübingen, Germany

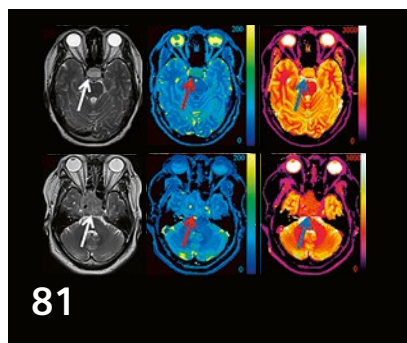
47 Magnetic Resonance Angiography with Ferumoxytol^{1,2}

J. Paul Finn, Kim-Lien Nguyen, et al.

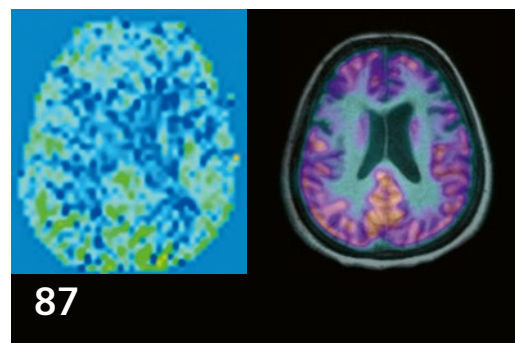
David Geffen School of Medicine at UCLA, Los Angeles, CA, USA



MSK MRI in children



MRF in brain tumors



PCASL in neurodegenerative disorders

60 3D Whole Heart Applications: Angiography and Delayed Enhancement¹

Jason Craft, et al.

St. Francis Heart Hospital, DeMatteis Research Center, Greenvale, NY, USA

87 Arterial Spin Labeling as a Potential Biomarker in Imaging of Various Neurodegenerative Disorders

Sandhya Mangalore, et al.

National Institute of Mental Health and Neurosciences, Bengaluru, India

Pediatric Imaging

66 Addressing Flow and Pulsation-Associated Artifacts in TOF-MRA in Children²

Ayaz Khan, et al.

St Jude Children's Research Hospital, Memphis, TN, USA

69 Musculoskeletal MRI in Children: How We Do It²

Małgorzata Grzywińska, Dominik Świętoń

University Clinical Centre in Gdansk, Poland

96 How-I-do-it: BLADE: Reducing Motion Artifacts in Uncooperative Patients with Acquired Brain Injury

Marta Cazzoli, et al.

IRCCS Fondazione Don Carlo Gnocchi Onlus, Milan, Italy

100 How-I-do-it: Feasibility of 3D Sequences for Median Nerve Imaging Using UltraFlex Large Coils and CAIPIRINHA on a 3T System

Yatin Sharma

Siemens Healthineers, Gurugram, India

Neurologic Imaging

81 Clinical Benefits of MRF in Brain Tumors³

Meiyun Wang, et al.

Henan Provincial People's Hospital & the People's Hospital of Zhengzhou University, Zhengzhou, China

104 Introducing Eva Eberlein

Head of the Gradient Coil and Shim Team

Siemens Healthineers, Erlangen, Germany

106 Introducing George Ferguson

Ultra-high field MSK applications developer

Siemens Healthineers, Erlangen, Germany

¹Work in progress. The system is currently under development and is not for sale in the U.S. and in other countries. Its future availability cannot be ensured.

²MR scanning has not been established as safe for imaging fetuses and infants less than two years of age. The responsible physician must evaluate the benefits of the MR examination compared to those of other imaging procedures.

³MR Fingerprinting is not commercially available in some countries. Due to regulatory reasons its future availability cannot be ensured.



Susie Y. Huang, M.D., Ph.D., is an Attending Radiologist in the Division of Neuroradiology and Athinoula A. Martinos Center for Biomedical Imaging in the Department of Radiology at the Massachusetts General Hospital, and an Assistant Professor of Radiology at Harvard Medical School, Cambridge, MA, USA.

Dr. Huang currently serves as the lead Principal Investigator on a \$14-million NIH BRAIN initiative multi-institutional collaborative grant to develop the next-generation Connectome MRI scanner for multiscale imaging of the human brain.



Bruce Rosen, M.D., Ph.D., is Professor of Radiology at the Harvard Medical School and Professor of Health Science and Technology at the Harvard-MIT Division of Health Sciences and Technology. He is Director of the Athinoula A. Martinos Center for Biomedical Imaging at Massachusetts General Hospital, Boston, MA, USA.

Dr. Rosen is the recipient of numerous awards in recognition of his contributions to the field of functional MRI and leads the activities of several large interdisciplinary and inter-institutional research programs including the NIH Blueprint-funded Human Connectome Project.



Daniel Paech, M.D., Ph.D., is Medical Director 7 Tesla MRI, at the German Cancer Research Center (DKFZ) in Heidelberg, Germany, and Senior Physician in the Department of Neuroradiology at the University Hospital Bonn, where he is Head of Neuro-Oncology Imaging.

Dr. Paech received the Walter Friedrich Award 2020 of the German Radiological Society for his research on "Metabolic imaging techniques at 7 Tesla ultra-high field MRI in neuro-oncological diseases". In 2022, he received the Kurt Decker Award of the German Congress for Neuroradiology for his research on X-nuclei and 7T MRI.

Life at the edge – exploring the limits of our “fields”

The most wonderful thing about magnetic resonance imaging is its remarkable ability to reinvent itself. What we can do to explore and exploit the natural laws of physics, learn about the biology of tissues, and apply that knowledge to help better understand disease in our patients has been constantly shifting and expanding over the last 50 years of MRI's existence. At nearly every conference we hear of new forms of image contrast to map, new quantitative measurements to make, new biology or clinical disorders we can now see that we couldn't before. Anatomy invisible before becomes visible, measure of tissue function expand from one organ to the next, and on its own and fused in real time with PET, imaging of molecular pathways moves from bench to bedside. This is why we love MR – it's always new.

Today of course is no exception. In just a few short years the use of artificial intelligence has provided an amazing boost in image clarity and resolution, and technologies like dense array coils combine now with novel image acquisition schemes to shorten our imaging times from tens of minutes to sometimes just seconds, with comprehensive multicontrast examinations in a few short

minutes (watch out CT!). And interestingly, these advances are now not only pushing the envelope on workflow, but they are also allowing us to revisit some of the means we once performed MRI in new and compelling ways – image quality that rivals “standard” 1.5T examinations are no longer limited to the complexity and footprint (and cost) of these larger magnets – this is expanding greatly our ability to provide access to patients in more and more settings, and setting new goals as we push for value-based care.

But with all of that said, there is another facet of MRI that has remained constant. The fundamentals of the physics of MRI tell us there is more signal to be seen as magnetic field strengths increase, and more ability to encode spatial properties both at the macroscopic scale of our images and at the microscopic scale of cells and tissues when our other “magnet”, the magnet field gradients, increase their power and speed. These “constants” in MR physics have in turn pushed MR engineers to keep a steady focus on increasing our fields, both static B_0 magnet and gradients G_{xyz} , to exploit the power that these higher and faster fields have, to map the underlying pathophysiology of our patients in both research and clinical settings.

Looked at over the five decades of MRI, the progress might appear slow but steady. Looked at more closely though and we can see that progress in these domains has been made in a more “stepwise” fashion – some of us are old enough to remember when the step to imaging at 1.5 Tesla was a remarkable engineering feat, and quickly brought MRI from its infancy into something that would look familiar to radiologists today. Gradient technology advances have followed a similar path – the first human diffusion images in stroke were acquired with 5 mT/m gradients and slew rates well below what was needed for single shot imaging (at 0.6T to boot!), it was the major advance in gradient systems now capable of echo planar imaging that brought diffusion imaging quickly into our routine clinical practices.

Today, we are lucky to be facing another of these important steps. Imaging magnets at 7 Tesla more than doubled the field strength of what was once “high field” MRI – though explored in research laboratories for several years, ultra-high field (UHF) 7 Tesla MR systems are now entering mainstream clinical practice. At the same time, through investments targeting how our human brains are wired, including the NIH Human Connectome Project and other major research initiatives, “Connectom” class gradient performance seen in laboratories is now poised to also move into the clinic. As with past leaps forward, we can predict that these new engineering capabilities will lead to wholly new ways to understand how our bodies work, and to detect and characterize what goes wrong in disease. But what can we anticipate these remarkable new machines will provide to our research community, and to clinical practice? Read on!

Our B₀ magnet – sometimes bigger really is better

High signal-to-noise-ratio (SNR) and increased spectral resolution at ultra-high field promise submillimeter anatomical resolution and new insights into human tissue function and metabolism. This information could be of key importance for diagnosis, prognosis, and treatment response monitoring in a wide spectrum of diseases.

As conventional neuroimaging techniques at typical clinical field strengths (≤ 3 Tesla) don't always provide sufficient metabolic and functional information, or adequate SNR to robustly measure these in individual patients, the advent of UHF MRI paves the way for many different imaging technologies that can provide additional insights into brain physiology and pathophysiological processes.

Generally, there is a fast-growing body of evidence that UHF MRI has the potential to improve depiction of anatomical substructures and therefore diagnostic confidence. Conventional high-resolution proton imaging is still the mainstay of clinical imaging at 7T. As one important example, multiple studies have provided evidence for an added clinical value of 7T MRI in the diagnostic work-up of patients with epilepsy. High-resolution anatomical imaging at 7 Tesla aids the identification of potential epileptogenic lesions, such as focal cortical dysplasias. A recent consensus report from the “7T Epilepsy Task Force” reported experience from 21 7T MRI centers including scans of over 2,000 patients together with recommendations for appropriate clinical indications, patient selection and preparation, acquisition protocols and setup, and technical challenges [1].

In many diseases, such as cancer, neurodegeneration, and neuroinflammation, morphologic changes often occur only at an advanced stage of illness. For instance in patients with brain tumors, current diagnostic approaches mainly detect changes associated with disease progression, such as blood brain barrier (BBB) disruption, necrosis, and edema in the case of aggressively growing tumors. However, tumor cells have distinct properties different from healthy tissue, such as altered metabolic pathways (e.g. Warburg effect) and increased proliferation rates.

Until today, PET imaging techniques have successfully targeted these characteristics mainly using (deoxy-2-[¹⁸F] fluoro-D-glucose) FDG-PET with great implications for patient care, particularly in body imaging. In the human brain, however, high ground level metabolic activity limits the potential of FDG-PET for the detection of cancer tissue. In this context, the increased SNR and the higher spectral resolution at 7 Tesla have enabled not only ultra-high

Nucleus	Relative sensitivity [%]	SNR relative to ¹ H [%]	I [ħ]	γ [MHz/T]	c [mol/L] of the isotope in-vivo
¹ H	100	100	1/2	42.6	79
²³ Na	9.25	35.0	3/2	11.3	0.041
³¹ P	6.63	16.4	1/2	17.2	0.003*
³⁵ Cl	0.356	3.64	3/2	4.2	0.027
¹⁷ O	0.0011	0.00815	5/2	-5.8	0.015

Table 1: Overview of the most commonly used X-nuclei for MRI and their physical properties.

I: spin, γ: gyromagnetic ratio, c: typical concentration of the isotope in vivo, ħ: Planck's constant. *Reproduced from [2].*

resolution anatomical imaging and improved MR spectroscopy, but also the introduction of new metabolic MR imaging technologies, in particular employing X-nuclei technology.

The term X-nuclei refers to all non-proton nuclei with a magnetic moment, such as sodium (^{23}Na), phosphorus (^{31}P), phosphorous (^{31}P), deuterium (^2H), potassium (^{39}K), and the oxygen-17 isotope (^{17}O). These nuclei are directly involved in many biological processes. However, the relatively low sensitivity and in vivo concentration pose challenges (Table 1).

Sodium ^{23}Na MRI is the currently best explored X-nuclei due to its high natural abundance in the human body and its relatively high gyromagnetic ratio compared to other X-nuclei. Sodium plays an important role in many physiological processes. Transmembrane sodium gradients control the transmission of action potentials, the maintenance of cell homeostasis and the regulation of physical properties such as pH, blood volume, and blood pressure. Therefore, sodium MRI has a variety of potential applications in order to study physiological and pathophysiological processes [3].

The tissue sodium concentration (TSC) has been shown to be increased in brain tumor tissue compared to normal-appearing white and gray matter regions (Fig. 1), and to be associated with different histologic and genetic subtypes, such as the isocitrate dehydrogenase (IDH) mutation status [4].

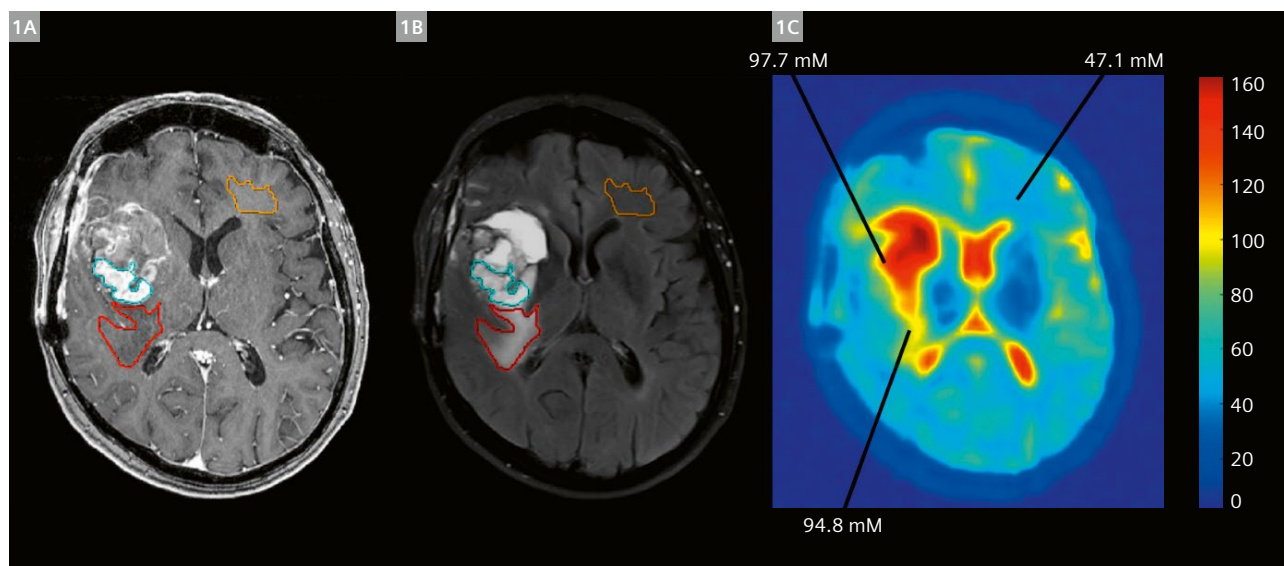
Abnormal TSC in brain tissue has also been demonstrated as a potential marker for neuroinflammatory processes, such as multiple sclerosis, and in neurodegener-

ative diseases, such as Alzheimer's disease, amyotrophic lateral sclerosis (ALS), and Huntington disease [3]. Overall, ^{23}Na MRI is emerging as a promising tool in the field of neuroimaging with broad applicability.

Another nucleus that has recently gained considerable attention is the oxygen-17 isotope (^{17}O). Oxygen-17 has a magnetic moment (spin 5/2), is non-toxic, and the only stable oxygen isotope that can be detected via MRI. The natural abundance of ^{17}O is very low (0.038%) [5]. However, the in vivo concentration of the isotope can be enhanced through inhalation of enriched $^{17}\text{O}_2$ gas during an MRI scan. The oxygen isotope is detectable only when it is bound to water (H_2^{17}O), which makes the approach a specific modality to measure the rate of oxidative phosphorylation at the mitochondrial membrane. Thus, ^{17}O MRI provides a direct window into oxygen-dependent tissue metabolism.

Clinical applications of ^{17}O MRI have so far been performed in study participants with brain tumors. Decreased cerebral metabolic rates of oxygen consumption (CMRO_2) have been reported in tumors of patients with gliomas (Fig. 2) [6]. This observation is in agreement with the theorem of Otto Warburg, who described a metabolic shift in cancer cells towards glucose fermentation, even in the presence of abundant oxygen. In addition to metabolic characterization of brain tumors, ^{17}O MRI offers great potential for studying oxygen metabolism in patients with stroke, and neurodegenerative diseases such as Alzheimer's or Parkinson's disease.

To date, X-nuclei methods have predominantly been investigated in experimental studies. However, with



1 Sodium MRI at 7 Tesla in a patient with right-sided fronto-temporal glioblastoma.

The images include a (1A) contrast-enhanced T1w MRI, (1B) T2 fluid-attenuated inversion recovery (FLAIR), (1C) sodium MRI. Three regions of interest have been selected on (1A, 1B) in the contrast-enhancing tumor region, the peritumoral edema, and contralateral normal appearing white matter. Corresponding sodium concentrations are additionally shown.

increasing magnetic field strengths and new technical developments, X-nuclei imaging may play an important role in routine clinical practice. Also in the context of artificial intelligence (AI) enhanced diagnostics, metabolic MRI methods have the potential to boost the performance of AI approaches by adding independent information compared to existing MR sequences.

The large majority of 7T MRI clinical studies have been performed in brain imaging, which is primarily due to the additional challenges, such as respiratory motion, B_0/B_1 inhomogeneities, and wave effects in body imaging (at 7T, the wavelength in tissue is shorter than the diameter of a human torso). In the near future, the increasing availability and technical advancements of parallel transmit (pTx) technology will permit the exploitation of further applications in human UHF imaging throughout the body and MSK systems [5].

UHF MRI already plays a key role in neuroscience and preclinical neural research, and its role in clinical diagnostics is certain to increase as more systems with clinical approval as medical devices are installed. In the future, even further increases in field strength may enhance our capabilities in clinical research and will certainly lead to significant advances in these imaging modalities.

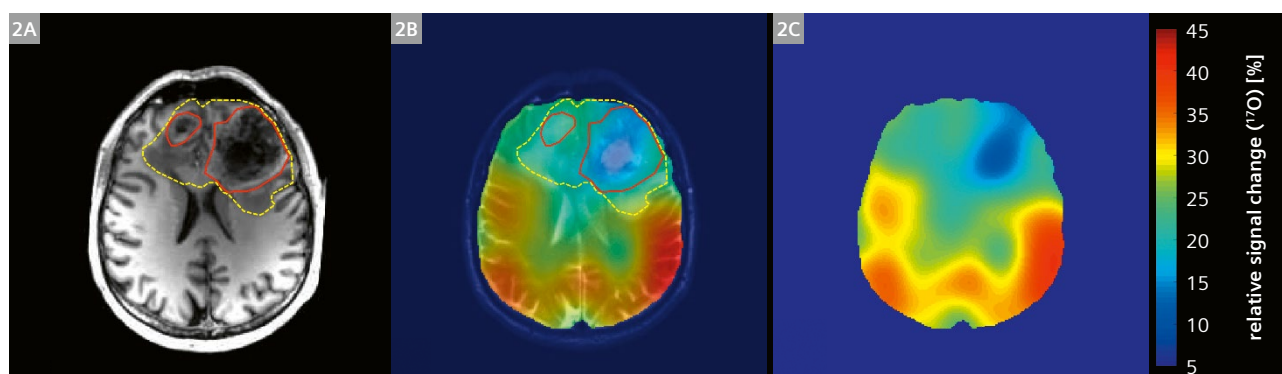
Gradients – not just for making pictures anymore

The gradient system is a key component of the MRI machine, being responsible for the spatial encoding in image generation and integral to controlling a range of physiological imaging contrasts, most notably diffusion-weighted MRI. The design and performance of the gradient system has substantial influence on the overall quality of the acquired images and has been the focus of intense engineering efforts over the last three decades in the quest for better image quality and ever-faster imaging speed.

Gradient performance is parameterized by the maximum gradient amplitude, which is measured in mT/m, and the slew rate, which describes how fast a gradient can attain a desired amplitude within a given amount of time and is measured in T/m/s. Since the inception of MRI, gradient amplitudes and slew rates have increased by orders of magnitude, roughly doubling every 10 years since the 1990's. In parallel, the push for stronger and faster gradients has been spurred by research applications, particularly in the brain. Early efforts to boost gradient performance for diffusion spectrum imaging led to the development of the AC88 head gradient by Siemens with a maximum gradient strength of 80 mT/m at a slew rate of 400 T/m/s. A seminal breakthrough in whole-body gradient design was achieved for the Human Connectome Project (HCP), culminating in the installation of the first Connectom¹ MRI scanner at the MGH Martinos Center in 2011, which featured a whole-body gradient with a peak gradient performance of 300 mT/m at a slew rate of 200 T/m/s. More recently, we have embarked on developing the next-generation Connectom scanner (Connectom 2.0)¹ in partnership with Siemens Healthineers, funded in part by the NIH BRAIN Initiative with the goal of comprehensive multi-scale mapping of structure and connectivity across the entire living human brain.

While advances in gradient technology have improved our understanding of the human brain through large-scale research efforts like the HCP and NIH BRAIN Initiative, the engineering advances required to achieve such strong gradient amplitudes and fast slew rates have directly informed and benefitted the radiological sciences and clinical imaging by encouraging the incorporation of stronger and

¹MAGNETOM Connectom is ongoing research. All data shown are acquired using a non-commercial system under institutional review board permission. Siemens Healthcare GmbH does not intend to commercialize the system.



2 Oxygen-17 MRI at 7 Tesla in a 63-year-old man with World Health Organization (WHO) grade IV glioblastoma. (2A) Axial slice on T2-weighted fast spin-echo image ($0.4 \times 0.4 \times 0.5 \text{ mm}^3$), (2B) T1-weighted magnetization-prepared rapid-acquisition gradient-echo image fused with a color-coded map of relative oxygen 17 (^{17}O) signal change, and (2C) without fusion of anatomical imaging. Regions of tumor tissue show a clearly reduced metabolic activity.

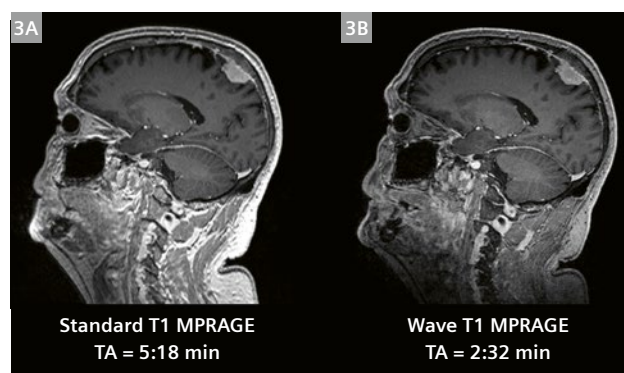
faster gradients into widely available products. The latest commercial scanners now feature integrated whole-body gradient systems with a maximum gradient amplitude of at least 80 mT/m, with maximum slew rates of at least 200 T/m/s; and with the Gemini gradient system² even 200 mT/m³ with a slew rate of 200 T/m/s.

Where does the future lie with such powerful technology, and how can we best leverage such advances to make a difference for our patients? Below, we highlight a few of the key clinical and research applications that will benefit most from such powerful gradients, listed in order of those that are closest to our current clinical practice to those that will advance our limits of detecting, understanding, and managing disease in patients across a range of pathologies.

Anatomical MRI: The need for speed

Stronger and faster gradients stand to benefit the workhorse of clinical MRI – multi-contrast anatomical MRI – by substantially reducing image acquisition times across the full range of 2D and 3D imaging sequences that are routinely used in clinical imaging protocols. In the last decade, fast MRI has become mainstream in clinical practice, no longer limited to echo planar imaging, or relegated to specialized protocols designated for motion-prone or acutely ill patients. The benefits of stronger gradients for image encoding are straightforward. As a case in point, for a 3D T1-weighted MPAGE sequence on the MGH Connectome¹ whole-body gradient system with G_{\max} of 300 mT/m and slew rate of 200 T/m/s compared to a standard whole-body gradient system with G_{\max} of 60 mT/m and slew rate of 200 T/m/s, the stronger gradients enable a reduction of repetition time by ~25% and reduction in echo time by ~50% through achieving shorter echo spacing, which translates into roughly ~25% reduction in acquisition time. Faster and stronger gradients act synergistically with AI-based tools, enabling higher acceleration factors that result in noisier images, which can then be cleaned up afterward with dedicated networks trained to reduce noise and sharpen images.

The push for shorter scan times has also led to the development of more efficient k -space sampling schemes for 2D and 3D imaging, which also benefit from better gradient performance, enabling such strategies to make it into the mainstream and introducing a range of novel fast imaging techniques to the clinic. Spiral k -space encoding makes efficient use of the gradient system hardware and has been used to achieve ultrashort echo times for real-time and rapid imaging applications. As another example, wave-controlled aliasing in parallel imaging (CAIPI) is a



3 Comparison of post-contrast three-dimensional T1-weighted magnetization prepared rapid acquisition gradient recalled echo (MPRAGE) images acquired with conventional parallel imaging and Wave-Controlled Aliasing in Parallel Imaging (CAIPI) encoding demonstrating a meningioma. Standard (3A) and Wave-CAIPI (3B) T1-weighted MPRAGE images show equivalent visualization of the dural-based enhancing mass along the parietal convexity. Both images were acquired on a 3T Siemens Healthineers MAGNETOM Prisma MRI scanner equipped with 80 mT/m maximum gradient strength and 200 T/m/s maximum slew rate. The Wave-CAIPI sequence was more than twice as fast as the standard sequence (acquisition time = 2:32 min for Wave-CAIPI compared to 5:18 min for the standard sequence). *Reproduced from [7].*

3D parallel imaging technique that is using sinusoidal gradients to create corkscrew-shaped k -space sampling trajectories in all three dimensions. Wave-CAIPI takes full advantage of the 3D coil sensitivity information when using the high-channel count receiver coils to provide high acceleration factors with negligible artifacts and noise penalty across a variety of contrasts. In general, higher gradient amplitudes and lower bandwidth generate more voxel spreading, which is beneficial for reconstructing cleaner images, while faster slew rates make it possible to fit more sinusoidal cycles per encoding period, diminishing the amount of artifact in the resulting images. The diagnostic performance of Wave-CAIPI has been shown to be equivalent to that of standard 3D anatomical sequences acquired with conventional parallel imaging across a variety of contrasts with reduced scan time and motion artifacts (Fig. 3) [8–11].

In short, fast MRI techniques take advantage of strong gradients and fast slew rates to enable more efficient, higher resolution anatomical images for diagnosis across a variety of contrasts with reduced scan time and concomitant motion artifacts.

Diffusion MRI: From connectational anatomy to the microstructure revolution

The advent of stronger gradients has been a boon to diffusion-weighted MRI by boosting the efficiency of diffusion encoding. Stronger gradients enable a given b -value to be achieved in less time, resulting in shorter echo times and less signal loss from T2 relaxation. Beyond the straight-

²Work in progress. The system is currently under development and is not for sale in the U.S. and in other countries. Its future availability cannot be ensured.

³≥ 200 (±3% for design tolerances)

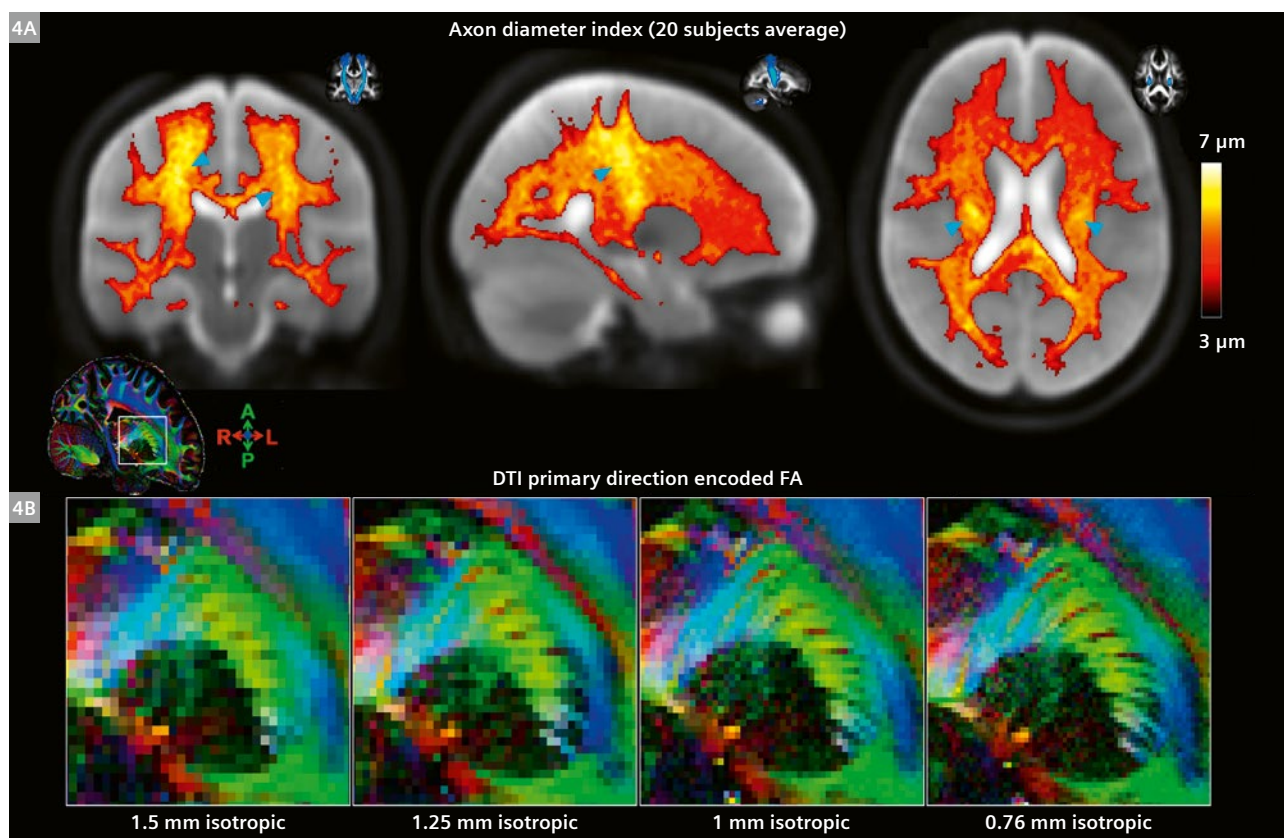
forward SNR argument, stronger gradients enable higher b-values to be achieved for better resolution of microscopic tissue structure and exquisite delineation of crossing fibers (Fig. 4). The increased signal-to-noise ratio can be deployed to increase the spatial resolution of diffusion MRI, enabling sub-millimeter voxel size, which benefits applications such as diffusion tractography in the deep brain, where white matter tracts coursing through the deep gray nuclei and brainstem are packed together tightly, making it very difficult to resolve such structures for important therapeutic applications such as deep brain stimulation and focused ultrasound targeting.

The availability of dedicated high-performance gradient coils with large maximum gradient amplitudes also enables new classes of diffusion MRI measurements to be performed and provides a more sensitive probe of gray and white matter microstructure in various neurological diseases. High gradient amplitudes benefit the estimation of tissue microstructural properties such as cellular size and density, axon diameter mapping, and the dimensions of the extracellular space, which opens the door to improving pathological specificity with the level of detail typically relegated to the realm of invasive tissue biopsies and

histological analysis, without the constraints of sampling bias or the risks associated with invasive procedures.

The advent of strong gradients for diffusion microstructural imaging may enable MRI to realize its true promise as a noninvasive imaging modality – monitoring disease activity and pathologic tissue change at the microscopic level in real-time, without the risk of radiation or the inherent risks of invasive sampling. The possibility of mapping tissue-level changes with a high degree of specificity might offer indicators of disease progression in a wide range of pathologic processes, such as increased cellular density within the tumor treatment bed, axonal loss and disability progression in multiple sclerosis, or impaired CSF clearance in neurodegenerative disorders such as Alzheimer's disease. Strong gradients will broaden our access as radiologists to a range of tissue-level parameters that are histologically and pathophysiologically relevant, offering new information to prompt a change in treatment course or management at an earlier disease stage, when such changes stand to make the biggest difference.

The greater availability of strong gradients for diffusion MRI will also enable the translation of novel diffusion-encoding paradigms to probe brain tissue microstructure



4 Benefits of strong gradients for diffusion MRI. **(4A)** In vivo axon diameter index maps enabled by high b-values using $G_{\max} \sim 200\text{--}300$ mT/m. Average axon diameter across 20 healthy subjects [12]. Blue arrowheads point to the corticospinal tracts, which show larger axonal diameter than the surrounding white matter. **(4B)** Fractional anisotropy (FA) maps of internal capsule at different spatial resolutions down to sub-millimeter 0.76 mm³ spatial resolution [13]. Reproduced from [14].

in patients, including oscillating-gradient waveforms, double-diffusion encoding, and q-space trajectory imaging. As a case in point, a recent study combined isotropic diffusion encoding with strong diffusion gradients to achieve high diffusion-weighting in highly restricted, spherical compartments in the cerebellar gray matter while suppressing signal arising from anisotropic water within axons. By gaining greater specificity to cellular signatures in the cerebellum, such spherical tensor encoding performed with high gradient strengths may enable the earlier identification of cerebellar gray matter loss in patients with hereditary ataxias such as spinocerebellar ataxia type 2, which selectively affects the granule and Purkinje cells. The ability to probe microscopic diffusion anisotropy in brain tumors using q-space trajectory imaging may enable the differentiation of relatively indolent tumors such as meningiomas from high-grade glial tumors based on their cellular morphology and composition.

The results of these and many other clinical research studies demonstrate the potential of high-gradient diffusion MRI to uncover changes in axonal and cellular microstructure and motivate the continued development, application, and dissemination of high-gradient technology for use in commercially available human MRI scanners. Just as advances in fiber technology, starting from under-sea cables to fiber optics and then the wireless revolution dramatically increased the accessibility and ease of communication, we believe that advances in gradient technology will increase the speed, availability, and clarity of imaging, while enabling the closer marriage between scientific discovery and clinical science to the benefit of patient care. Moving Connectome-like gradient strengths out of a few dedicated research facilities into the hands of radiologists and imaging scientists around the world promises to open up a whole new generation of clinical applications and discovery.

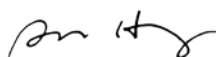
Conclusion

It is clear that in addition to the remarkable applications of the computational tools of AI and machine learning which we hear so much about today, the fundamentals of MR physics will continue to drive the benefits of, indeed the necessity for, further advances in the foundational components of our MRI systems: the primary magnetic fields which control and manipulate our MR signals, B_0 , and gradients. We are fortunate to be witnessing yet another key step forward in these technologies with the arrival of 7T systems for clinical and broad translational research

use, and “Connectom” class gradients for widespread applications outside select laboratories. As it has for four decades now, MRI continues to excite our imaginations for a boundless future.

References

- Opheim G, van der Kolk A, Bloch KM, Colon AJ, Davis KA, Henry TR, et al. 7T Epilepsy Task Force Consensus Recommendations on the Use of 7T MRI in Clinical Practice. *Neurology*. 2021;96(7):327-41.
- Ladd ME in: Schlegel W, Karger CP, Jäkel O. *Medizinische Physik: Grundlagen–Bildgebung–Therapie–Technik*: Springer-Verlag; 2018.
- Madelin G, Lee J-S, Regatte RR, Jerschow A. Sodium MRI: methods and applications. *Progress in nuclear magnetic resonance spectroscopy*. 2014;79:14-47.
- Regnery S, Behl NGR, Platt T, Weinfurter N, Windisch P, Deike-Hofmann K, et al. Ultra-high-field sodium MRI as biomarker for tumor extent, grade and IDH mutation status in glioma patients. *NeuroImage: Clinical*. 2020;28:102427.
- Platt T, Ladd ME, Paech D. 7 Tesla and Beyond: Advanced Methods and Clinical Applications in Magnetic Resonance Imaging. *Investigative Radiology*. 2021;56(11):705-25.
- Paech D, Nagel AM, Schultheiss MN, Umthum R, Regnery S, Scherer M, et al. Quantitative Dynamic Oxygen 17 MRI at 7.0 T for the Cerebral Oxygen Metabolism in Glioma. *Radiology*. 2020;295(1):181-9.
- Vachha B, Huang SY. MRI with ultrahigh field strength and high-performance gradients: challenges and opportunities for clinical neuroimaging at 7 T and beyond. *Eur Radiol Exp*. 2021;5(1):35.
- Conklin J, Longo MGF, Cauley SF, Setsompop K, Gonzalez RG, Schaefer PW, et al. Validation of Highly Accelerated Wave-CAIPI SWI Compared with Conventional SWI and T2*-Weighted Gradient Recalled-Echo for Routine Clinical Brain MRI at 3T. *AJNR Am J Neuroradiol*. 2019;40(12):2073-80.
- Goncalves Filho ALM, Conklin J, Longo MGF, Cauley SF, Polak D, Liu W, et al. Accelerated Post-contrast Wave-CAIPI T1 SPACE Achieves Equivalent Diagnostic Performance Compared With Standard T1 SPACE for the Detection of Brain Metastases in Clinical 3T MRI. *Front Neurol*. 2020;11:587327.
- Longo MGF, Conklin J, Cauley SF, Setsompop K, Tian Q, Polak D, et al. Evaluation of Ultrafast Wave-CAIPI MPRAGE for Visual Grading and Automated Measurement of Brain Tissue Volume. *AJNR Am J Neuroradiol*. 2020;41(8):1388-96.
- Polak D, Cauley S, Huang SY, Longo MG, Conklin J, Bilgic B, et al. Highly-accelerated volumetric brain examination using optimized wave-CAIPI encoding. *J Magn Reson Imaging*. 2019;50(3):961-74.
- Huang SY, Tian Q, Fan Q, Witzel T, Wichtmann B, McNab JA, et al. High-gradient diffusion MRI reveals distinct estimates of axon diameter index within different white matter tracts in the in vivo human brain. *Brain Struct Funct*. 2020;225(4):1277-91.
- Wang F, Dong Z, Tian Q, Liao C, Fan Q, Hoge WS, et al. In vivo human whole-brain Connectom diffusion MRI dataset at 760 microm isotropic resolution. *Sci Data*. 2021;8(1):122.
- Gudino N, Litten S. Advancements in Gradient System Performance for Clinical and Research MRI. *J Magn Reson Imaging*. 08 September 2022.



Susie Huang



Bruce Rosen



Daniel Paech

Building a Global Power of Experience in Diagnostic Imaging – Lessons from Africa's COVID-19 Response

Udunna Anazodo, Ph.D.^{1,2}; Iris Asllani, Ph.D.^{3,4}; Abiodun Fatade, MBBS²

¹Montreal Neurological Institute, McGill University, Montreal, Quebec, Canada

²Medical Artificial Intelligence (MAI) Lab, Crestview Radiology Ltd, Lagos, Nigeria

³Department of Biomedical Engineering, Rochester Institute of Technology, New York, NY, USA

⁴Department of Neuroscience and Imaging, Brighton and Sussex Medical School, University of Sussex, Brighton, UK

Nigeria's experience with Ebola shows us how having trained experts in place can make the difference when confronting unexpected health threats.

The U.S. Centers for Disease Control and Prevention (CDC), 2016

As we collectively resume our daily life in the post-pandemic 'new normal' and reflect on the varying trials and tribulations brought on by the COVID-19 pandemic, some have argued that what we lived through in the past two years was a 'syndemic' – the aggregation of the acute infectious SARS-CoV-2 and chronic noncommunicable diseases (NCDs), with their interaction increasing disease susceptibility and worsening health outcomes [1, 2]. In all likelihood, the poor management of the growing prevalence of NCDs, due primarily to a fragmented global public health policy, created the perfect storm for a COVID-19 syndemic [1]. Nonetheless, as the number of COVID-19 cases worldwide continue to trend downwards, the growing burden of NCDs, especially in low resourced areas, remains a threat to post-pandemic recovery and to the sustainability of health systems worldwide [3].

The pandemic highlighted the need for "medicine without borders", including development of accurate and easily implementable diagnostic tools. Here, we focus on high value diagnostic imaging, particularly CT and MRI services, as the global demand has risen over the past two decades as the technological innovations of these services become rapidly adopted as standard of care to manage the growing burden of NCDs. Thirteen of the twenty leading causes of deaths worldwide are NCDs, with cardiovascular diseases, cancers, respiratory diseases, and dementia lead-

ing the way (Fig. 1) [4, 5]. A staggering majority (70–80%) of these deaths occur in low-to-middle income countries (LMICs) [4]. Even in Sub-Saharan Africa, premature mortality from NCDs is on track to outpace the combined deaths from communicable, maternal, neonatal, and nutritional diseases by 2030 [4]. Not surprising, deaths from heart disease and cancer in 2019 (the latest global numbers available) were far greater than the total number of deaths attributed to COVID-19 from January 2020 to September 2022 (Fig. 1) [6].

What's even more surprising is that Africa seems to have fared relatively well with the COVID-19 pandemic, or syndemic, with a fewer number of COVID-19 cases and deaths compared to other regions of the world [6, 7], despite having the lowest vaccination rate in the world [7]. This is quite remarkable given early predictions of worse outcomes considering Africa's notoriously weak healthcare systems and its perennial lack of health infrastructure and skilled workforce [8–10]. Although the jury is still out as to why Africa seemingly weathered the COVID-19 storm, wave after wave, there is a general understanding that the region's level of preparedness from lessons of decades of battling epidemic infectious diseases may have conferred the *Power of Experience* to manage COVID-19 relatively well [7–12].

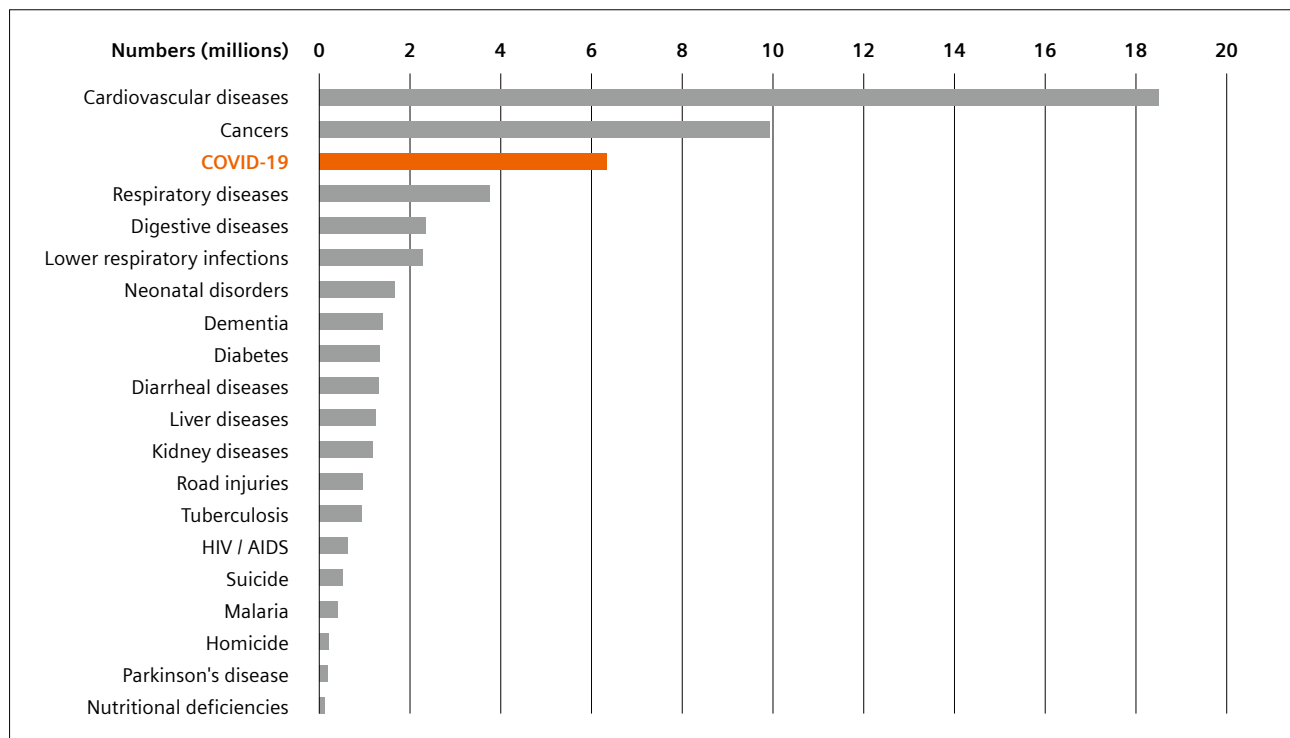
Are there lessons from Africa's COVID-19 experience that can be gleaned to inform pragmatic strategies that will strengthen diagnostic imaging services to address global threats from NCDs? Given that 80% of the world's population who largely resides in low-resourced areas is the most vulnerable but do not have access to adequate diagnostic imaging and must contend with poorly maintained equipment sporadically centralized in major cities in centers that are understaffed and lack skilled personnel, it is crucial that any wins in one health sector in LMICs is unweariedly and efficiently adapted to other sectors.

COVID-19 lessons from Africa: Think Omicron!

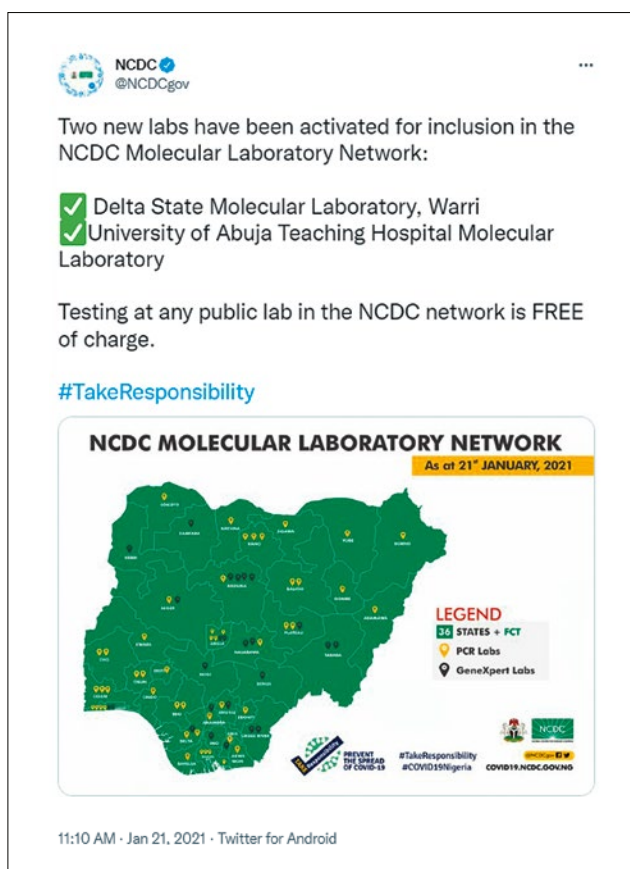
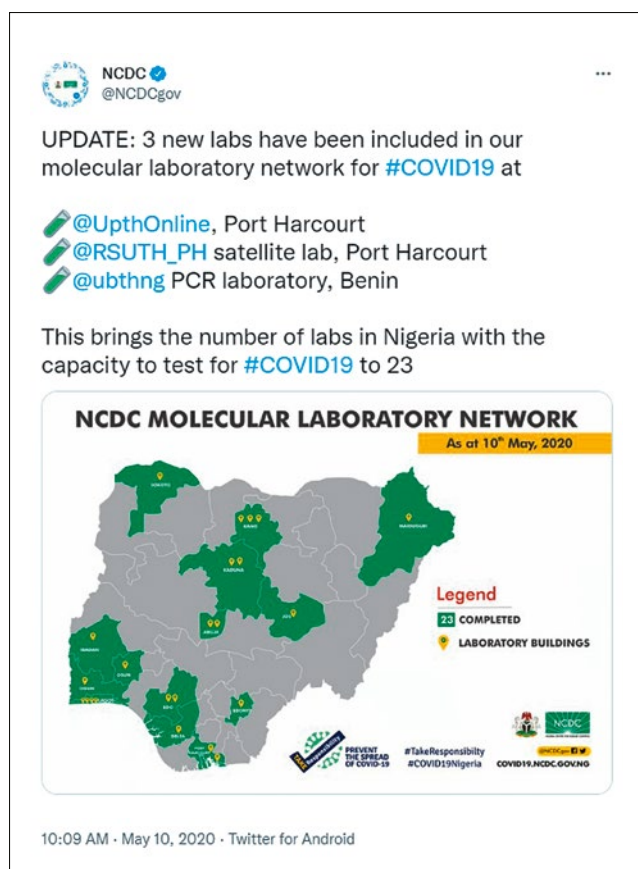
Precisely one year before COVID-19 took the world by storm, Nature ran a news feature on February 20, 2019, with the following headline, “This Nigerian doctor might just prevent the next deadly pandemic” [13]. The author, Amy Maxmen, was writing about Dr. Chikwe Ihekweazu, the first Director General of Nigeria Centre for Disease Control (NCDC), who completed his medical training at the University of Nigeria in Nsukka, Nigeria, prior to receiving his Master’s in Public Health from Heinrich Heine University of Düsseldorf, Germany, and subsequent stints as a Medical Epidemiologist in Germany and the UK. The article described the ‘step change’ in Nigeria’s pandemic preparedness with the arrival of Dr Ihekweazu as head of the fledgling NCDC in 2016, during the 2014–16 Ebola crisis [13]. Armed with a measly \$4 million budget in 2018 (0.036% of the US CDC’s annual budget in the same year) and lessons from several epidemics (2016 Polio, 2016–17 Meningitis, 2018 Yellow fever, Lassa fever and Cholera), as well as a healthy political will from the Nigerian Government to support the NCDC and their leadership, Dr Ihekweazu did what Africans generally do – do much with little. The good doctor at the outset made “careful choices” [13] with his scarce resources and created a power of experience in COVID-19 management by:

- I. Forming “real partnerships not a master-servant relationship” with US CDC [14] and other international public health institutions [15] to **train** epidemiologists and biologists in place at the NCDC and use his sheer dedication to attract Nigerians abroad to join the NCDC – “an experiment in brain gain” [13].
- II. Building a regional **network** of molecular labs with the capacity to monitor pathogens and surveillance offices in each state in Nigeria linked to the national NCDC headquarter in the nation’s capital, Abuja to prevent and respond to infectious disease outbreaks in a coordinated manner.
- III. Strategically equipping regional labs with **infrastructure** for high quality diagnostics capacity including Polymerase Chain Reaction (PCR) machines, rapid antibody sensitivity diagnostic systems, and genomic sequencing and immunological testing systems.

When COVID-19 hit Nigeria in March of 2020, the NCDC had 6 molecular labs judiciously distributed across the country with capacity for PCR COVID-19 testing and other 6 in the process of being completed [16]. By May 2020, the test capacity had jumped to 23 labs across the country and, within 10 months, in January 2021, all 36 states in the country had molecular labs equipped with skilled



1 2019 worldwide number of deaths by cause [5].



2 Strategically equipping regional labs with infrastructure for high quality diagnostics capacity.

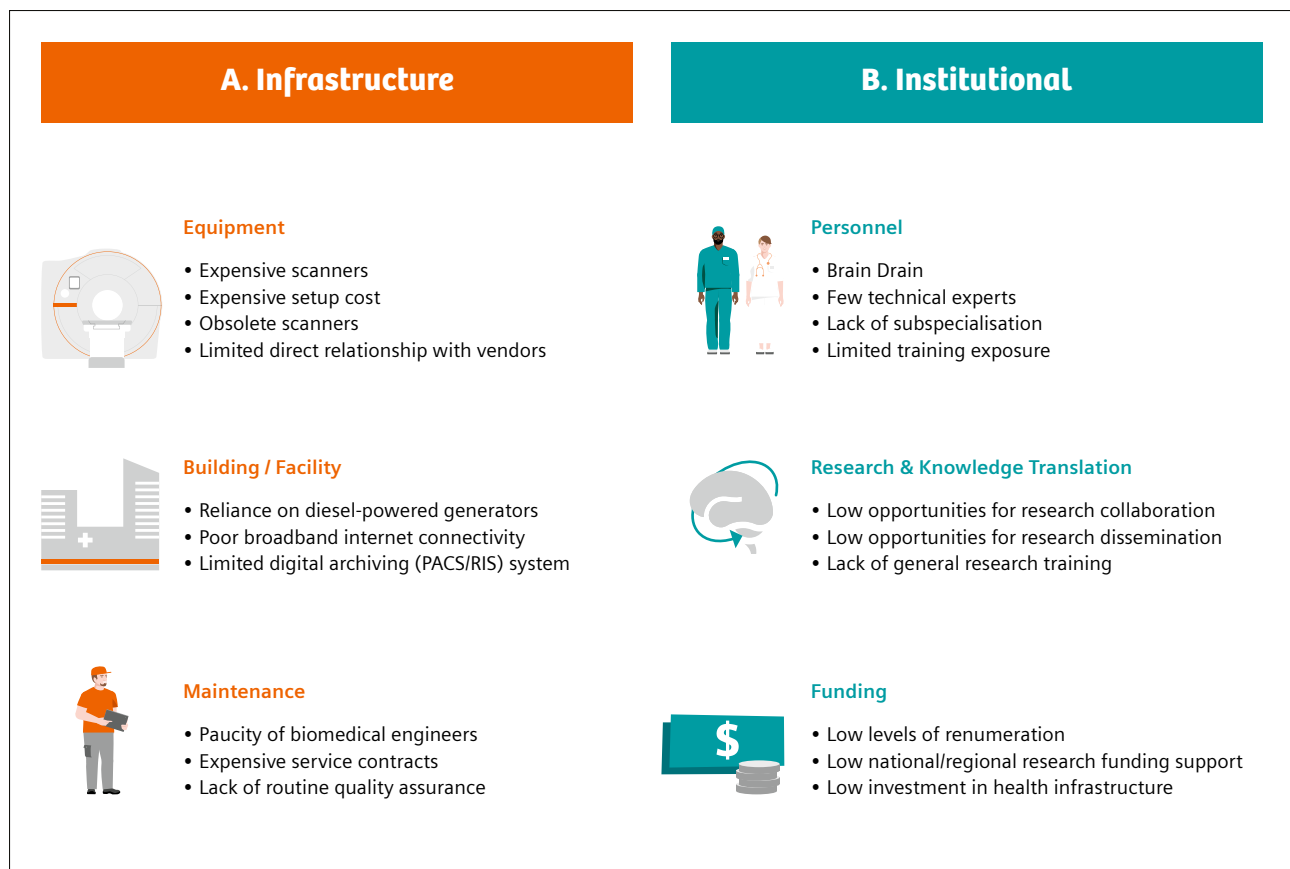
personnel, infrastructure for COVID-19 testing, and linkage to rapid viral genome sequencing centers (Fig. 2). These resources were rapidly deployed to detect and track the emerging COVID-19 threat [16].

While Dr Ihekweazu and his team at NCDC were preparing Nigeria to address COVID-19, the Africa Center for Disease Control and Prevention (Africa CDC), formed in 2017, following the Ebola crisis, leaped into action in February 2020, days after the 1st case of COVID-19 was reported in Egypt [7], to form a Joint Continental Strategy with national public health institutions across the region. This continent-wide collaboration, still in place, provided the coordinated platform to share resources, work together in a pan-regional network, and communicate efforts, including implementation of lockdowns and restrictions [5]. More importantly, this continent-wide network, supported by scaled-up local capacity in surveillance and genomics, resulted in rapid discovery of several COVID-19 variants across Africa, including the now infamous Omicron variant, sampled in Botswana, and sequenced by the Network for Genomic Surveillance in South Africa [7, 17].

Now, imagine if Africa had the standard global support – the mismatched donated low-cost and low-resolution health technology, in this case, rapid kits or PCR with limited and isolated capacity for viral genome sequencing – if that were the case, the world would not have benefited from the African discovery of Omicron. Generally speaking, if low-resourced settings around the world were not empowered to develop and sustain their own local public health systems, the COVID-19 pandemic/syndemic may have had a more dire outlook. Therefore, we must lose no time to adopt this winning strategy to other healthcare sectors in LMICs.

Closing global gaps in diagnostic imaging

What Africa got right [7] with COVID-19 and a global lesson with clear relevance to diagnostic imaging is the need to work together as a global community to create the power of experience, the rich local expertise and capacity that will enable each country and each region to meet their pertinent and unique health care challenges.



3 Drivers of limited access to MRI in Africa. *Figure adapted from [19].*

The question then is: How do we, as a global imaging community, work with those from the least-resourced areas to close longstanding inequities and enable our colleagues in Africa to address their overlapping complex imaging barriers (Fig. 3) so that the region's poor are provided with adequate access to clinically valuable diagnostic imaging?

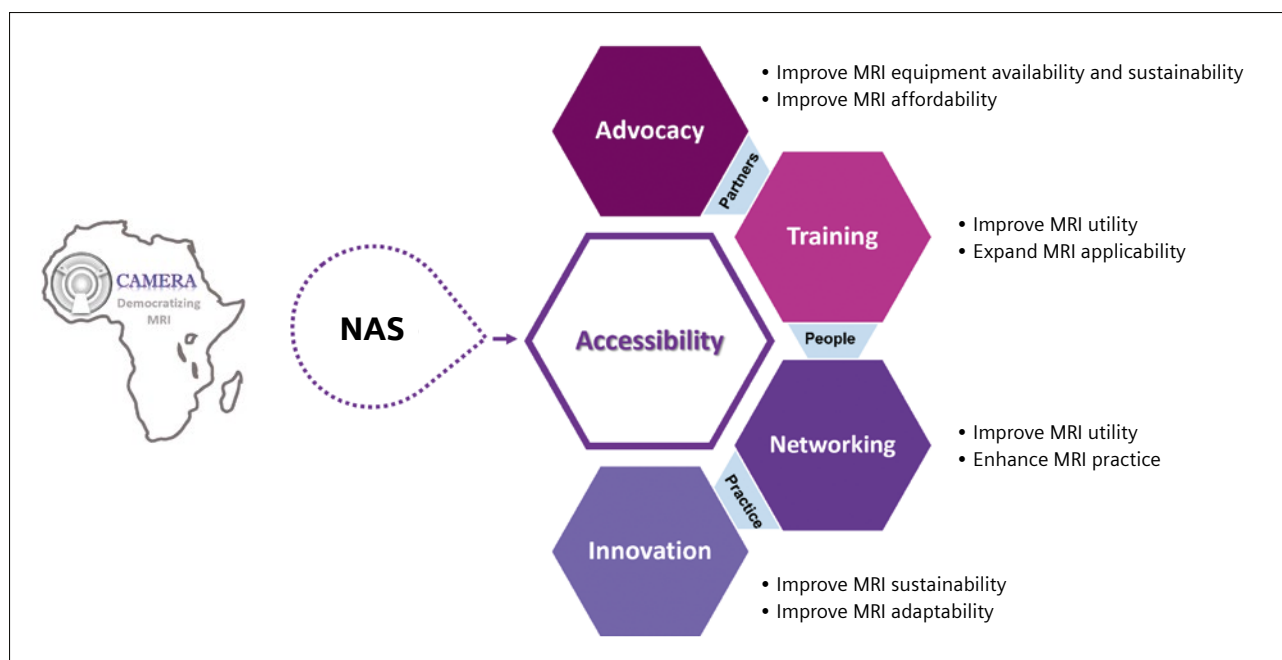
In October 2019, we set out to do just that. We formed the Consortium for Advancement of MRI Education and Research in Africa (CAMERA), as a working group of the European Society of Magnetic Resonance in Medicine and Biology (ESMRMB), to address challenges to MRI access in Africa by strengthening local capacity for clinical use of MRI and expediting research translation of local MRI innovations. Since then, we have grown to become a global network of MRI experts from all disciplines (radiology, radiography, physics, biomedical engineering) and emerging fields (computational imaging and artificial intelligence) with a clear vision [18] and strategy, gleaned from Africa's COVID-19 lessons, to create the unbroken chain of resources and expertise in MRI across Africa [19]. In 2020 and 2021, we leveraged the general slowdown in radiology services during the COVID-19 lockdowns to conduct a Needs Assessment Study (NAS) to identify MRI

capacity gaps and understand the general landscape of MRI in the region [19]. Our NAS captured needs as well as opportunities along four central priorities:

- 1) availability and access,
- 2) personnel training and education,
- 3) research translation, and
- 4) sustainable technology [19].

Based on the NAS findings, we formulated a framework (Fig. 4) to address these four priorities and the intricate barriers that accompany them (Fig. 3) [19].

We discovered that overall, the percentage of high field 1.5T MRI in Sub-Saharan Africa is growing and predominantly installed and operated at private clinics [19]. Furthermore, these scanners are severely (92%) underutilized, scanning less than 15 patients per day, per scanner, a far cry from the potential capacity of MRI, especially for clinics that service relatively large geographical areas [19]. Our study found that one of the major contributors to the under-utilization of MRI in the region is the perpetual and persistent lack of trained expertise to scan (radiographers), interpret (radiologists), develop,



4 The CAMERA conceptual framework. *Figure adapted from [19].*

or optimize protocols, as well as process high quality images (physicists) and maintain (engineers) the scanners [19]. To address these issues, we are leveraging the existing MRI infrastructure in the region to develop local training and continuing education programs and create regional networking opportunities to provide our African colleagues with the power of experience in MRI diagnostics [19].

Training game changers and creating catalysts for MRI innovation in Africa

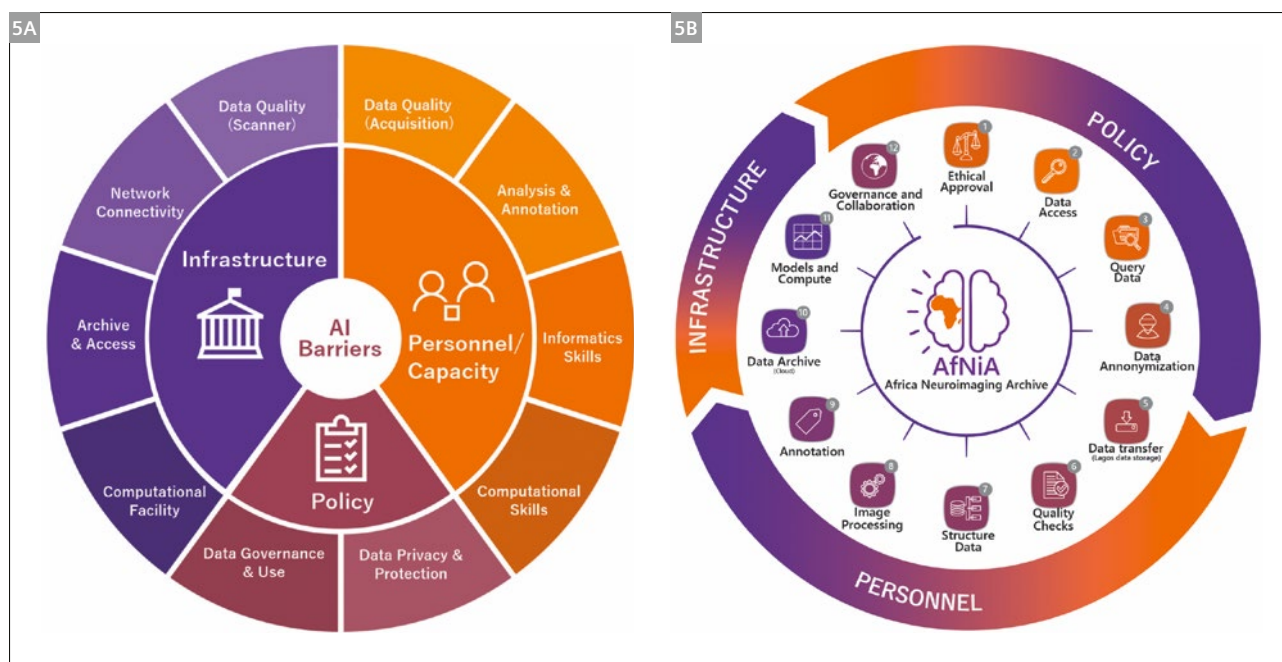
In October 2022 at the Association of Radiologists in Nigeria (ARIN) annual meeting, we launched the Africa Neuroimaging Archive (AfNiA), one of the key initiatives at CAMERA and funded by the Lacuna Fund [20], with the overarching aim of providing the power of experience in artificial intelligence (AI) applications in MRI diagnostics in low-resourced settings [21]. Specifically, AfNiA is a collaborative framework to enable ethical data share and aggregation of fragmented expertise, disciplines, resources, and pipelines required to effectively apply AI imaging solutions to transform diagnostic imaging care in the African setting (Fig. 5).

We have created the AfNiA ecosystem using glioma MRI diagnostics as an optimal use case and catalyst for the design, implementation, and validation of its 12 nodes (Fig. 5B). We chose glioma diagnostics to leverage the decade-long collaborative global efforts in glioma AI imaging applications by the computational

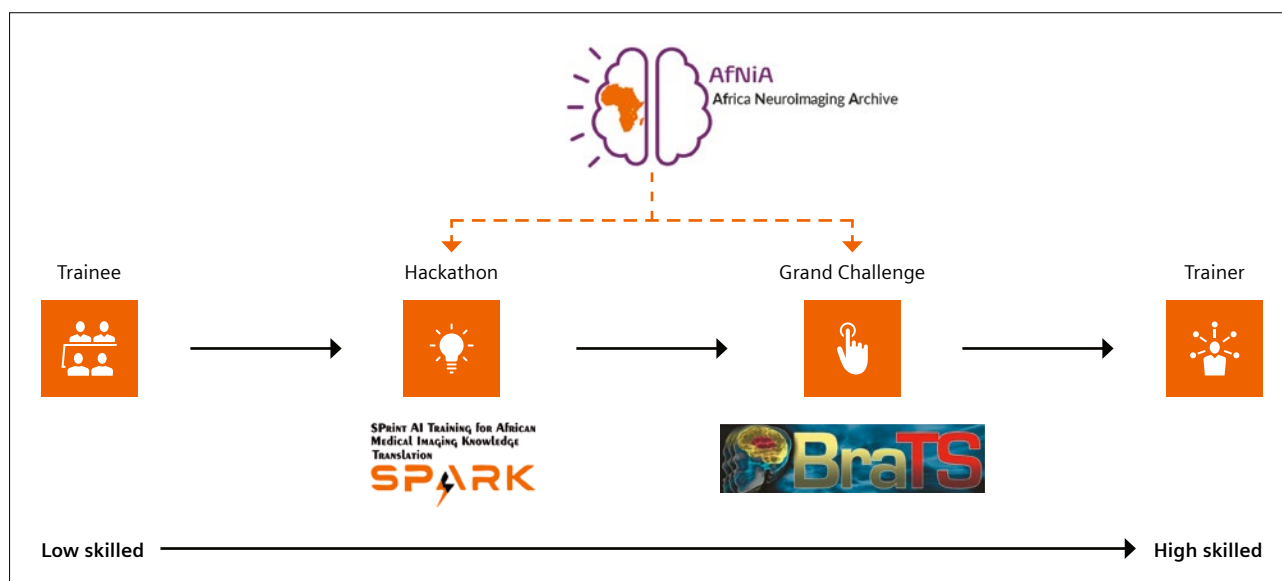
imaging community through the RSNA/ACR/MICCAI Brain Tumor Segmentation (BraTS) challenge [22]. Although the BraTS challenge has provided several promising models, some segmenting tumors with precision comparable to manual expert reads [23], it is unclear if these models can be applied to African populations who need AI-assisted diagnosis the most [22]. Starting with data, we are aggregating retrospective brain MRI scans from clinics across Africa, including clinics that do not have access to PACS to curate, annotate, and archive the data for public use in the upcoming BraTS challenge.

Moreover, to address the lack of region-specific data governance provisions, policies for ethical use are being developed to govern access to curated data and ensure that AI solutions created using AfNiA will directly benefit the local communities who own and provide the data. This effort is crucial in Africa, where medical data is overwhelmingly provided from out-of-pocket patient expenses, and as such require direct benefit considerations [19]. Using the data governance mechanism, we will link local clinics to the wider imaging community and among themselves to enable co-creation of AI solutions in a global peer-to-peer collaborative network.

Lastly, to meaningfully create a rich local experience in AI imaging capacity, as part of AfNiA, we have developed the SPARK (Sprint AI Training for African Medical Imaging Knowledge Translation) program as a train-the-trainer workshop and hackathon (Fig. 6) to rapidly establish game changers that will drive AI imaging innovations locally.



5 (5A) AI challenges in healthcare. (5B) The AfNiA ecosystem.



6 Train-the-trainer concepts to meaningfully create a rich local experience in AI imaging capacity.

The SPARK training program, which is planned to run for the first time in Summer 2023, will use RAD-AID's *Teach-Try-Use* [24] approach to train a multi-disciplinary team on data collection, AI model development, and clinical evaluation. The aim is to equip the trainees with competent skills to participate in the next 2023 BraTS challenge with models that have a clear chance of winning the challenge.

SPARK and AfNiA will operate out the Medical Artificial Intelligence (MAI) lab, strategically situated within Crestview Radiology Ltd, Lagos, Nigeria – a local clinic not affiliated with an academic institution, to ensure that AI models being developed can be swiftly and directly deployed to clinic (i.e., rapid model-to-clinic or bench-to-bedside).

Democratizing diagnostic imaging to advance global health

As novel innovations in mobile and low-cost imaging technology such as the 0.55T MRI system MAGNETOM Free.Max (Siemens Healthcare, Erlangen, Germany) continue to make their way into clinics, especially those in low-resourced settings, imaging communities such as the Radiological Society of North America, can partner with vendors who are starting to break barriers with these systems, to provide local communities around the world with the power of experience to address their global health challenges using high value diagnostic imaging. Considering how crucial low field MRI is to the democratization of diagnostic imaging and the surge of research and development in this field, collaborative multi-national and multi-institutional efforts should be strongly encouraged, especially those aimed at open sharing of resources, to readily include low-resourced settings. One such exemplary effort is the recent in situ assembly of a low field MRI system [25] at Dr Johnes Obungoloch's MRI lab at the

Mbarara University of Science and Technology (MUST), Uganda (Fig. 7). The MRI system was developed at Leiden University Medical Center, the Netherlands, by Professor Andrew Webb and constructed at MUST by a team of international MRI scientists (Fig. 7) supported by Professor Steven Schiff's group at Yale University, New Haven, CT, USA. This first MRI system collaboratively built in Africa under a resource-limited setting and the accompanying MRI training provided to local scientists is the power of experience that will catalyze research projects pertinent to increasing MRI capacity to meet the region's healthcare needs and ambitions.

If COVID-19 has taught us anything, it is that we must now practice 'medicine without borders', to Think Globally while Acting Locally, to now go further together, so we can as Professor Daniel K Sodickson, former President of ISMRM eloquently stated at the ISMRM-ESMRMB 2018 Mansfield Lecture, marshal all our disruptive innovative forces to continue to create new ways of seeing [26].



AndrewWebb @AndrewW56450446 · Sep 24

Building low field MRI systems in Africa, aided by Wouter Teeuwisse and Tom O'Reilly



7 Assembly of a low field MRI system at Mbarara University of Science and Technology (MUST), Uganda, Africa.

References

- 1 Horton R. Offline: COVID-19 is not a pandemic. *Lancet*. 2020;396(10255):874.
- 2 Di Guardo G. CoViD-19, a “syndemic” rather than a “pandemic” disease. *BMJ*. 2020;370:m3702.
- 3 Wilkinson E. UK Government urged to recognize post-COVID cancer backlog. *Lancet Oncology*. 2021;22(7):910.
- 4 Ezzati M, Pearson-Stuttard J, Bennett JE, Mathers CD. Acting on non-communicable diseases in low- and middle-income tropical countries. *Nature*. 2018;559(7715):507-516.
- 5 Our World in Data. Deaths by cause, World 2019. <https://ourworldindata.org/causes-of-death> [Accessed on September 27, 2022].
- 6 World Health Organization (WHO) Coronavirus (COVID-19) Dashboard. <https://covid19.who.int/> [Accessed on September 27, 2022].
- 7 Happi CT, Nkengasong JN. Two years of COVID-19 in Africa: lessons for the world. *Nature*. 2022;601:22-25.
- 8 Nordling L. The Pandemic appears to have spared Africa so far. Scientists are struggling to explain why. *Science*. 2020 Aug 11.
- 9 Ofotokun I, Sheth AN. Africa’s COVID-19 Experience – A Window of Opportunity to Act. *JAMA Network Open*. 2021;4(9):e2124556.
- 10 Chitungo I, Dzobo M, Hlongwa M, Dzinamarira T. COVID-19: Unpacking the low number of cases in Africa. *Public Health Pract (Oxf)*. 2020;100038.
- 11 Tessema GA, Kinfu Y, Dachew BA, Tesema AG, Assefa Y, Alene KA, et al. The COVID-19 pandemic and healthcare systems in Africa: a scoping review of preparedness, impact and response. *BMJ Global Health*. 2021;6:e007179.
- 12 Soy A. Coronavirus in Africa: Five reasons why COVID-19 has been less deadly than Elsewhere. *Global Development Commons*. United Nations International Children’s Emergency Fund (UNICEF). October 9, 2020. <https://gdc.unicef.org/resource/coronavirus-africa-five-reasons-why-covid-19-has-been-less-deadly-elsewhere> [Accessed on September 27, 2022].
- 13 Maxmen A. This Nigerian doctor might just prevent the next deadly pandemic. *Nature* 2019;566,310-313.
- 14 Centers for Disease Control and Prevention (CDC). CDC in Nigeria. <https://www.cdc.gov/globalhealth/countries/nigeria/> [Accessed on September 27, 2022].
- 15 German Federal Ministry of Health. Fighting COVID-19: Support to West Africa-Module <https://ghpp.de/en/projects/afrolabnet/fighting-covid-support-to-west-africa/> [Accessed on September 27, 2022].
- 16 Nigeria Centre for Disease and Control (NCDC). COVID-19 Dashboard. <https://covid19.ncdc.gov.ng/report/> [Accessed on September 27, 2022].
- 17 Tegally H, Wilkinson E, Giovanetti M, Iranzadeh A, Fonseca V, Giandhari J, et al. Detection of a SARS-CoV-2 variant of concern in South Africa. *Nature*. 2021;592(7854):438-443.
- 18 <https://www.cameramriafrika.org/> [Accessed on September 27, 2022].
- 19 Anazodo UC, Ng JJ, Ehiogu B, Obungoloch J, Fatade A, Mutsaerts HJMM, et al. The Consortium for Advancement of MRI Education and Research in Africa (CAMERA). A Framework for Advancing Sustainable MRI Access in Africa. *NMR Biomedicine*. 2022. doi: 10.1002/nbm.4846
- 20 Lacuna Fund. Announcing Awards for Health Datasets. <https://lacunafund.org/announcing-awards-for-health-datasets/>. Published May 19, 2022. [Accessed May 22, 2022].
- 21 Anazodo U C, Adewole M, Dako F. AI for Population and Global Health in Radiology. *Radiol Artif Intell*. 2022;4(4):e220107.
- 22 Menze BH, Jakab A, Bauer S, Kalpathy-Cramer J, Farahani K, Kirby J, et al. The Multimodal Brain Tumor Image Segmentation Benchmark (BRATS). *IEEE Trans Med Imaging*. 2015;34(10):1993-2024.
- 23 Kouli O, Hassane A, Badran D, Kouli T, Hossain-Ibrahim K, Steele JD. Automated brain tumor identification using magnetic resonance imaging: A systematic review and meta-analysis. *Neurooncol Adv*. 2022;4(1):vdac081.
- 24 <https://rad-aid.org/artificial-intelligence/> [Accessed September 27, 2022].
- 25 de Vos B, Parsa J, Abdulrazaq Z, Teeuwisse WM, Van Speybroeck CDE, de Gans DH, et al. Design, Characterisation and Performance of an Improved Portable and Sustainable Low-Field MRI System. *Front Phys*. 2021.9:701157.
- 26 Warnert EAH, Nayak K, Menon R, Rice C, Port J, Morris EA, et al. Resonate: Reflections and recommendations on implicit biases within the ISMRM. *J Magn Reson Imaging*. 2019;49(6):1509-1511.

Contact

Udunna C. Anazodo, Ph.D.
 Assistant professor of neurology and neurosurgery
 Montreal Neurological Institute at McGill University
 3801 Rue University
 Montréal, QC H3A 2B4
 Canada
udunna.anazodo@mcgill.ca



Udunna Anazodo, Ph.D.



Iris Asllani, Ph.D.



Abiodun Fatade, MBBS

Breast MRI in India: Practice and Challenges

Pratiksha Yadav, MBBS, M.D., Ph.D.

Dr. D. Y. Patil Medical College, Hospital and Research Centre, Dr. D. Y. Patil Vidyapeeth, Pune, India

Background

Breast cancer is one of the most common malignancies in women worldwide, and the leading cause of cancer mortality. Although the incidence of breast cancer is thought to be higher in developed countries, it is also increasing in developing countries, where the majority of cases are detected at already advanced stages. According to data from Surveillance Epidemiology and End Results Program (SEER), there were 231,840 new cases of breast cancer in 2015, and 14% of those were newly detected cases. In the same year, breast cancer resulted in an estimated 40,290 deaths, which constituted 6.8% of all cancer deaths [1].

In India, the age-adjusted incidence of breast cancer is 25.8 per 100,000, which is lower than in the United Kingdom, where it is 95 per 100,000. However, the mortality rate is about 12.7 versus 17.1 per 100,000 respectively [2]. The global burden of breast cancer cases is expected to be about 2 million by 2030, with an increasing proportion of cases from developing countries [3, 4]. Breast cancer incidence in India varies across the country. Breast carcinomas in younger women are more aggressive than in older women, and studies suggest that breast cancer diagnoses peak at about 40–50 years of age in Indian women [7]. Indian women with breast cancer are estimated to be one decade younger than respective women in western countries [5–7]. Diagnosis of breast cancer at advanced stages contributes to the high mortality rate in Indian women.

Early detection is key for better prognosis. As lumps are not typically associated with pain, this leads to a delay in seeking diagnosis and treatment, and most of the symptomatic patients are already at stage II or III. The late diagnosis can be attributed to less awareness and limited access to diagnostic and treatment facilities in rural and suburban areas. India has no national screening program, and many women cannot afford

the expensive examinations that would be required. Middle- and low-income countries face infrastructure and resource constraints, which are obstacles to improving breast cancer outcomes with early detection and treatment.

There are vast differences in the availability of breast imaging infrastructure and expert radiologists between big cities, rural regions, and suburban areas [8]. On one side, bigger cities have state-of-the-art infrastructure and expert radiologists who excel at early detection of breast cancer. On the other side, in rural and suburban areas, many breast cancer cases are missed or wrongly diagnosed as benign due to a lack of adequate diagnostic availability.

It is a real challenge that, in India, women present at late stages of breast cancer with large lumps, secondary changes of malignancy, multiple lesions, and sometimes bilateral cancer or metastatic lesions in the contralateral breast.

Magnetic resonance imaging (MRI) has exceptional sensitivity to detect breast lesions that sometimes might remain undetected on X-ray mammography, i.e. in women with dense breast tissue, which is more common in the aforementioned age range of 40–50. Dynamic contrast-enhanced MRI (DCE-MRI) is the most sensitive method for the detection of breast carcinomas, with reported sensitivities greater than 90% [9]. Even though both fat-suppressed T1- and T2-weighted MRI and DCE-MRI are excellent techniques for the characterization of breast lesions, sometimes it is not possible to distinguish between benign and malignant lesions using only these methods. Diffusion-weighted imaging (DWI) is a technique where the image contrast is derived from differences in the diffusion rate of water molecules in normal and pathological tissues. Malignant lesions, which typically have a higher degree of cellularity, demonstrate restricted diffusion. Studies have demonstrated that multi-parametric MRI of

the breast using DCE-MRI and DWI together significantly improve the diagnostic accuracy [10, 11].

To overcome the limitation in specificity of DCE-MRI [12], other functional MRI parameters can be used in multi-parametric MRI to primarily improve the specificity of breast MRI.

My practice in breast MRI

At our institution we use a dedicated 16-channel breast imaging coil on a 1.5T MAGNETOM Avanto and an 18-channel breast imaging coil on a 3T MAGNETOM Vida scanner (Siemens Healthcare, Erlangen, Germany). Patients lie prone with both breasts in the apertures of the coil. Compression is not applied but both breasts are softly fixed using foam.

Protocol and scanning parameters

The MRI sequences acquired are T2W, non-enhanced T1W, dynamic post-contrast T1W, and DWI. The sequence parameters are listed in Table 1.

The dynamic T1W sequences are acquired in transverse plane for better assessment of both breasts. A T1W with SPAIR fat suppression is acquired before the intravenous injection of contrast agent. The contrast, MultiHance (gadobenate dimeglumine; Bracco Imaging, Milan, Italy), is administered at 0.1 mmol per kilogram of body weight, followed by a 20 mL flush of saline using a power injector set at a flow rate of 2 mL/s. After the intravenous contrast injection, five T1W post-contrast series are acquired to evaluate the enhancement characteristic of the lesion.

Postprocessing and reading

The reading and interpretation of a breast MRI examination is performed following the American College of Radiology BI-RADS guidelines to differentiate benign and malignant lesions. It starts by analyzing first the pre-contrast T1W

images, then the post-contrast images, and the post-processing information.

Subtraction images are obtained by subtracting the T1W pre-contrast images from the post-contrast series. Then, the maximum intensity projection (MIP) of the post-contrast images is also obtained.

Kinetic analysis is performed by calculating the mean curve in the region of interest (ROI) from the dynamic scans. The type of post-contrast enhancement is analyzed in each lesion (foci enhancement, mass or non-mass enhancement). The evaluation of the enhancement kinetics involves assessing the contrast uptake in the early post-contrast phase (wash-in), the peak of lesion enhancement, and the wash-out. In a type I curve, there is persistent enhancement with continued increased signal intensity throughout the dynamic phase. A type II curve has a plateau pattern, in which the signal intensity of the lesion remains approximately constant in the delayed phase. A type III curve shows early uptake and early wash-out.

Apparent Diffusion Coefficient (ADC) maps are obtained on the workstation.

In vivo high-resolution MR spectroscopy (MRS) is performed using a single-voxel proton spectroscopy method with spectral lipid suppression and weak water suppression. Postprocessing is performed using a spectroscopy evaluation tool available at the MR console, and metabolite information is obtained for the ROI.

After reading and interpretation of the data, the diagnosis is correlated with the histopathological analysis following core biopsy or surgical excision.

My clinical and research experience with breast MRI

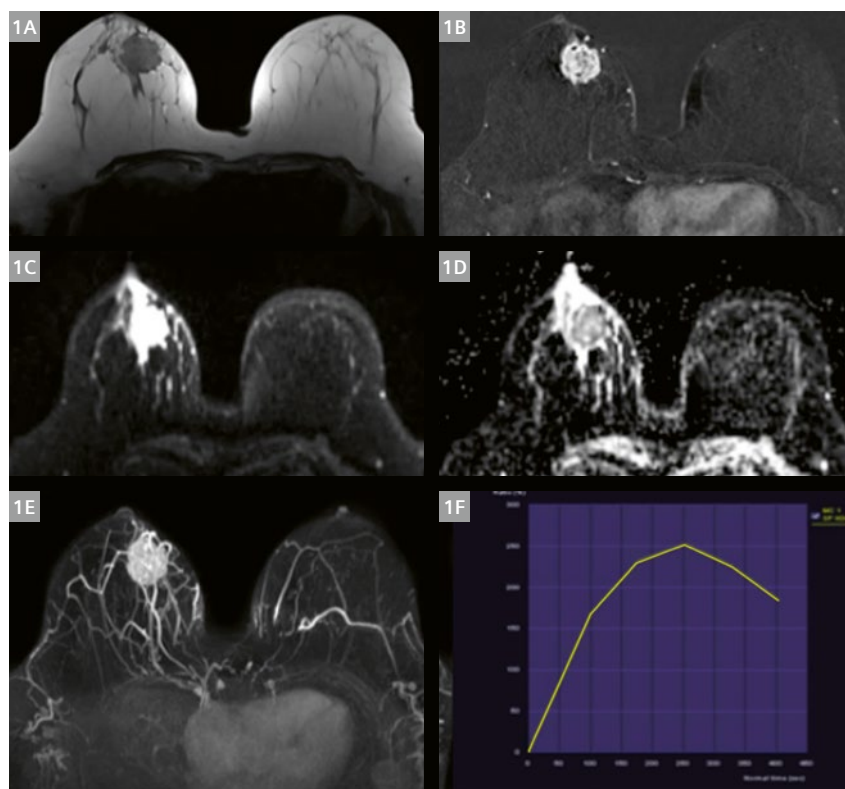
Indian women often have a dense fibroglandular pattern, so there are more chances that lesions are missed on

Sequence	Orientation	TR/TE (ms)	FOV read (mm)	Slice thickness (mm)	Base resolution	Phase Resolution (%)	b-value (s/mm ²)
T2W STIR	Transverse	3800/70	300	3	448	70	–
T2W STIR	Coronal	3800/79	300	3	448	70	–
T2W	Transverse	3000/71	320	3	448	70	–
DWI	Transverse	6800/70	360	3	360	50	0, 800, 1500
T1W SPAIR pre/post-contrast	Transverse	6.13/3.30	320	0.8	448	80	–
T1W SPAIR	Transverse	4.54/1.73	320	1.5	448	90	–
T1W SPAIR	Sagittal	4.58/1.96	230	1	230	70	–

Table 1: Sequence parameters

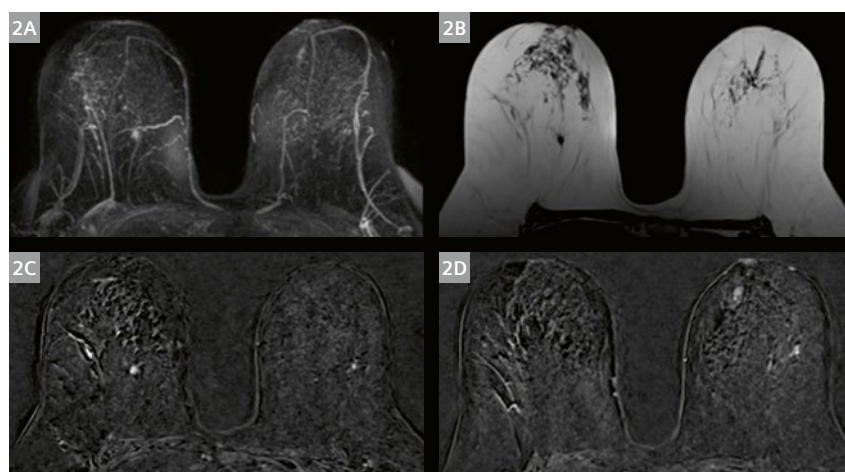
mammography (Fig. 6). However, MRI is very good at detecting even small lesions in the dense breast parenchyma and is highly sensitive for the detection of breast carcinoma (Fig. 2). MRI has multiple indications such as preoperative evaluation for staging (Fig. 1), treatment monitoring, detection of disease recurrence, screening for high-risk women (Fig. 2), assessment of breast implants, and as a problem-solving tool for indeterminate findings on

mammography and ultrasonography. MRI is also useful in the evaluation of multicentric breast cancer (Fig. 3) and bilateral breast cancer (Fig. 4). Advanced MRI techniques and various functional MRI parameters can help improve the characterization of breast cancer lesions. MR spectroscopy is helpful in cases of granulomatous mastitis, which is very common in India and typically gives indeterminate imaging findings on conventional imaging techniques

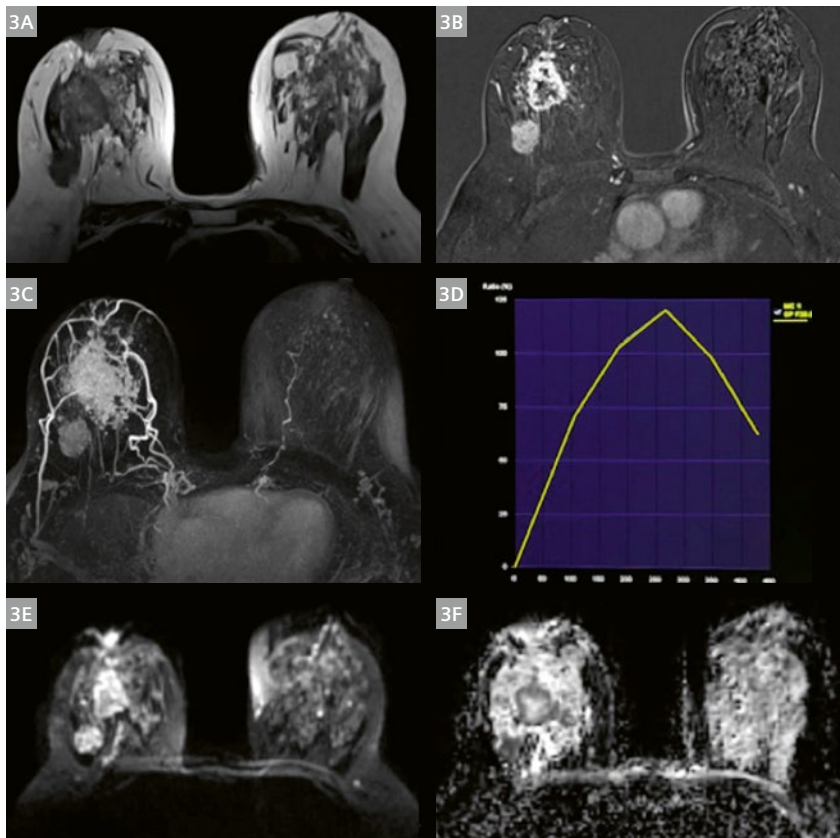


1 Invasive ductal carcinoma

(1A) Axial T2W image showing an irregular-shaped mass with irregular margins in the upper inner quadrant of the right breast. (1B) Axial T1W FS dynamic post-contrast subtracted image showing heterogeneous internal enhancement of the mass. (1C) Axial DWI (b-value 800 s/mm²) showing the mass with restricted diffusion. (1D) Corresponding ADC map of the mass characterized by low ADC. (1E) MIP of the dynamic contrast-enhanced T1W images. (1F) The mass showed a type III kinetic curve of contrast enhancement, with early uptake and early wash-out.

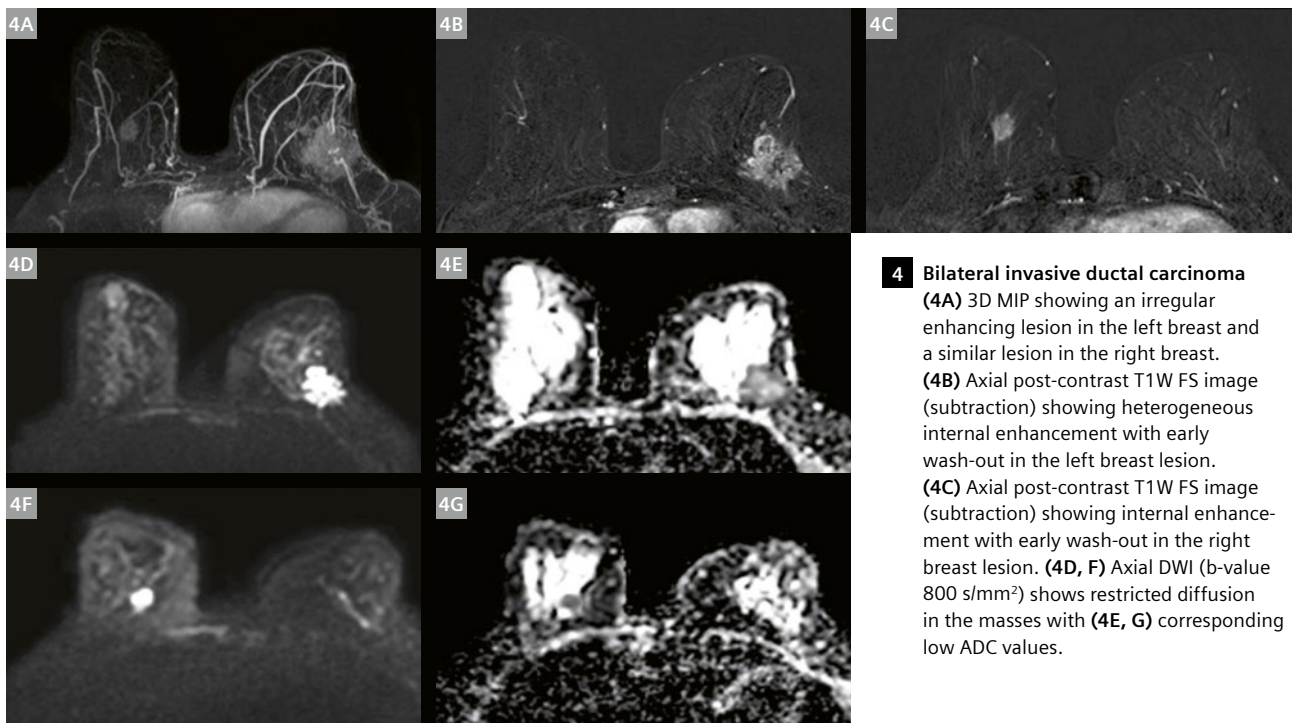


2 61-year-old woman with suspected invasive ductal carcinoma detected on screening mammography. MRI was performed to confirm and evaluate the left breast lesion, which turned out to be benign. (2A) MIP of the dynamic contrast-enhanced T1W images. (2B) Axial T2W image showing hypointense spiculated mass in the right breast. (2C) Axial T1W FS dynamic post-contrast subtracted image showing enhancing mass in the central region of the right breast. (2D) Mild type I enhancement of the lesion in the left breast, which turned out to be benign on regular follow-ups.



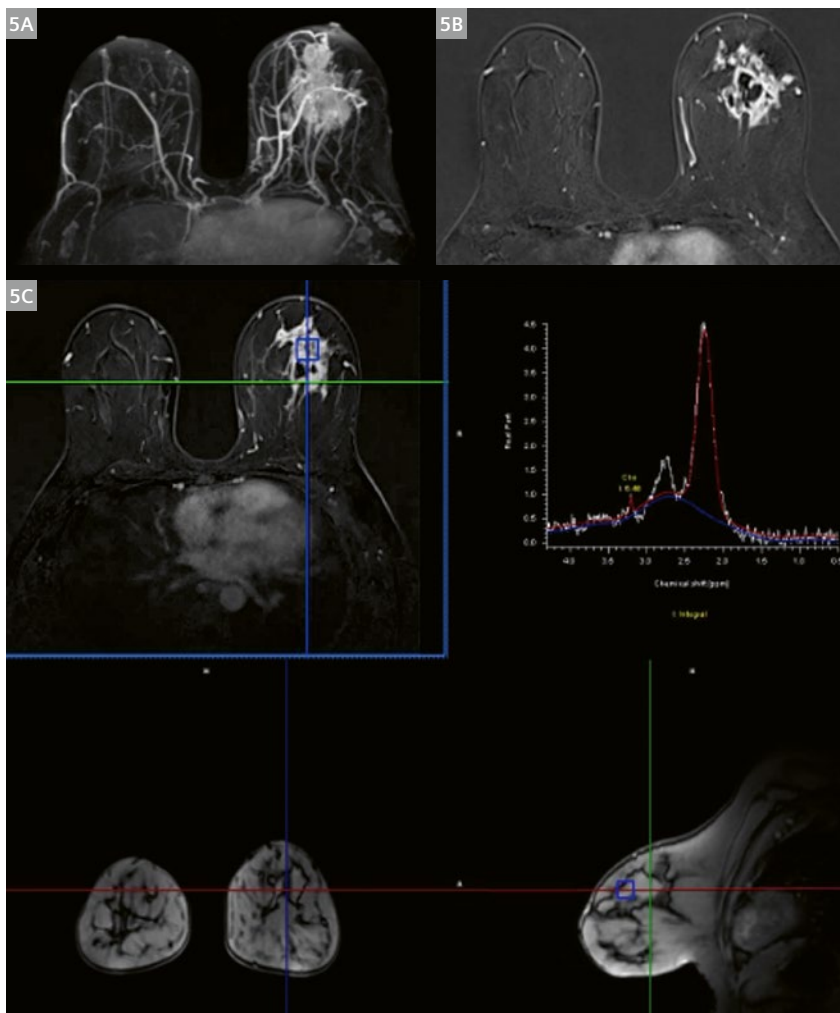
3 Multicentric breast cancer

in a 41-year-old patient. **(3A)** Axial T2W image showing two ill-defined, irregular masses in the right breast with irregular margins and architectural distortion. Nipple areolar complex was involved with retraction of the nipple. **(3B)** Axial post-contrast T1W FS image showing heterogeneous rim enhancement of the largest mass and heterogeneous internal enhancement of the other mass. Multiple small enhancing foci can be seen in the adjacent parenchyma. **(3C)** 3D MIP showing the multicentric carcinoma with intense heterogeneous enhancement with **(3D)** type III kinetic curve. **(3E)** Axial DWI showed restricted diffusion in the masses with **(3F)** corresponding low ADC values.



4 Bilateral invasive ductal carcinoma

(4A) 3D MIP showing an irregular enhancing lesion in the left breast and a similar lesion in the right breast. **(4B)** Axial post-contrast T1W FS image (subtraction) showing heterogeneous internal enhancement with early wash-out in the left breast lesion. **(4C)** Axial post-contrast T1W FS image (subtraction) showing internal enhancement with early wash-out in the right breast lesion. **(4D, F)** Axial DWI (b-value 800 s/mm²) shows restricted diffusion in the masses with **(4E, G)** corresponding low ADC values.



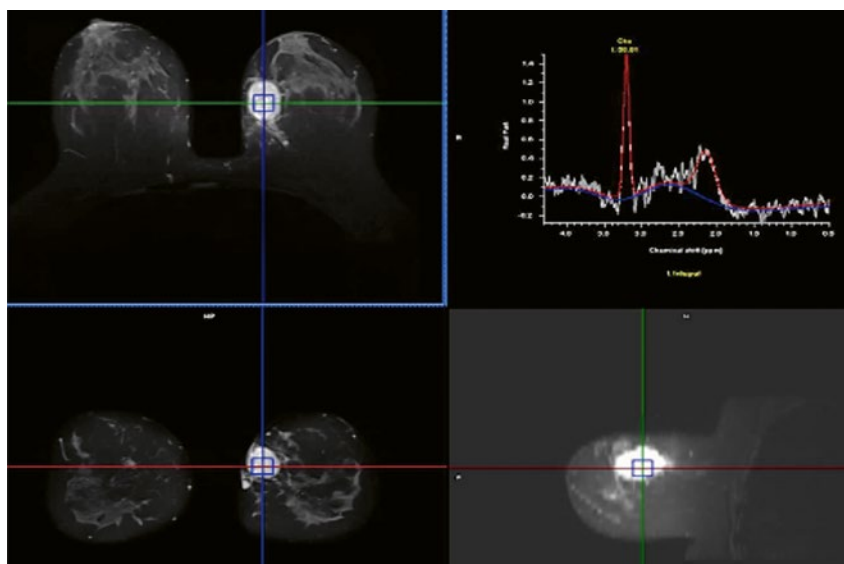
5 Granulomatous mastitis with abscess

(5A) 3D MIP showed heterogeneous diffuse enhancement. (5B) Axial T2 FS dynamic contrast image showed diffuse enhancement and an abscess with rim enhancement. (5C) MR spectroscopy showed low Choline level in the lesion.



6 Ductal carcinoma in situ

A 43-year-old woman presented with bloody nipple discharge from the right nipple. (6A) Digital breast mammogram (MLO) views. (6B) 3D MIP showed non-mass enhancement in the right breast. (6C) Axial post-contrast T1W FS image (subtraction) showing non-mass enhancement. Histopathology: invasive ductal carcinoma with DCIS.



7 MR spectroscopy

A 28-year-old patient with MRS showing a Choline peak in malignant phyllodes.

such as ultrasound or X-ray mammography (Figs. 5, 6). On MR spectroscopy, high Choline was found in most of the malignant lesions (Fig. 7), so MRS can be useful in the differentiation of benign and malignant breast lesions, but also in predicting the aggressiveness of tumors, and for monitoring response to neoadjuvant chemotherapy. MR Ductography is another non-invasive imaging technique that can be useful in the evaluation of intraductal lesions.

In India, when patients present with large masses it is very common to perform a radical mastectomy. However, in bigger cities there is now increasing awareness about breast cancer among women who prefer the option of conservative breast surgery. MRI is extremely helpful for adequate planning, management, and follow-up. As breast carcinomas are being detected in more and more young women in India, breast MRI is gaining a crucial role as it is safe, radiation-free, and very useful even in dense breast parenchyma.

Conclusion

Breast MRI is a highly sensitive examination to detect breast carcinoma. It has excellent tissue contrast with high sensitivity, however the specificity is still relatively low. To overcome the limitations in the specificity of contrast-enhanced MRI, additional functional MRI parameters such as diffusion-weighted imaging and MR spectroscopy can be used for a multiparametric evaluation of the breast. As shown in various research studies [10, 11], such a multiparametric breast MRI approach has significantly improved the diagnostic accuracy of breast MRI at our institution and has the potential to reduce unnecessary biopsies.

References

- 1 American Cancer Society. Breast Cancer Facts & Figures 2015-2016 [Internet]. Atlanta: American Cancer Society, Inc. 2015 [accessed on 6 October 2022]. Available from: <https://www.cancer.org/research/cancer-facts-statistics/breast-cancer-facts-figures.html>.
- 2 Ferlay J, Soerjomataram I, Ervik M, Dikshit R, Eser S, Mathers C, et al. Estimated Cancer Incidence, Mortality and Prevalence Worldwide in 2012. v1.0 (IARC CancerBase No. 11). [accessed on 6 October 2022]. Available from: <https://publications.iarc.fr/Databases/Iarc-Cancerbases/GLOBOCAN-2012-Estimated-Cancer-Incidence-Mortality-And-Prevalence-Worldwide-In-2012-V1.0-2012>.
- 3 Jemal A, Bray F, Center MM, Ferlay J, Ward E, Forman D. Global cancer statistics. *CA Cancer J Clin*. 2011;61(2):69–90.
- 4 Sung H, Ferlay J, Siegel RL, Laversanne M, Soerjomataram I, Jemal A, et al. Global Cancer Statistics 2020: GLOBOCAN Estimates of Incidence and Mortality Worldwide for 36 Cancers in 185 Countries. *CA Cancer J Clin*. 2021;71(3):209–249.
- 5 National Cancer Registry Programme. Three-year report of the population based Cancer Registries, 2012-2014. [Internet]: Indian Council of Medical Research, Bangalore. 2016 [accessed on 6 October 2022]. Available from: https://www.ncdirindia.org/All_Reports/PBCR_REPORT_2012_2014/ALL_CONTENT/Printed_Version.htm.
- 6 Chopra B, Kaur V, Singh K, Verma M, Singh S, Singh A. Age shift: breast cancer is occurring in younger age groups—is it true? *Clin Cancer Investig J*. 2014;3(6):526–29.
- 7 Thangjam S, Laishram RS, Debnath K. Breast carcinoma in young females below the age of 40 years: a histopathological perspective. *South Asian J Cancer*. 2014;3(2):97–100.
- 8 Mehrotra R, Yadav K. Breast cancer in India: Present scenario and the challenges ahead. *World J Clin Oncol*. 2022 Mar 24;13(3):209–218.
- 9 Boetes C, Barentsz JO, Mus RD, van der Sluis RF, van Erning LJ, Hendriks JH, et al. MR characterization of suspicious breast lesions with a gadolinium-enhanced TurboFLASH subtraction technique. *Radiology*. 1994;193(3):777–81.

- 10 Yadav P, Chauhan S. Effectivity of combined diffusion-weighted imaging and contrast-enhanced MRI in malignant and benign breast lesions. *Pol J Radiol.* 2018;83:e82–e93.
- 11 Yadav P, Harit S, Kumar D. Efficacy of high-resolution, 3-D diffusion-weighted imaging in the detection of breast cancer compared to dynamic contrast-enhanced magnetic resonance imaging. *Pol J Radiol.* 2021;86:e277–e286.

- 12 Heiberg EV, Perman WH, Herrmann VM, Janney CG. Dynamic sequential 3D gadolinium-enhanced MRI of the whole breast. *Magn Reson Imaging.* 1996;14(4):337-48.



Contact

Professor Pratiksha Yadav, M.D., Ph.D.
 Head, Interventional Radiology
 Director, Breast Imaging Fellowship, Women Imaging Fellowship
 Dr. D. Y. Patil Medical College, Hospital and Research Centre
 Pimpri
 Pune, 411018
 India
 Tel.: +9120 27805900
 yadavpratiksha@hotmail.com

Advertisement

iBreastExam™

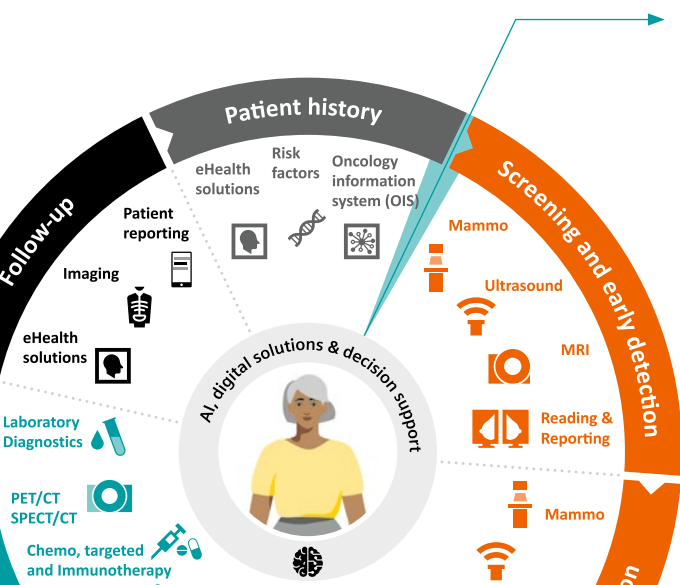
With iBreastExam™, augment and document your Clinical Breast Exams (CBEs) reliably, quickly, and painlessly.

All in your office!

iBreastExam™ has been used with more than a half million women in 12 countries.

Why iBreastExam™?

- Create a record of your CBEs in a consistent digital format
- Easily incorporate reports into EMR systems and workflows
- Potentially find hard to palpate lesions
- Reassure patients with dense breasts and those who fall outside of routine mammography guidelines
- Documentation using iBreastExam™ supports your clinical expertise and reinforces any decision to seek further diagnostic imaging
- Backed by multiple, peer-reviewed studies demonstrating sensitivity and specificity



An essential component of the 360-degree breast care portfolio

iBreastExam™ is ...

... US FDA cleared for breast lesion documentation during CBEs
 ... non-invasive, radiation-free breast examination device
 ... usable virtually anywhere and for all adult women

iBreastExam™ is NOT ...

... a screening tool for breast cancer
 ... a replacement for mammogram, Ultrasound, or MRI

For details please contact your local Siemens Healthineers sales representative or mail to
accessorysolutions@siemens-healthineers.com

High-Resolution Accelerated Prostate TSE Axial Imaging with Deep Learning Reconstruction at 3 Tesla

Edouard Reizine, M.D.¹; Wafa Boughanmi, M.D.¹; Aurélien Massire, Ph.D.²; Elisa Roccia, Ph.D.³; Dominik Nickel, Ph.D.³; Thomas Benkert, Ph.D.³; Alain Luciani, Ph.D., M.D.^{1,4,5}

¹Service d'Imagerie Médicale, AP-HP, Hôpitaux Universitaires Henri Mondor, Créteil, France

²Siemens Healthcare SAS, Saint-Denis, France

³Siemens Healthineers, Erlangen, Germany

⁴Faculté de Santé, Université Paris-Est Créteil, Créteil, France

⁵INSERM IMRB, U 955, Equipe 18, Créteil, France

Introduction

Multiparametric MRI is a crucial tool for prostate cancer detection, staging, active surveillance, and now also prior to biopsies (MRI-targeted biopsies). The guidelines for prostate imaging (PI-RADS [1]) currently recommend a protocol that consists of several MR sequences: T2-weighted (T2w), diffusion-weighted imaging (DWI), and dynamic contrast-enhanced (DCE) imaging. Notably, the T2w turbo spin echo (TSE) sequence should be acquired in the axial plane, with a slice thickness of 3 mm without gaps, and high in-plane spatial resolution. The increased demand for prostate MRI examinations observed in the past years requires to adequately respond by reducing the examination times in order to increase throughput on the one hand and to minimize the table time for the patient on the other. Indeed, this is especially problematic as prostate cancer commonly affects elderly men, who may have difficulties remaining motionless during long MRI examinations.

Deep learning reconstruction has played a key role in tackling this challenge, as it has been proven to reduce acquisition times with comparable, and often improved,

image quality and diagnostic accuracy compared to standard reconstruction techniques [2–4]. Initially Siemens Healthineers' deep learning reconstruction solution, Deep Resolve, consisted of Deep Resolve Gain and Deep Resolve Sharp.

- Deep Resolve Gain [5] mitigates thermal noise by incorporating prior knowledge of the noise characteristics into the image reconstruction, performing denoising of the data in image space. The enhanced SNR can be used to accelerate the acquisition by either increasing the acceleration factor in parallel imaging or by reducing the number of averages.
- Deep Resolve Sharp improves the image sharpness by reconstructing a high-resolution image from low-resolution data using a deep neural network. In particular it suppresses truncation artifacts in *k*-space and allows to avoid conventional *k*-space filtering. This enables to achieve image resolutions that would not be possible to achieve using conventional reconstruction.

When we first tested Deep Resolve Gain and Sharp at the Henri Mondor hospital, we were convinced by the results and decided to immediately implement it in our clinical practice. Deep Resolve is indeed now the standard of operation for prostate MR imaging at our institution.

This deep learning reconstruction technology has now gone one step further with the introduction of Deep Resolve Boost, which is even more powerful, bringing the results to a new level.

Deep Resolve Boost for TSE

Deep Resolve Boost replaces the conventional image reconstruction with a deep neural network [2]. The network architecture has similarities to an iterative image reconstruction and receives undersampled raw data as well as pre-estimated coil sensitivity maps as input. High quality images are then obtained by alternating between a parallel imaging model that relates images to acquired data and a deep learning-based regularization that enhances image quality. The main benefit of this technology is the ability to reduce the acquisition time without compromising SNR or image quality, as described in several publications [3, 6]. The outcome of the reconstruction can be further improved by combining Deep Resolve Boost with Deep Resolve Sharp.

Materials and methods

At our institution we had access to a research implementation of Deep Resolve Boost for TSE¹. All patients underwent a prostate examination in our clinical 3T MR system (MAGNETOM Vida; Siemens Healthcare, Erlangen, Germany) with XT gradients, an 18-channel body array and a 72-channel spine array. We acquired three MR sequences:

- Transverse 2D T2w TSE reconstructed with Deep Resolve Gain and Sharp
- Transverse 2D T2w TSE reconstructed with the research implementation of Deep Resolve Boost¹
- Transverse 2D diffusion single-shot EPI with 3 b-values (50, 1000, 1500 s/mm²)

The acquisition parameters of the T2-weighted sequences are shown in Table 1.

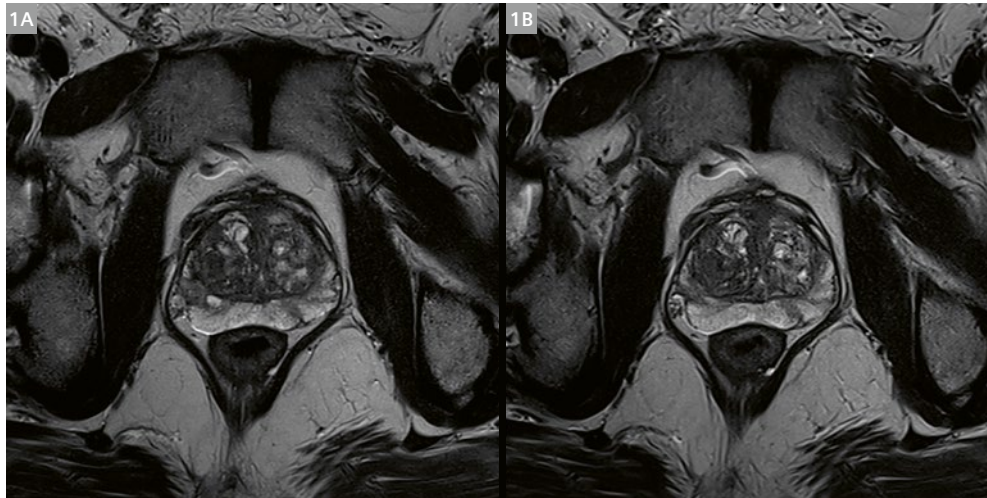
We present a series of clinical cases which show that Deep Resolve Boost for TSE provides at least similar image quality and diagnostic information as the more time-intensive Deep Resolve Gain and Sharp TSE acquisition, which is now the clinical standard at our institution.

¹With software version syngo MR XA50 Deep Resolve Boost is available for MAGNETOM Vida.

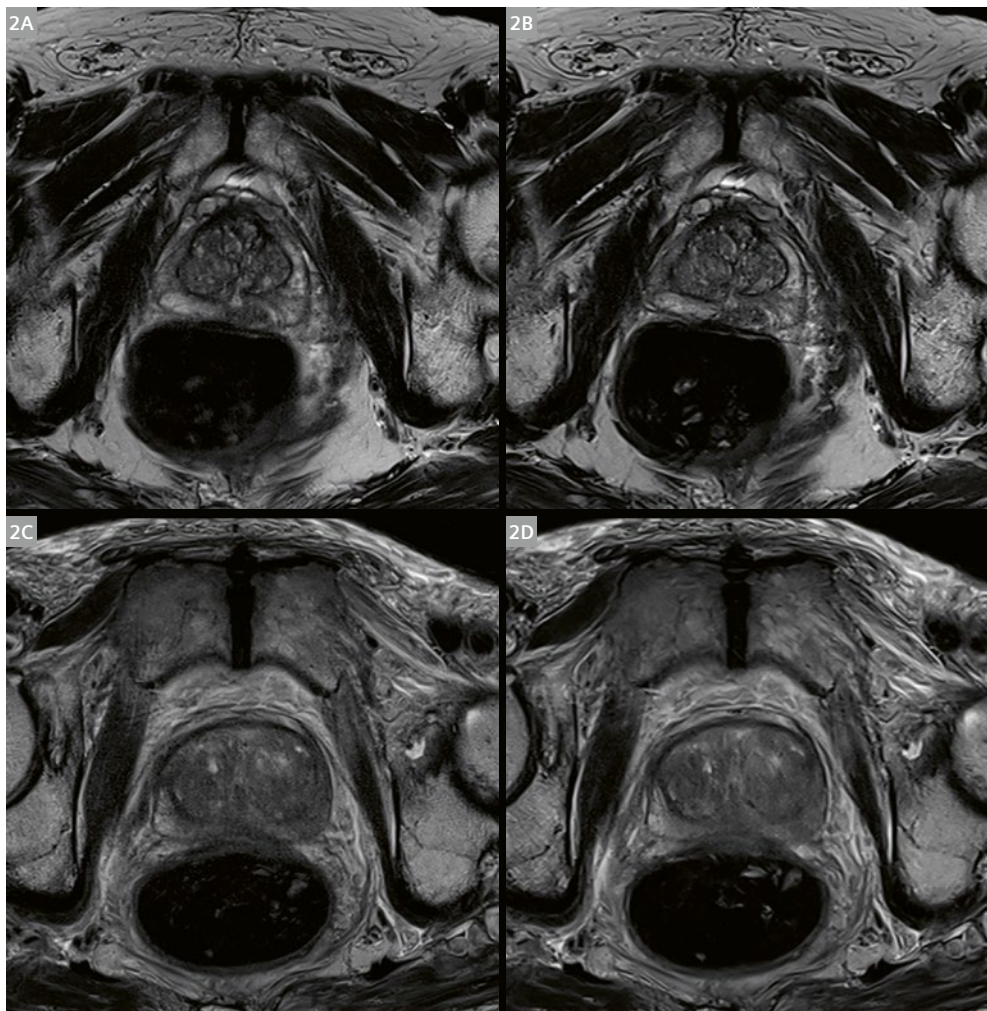
	Deep Resolve Gain and Sharp TSE	Deep Resolve Boost TSE
Scan time (min:s)	3:16	1:50
FOV (mm ²) / phase oversampling	160 × 160 / 145%	180 × 180 / 200%
TE (ms)	116	104
TR (ms)	3380	3850
Reconstructed voxel size (mm ³)	0.26 × 0.26 × 3	0.24 × 0.24 × 3
Nb excitations	2	1
Matrix size	304 × 304 × 26	368 × 368 × 26
Acceleration technique	GRAPPA 2 (Auto -32)	GRAPPA 3 (TSE/Sep -24)
Flip angle (°)	133	160
Turbo factor	23	25
Phase resolution (%)	85	85
Bandwidth (Hz/Px)	201	200
Nb concatenations	2	2

Table 1: Acquisition parameters of the T2-weighted sequences.

Cases



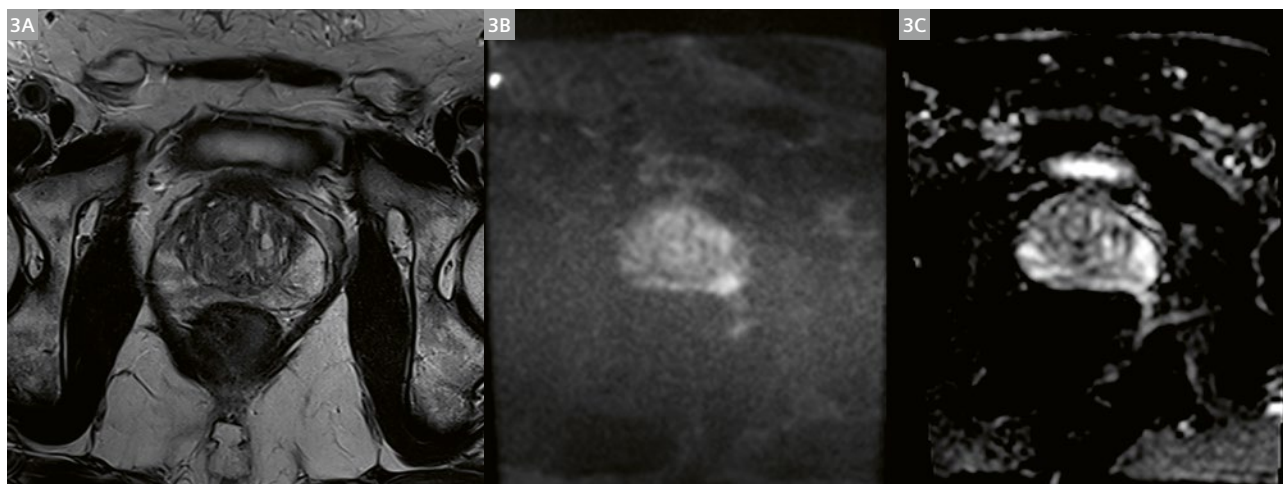
- 1** A 72-year-old patient (Density PSA = 0.09 ng/ml²) with bilateral PI-RADS 2 lesions in the middle peripheral zones of the prostate. T2-weighted TSE using **(1A)** Deep Resolve Gain and Sharp and **(1B)** Deep Resolve Boost. Deep Resolve Boost provides comparable image quality with a 41% scan time reduction.



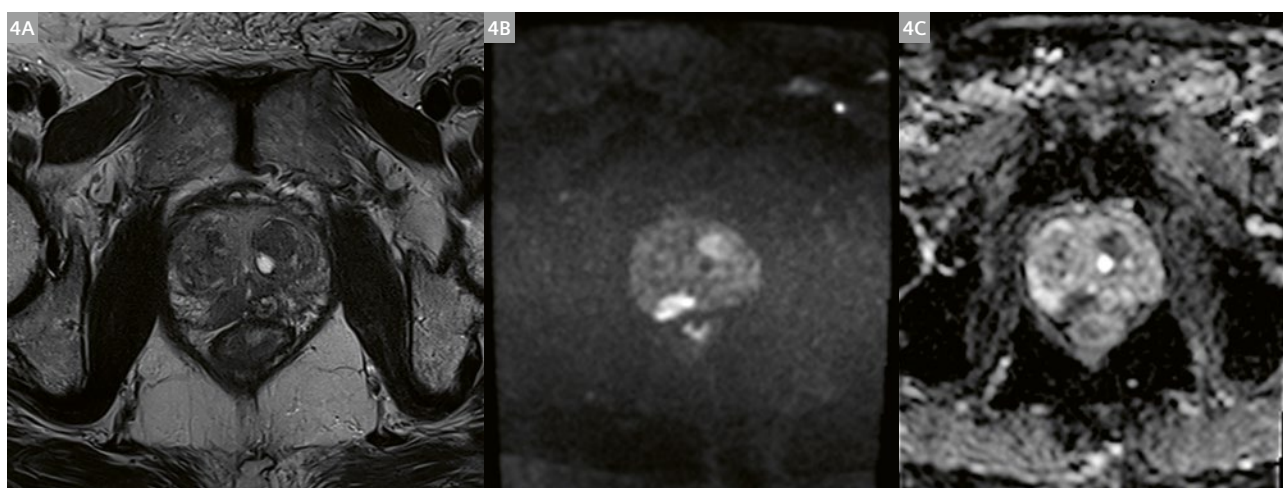
- 2** A 77-year-old patient (PSA = 1.7 ng/ml; density PSA = 0.05 ng/ml²) with bilateral PI-RADS 2 lesions in the middle peripheral zones of the prostate. T2-weighted TSE using **(2A)** Deep Resolve Gain and Sharp and **(2B)** Deep Resolve Boost.

An 83-year-old patient (PSA = 14.8 ng/ml; density PSA = 0.29 ng/ml²) with a PI-RADS 4 lesion in the right postero-medial middle peripheral zone of the prostate. T2-weighted TSE using **(2C)** Deep Resolve Gain and Sharp and **(2D)** Deep Resolve Boost.

For both patients, motion artefacts in the Deep Resolve Boost images are reduced thanks to the shorter acquisition time (1 average), allowing sharper delineation of the anatomical structures.



3 A 59-year-old patient (PSA: 4.2 ng/mL; density PSA = 0.10 ng/mL²) with bilateral PI-RADS 2 lesions in the middle peripheral zones of the prostate. T2-weighted TSE using **(3A)** Deep Resolve Boost. **(3B)** Trace DWI image with b-value 1500 s/mm², **(3C)** ADC map.



4 A 81-year-old patient (PSA: 12 ng/mL; density PSA = 0.33 ng/mL²) with a PI-RADS 5 lesion in the right posteromedial apical peripheral zone of the prostate. T2-weighted TSE using **(4A)** Deep Resolve Boost. **(4B)** Trace DWI image with b-value 1500 s/mm², **(4C)** ADC map.

Conclusion

Compared to Deep Resolve Gain and Sharp, Deep Resolve Boost allowed us to decrease the acquisition time of the T2w TSE acquisition by 41% (Fig. 1), as only 1 average was acquired compared to the 2 averages of the Deep Resolve Gain and Sharp scan, with comparable image quality. One of the benefits of the shorter acquisition time was the reduction of artefacts due to either voluntary or involuntary patient motion (Fig. 2), which is one of the challenges of prostate imaging. No evident artefacts were observed. There is an increasing body of evidence from clinical studies and scientific publications that these physics-guided deep learning reconstruction approaches

provide reliable and robust image information with anatomical fidelity.

These results are also in line with the published literature, which has reported significant time savings, as well as comparable image quality and diagnostic confidence for staging prostate lesions when compared to conventional acquisitions [2–4, 7].

The adoption of Deep Resolve in our clinical workflow has helped us to match the increased demand of prostate MRI examinations at our institution and we are confident that further improvements in acquisition time and spatial resolution can be achieved.

References

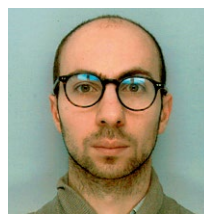
- Weinreb JC, Barentsz JO, Choyke PL, Dornud F, Haider MA, Macura KJ, et al. PI-RADS Prostate Imaging – Reporting and Data System: 2015, Version 2. Eur. Urol. 2016; 69, 16–40.
- Gassenmaier S, Afat S, Nickel D, Mostapha M, Herrmann J, Othman AE. Deep learning-accelerated T2-weighted imaging of the prostate: Reduction of acquisition time and improvement of image quality. Eur J Radiol. 2021;137:109600.
- Gassenmaier S, Afat S, Nickel MD, Mostapha M, Herrmann J, Almansour H, Nikolaou K, Othman AE. Accelerated T2-Weighted TSE Imaging of the Prostate Using Deep Learning Image Reconstruction: A Prospective Comparison with Standard T2-Weighted TSE Imaging. Cancers (Basel). 2021;13(14):3593.
- Kim EH, Choi MH, Lee YJ, Han D, Mostapha M, Nickel D. Deep learning-accelerated T2-weighted imaging of the prostate: Impact of further acceleration with lower spatial resolution on image quality. Eur J Radiol. 2021;145:110012.
- Dehem J, Kannengießer S, Hoelscher UC. Initial Clinical Experience with an Iterative Denoising Algorithm Applied to Reduced-data 2D Turbo Spin Echo Acquisitions. *MAGNETOM Flash*. 2021;(78)2:22-28.
- Herrmann J, Gassenmaier S, Nickel D, Arberet S, Afat S, Lingg A, et al. Diagnostic Confidence and Feasibility of a Deep Learning Accelerated HASTE Sequence of the Abdomen in a Single Breath-Hold. Invest Radiol. 2021;56(5):313–319.
- Johnson PM, Tong A, Donthireddy A, Melamud K, Petrocelli R, Smereka P, Qian K, Keerthivasan MB, Chandarana H, Knoll F. Deep Learning Reconstruction Enables Highly Accelerated Biparametric MR Imaging of the Prostate. J Magn Reson Imaging. 2022;56(1):184-195.

Contact

Professor Alain Luciani, Ph.D., M.D.
 HU Henri Mondor
 Medical Imaging Department
 APHP, UPEC University
 51 Avenue Mal De Lattre De Tassigny
 94000 Créteil
 France
 alain.luciani@aphp.fr



Alain Luciani, Ph.D., M.D.



Edouard Reizine, M.D.



Wafa Boughanmi, M.D.

Advertisement

PI-RADS 2.1 Standardized Prostate MRI Reporting

David Jean Winkel, M.D. and
 Hanns-Christian Breit, M.D.

University Hospital Basel,
 Switzerland



PI-RADS 2.1 Standardized Prostate MRI Reporting

Peripheral Zone (PZ) Transition Zone (TZ)

Score

1 2 3 4 5

Contrast-enhanced MRI

Prostate Volume Measurement

Decision tree for final PI-RADS score

Overall PI-RADS score

SIEMENS Healthineers

Get your free copy of the PI-RADS poster at
www.magnetomworld.siemens-healthineers.com/publications/subscriptions/mri-poster

Improving Patients' Experience of MRI: Why and How Reducing Stress and Anxiety in Patients May Enhance Clinical Operations

Janika Madl^{1,2}; Susanne Bay²; Rolf Janka³

¹Chair of Health Psychology, Friedrich-Alexander-Universität Erlangen-Nürnberg, Erlangen, Germany

²Siemens Healthineers, Erlangen, Germany

³Department of Radiology, Universitätsklinikum Erlangen, Germany

Introduction

Magnetic resonance imaging (MRI) is non-invasive and painless, with excellent spatial resolution and soft-tissue contrast. These numerous benefits have rendered MRI one of the most important diagnostic tools in modern medicine. In Germany, 150 MRI examinations are performed per 1,000 inhabitants every year [1]. Yet, MRI also has substantial drawbacks: Most MRI protocols are time-consuming and very dependent on the patient's cooperation and ability to lie motionless. One of the main roots for disruptions to MRI workflows is stress and anxiety in patients, who often experience MRI as uncomfortable and frightening [2, 3]. Beyond creating a negative patient experience, feelings of anxiety and stress may relate to unexpected patient-related events such as motion artifacts, the need for sedation, or failed scans; these events result in a substantial amount of revenue lost [4–6]: Andre et al. [4] calculated that US\$ 115,000 are lost per scanner every year due to unexpected patient behavior.

The aim of this article is to provide a holistic picture of patients' experience of MRI, related unexpected behaviors and consequences, and approaches to improve the situation for all concerned: patients, healthcare staff, and the medical institutions. The focus is to provide insights into the "Patient Experience (PX) in MRI" collaboration project between Siemens Healthineers, the Chair of Health Psychology (FAU Erlangen-Nürnberg), and Universitätsklinikum Erlangen, Department of Radiology. During this collaboration project, two empirical studies and one systematic review with meta-analysis were conducted and will be presented in the following.

Take-home points

- Although most patients tolerate MRI well, a substantial number of patients experience clinically relevant levels of anxiety; related unexpected patient behaviors disturb clinical workflows and impede efficiency of healthcare providers.
- Patients' response to MRI depends on many different factors; previous negative experiences with MRI and female sex seem to be particularly predictive of a negative patient experience.
- In order to address individual patients' needs, different materials for patient preparation should be offered: Not only informational material, but also measures to support active modulation of anxiety, e.g., relaxation exercises.
- Patients who experience high levels of stress or anxiety tend to lie less still, which may provoke motion artifacts and the need for scan repetitions, thereby prolonging procedural times. Therefore, reducing stress and anxiety in patients might not only improve the patient experience, but also lead to clinical workflows running more smoothly.

Patients' experience of MRI: An introduction

How patients experience MRI has been a topic of interest since the very beginnings of MRI. In the course of MRI paving its way from the 1980s on, it soon became apparent that many patients fear this medical "coffin" [7]; Figures 1A and 1B show that, indeed, early MRIs resembled "mechanical monster[s]" [7]. Since then, many technological advancements have made MRI more patient-friendly: Recent MRI machines produce less noise, are equipped with shorter, wider bores that are open at both ends, and acquire images much quicker, thereby reducing scan duration [8, 9]. Some studies report that these advancements have resulted in reduced levels of stress and anxiety, as well as related operational issues [6, 10, 11]. Yet, others find that – although most patients tolerate MRI well – stress and anxiety are still widespread phenomena reaching levels that are considered clinically relevant in around 30% of patients [12, 13]. Two questions arise from these findings:

- 1) What factors differentiate patients who fear MRI from the rest?
- 2) To what extent have technical advancements brought about improvements regarding the patient experience of MRI examinations and related behaviors?

Adequate patient preparation seems to be most decisive in preventing a negative patient experience and fostering smooth clinical workflows

In our "baseline" study, our aim was to analyze patients' response to MRI in detail including influencing factors and consequences [12]. We thereby considered patients' psychological response (i.e., anxiety), the physiological response (i.e., salivary stress markers), and operational effects on clinical processes (i.e., scan repetitions due to motion artifacts, scan duration).

The study was conducted in the department of radiology of Universitätsklinikum Erlangen. We examined anxiety and physiological stress markers in 96 patients undergoing MRI ($M = 49$ years, 61.5% female). Anxiety was assessed via questionnaires before and after MRI; at the same time-points, we took saliva samples to measure salivary stress markers (cortisol, alpha-amylase).

In general, most patients tolerated MRI well. Yet, every third patient experienced moderate to severe levels of anxiety in anticipation of the examination and experienced relief only after having endured the examination. As suggested by Ahlander et al. [14], this implies that efforts to improve the patient experience might be most effective



1 (1A, B) While the first MAGNETOM MRI scanner from 1983 [41] might have been a scary sight, only a few years later product development focused also on patient comfort. (1C) In 1993, Siemens introduced the 0.2T MAGNETOM Open. (1D, E) In 1996 the product line around MAGNETOM Symphony featured a flared bore. (1F) In 2004 MAGNETOM Espree was the world's first 1.5-tesla system with a 70-centimeter opening. (1G) Today a relaxing atmosphere, noise reduction and fast sequences make MRI easier to tolerate.

when applied in advance. Materials for patient preparation can only reduce anticipatory anxiety when given with sufficient lead time, ideally a few days/weeks before the examination.

We examined a broad range of potentially influencing factors (sex, age, positioning, accompanying persons, pain, previous experiences, examined body part) and found them to interact with patients' response in a complex way. Women receiving breast examinations had a particularly high risk of anxiety. This is in line with previous studies that reported a more negative response to MRI in women vs. men [6, 12, 15]. Further, we found that negative experiences made during previous MRI examinations significantly predicted a negative experience during the current examination. That means that patients who once have a negative MRI experience tend to keep on having bad experiences. When integrating our results on the impact of age and positioning with other studies, the state of research appears to be less clear [6, 12, 16–18]. Most certainly, it can be deduced that patients differ considerably regarding their response to MRI and their needs, which is why they also require different approaches to address these needs.

Furthermore, we found evidence of a link between patients' experience and clinical workflows: Patients' response to MRI predicted the probability of scan repetitions and scan duration [12], thereby supporting previous results that reported a connection between the patient experience and the prevalence of unexpected patient-related events [5, 19–22]. For example, an increase of 1 nmol/L in the stress marker salivary cortisol predicted a prolongation of the scan duration of more than 4 minutes [12].

Apart from individual factors that influence patients' experience of MRI, technological advancements have been proposed that aim to have a positive impact on stress and anxiety as well as related behavioral issues in patients. Yet, until now, no systematic review has summarized the patient experience of MRI, related unexpected patient behaviors, and their evolution along with technological advancements holistically. We sought to overcome this research gap in a systematic review with a meta-analysis that we conducted on patients' response to MRI, its effects (i.e., unexpected patient behaviors related to stress and anxiety), and their evolution over time [20].

Evolution of patients' experience of MRI and related unexpected patient behaviors over time: A systematic review and meta-analysis

We searched four databases and screened more than 12,000 studies. Meta-analysis of 44 studies revealed that, despite the common understanding of patient anxiety, there have been no significant improvements over time in the amount of anxiety experienced: Average values of reported anxiety were close to the cut-off considered

as clinically relevant and around 4% of patients reported to be unwilling to undergo further MRI examinations. Similarly, the rates of unexpected patient-related events such as no-shows, failed scans, motion artifacts, and sedation, have not significantly reduced over time. While these findings could be traced back to statistical issues or the fact that we had to use the year of study publication as an indicator of MRI technology as more exact data on scanner technology was unavailable for most studies, it might as well reflect the fact that patients still experience substantial stress and anxiety in the context of MRI. An additional interesting finding was that claustrophobia significantly moderated the overall number of unexpected patient events. The rates of unexpected behaviors such as no-shows, motion artifacts, failed scans, and sedation were higher in patient groups with higher levels of claustrophobia. This supports the notion of a link between the patient experience and clinical workflows as has been postulated previously [5, 19, 21, 22].

Based on the results of the baseline study and meta-analysis, it can be concluded that stress and anxiety in patients have always been and still are a relevant topic in the context of MRI. In short, technological advancements of the MRI scanners alone might not be sufficient to improve the patient experience of MRI or related unexpected events – at least until now. There seems to be a need for interventions that target patients' needs more explicitly. The evidence generally suggests that MRI-related patient anxiety and related effects can be prevented when we enrich standard care and properly address patients' needs.

How patient's experience of MRI can be improved: An overview

A wide variety of interventions to improve patients' experience of MRI has been developed and tested in the past. Approaches range from easy-to-implement measures to very elaborate and complex ones: From the supply of music or having someone accompany the patient, to variations in patient positioning or the environment, mock MRI, aromatherapy, amended patient information, distraction via VR, hypnosis and other relaxation strategies, to communication training for the medical personnel.

Many of these approaches have been proven to be effective (see Munn et al. [17] for an overview), but this article will focus on interventions specifically targeted at patient preparation.

Two major types of interventions for patient preparation can be distinguished:

- The aim of informational interventions is to reduce ambiguity and feelings of uncertainty that may constitute a stressor for patients [2, 23, 24]. Although

many studies report beneficial effects of additional information, others find even negative effects when information is provided exclusively [17].

- A different approach aims at enhancing a patient's ability to cope with the stressful situation more successfully, e.g., via relaxation techniques [25, 26]. Although consistently positive, the effect sizes of these interventions vary considerably [17].

The majority of the literature points toward substantial benefits of interventions to improve the MRI patient experience; yet, some questions remain unresolved: Why do some studies report positive effects of informational interventions but others don't? Where do the considerable variations in the reported effect sizes of coping interventions trace back to? And is there a link between patient experience and clinical processes?

Patient preparation should cover different needs of patients

In order to address these questions and help to enhance the patient experience of MRI, we developed a patient

education toolkit (see Fig. 2) in collaboration with Siemens Healthineers MR marketing and tested it in clinical trial. We based our approach on the assumptions of the "Model of Coping Modes" [27, 28], which may contribute to explaining the inconsistencies described above. The model describes different ways of coping with stress-inducing situations that people tend to employ habitually. The model proposes vigilance and cognitive avoidance as two basic dimensions of how attention shifts when facing stressful situations. While cognitive avoidance means the tendency to divert attention from threatening cues to reduce the bodily arousal induced by these, vigilance refers to the opposite: An increased focus on threatening cues to enhance knowledge about the situation and reduce feelings of uncertainty [25, 27]. Figure 3 depicts the four coping styles that can be differentiated on the basis of these two dimensions. According to this scheme, it can be expected that sensitizers benefit from receiving additional information: It should enable them to reduce feelings of uncertainty successfully. By contrast, repressors should benefit from distraction and relaxation, which supports distracting attention away from the threatening cues that induce arousal.



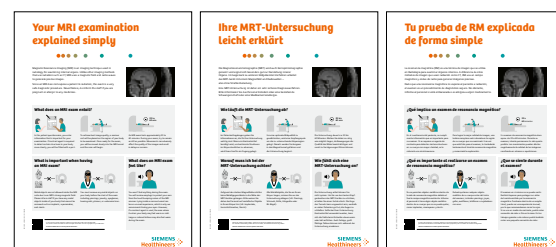
MRI Patient Education Toolkit

www.magnetomworld.siemens-healthineers.com/toolkit/mri-patient-education

Patient Education Video



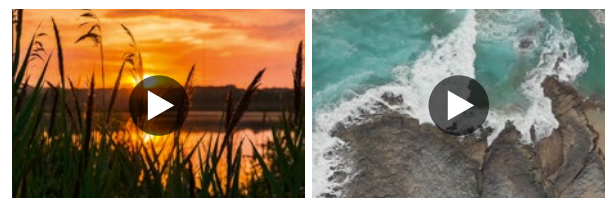
Patient Education Poster



Children's Book and Movie



Patient Meditation



2 QR code for access to the Patient Education Toolkit including the two patient preparation videos and the MRI book for children.

Patient preparation that matches the coping style (“congruent preparation”) has been shown to improve patient-related outcomes such as pain, anxiety, and adaptation in other medical fields like surgery [29, 30], cardiac catheterization [31], cancer survivorship care [32], or colonoscopy [33]. We therefore hypothesized the same pattern to apply to MRI patients: We expected the psychological and physiological response of patients to improve when they received an intervention congruent with their coping style vs. when they received incongruent preparation or no additional preparation (i.e., standard care control group).

We tested this assumption in a study with a randomized controlled design with 142 patients. While sitting in the waiting room, the patients randomly watched one of two videos developed to address the needs of sensitizers (information video) or repressors (relaxation video) or received standard care (no video). Both videos can be accessed via the QR code presented in Figure 2. We assessed the patients’ psychological and physiological responses to the examination, their evaluation of the videos, and recorded procedural outcomes (scan duration, repeated scans, interruptions). Anxiety was assessed via questionnaires on arrival at the hospital, after watching the video (or after a comparable amount of time in the control group), and after MRI. Cortisol as a physiological stress marker was assessed on arrival and after the MRI scan.

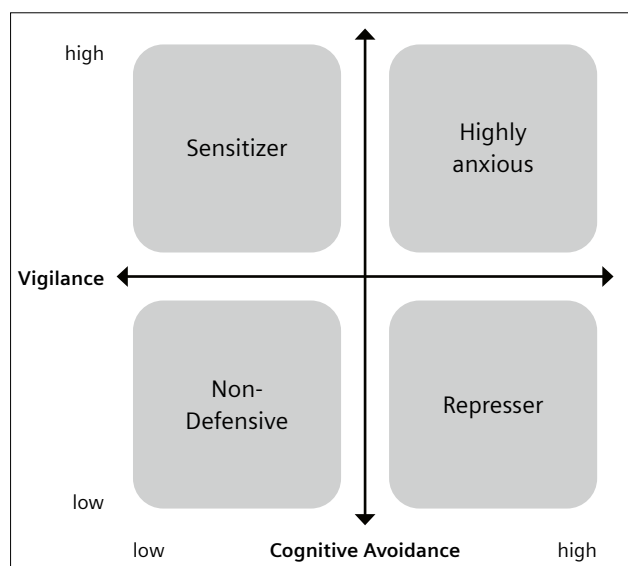
We found that cortisol levels were elevated compared with a “normal” day, which meant that undergoing MRI induced physiological stress in patients [34]. As cortisol still followed its normal circadian rhythm, we concluded that

this elevation most likely reflected anticipatory effects, which is in line with our findings from the baseline study [12]. The videos were very well received by the patients [35]: Almost all reported that they found them helpful and that they increased their confidence regarding the examination; whereby the information video was evaluated even more positively. When the patients’ preparation matched their coping style, anxiety decreased even before MRI, whereas this relief was only observed after the examination in patients whose preparation did not fit their needs. Beyond the positive effects at the patient level, we also found scan duration to be 10–20% shorter in the interventional groups and, descriptively, rates of scan repetitions or interruptions were 30–50% lower. Although our hypotheses were supported on a descriptive level, results failed to reach statistical significance. We believe that this is most likely due to power issues but there has, as yet, been no statistical confirmation of the effects on clinical processes and results must be interpreted with caution.

Improving patients’ experience of MRI by addressing individual needs in advance can reduce stress and anxiety in patients and support smooth clinical workflows

Anxiety and stress in patients have always been and still are relevant phenomena in the context of MRI examinations. Based on the results of our studies [12, 34, 35] and the consideration of Ahlander et al. [14], we suggest that patients’ response to MRI is most negative in anticipation of the examination. Therefore, changing the way patients are prepared for MRI seems to be a crucial step for improving MRI-related healthcare. Enriching standard care with additional patient preparation can have a positive impact on patients’ experience of MRI. Our research suggests that patients vary greatly regarding their needs. Therefore, considering interindividual differences in patients’ needs may be a promising approach to reduce stress and anxiety in patients most effectively. We therefore suggest that medical institutions should start providing tailored medicine, also in respect to the patient experience. This may be achieved by providing a variety of different materials for patients to choose from – or amendments of standard care, when thinking more generally. Thereby, it seems to be crucial to reach out to patients in advance: Providing patients with the opportunity to prepare themselves according to their own needs in a calm environment has the potential to maximize the beneficial effects.

Apart from being a relevant end in itself, we found in line with previous research that improving the patient experience could also have beneficial effects on clinical



3 The Model of Coping Modes (based on Krohne [42]).

workflows [5, 12, 17, 19, 21, 35–37]. Research suggests that patients who are calmer are less likely to be no-shows, have a lower need for sedation, premature terminations are less likely to happen, and patients move less, which could result in less need for scan repetitions and therefore shorter scan duration times [17, 19, 21, 36–40]. These effects might be even more pronounced when considering that time for patient education and preparation could also be reduced if patients were to arrive in an enhanced state of preparation. We therefore propose that improving the patient experience could result in positive effects for all stakeholders: Patients will be more relaxed, which also reduces stress for the medical personnel; furthermore, workflows will run more smoothly, thereby also increasing the revenue of an institution.

References

- OECD. Magnetic resonance imaging (MRI) exams 2021.
- Carlsson S, Carlsson E. 'The situation and the uncertainty about the coming result scared me but interaction with the radiographers helped me through': a qualitative study on patients' experiences of magnetic resonance imaging examinations. *J Clin Nurs* 2013;22:3225–3234.
- Törnqvist E, Månsson A, Larsson E-M, Hallström I. It's like being in another world – patients' lived experience of magnetic resonance imaging. *J Clin Nurs* 2006;15:954–961.
- Andre JB, Bresnahan BW, Mossa-Basha M, Hoff MN, Smith CP, Anzai Y, et al. Toward quantifying the prevalence, severity, and cost associated with patient motion during clinical MR examinations. *J Am Coll Radiol* 2015;12:689–695.
- Dantendorfer K, Amering M, Bankier A, Helbich T, Prayer D, Youssefzadeh S, et al. A study of the effects of patient anxiety, perceptions and equipment on motion artifacts in magnetic resonance imaging. *Magn Reson Imaging* 1997;15:301–306.
- Dewey M, Schink T, Dewey CF. Claustrophobia during magnetic resonance imaging: Cohort study in over 55,000 patients. *J Magn Reson Imaging* 2007;26:1322–1327.
- Notini E. Panic. *JAMA J Am Med Assoc* 1988;259:897.
- Brunnquell CL, Hoff MN, Balu N, Nguyen XV, Oztek MA, Haynor DR. Making magnets more attractive: Physics and engineering contributions to patient comfort in MRI. *Top Magn Reson Imaging* 2020;29:167–174.
- Rinck PA. Magnetic resonance in medicine: A critical introduction. 12th ed. 2018.
- Enders J, Zimmermann E, Rief M, Martus P, Klingebiel R, Asbach P, et al. Reduction of claustrophobia with short-bore versus open magnetic resonance imaging: A randomized controlled trial. *PLoS ONE* 2011;6:e23494.
- Michel SC, Rake A, Götzmann L, Seifert B, Ferrazzini M, Chaoui R, et al. Pelvimetry and patient acceptability compared between open 0.5-T and closed 1.5-T MR systems. *Eur Radiol* 2002;12:2898–2905.
- Madl J, Janka R, Bay S, Rohleder N. MRI as a stressor: The psychological and physiological response of patients to MRI, influencing factors, and consequences. *J Am Coll Radiol* 2022;19:423–432.
- Sadigh G, Applegate KE, Saindane AM. Prevalence of unanticipated events associated with MRI examinations: A benchmark for MRI quality, safety, and patient experience. *J Am Coll Radiol* 2017;14:765–772.
- Ahlender B-M, Engvall J, Maret E, Ericsson E. Positive effect on patient experience of video information given prior to cardiovascular magnetic resonance imaging: A clinical trial. *J Clin Nurs* 2018;27:1250–1261.
- Harris LM, Menzies RG, Robinson J. Predictors of panic symptoms during magnetic resonance imaging scans. *Int J Behav Med* 2001;8:80–87.
- Eshed I, Althoff CE, Hamm B, Hermann K-GA. Claustrophobia and premature termination of magnetic resonance imaging examinations. *J Magn Reson Imaging* 2007;26:401–404.
- Munn Z, Jordan Z. Interventions to reduce anxiety, distress and the need for sedation in adult patients undergoing magnetic resonance imaging: a systematic review. *Int J Evid Based Healthc* 2013;11:265–274.
- Tazegul G, Etcioğlu E, Yildiz F, Tuney D. Can MRI related patient anxiety be prevented? *Magn Reson Imaging* 2014;33:180–183.
- Ladapo JA, Spritzer CE, Nguyen XV, Pool J, Lang E. Economics of MRI Operations After Implementation of Interpersonal Skills Training. *J Am Coll Radiol* 2018;15:1775–1783.
- Madl JEM, Nieto Alvarez I, Amft O, Rohleder N, Becker L. The psychological, physiological, and behavioral responses of patients to magnetic resonance imaging (MRI): A systematic review and meta-analysis. Under Revision.
- Powell R, Ahmad M, Gilbert FJ, Brian D, Johnston M. Improving magnetic resonance imaging (MRI) examinations: Development and evaluation of an intervention to reduce movement in scanners and facilitate scan completion. *Br J Health Psychol* 2015;20:449–465.
- Thompson MB, Coppens NM. The effects of guided imagery on anxiety levels and movement of clients undergoing magnetic resonance imaging: *Holist Nurs Pract* 1994;8:59–69.
- Krohne HW. Stress und Stressbewältigung bei Operationen. 1. Auflage. Berlin Heidelberg: Springer; 2017.
- Mackenzie R, Sims C, Owens RG, Dixon AK. Patients' perceptions of magnetic resonance imaging. *Clin Radiol* 1995;50:137–143.
- Krohne, de Bruin JT. Stress bei medizinischen Eingriffen: Kritischer Überblick über verschiedene Interventionsansätze. *Z Für Med Psychol* 1998;7:3–39.
- Miller SM, Combs C, Stoddard E. Information, coping and control in patients undergoing surgery and stressful medical procedures. In: Steptoe A, Appels A, editors. *Stress Pers. Control Health*, Chichester, UK: Wiley; 1989, p. 107–130.
- Krohne HW. Vigilance and cognitive avoidance as concepts in coping research. In: Krohne HW, editor. *Atten. Avoid. Strateg. Coping Aversiveness*, Seattle: Hogrefe & Huber; 1993, p. 19–50.
- Krohne HW. Individual differences in emotional reactions and coping. In: Davidson RJ, Goldsmith HH, Scherer KR, editors. *Handb. Affect. Sci.*, New York: Oxford University Press; 2003, p. 698–725.
- Krohne HW, El-Giamal M. Psychologische Operationsvorbereitung, Stressbewältigung und perioperativer Status. *Z Für Gesundheitspsychologie* 2008;16:183–195.
- Martelli MF, Auerbach SM, Alexander J, Mercuri LG. Stress management in the health care setting: Matching interventions with patient coping styles. *J Consult Clin Psychol* 1987;55:201–207.
- Ludwick-Rosenthal R, Neufeld RWJ. Preparation for undergoing an invasive medical procedure: Interacting effects of information and coping style. *J Consult Clin Psychol* 1993;61:156–164.

- 32 de Rooij BH, Ezendam NPM, Vos MC, Pijnenborg JMA, Boll D, Kruitwagen RFPM, et al. Patients' information coping styles influence the benefit of a survivorship care plan in the ROGY Care Trial: New insights for tailored delivery. *Cancer* 2019;125:788–797.
- 33 Morgan J, Roufeil L, Kaushik S, Bassett M. Influence of coping style and precolonoscopy information on pain and anxiety of colonoscopy. *Gastrointest Endosc* 1998;48:119–127.
- 34 Madl JEM, Sturmbauer SC, Janka R, Bay S, Rohleder N. Preparing patients according to their individual coping style improves patient experience of magnetic resonance imaging. *J Behav Med* 2022. <https://doi.org/10.1007/s10865-022-00361-y>.
- 35 Madl JEM, Janka R, Bay S, Sturmbauer S, Rohleder N. Effects of video-based patient preparation for MRI on clinical processes and patient experience. Under Revision.
- 36 Ali SH, Modic ME, Mahmoud SY, Jones SE. Reducing clinical MRI motion degradation using a prescan patient information pamphlet. *Am J Roentgenol* 2013;200:630–634.
- 37 Norbash A, Yucel K, Yuh W, Doros G, Ajam A, Lang E, et al. Effect of team training on improving MRI study completion rates and no-show rates: Improving MRI Study Completion Rates. *J Magn Reson Imaging* 2016;44:1040–1047.
- 38 Andre JB, Johansson K. Relaxed patients, reduced motion, improved productivity. *FieldStrength* 2016;1:11–15.
- 39 Lang EV, Ward C, Laser E. Effect of team training on patients' ability to complete MRI examinations. *Acad Radiol* 2010;17:18–23.
- 40 Törnqvist E, Månsson A, Larsson E-M, Hallström I. Impact of extended written information on patient anxiety and image motion artifacts during magnetic resonance imaging. *Acta Radiol* 2006a;47:474–480.
- 41 Zenger I. Magnetic Resonance Imaging at Siemens. A success story. Erlangen, Germany: Siemens Healthcare AG; 2014. https://marketing.webassets.siemens-healthineers.com/1800000001929766/ef6a5e27aaf7/Siemens_MRI_MAGNETOM-World_Case-Study_success-story-Hellwich_1800000001929766.pdf
- 42 Krohne HW. Angst und Angstbewältigung. Stuttgart: Kohlhammer; 1996.



Contact

Janika Madl, M.Sc.
Chair, Health Psychology
Friedrich-Alexander-University
Erlangen-Nürnberg
Nägelsbachstrasse 49a
91052 Erlangen
Germany
janika.madl@fau.de

Advertisement

What happens when you have an MRI scan?

Help your little patients lose their fear – with Lottie

Lottie is an adventurous little lamb that loves to skateboard. But poor Lottie had an accident and may have broken her ankle. Now instead of leaping, she can only limp. Lottie is off to the hospital for an MRI scan. This engaging story by Professor Rolf Vosschenrich and Sylvia Graupner explains to children what it's like to have an MRI scan in a way they can understand.

We offer Lottie's story as a children's book in 15 languages (PDF) and as video in 5 languages. You can also order hard copies of the book in German, English, and Spanish.

The material is available at
www.siemens-healthineers.com/magnetom-world

Go to > Publications > MR Basics



Artificial Intelligence: Learning About the Future of Cardiovascular MR

Kerstin Hammernik, Ph.D.¹ and Thomas Küstner, Ph.D.²

¹Technical University of Munich, Germany / Imperial College London, UK

²University Hospital Tübingen, Germany

Over the past 40 years, cardiovascular magnetic resonance (CMR) has evolved from an esoteric research tool to an indispensable clinical tool that routinely changes patient management across the breadth of modern cardiovascular practice. CMR is a versatile, non-invasive imaging modality that provides a comprehensive assessment of multiple parameters for cardiac function and morphology in a single protocol. It plays a major role in the diagnosis and management of cardiovascular disease (CVD). The prevalence of CVD is increasing annually and the conditions are among the leading causes of morbidity and mortality worldwide. This requires improvements in assessing, diagnosing, treating, and monitoring CVD patients. CMR will play a central role in achieving these goals. However, there remain major challenges for the widespread use of this technique:

- (a) Complex technology with many pulse sequences and parameters to choose from
- (b) Manual data analysis and interpretation
- (c) Inherent cardiac and respiratory motion
- (d) Duration of the examination

Methods using artificial intelligence (AI) have been proposed to address these challenges, but have also given rise to new questions about the methods' reliability, accuracy, generalizability, and robustness. In order to shape the future of CMR and establish where and how AI can play a role in it, we will showcase some CMR applications and scenarios that reflect the abovementioned challenges. We will highlight some AI methods for each step of the CMR processing chain and conclude with thoughts on remaining challenges and opportunities.

Learning about the heart in higher dimensions

CMR enables the acquisition of morphological, functional, and quantitative tissue parameters. Various sequences are devised that represent powerful tools for the non-invasive characterization of congenital or acquired CVDs, including ischemia, valvular diseases, and ischemic and non-ischemic cardiomyopathies. Cardiac function is commonly assessed with continuous acquisitions (cine, real-time) over multiple

cardiac cycles. Perfusion imaging permits the assessment of physiologic and pathophysiologic functional parameters. First-pass perfusion is the clinical standard for measuring myocardial blood flow and detecting myocardial ischemia. Cardiac viability is traditionally studied with a gadolinium-based contrast agent in late gadolinium enhancement. Cardiovascular flow by phase-contrast imaging measures the velocity of blood in the cardiac chambers and great vessels. Coronary magnetic resonance angiography (CMRA) has the potential to diagnose coronary artery diseases. Quantitative CMR techniques like T1, T2, or T1rho mapping provide characterization of tissue properties that distinguish healthy from diseased tissue. More recently, MR fingerprinting¹ and MR multitasking have been proposed to provide multi-parametric data in a continuously measured acquisition under a free-movement scenario (with respiration and a beating heart). Multi-parametric CMR offers the promise of a more accurate diagnosis, early disease detection, and monitoring over time or of response to therapy [1].

These applications require either high spatial and/or temporal resolution, should ideally be acquired in 3D with whole-heart coverage to avoid slice misalignments or to allow reformatting into arbitrary image orientations, or are susceptible to cardiac and respiratory motion. The achievable image quality must be sufficient to detect and characterize CVDs, and is thus an inherent trade-off between imaging resolution, scan time, and signal-to-noise ratio (SNR), which are overall challenging requirements to meet. Moreover, to fully utilize the available information and/or to resolve the individual factors (motion, relaxivity, perfusion, etc.), joint data processing of all acquired data should be performed. This in turn yields high-dimensional data processing for CMR. To give an example, 5D cine imaging provides 3D spatial information of respiratory (1D) and cardiac (1D) motion-resolved data. If we jointly reconstruct motion-resolved data, we can share spatiotemporal information, i.e., sharing samples at a spatial location

¹MR Fingerprinting is not commercially available in some countries. Due to regulatory reasons its future availability cannot be ensured.

between different respiratory/cardiac motion states by accounting for the underlying motion between motion states. The benefit is increased sampling efficiency and higher sampling density, which in turn can result in improved image quality. Furthermore, high-dimensional data processing naturally lends itself to the combination of several data processing steps, as shown in Figure 1. In our 5D cine example, the image reconstruction is combined with a motion correction/estimation procedure. The combination could also expand across several processing steps and we could develop a single AI network that performs this task for us. Let us say we are actually interested in assessing the left ventricular function using the 5D cine imaging. We could thus combine reconstruction, motion estimation, and image segmentation (to obtain left ventricular functional parameters) using as input the acquired MR raw data and outputting the left ventricular functional parameters (ejection fraction, end-systolic volume, and so on). While joint processing has its benefits, one could also be interested in obtaining the intermediate results of this joint processing chain – to perform quality assurance, for instance, or to further visually assess morphology and function. However, depending on the selected setup, architecture, and scenario, this may no longer be easily possible. On the other hand, we could have developed individual and finely tuned AI networks for each of the tasks. For the 5D cine example, an image reconstruction network is followed by an image registration network that merges individually reconstructed motion states on which a subsequent image segmentation network is performed. Intermediate results (reconstructed image, motion fields, segmentation masks) would be available, but we would lose the possibility to share information between and within processing steps.

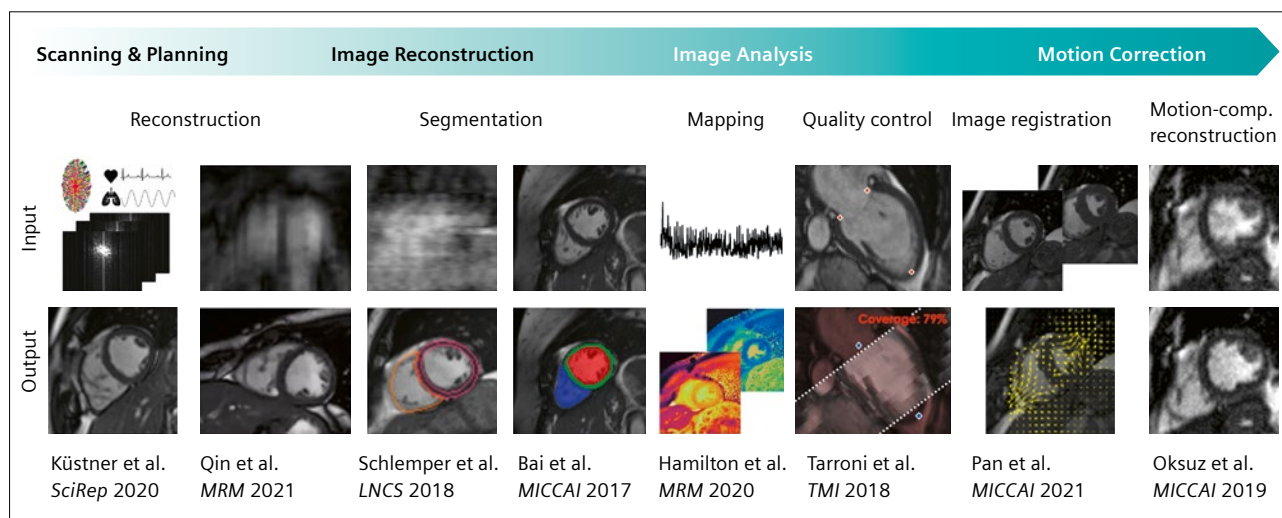
While the concepts of joint processing sound intriguing and have already been studied in several research settings, applying them to a clinical scenario in a reliable fashion is challenging. Furthermore, high-dimensional AI-based data processing is not trivial and currently still limited in most cases by the available graphics processing unit (GPU) memory and the availability of network building blocks to process data beyond 3D [2].

AI forming the CMR workflow

For a conventional CMR examination, several individual sequences are acquired, for which different processing steps are conducted. These include image acquisition, image formation, and diagnosis, as illustrated in Figure 1. These processing steps could be performed individually with highly optimized and tuned AI networks, or several steps could be combined end-to-end for outputting multiple results in so-called multi-tasking networks. While AI has the potential to improve each step of the imaging pipeline, it should be seen as a support for clinicians, not a replacement.

Scanning and planning

The most tedious and time-consuming part of CMR is planning the cardiac scan. The image quality depends on the experienced technician responsible for acquiring the data, and uncertainties might be introduced by incorrect planning. AI has the potential to speed up the whole planning workflow, resulting in increased patient comfort and reduced healthcare costs. Also, AI-supported planning allows for more standardized cardiac scans and reduces the complexity of cardiac view planning. Siemens Healthineers provides a solution for AI-based view planning with its myExam Cardiac Assist tool [3, 4].



1 Overview of clinical workflow supported by several artificial intelligence (AI) methods. Different AI solutions along the imaging and processing chain are illustrated for cardiac cine imaging. The inputs and outputs of the proposed AI techniques are also shown.

Image reconstruction

Traditional image reconstruction techniques suffer from long reconstruction times and limitations in acceleration under Cartesian sampling patterns. Furthermore, prior knowledge of the reconstructed images needs to be incorporated into the reconstruction procedure. However, this prior information is often too simple to characterize the complex medical images. AI provides the opportunity to gain this prior knowledge directly from the data. Dictionary learning is an early example of data-driven learning in Compressed Sensing (CS)-based MRI reconstruction, and involves learning directly from undersampled data how the individual dictionary entries should be combined. AI-based solutions now achieve image quality similar or superior to classic CS-based approaches, while reducing the reconstruction time tremendously from minutes and hours to seconds. Furthermore, the learned priors can deal with the characteristic, coherent backfolding artifacts that appear in Cartesian sampling schemes, which are standard in the clinical workflow.

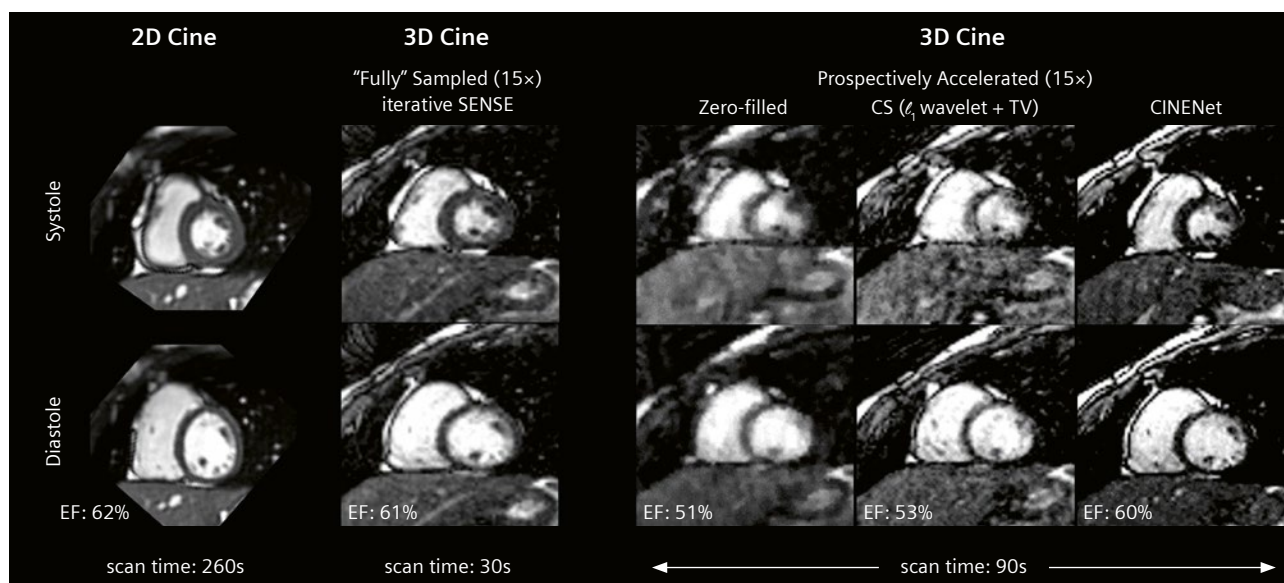
However, learning only a data-driven image prior is not enough, and special care needs to be taken with the acquired k -space data. While purely image-driven networks are able to produce realistic-looking images, the images themselves are not consistent with the acquired k -space data. We refer the interested reader to a previous article in MAGNETOM Flash and to book chapters [5, 6] for more information on how to include the acquired k -space into a

reconstruction network. In the current article, we focus on the application of AI-based solutions to (high-dimensional) CMR, including static and dynamic imaging.

Fuin et al. proposed a multi-scale variational network for CMRA [7]. For this static application, the reconstruction time could be reduced from ~5 minutes for a CS-based approach to ~14 seconds for the proposed learning-based approaches. Comparable image quality was achieved between the fully sampled reference scan and the 9× accelerated scan. The results show that the acquisition time can be reduced from 18:55 minutes for the fully sampled reference scan to 2:34 minutes for the 9× accelerated acquisition, while the image quality stays comparable.

An alternative approach for shortening the scan time while simultaneously increasing spatial resolution is to use AI-based super resolution. Images are acquired at a low image resolution and retrospectively reconstructed to the high-resolution target. This approach has been successfully applied to cardiac cine [8, 9] and CMRA [10, 11].

In the context of cine image reconstruction, Schlemper et al. proposed a data-consistent convolutional neural network (CNN), performing alternating single-coil data-consistency steps and image denoising with a 5-layer CNN [12]. This approach was improved by a recurrent approach to propagate information through the time dimensions and between iterations [13]. Separated convolutions in the spatial domain and temporal domain further improve reconstruction quality, yielding more accurate functional



2 Physics-guided deep learning-based image reconstruction for cardiac cine imaging. High imaging acceleration (15×) enables the acquisition of a 3D cardiac cine with isotropic resolution and left ventricular coverage in a single breath-hold of < 10 seconds. A deep learning-based image reconstruction, CINeNet, provides high image quality in contrast to the zero-filled reconstruction (input to network) or a Compressed Sensing (CS) reconstruction. CINeNet reconstruction of accelerated scan (9 seconds) is in good accordance with a separate (slightly accelerated, 2.5×) 3D cine (30 seconds) and a conventional multi breath-hold 2D cine (260 seconds). The 3D cine with CINeNet reconstruction shows high agreement with the conventional 2D cine in terms of left ventricular ejection fraction (EF).

parameters [14] and allowing for accelerated 3D cine reconstruction [15]. An example for accelerated single-breath-hold 3D cine reconstruction compared to conventional multi-slice multi-breath-hold 2D reconstruction is depicted in Figure 2. The aforementioned approaches operate directly on the full image, but low-rank and sparse priors are less frequently studied. Building on the success of unrolled networks, recent works focus on learning a structured low-rank prior [16] or low-rank plus sparse decomposition [17] in the context of dynamic MRI reconstruction.

While most approaches apply CNNs primarily in the image domain, hybrid networks exploit information in complementary domains. Due to the dynamic component in cine images, we can exploit the data in various domains. Exploiting all available data in various spaces pushes the reconstruction results further. El-Rewaify et al. use both k -space and image domain information for radial imaging, implementing CNNs in both domains [18]. Complementary information in k - t and x - f space was studied in Qin et al. [19].

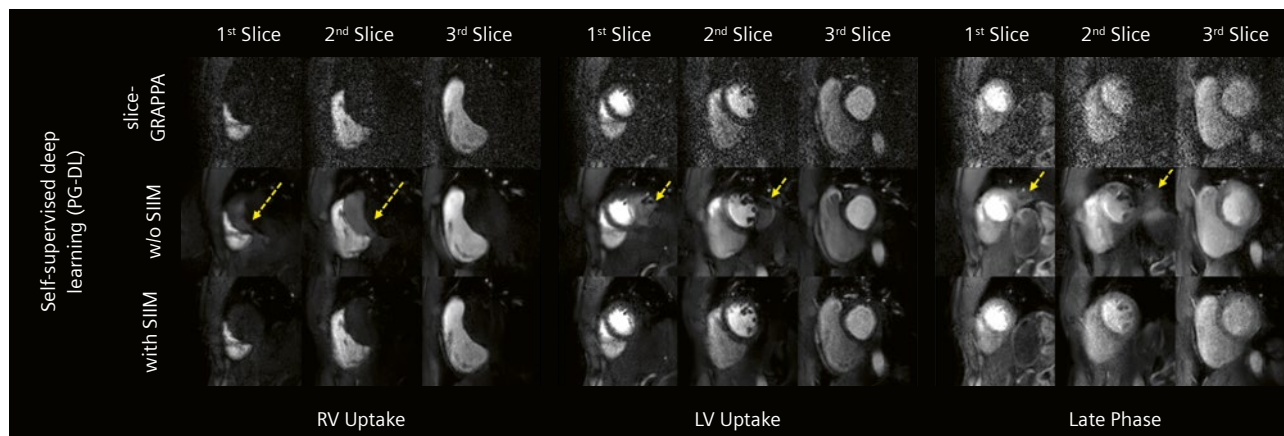
All aforementioned reconstruction approaches assume that fully sampled training data are available. The fully sampled data serve as a reference during training. However, training data is not always available, and is sometimes even impossible to acquire. Yaman et al. proposed a self-supervised learning approach that uses only the acquired training data points, with application to late gadolinium enhancement as depicted in Figure 3 [20]. The sampled data points are split into two disjoint sets, where the first set is used in the data consistency units of the unrolled reconstruction network, and the second set is used to evaluate the loss function during training directly in k -space.

Image analysis

CMR image segmentation and quantitative evaluation can be a challenging, time-consuming, and operator-intensive task. Segmentation of the chambers and myocardium is a mandatory postprocessing task. Automation of these tasks can therefore significantly reduce the time required for CMR image assessment.

AI-based solutions for image segmentation have been shown to be highly accurate and fast [21]. Considerable efforts have been directed toward cine imaging, as it is considered the gold standard for the assessment of cardiac chamber volumes and function [22]. The work of Morales et al. provided additional myocardial strain measures [23]. Segmentation methods have also been paired with predictions of important markers for cardiovascular disease, such as volume of pericardial adipose tissue [24] and scar-tissue areas [25]. Fahmy et al. automatically quantified left ventricular mass and scar volume in late gadolinium enhanced imaging [26], which showed strong agreement between the automated segmentations and the manual delineations. Farrag et al. [27] investigated the propagation of segmentation masks derived from cine imaging for the accurate segmentation of myocardial tissue in T1 mapping of a shMOLLI sequence. In contrast, the work of Hann et al. [28] segmented the myocardium directly in the shMOLLI data.

Segmentations have also been shown to provide valuable information for image reconstruction and motion correction tasks. Joint learning of motion estimation and segmentation for cine imaging was proposed by Qin et al. [29]. The results suggested that an efficient motion estimation network can bypass the need for high-quality reconstructions to achieve accurate image segmentation,



3 Physics-guided deep learning-based image reconstruction for dynamic contrast-enhanced MRI. A three-slice myocardial perfusion in the right ventricle (RV) uptake, left ventricle (LV) uptake and late phase is shown for different reconstruction techniques. A split slice-GRAPPA (top row) is compared to two self-supervised deep learning solutions (middle and bottom row) [63]. The difference between the deep learning methods is the use of signal intensity informed multi-coil (SIIM) encoding, which better models the underlying MR physics as indicated by the yellow arrows. Image courtesy of Mehmet Akçakaya.

indicating the superiority of high-dimensional data processing. Sun et al. [30] proposed a unified deep network architecture for joint image reconstruction and segmentation. The reconstruction and segmentation networks share network parts, acting as intrinsic regularizers for each other, while unshared network parts act specifically to the task (reconstruction or segmentation). Their results suggest that training a joint network is beneficial for high-quality segmentation of undersampled k -space data. While most multi-task networks aimed for an intermediate reconstructed image, Schlemper et al. [31] bypassed this step and directly predicted segmentation maps from highly undersampled dynamic CMR images of the UK Biobank data. Their results indicate that clinical parameters can be computed within an error of 10% if at least 10 lines are acquired for each cardiac phase using Cartesian sampling.

As sufficient image quality is a crucial factor in any further downstream task, Tarroni et al. devised an automated cardiac quality control [32]. The heart coverage, existence of inter-slice motion, and myocardial to blood pool contrast are automatically assessed. Their findings enable a reproducible and objective setting for large-scale and automated data processing.

Neural networks have also been proposed for quantitative CMR imaging to allow for accelerated myocardial tissue characterization. Jeelani et al. estimated quantitative T1 maps from a MOLLI sequence [33, 34]. The work of Fahmi et al. paired the quantification network with a segmentation to target the maps toward the myocardium [35].

For multi-parametric acquisitions in MR fingerprinting, AI solutions have been initially proposed for non-cardiac applications [36] in order to bypass dictionary simulation and pattern matching and thereby reduce computation time and memory requirements. In CMR fingerprinting, sequence timings depend on the subject's cardiac rhythm.

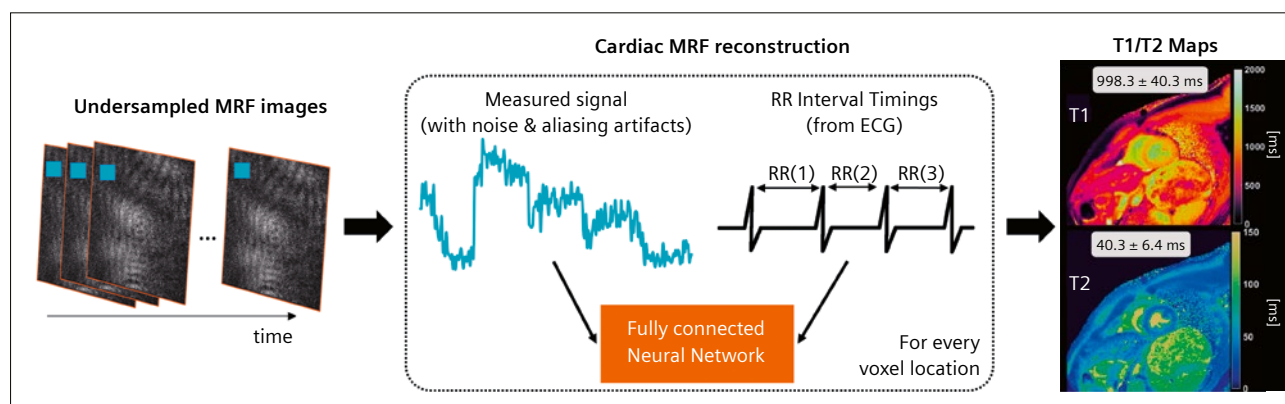
Hamilton et al. proposed an estimation of T1 and T2 maps directly from undersampled spiral images showcasing rapid and robust predictions [37], as depicted in Figure 4.

Myocardial tissue characterization has also been studied in the context of radiomics. In radiomics, the image data is converted into mineable high-dimensional data using a large number of handcrafted features targeted toward the image intensity, and structural and textural information. These features are then used to perform segmentation of myocardial tissue [38], differentiate between acute and chronic infarction [39], differentiate between causes of myocardial hypertrophy [40], discriminate between hypertensive heart disease and hypertrophic cardiomyopathy patients [41], and quantify myocardial inflammation [42].

Beyond purely imaging-focused approaches, AI methods have also been used to predict outcomes in patients with various cardiovascular diseases [43] and identify relationships between cardiac morphology and non-imaging information as provided by genetic variations [44].

Motion correction

Physiological motion is still one of the major extrinsic sources of image artifacts and requires appropriate handling during acquisition or reconstruction. In the case of CMR, we are primarily dealing with respiratory and cardiac motion, which result in non-rigid deformations of the heart and its surrounding environment. Respiratory motion and cardiac motion are in most solutions regarded as periodic, but they do not necessarily have a fixed frequency throughout the scan. In other words, a subject might hold their breath, or a heartbeat might be skipped and should therefore be treated as cyclic rather than periodic. Simplifications in modeling and correcting motion may be necessary to handle the motion problem and to build an appropriate AI solution.



4 Deep learning-based magnetic resonance fingerprinting (MRF) for myocardial tissue mapping [37]. A cardiac MRF sequence collects data within an ECG-triggered window under breath-hold from which the temporal fingerprint (measured signal) can be extracted for every voxel location. Together with the heart-rate interval timings, a fully connected neural network estimates the T1 and T2 values at each voxel location. Image courtesy of Jesse Hamilton.

AI-based image registration methods have been proposed to map motion states in motion-resolved images, outputting a motion field of the moving anatomies. Mappings can be expressed between a pair of images (e.g., end-systolic frame to end-diastolic frame), known as pairwise registration, or between a group of images (several diastolic frames) to a target image (end-systolic frame), known as groupwise registrations. Large non-rigid motion across multiple temporal frames can occur, and in the case of 2D imaging the existence of through-plane motion complicates the motion estimation process. Moreover, estimated motion fields should be diffeomorphic, i.e., a forward motion (end-systolic to end-diastolic) can be easily inverted to a backward motion (end-diastolic to end-systolic).

A fast and reliable motion estimation is therefore required that correlates these short- and long-term correspondences. AI methods have been proposed to operate on the reconstructed motion-resolved images (i.e., in the image domain) for pairwise registrations [45–47] or groupwise registrations [48]. Alternatively, registration could be carried out directly on the acquired raw k -space data [49]. Since it is often of interest to estimate motion from as little data as possible (providing high temporal motion resolution), motion estimation procedures have been challenged with data from accelerated acquisitions [49–51].

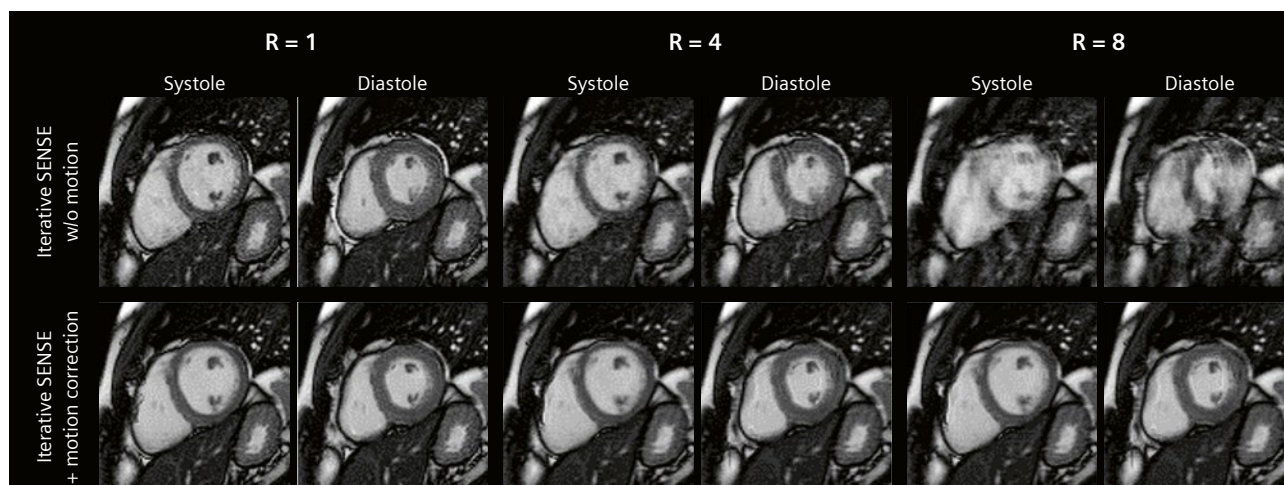
Instead of outputting a motion field, joint motion-compensated image reconstruction networks have been studied. Motion estimations are embedded with the reconstruction process in order to exploit the high-dimensional data [52–54], as highlighted in Figure 5. Further combinations with segmentation have been studied in [55], which introduced a joint framework for motion artifact detection, correction in k -space, and image segmentation. In this

setting, the motion correction problem is reformulated as a reconstruction task. The motion artifact network detects motion-affected lines in k -space, which are then signaled to the reconstruction part for removal, yielding a motion-corrected image from which segmentations are derived. The results showed that joint processing was superior to sequential processing.

Adversarial training strategies as proposed in [56, 57] aim to correct for the motion in the image domain. These networks consist of two parts: a generator network which predicts motion-corrected images from simulated motion-corrupted ones, and a discriminator which tries to distinguish between the generated motion-corrected images (from generator) and real motion-corrected images. The goal is to fool the discriminator network to generate images that look like real motion-corrected images. Alternatively, motion embeddings can be learned with variational autoencoders that allow to distinguish between motion-affected and motion-corrected scans [58].

Current challenges, opportunities, and limitations

CMR imaging offers a great opportunity for deep learning due to the redundancy and the high dimensionality of the data. However, we also face challenges regarding acquisition time, SNR, the trade-off between spatial and temporal resolutions, and different types of motion, e.g., cardiac and respiratory motion, which makes the application of deep learning techniques more demanding. While deep learning approaches often outperform CS-based approaches in terms of pixel-wise quantitative scores, these approaches might tend to over-blur the temporal component. However, a



5 Motion-compensated image reconstruction for cardiac cine imaging. An image reconstruction is paired with a motion estimation network. The impact of sharing the available spatiotemporal information in a motion-corrected image reconstruction (bottom row) is shown in comparison to performing only a non-motion-informed image reconstruction (top row). For higher accelerations, sharing spatiotemporal data allows to increase sampling density and thereby improve image quality.

high resolution of the temporal dynamics is crucial for diagnosis and to detect subtle pathologies.

When using deep learning techniques, it is challenging to evaluate the quality and robustness of reconstruction approaches, especially in the case of subtle pathologies. However, we might get trapped in overly optimistic results if we use simulated data and neglect the unprocessed raw *k*-space data [59]. In a different line of work, the robustness of neural networks to small adversarial perturbations at the input was investigated [60]. Robustness of neural networks to changes in anatomy was studied in the context of static 2D imaging in [61], showing that domain shift has a marginal impact on image reconstruction when using unrolled networks and moderate acceleration. This observation regarding domain shift is different to image analysis tasks, where a subtle change might lead to mis-segmentation, for instance.

Deep learning approaches were intensively and individually studied in the context of scan planning, accelerated acquisition and reconstruction, and image analysis. While we often focus only on one part of this full imaging pipeline, deep learning provides many more opportunities to improve the whole workflow of CMR image acquisition for analysis and diagnosis. Future investigations of deep learning approaches will go deeper in supporting the choice of exam based on actual physiological scan parameters such as heart rate, or on the patient information obtained during the scan. Deep learning techniques will also support further acceleration in scan time to enable real-time interventional cardiac MRI [62]. We also observe a trend towards embedding different elements of the imaging pipeline into a deep learning approach and training this network end-to-end as shown in multi-task networks, or exploiting the available data, e.g., via motion fields, which will form the future of learning-based CMR imaging.

Acknowledgments

The authors would like to thank Jesse Hamilton and Mehmet Akçakaya for providing materials for the figures, and Teresa Correia, Tevfik Ismail, Wendy Strugnell, Chiara Coletti, Masa Bozic-Iven, Sebastian Weingärtner, and Gastao Cruz for the discussions.

References

- Ismail TF, Strugnell W, Coletti C, Božić-Iven M, Weingärtner S, Hammernik K, et al. Cardiac MR: From Theory to Practice. *Front Cardiovasc Med*. 2022;9:826283.
- Hammernik K, Kuestner T, Rueckert D. Machine Learning in MRI Reconstruction. In: Akçakaya M, Doneva M, Prieto C, editors. *Magnetic Resonance Image Reconstruction Theory, Methods, and Applications*. Elsevier; 2022. ISBN: 9780128227268. In press.
- Thomas SJ, Bryant MG, Radvan J, Speier P, Mueller E, Schmidt M, et al. The need for speed – adenosine stress MRI in less than 30 minutes. *J Cardiovasc Magn Reson*. 2013;15(Suppl 1):E24.
- Wang K, Zhang W, Li S, Bi X, Schmidt M, An J, et al. Free-Breathing 10-Min Cardiac MRI Protocol at 3.0T: Single-Center Experience. *Biomedical Journal of Scientific & Technical Research*. 2022;41(1):32365-32373.
- Hammernik K, Knoll F, Rueckert D. Deep Learning for Parallel MRI Reconstruction: Overview, Challenges, and Opportunities. *MAGNETOM Flash*. 2019;75:10-15.
- Hammernik K, Knoll F. Chapter 2 – Machine learning for image reconstruction. In: Zhou SK, Rueckert D, Fichtinger G, editors. *Handbook of Medical Image Computing and Computer Assisted Intervention*. Academic Press; 2020. p. 25–64.
- Fuin N, Bustin A, Küstner T, Oksuz I, Clough J, King AP, et al. A multi-scale variational neural network for accelerating motion-compensated whole-heart 3D coronary MR angiography. *Magn Reson Imaging*. 2020;70:155–167.
- Lin JY, Chang YC, Hsu WH. Efficient and Phase-aware Video Super-resolution for Cardiac MRI. *arXiv*. 10626 [eess.IV].
- Steeden JA, Quail M, Gotschy A, et al. Rapid whole-heart CMR with single volume super-resolution. *J Cardiovasc Magn Reson*. 2020;22:56.
- Küstner T, Munoz C, Psenicny A, Bustin A, Fuin N, Qi H, et al. Deep-learning based super-resolution for 3D isotropic coronary MR angiography in less than a minute. *Magn Reson Med*. 2021;86(5): 2837–2852.
- Ishida M, Nakayama R, Uno M, et al. Learning-based super-resolution technique significantly improves detection of coronary artery stenoses on 1.5T whole-heart coronary MRA. *J Cardiovasc Magn Reson*. 2014;16 (Suppl 1), P218.
- Schlemper J, Caballero J, Hajnal JV, Price AN, Rueckert D. A Deep Cascade of Convolutional Neural Networks for Dynamic MR Image Reconstruction. *IEEE Trans Med Imaging*. 2018;37(2):491–503.
- Qin C, Schlemper J, Caballero J, Price AN, Hajnal JV, Rueckert D. Convolutional Recurrent Neural Networks for Dynamic MR Image Reconstruction. *IEEE Trans Med Imaging*. 2019;38(1):280–290.
- Sandino CM, Lai P, Vasanaawala SS, Cheng JY. Accelerating cardiac cine MRI using a deep learning-based ESPIRiT reconstruction. *Magn Reson Med*. 2021;85(1):152–167.
- Küstner T, Fuin N, Hammernik K, Bustin A, Qi H, Hajhosseiny R, et al. CINeNet: deep learning-based 3D cardiac CINE MRI reconstruction with multi-coil complex-valued 4D spatio-temporal convolutions. *Sci Rep*. 2020;10:13710.
- Ke Z, Huang W, Cui ZX, Cheng J, Jia S, Wang H, et al. Learned Low-Rank Priors in Dynamic MR Imaging. *IEEE Trans Med Imaging*. 2021;40(12):3698–3710.
- Huang W, Ke Z, Cui ZX, Cheng J, Qiu Z, Jia S, et al. Deep low-Rank plus sparse network for dynamic MR imaging. *Medical Image Analysis*. 2021;73:102190.
- El-Rewaify H, Fahmy AS, Pashakhanloo F, Cai X, Kucukseymen S, Csecs I, et al. Multi-domain convolutional neural network (MD-CNN) for radial reconstruction of dynamic cardiac MRI. *Magn Reson Med*. 2021;85(1):1195–1208.
- Qin C, Duan J, Hammernik K, Schlemper J, Küstner T, Botnar R, et al. Complementary time-frequency domain networks for dynamic parallel MR image reconstruction. *Magn Reson Med*. 2021;86(6):3274–3291.
- Yaman B, Shenoy C, Deng Z, Moeller S, El-Rewaify H, Nezafat R, et al. Self-Supervised Physics-Guided Deep Learning Reconstruction for High-Resolution 3D LGE CMR. *IEEE 18th International Symposium on Biomedical Imaging (ISBI)*, 2021, pp. 100–104.
- Bernard O, Lalande A, Zotti C, Cervenansky F, Yang X, Heng PA, et al. Deep Learning Techniques for Automatic MRI Cardiac Multi-Structures Segmentation and Diagnosis: Is the Problem Solved? *IEEE Trans Med Imaging*. 2018;37(11):2514–2525.
- Bai W, Sinclair M, Tarroni G, Oktay O, Rajchl M, Vaillant G, et al. Automated cardiovascular magnetic resonance image analysis

- with fully convolutional networks. *J Cardiovasc Magn Reson*. 2018;20(1):65.
- 23 Morales MA, van den Boomen M, Nguyen C, Kalpathy-Cramer J, Rosen BR, Stultz CM, et al. DeepStrain: A Deep Learning Workflow for the Automated Characterization of Cardiac Mechanics. *Front Cardiovasc Med*. 2021;8:730316.
 - 24 Bard A, Raisi-Estabragh Z, Ardissono M, Lee AM, Pugliese F, Dey D, et al. Automated Quality-Controlled Cardiovascular Magnetic Resonance Pericardial Fat Quantification Using a Convolutional Neural Network in the UK Biobank. *Front Cardiovasc Med*. 2021;8:677574.
 - 25 Chen J, Yang G, Gao Z, Ni H, Angelini E, Mohiaddin R, et al. Multiview two-task recursive attention model for left atrium and atrial scars segmentation. *arXiv:1806.04597 [cs.CV]*.
 - 26 Fahmy AS, Rausch J, Neisius U, Chan RH, Maron MS, Appelbaum E, et al. Automated Cardiac MR Scar Quantification in Hypertrophic Cardiomyopathy Using Deep Convolutional Neural Networks. *JACC Cardiovasc Imaging*. 2018;11(12):1917–1918.
 - 27 Farrag NA, White JA, Ukwatta E. Semi-automated myocardial segmentation in native T1-mapping CMR using deformable non-rigid registration of CINE images. In: *Medical Imaging 2019: Biomedical Applications in Molecular, Structural, and Functional Imaging*. SPIE Conference Series. 2019;10953.
 - 28 Hann E, Ferreira VM, Neubauer S, Piechnik SK. Deep Learning for Fully Automatic Contouring of the Left Ventricle in Cardiac T1 Mapping. *CMR 2018 – A Joint EuroCMR/SCMR Meeting Abstract Supplement*. ID# 376365.
 - 29 Qin C, Bai W, Schlemper J, Petersen SE, Piechnik SK, Neubauer S, et al. Joint Learning of Motion Estimation and Segmentation for Cardiac MR Image Sequences. *arXiv:2018.1806.04066 [cs.CV]*.
 - 30 Sun L, Fan Z, Ding X, Huang Y, Paisley J. Joint CS-MRI Reconstruction and Segmentation with a Unified Deep Network. *Lecture Notes in Computer Science (including subseries Lecture Notes in Artificial Intelligence and Lecture Notes in Bioinformatics)*. 2019;11492 LNCS:492–504.
 - 31 Schlemper J, Oktay O, Bai W, Castro DC, Duan J, Qin C, et al. Cardiac MR Segmentation from Undersampled *k*-space Using Deep Latent Representation Learning. In: Frangi A, Schnabel J, Davatzikos C, Alberola-López C, Fichtinger G (eds). *Medical Image Computing and Computer Assisted Intervention – MICCAI 2018*. MICCAI 2018. *Lecture Notes in Computer Science*. 2018;11070.
 - 32 Tarroni G, Bai W, Oktay O, Schuh A, Suzuki H, Glocker B, et al. Large-scale Quality Control of Cardiac Imaging in Population Studies: Application to UK Biobank. *Sci Rep*. 2020;10:2408.
 - 33 Jeelani H, Yang Y, Zhou R, Kramer CM, Salerno M, Weller DS. A Myocardial T1-Mapping Framework with Recurrent and U-Net Convolutional Neural Networks. In: *IEEE 17th International Symposium on Biomedical Imaging (ISBI)*. 2020:1941–1944.
 - 34 Martini N, Della Latta D, Santini G, Valvano G, Barison A, Avoglierio F, et al. Automatic AHA model segmentation of cardiac T1 maps with deep learning. *Proc Intl Soc Mag Reson Med*. 2018;26:1047.
 - 35 Fahmy AS, El-Rewaify H, Nezafat M, Nakamori S, Nezafat R. Automated analysis of cardiovascular magnetic resonance myocardial native T1 mapping images using fully convolutional neural networks. *J Cardiovasc Magn Reson*. 2019;21(1):7.
 - 36 Cohen O, Zhu B, Rosen MS. MR fingerprinting Deep ReConstruction Network (DRONE). *Magn Reson Med*. 2018;80(3):885–894.
 - 37 Hamilton JI, Curry D, Rajagopalan S, Seiberlich N. Deep learning reconstruction for cardiac magnetic resonance fingerprinting T1 and T2 mapping. *Magn Reson Med*. 2021;85(4):2127–2135.
 - 38 Kotu LP, Engan K, Skretting K, Måløy F, Orn S, Woie L, et al. Probability mapping of scarred myocardium using texture and intensity features in CMR images. *Biomed Eng Online*. 2013;12:91.
 - 39 Larroza A, López-Lereu MP, Monmeneu JV, Gavara J, Chorro FJ, Bodí V, et al. Texture analysis of cardiac cine magnetic resonance imaging to detect nonviable segments in patients with chronic myocardial infarction. *Med Phys*. 2018;45(4):1471–1480.
 - 40 Schofield R, Ganeshan B, Kozor R, Nasir A, Endozo R, Groves A, et al. CMR myocardial texture analysis tracks different etiologies of left ventricular hypertrophy. *J Cardiovasc Magn Reson*. 2016;18(Suppl 1):O82.
 - 41 Neisius U, El-Rewaify H, Nakamori S, Rodriguez J, Manning WJ, Nezafat R. Radiomic Analysis of Myocardial Native T1 Imaging Discriminates Between Hypertensive Heart Disease and Hypertrophic Cardiomyopathy. *JACC Cardiovasc Imaging*. 2019;12(10):1946–1954.
 - 42 Baeßler B, Schaarschmidt F, Treutlein M, Stehning C, Schnackenburg B, Michels G, et al. Re-evaluation of a novel approach for quantitative myocardial oedema detection by analysing tissue inhomogeneity in acute myocarditis using T2-mapping. *Eur Radiol*. 2017;27(12):5169–5178.
 - 43 Kotu LP, Engan K, Borhani R, Katsaggelos AK, Ørn S, Woie L, et al. Cardiac magnetic resonance image-based classification of the risk of arrhythmias in post-myocardial infarction patients. *Artif Intell Med*. 2015;64(3):205–15.
 - 44 Biffi C, de Marvao A, Attard MI, Dawes TJW, Whiffin N, Bai W, et al. Three-dimensional cardiovascular imaging-genetics: a mass univariate framework. *Bioinformatics*. 2018;34(1):97–103.
 - 45 Pan J, Rueckert D, Kuestner T, Hammernik K. Efficient Image Registration Network for Non-Rigid Cardiac Motion Estimation. In: Haq N, Johnson P, Maier A, Würfl T, Yoo J (eds). *Machine Learning for Medical Image Reconstruction*. *MLMIR 2021. Lecture Notes in Computer Science*. 2021;12964. Springer, Cham.
 - 46 Morales MA, Izquierdo-Garcia D, Aganj I, Kalpathy-Cramer J, Rosen BR, Catana C. Implementation and Validation of a Three-dimensional Cardiac Motion Estimation Network. *Radiol Artif Intell*. 2019;1(4):e180080.
 - 47 Upendra RR, Wentz BJ, Shontz SM, Linte CA. A Convolutional Neural Network-based Deformable Image Registration Method for Cardiac Motion Estimation from Cine Cardiac MR Images. *Comput Cardiol* (2010). 2020;47:10.22489/CinC.2020.204.
 - 48 Qi H, Hajhosseiny R, Cruz G, Küstner T, Kunze K, Neji R, et al. End-to-end deep learning nonrigid motion-corrected reconstruction for highly accelerated free-breathing coronary MRA. *Magn Reson Med*. 2021;86(4):1983–1996.
 - 49 Küstner T, Pan J, Qu H, Cruz G, Gilliam C, Blu T, et al. LAPNet: Non-Rigid Registration Derived in *k*-Space for Magnetic Resonance Imaging. In: *IEEE Transactions on Medical Imaging*. 2021;40(12):3686–3697.
 - 50 Hammernik K, Pan J, Rueckert D, Küstner T. Motion-Guided Physics-Based Learning for Cardiac MRI Reconstruction. In: *55th Asilomar Conference on Signals, Systems, and Computers*. 2021:900–907.
 - 51 Huttinga NRF, van den Berg CAT, Luijten PR, Sbrizzi A. MR-MOTUS: model-based non-rigid motion estimation for MR-guided radiotherapy using a reference image and minimal *k*-space data. *Phys Med Biol*. 2020;65(1):015004.
 - 52 Seegoolam G, Schlemper J, Qin C, Price A, Hajnal J, Rueckert D. Exploiting Motion for Deep Learning Reconstruction of Extremely-Undersampled Dynamic MRI. In: Shen D, Liu T, Peters TM, Staib LH, Essert C, Zhou S, et al. (eds). *Medical Image Computing and Computer Assisted Intervention – MICCAI 2019*. *Lecture Notes in Computer Science*. 2019;11767. Springer, Cham.
 - 53 Küstner T, Pan J, Gilliam C, Qi H, Cruz G, Hammernik K, et al. Self-Supervised Motion-Corrected Image Reconstruction Network for 4D Magnetic Resonance Imaging of the Body Trunk. *APSIPA Transactions on Signal and Information Processing*. 2022;11(1):e12.

- 54 Qi H, Hajhosseiny R, Cruz G, Kuestner T, Kunze K, Neji R, et al. End-to-end deep learning nonrigid motion-corrected reconstruction for highly accelerated free-breathing coronary MRA. *Magn Reson Med*. 2021;86(4):1983–1996.
- 55 Oksuz I, Clough JR, Ruijsink B, Anton EP, Bustin A, Cruz G, et al. Deep Learning-Based Detection and Correction of Cardiac MR Motion Artefacts During Reconstruction for High-Quality Segmentation. *IEEE Trans Med Imaging*. 2020;39(12):4001–4010.

Contact

Kerstin Hammernik, Ph.D.
AI in Healthcare and Medicine
Technical University of Munich
Boltzmannstr. 3
85748 Garching
Germany
k.hammernik@tum.de



Thomas Küstner, Ph.D.
University Hospital Tübingen
Hoppe-Seyler-Straße 3
72076 Tübingen
Germany
thomas.kuestner@med.uni-tuebingen.de



- 56 Zhang Y, Zhang W, Zhang Q, Yang J, Chen X, Zhao S. CMR motion artifact correction using generative adversarial nets. *arXiv:1902.11121 [cs.CV]*.
- 57 Küstner T, Armanious K, Yang J, Yang B, Schick F, Gatidis S. Retrospective correction of motion-affected MR images using deep learning frameworks. *Mag Reson Med*. 2019;82(4):1527–1540.
- 58 Ghodrati V, Bydder M, Ali F, Gao C, Prosper A, Nguyen KL, et al. Retrospective respiratory motion correction in cardiac cine MRI reconstruction using adversarial autoencoder and unsupervised learning. *NMR Biomed*. 2021;34(2):e4433.
- 59 Shimron E, Tamir JI, Wang K, Lustig M. Implicit data crimes: Machine learning bias arising from misuse of public data. *Proc Natl Acad Sci U S A*. 2022;119(13):e2117203119.
- 60 Antun V, Renna F, Poon C, Adcock B, Hansen AC. On instabilities of deep learning in image reconstruction and the potential costs of AI. *Proc Natl Acad Sci U S A*. 2020;117(48):30088–30095.
- 61 Hammernik K, Schlemper J, Qin C, Duan J, Summers RM, Rueckert D. Systematic evaluation of iterative deep neural networks for fast parallel MRI reconstruction with sensitivity-weighted coil combination. *Magn Reson Med*. 2021;86(4):1859–1872.
- 62 Jaubert O, Montalt-Tordera J, Knight D, Coghlan GJ, Arridge S, Steeden JA, et al. Real-time deep artifact suppression using recurrent U-Nets for low-latency cardiac MRI. *Magn Reson Med*. 2021;86(4):1904–1916.
- 63 Yaman B, Hosseini SAH, Moeller S, Ellermann J, Uğurbil K, Akçakaya M. Self-supervised learning of physics-guided reconstruction neural networks without fully sampled reference data. *Magn Reson Med*. 2020;84(6):3172–3191.

Advertisement

Learn more about Deep Learning Image Reconstruction

Introduction to Deep Learning for MR Image Reconstruction

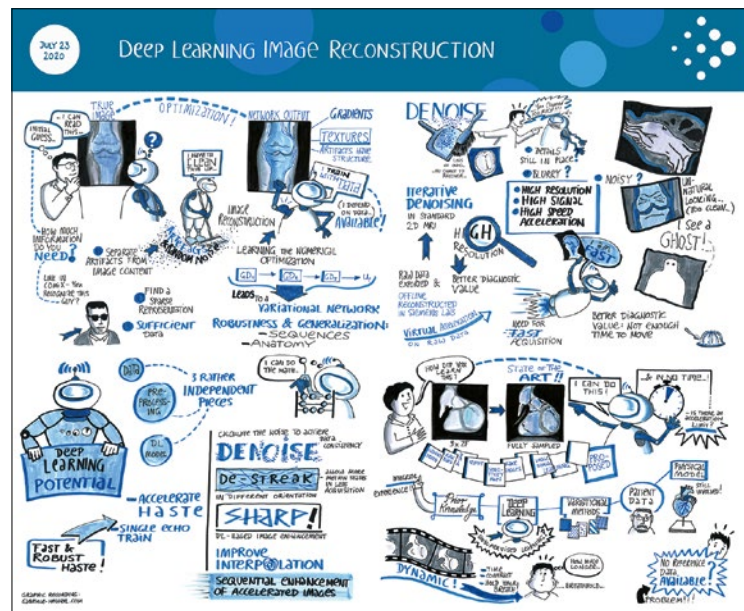
Florian Knoll, PhD
(New York University, New York, NY, USA)

Deep Learning Image Reconstruction – State of the Art

Kerstin Hammernik, PhD
(Imperial College London, UK)

Iterative Denoising and Increased Acquisition Speed

Johan Dehem, MD
(Yan Yperman Ziekenhuis, Ieper, Belgium)



Don't miss this valuable source of information
siemens-healthineers.com/MWS2020-recordings

Graphic Recording: www.gabriele-heinzel.com

Magnetic Resonance Angiography with Ferumoxytol

J. Paul Finn, M.D.^{1,2}; Takegawa Yoshida, M.D.¹; Ashley Prosper, M.D.¹; Arash Bedayat, M.D.¹; Cameron Hassani, M.D.¹; Puja Shahrouki, M.D.¹; Kim-Lien Nguyen, M.D.^{1,2,3}

¹Diagnostic Cardiovascular Imaging Section, Department of Radiological Sciences, David Geffen School of Medicine at UCLA, Los Angeles, CA, USA

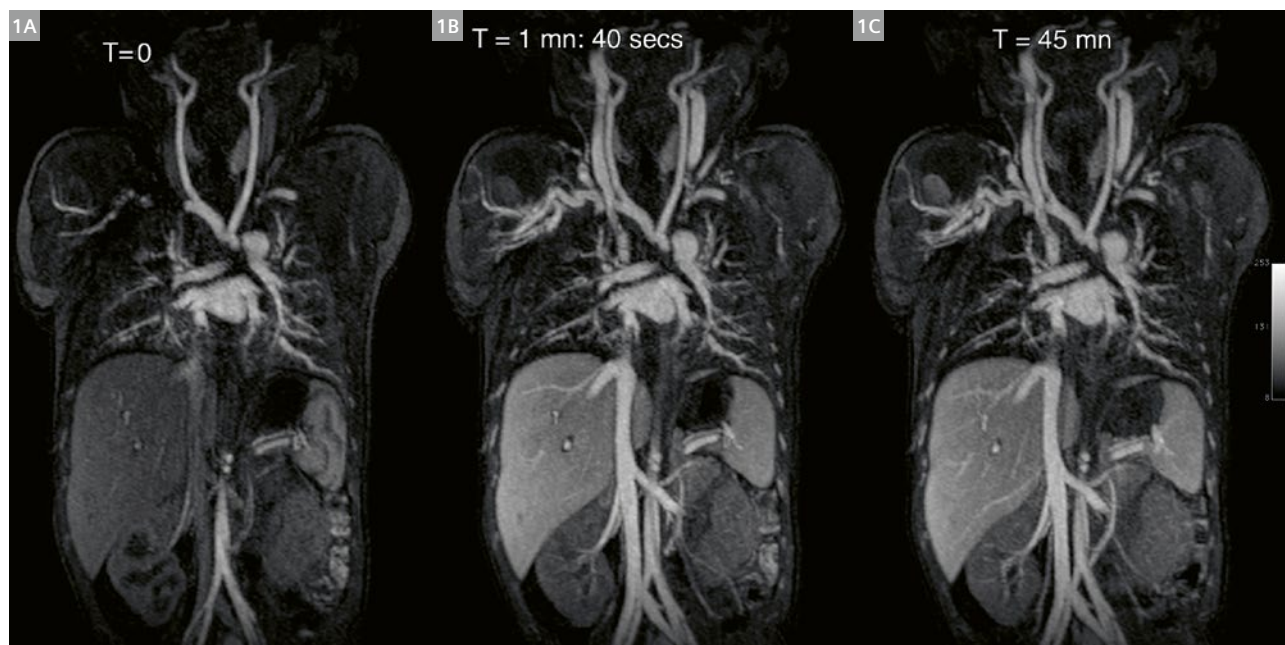
²Physics and Biology in Medicine Graduate Program, University of California, Los Angeles, CA, USA

³Division of Cardiology, David Geffen School of Medicine at UCLA and VA Greater Los Angeles Healthcare System, Los Angeles, CA, USA

Introduction

In the more than three decades since magnetic resonance angiography (MRA) was introduced into clinical practice, resolution and imaging speed have improved dramatically. Parallel imaging and advances in coil technology have slashed acquisition times through undersampling, while data processing power has exploded. More recent developments in compressed sensing and deep learning hold promise for still more aggressive undersampling schemes as they usher in an exciting new era of technical innova-

tion. Today, MRA studies are, on average, faster to acquire with greater coverage and higher resolution than 10 years ago, at which time MRA use was growing at a fast pace [1, 2]. However, an analysis of MRA utilization trends over the past decade suggests that its use is steadily decreasing, while the use of X-ray CT angiography (CTA) is steadily increasing [3]. The reasons underlying this trend will require further analysis, but relevant factors in the choice of test include ease of access, diagnostic accuracy, image



1 3-day-old¹ male patient with hypoplastic aortic arch and coarctation. Coronal thin MIP images from ferumoxytol enhanced MRA in the arterial (1A), venous (1B) and late venous (1C) phases at 3T. Note the stable intravascular signal in the 43-minute interval between the early and late venous phases. Reproduced from [30] with permission.

¹Siemens Healthineers Disclaimer: MR scanning has not been established as safe for imaging fetuses and infants less than two years of age. The responsible physician must evaluate the benefits of the MR examination compared to those of other imaging procedures. Note: This disclaimer does not represent the opinion of the authors.

quality, workflow, cost and safety. Modern CTA has made impressive strides in all of these spaces, raising the bar in a point to point face off [4]. Nonetheless, in certain areas, MRA is still firmly rooted in clinical practice (e.g., 3D Time of Flight MRA in the brain) and is an effective alternative to CTA when iodinated contrast agents are contraindicated or when vascular calcification is problematic. Also, MR technology has unique advantages for imaging the vessel wall and plaque composition [5]. Outside of the brain, contrast enhanced MRA (CEMRA) has out-performed non-contrast techniques for most applications, but the association of gadolinium with nephrogenic systemic fibrosis [6, 7] and gadolinium retention in brain [8, 9] has unwound the common practice of using high dose gadolinium for CEMRA. Although there is strong evidence supporting the safety of the macrocyclic gadolinium-based contrast agents (GBCAs) in patients with renal impairment [10], persistent concerns about gadolinium brain deposition [8, 11] have tempered enthusiasm for GBCA enhanced studies in several patient groups. For all of the above reasons, the landscape of advanced, non-invasive vascular imaging is very much in flux.

Against this background, ferumoxytol (Sandoz Inc, Princeton, NJ, USA: Feraheme®, Covis Pharma GmbH, Zug, Switzerland) has emerged as a diamond in the rough that can address many of the limitations faced by both gadolinium-based MRA and iodine-based CTA [12–17]. Ferumoxytol is an iron nanoparticle with a mean particle diameter of 30 nm [13, 14], placing it in the class of ultra-small, superparamagnetic iron oxide (USPIO) agents. It is approved in the U.S. for intravenous iron replacement therapy in patients with all levels of renal impairment, as well as in those with normal renal function [18]. Ferumoxytol is effectively a pure blood-pool agent with remarkable MRI properties that has proved to be a powerful off-label vascular imaging agent where other agents may be contraindicated or ineffective [13–15].

In our practice at UCLA, ferumoxytol enhanced MRA (FEMRA) has been requested in growing numbers over the past eight years for patients with renal failure and in other patient groups where its advantages have become evident. In this paper, we address several clinical applications where we have found the off-label use of FEMRA effective and reliable.

Ferumoxytol compared to the extracellular GBCAs

Without doing an exhaustive dive into the physico-chemical properties of the individual agents, below we highlight relevant characteristics that distinguish ferumoxytol from the broad class of extracellular GBCA.

Biodistribution and pharmacokinetics

Once injected, ferumoxytol remains unaltered in the blood with a nominal half-life of 15 hours. Its distribution volume is the blood volume, which is about 5 liters in a typical adult. It is not excreted by the kidneys or the liver and so does not appear in urine or bile. Rather, ferumoxytol is slowly taken up by white blood cells (macrophages) in liver, spleen and bone marrow and the iron is incorporated into the red blood cell synthesis pathway. The GBCAs on the other hand, once injected, begin to diffuse into the entire extracellular fluid space immediately. Their blood half-life (depending on renal function) is on the order of two minutes for the distribution phase and 90 minutes for the elimination phase [19]. The distribution volume for the GBCAs is the volume of the extracellular fluid space, which is about 15 liters in a typical adult. So, within two minutes of injection, the GBCAs become three times more diluted than ferumoxytol and their blood concentration drops further due to renal excretion. It should be noted that iron is an essential component of normal cellular metabolism, such that iron deficiency has far reaching consequences [20].

Relaxivity

The T1 relaxivity of ferumoxytol is about three times that of the currently available macrocyclic GBCAs [13, 21]. So, when coupled with its smaller distribution volume (less dilution) and slow clearance from the blood, ferumoxytol exhibits about a ten-fold advantage when compared to the GBCAs at comparable doses. The steady state distribution of ferumoxytol is established within two to five minutes of administration and thereafter uniformly high signal persists in all blood vessels and in all vascular territories.

Vascular specificity

Because ferumoxytol does not diffuse into the extravascular tissue spaces, it maintains a high gradient in concentration between blood vessels and their surroundings. This preserves the sharpness of vessel borders and makes the task of region-growing easier for post processing algorithms, such as volume rendering (VR). On the other hand, with GBCAs, once the first pass is over, enhancement of soft tissues diminishes the concentration gradient between blood vessels and their surroundings also decreases.

Image contrast basis

In addition to high T1 relaxivity, ferumoxytol also has potent T2 relaxivity [21], whereas the GBCAs do not. The T2 property can be exploited to huge advantage for black blood imaging without any requirement for magnetization preparation schemes such as double inversion or diffusion sensitization [22]. So, with appropriate image weighing, ferumoxytol can produce reliable bright blood imaging and also reliable black blood imaging. The GBCAs exhibit weak

T2 relaxivity and their T1 effects undermine black blood imaging with commonly used preparation schemes. Beyond vessel imaging, strong T2 contrast can be seen with ferumoxytol at much shorter TEs than with the GBCAs. This has relevance for improved T2-weighted imaging of solid organs, such as liver, and for susceptibility-weighted imaging in all regions, including the brain [23].

Cardiovascular imaging

For ferumoxytol in the heart, there are several noteworthy observations. Because it does not diffuse into the interstitial (extravascular) fluid space, ferumoxytol does not enhance myocardial scar. However, its intravascular fidelity could be leveraged for estimation of fractional blood volume distribution [24]. Ferumoxytol should not be used for applications such as late gadolinium enhancement, where GBCAs may have greater strengths due to their extracellular properties. Second, ferumoxytol does not play well with TrueFISP sequences (because of its T2 effects) and the preferred cardiac cine sequence with ferumoxytol is T1 FLASH. Due to its potent and persistent shortening of the blood T1, ferumoxytol offsets the saturation that can plague non-contrast FLASH cine, such that high quality images are routinely achievable even in patient with poor cardiac function. FLASH is also relatively immune to the B_0 and B_1 non-uniformity that complicates TrueFISP cine at 3T and in patients with implanted cardiac devices [25].

Field strength compatibility

Like CEMRA with the GBCAs, FEMRA can be performed at 1.5T and 3T. Also, there is evidence of its potential at 0.5T [26].

Multi-station and repeated acquisitions

As already noted, the steady state concentration of ferumoxytol in the blood is constant. For this reason, multiple overlapping stations can be acquired reliably, without having to 'keep up with' a traveling bolus of contrast. These individual stations can then be composed into a single, large field of view image using 'Image Compose'. For the same reason, if the patient moves or does not follow breath-held instructions on the first attempt, the acquisition can be repeated with no penalty in image contrast.

Safety

Ferumoxytol is approved in the U.S. for therapy in patients with renal failure and can be used (off-label) as an alternative to the iodinated X-ray agents and the GBCAs as appropriate. The U.S. Food and Drug Administration (FDA) has warned against rapid injection of ferumoxytol due to the possibility of severe hypersensitivity reactions reported during its therapeutic use [27]. Although severe reactions have not been reported during diagnostic use of ferumoxytol [28], we strongly recommend following FDA guidelines

with slow infusion and physiological monitoring. In our practice, minor infusion reactions have occurred in less than 1% of patients and in multicenter experience, mild reactions occurred in < 2% of injections [28]. Sometimes called 'Fishbane' reactions, these are self-limiting symptoms thought to be mediated through release of complement and typically manifest as chest tightness, flushing of the skin, back pain, or 'trouble taking a breath'. Whereas vital signs are stable with Fishbane reactions, without bronchospasm hypotension, tachycardia or hypoxia, they may be distressing to patients (and staff) who have not been made aware that such symptoms may occur. In that case, patients and MRI staff may become anxious and distressed and confuse the episode with severe allergy. Management is supportive and generally requires only pausing the infusion, checking vital signs and reassuring the patient. Symptoms usually resolve within five minutes, without drug intervention. Once symptoms resolve, the infusion can be restarted slowly and symptoms generally do not recur. Although our numbers are not sufficient to draw any firm conclusions about who is more or less likely to exhibit symptoms, anecdotally we have observed a cluster in young patients (four of six total were in the age range from teens to thirties) and rarity in elderly patients. Failure to recognize Fishbane reactions for what they are may result in inappropriate escalation of care and administration of potent drugs that have potentially serious side effects. If a true allergic anaphylactic reaction occurs, as it may with any injected agent, it should be managed in the same manner as other severe hypersensitivity reactions due to the GBCAs or iodinated contrast agents.

Availability

Currently, ferumoxytol is available only within the U.S. and is marketed as Feraheme (Covis Pharma GmbH, Zug, Switzerland). Within the past year, a generic version of ferumoxytol has become available in the U.S., marketed by Sandoz, a Division of Novartis (Sandoz Inc., Princeton, NJ, USA).

Clinical experience

In our experience of more than 1,500 studies in more than 1,300 patients at UCLA, ferumoxytol has been used successfully in the following broad areas:

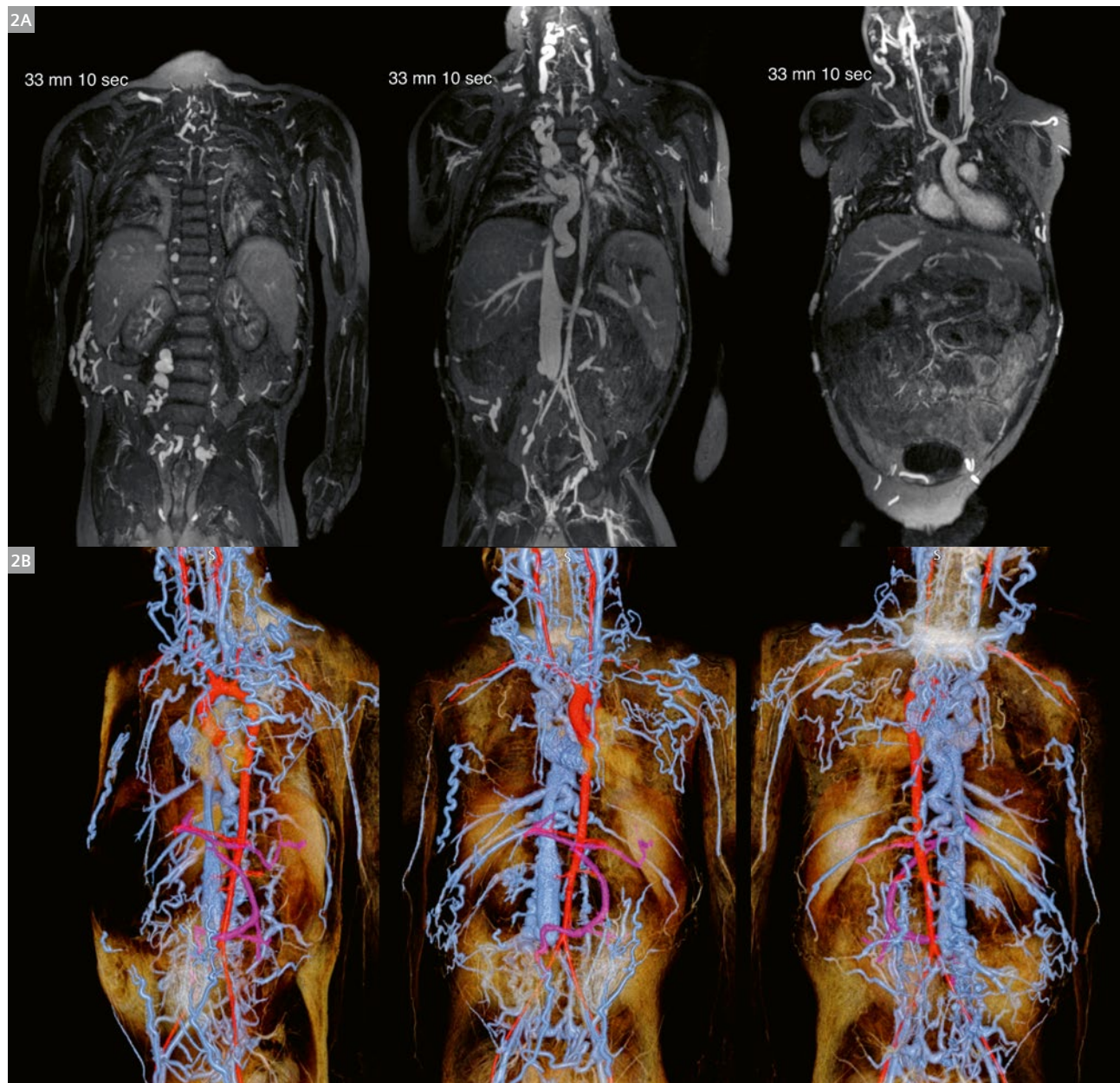
- (1) Venography: venous access mapping, central or peripheral venous occlusion, pre-operative planning for venous intervention, evaluation of the portal and hepatic venous system
- (2) Arteriography: aortic aneurysm and dissections, renal transplant vascular imaging, peripheral
- (3) Cardiovascular: congenital heart disease, implanted cardiac devices
- (4) MRA in claustrophobic patients

Venography

Ferumoxytol in the steady state produces equivalent high contrast in both arteries and veins and MR venography with ferumoxytol is poised to set a new gold standard [29, 30].

Venous thrombosis and occlusion are increasingly frequent and potentially devastating complications of treatment in patients with malignancy and organ failure

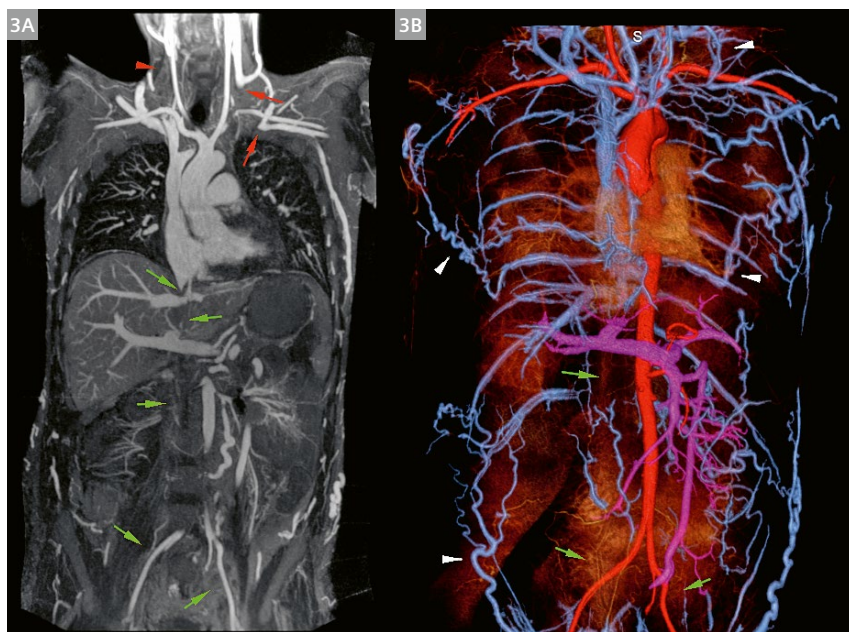
[31]. However, imaging of central veins may be impossible with ultrasound [31] and even modern CT may require high contrast doses and is prone to timing errors [32]. While non-contrast magnetic resonance venography (MRV) techniques have been applied to the central veins [33, 34], they are flow-dependent, relatively slow and are sensitive to motion artifact. Non-contrast MRV is nowadays used sparingly, outside of the brain.



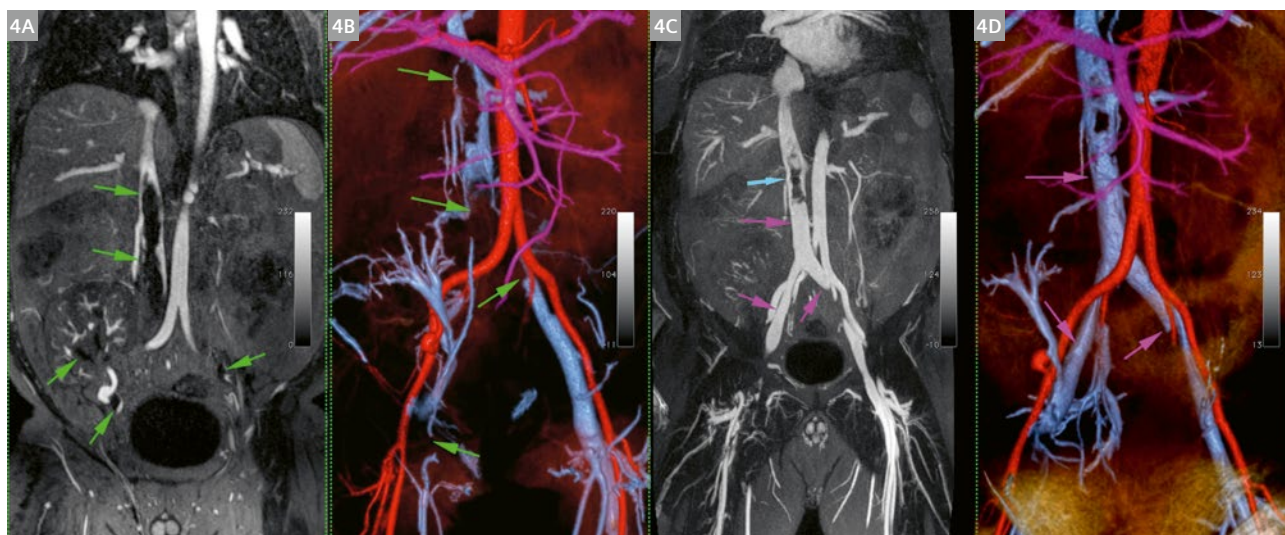
2 Ferumoxytol enhanced MRA (FEMRA) on a 3T MAGNETOM Trio a Tim system scanner in a 10-year-old boy with chronic renal failure requiring venous access. FEMRA at 30 minutes post injection show extensive venous occlusion in the chest and pelvis with extensive collateralization (2A, B). Color volume rendering highlights the numerous venous collaterals (2B, blue). Systemic arteries are rendered in red and portal vein tributaries in magenta (2B). Reproduced from [30] with permission.

Contrast enhanced MR Venography (CEMRV) with gadolinium has been used successfully with both blood pool and extracellular agents. However, in patients with severe renal impairment, clinicians remain hesitant to request gadolinium enhanced studies, a trend exacerbated by the recent reports of gadolinium deposition in brain and bone.

Ferumoxytol is, in many ways, an ideal agent for venous imaging. Following injection, there may be great variability in the time taken for veins in different anatomic regions to enhance. Because of its long vascular half life, ferumoxytol will eventually make its way to all patent blood vessels.



3 Ferumoxytol enhanced MRV on a 1.5T in a 33-year-old male with end-stage renal disease on hemodialysis who required venous mapping prior to central venous access. FE-MRV maximum intensity projection (**3A**) and color 3D volume rendering (**3B**) show occluded right internal jugular and subclavian veins (red arrows in **3A**), non-visualized occluded right internal jugular vein (**3A**, red arrowhead) and complete occlusion of the entire inferior vena cava and common iliac veins (**3A** and **B**, green arrows). Collateral veins are highlighted in **B** (white arrowheads). The study was completed in two breath-holds, with overlapping stations in Image Compose. *Reproduced from [29] with permission.*

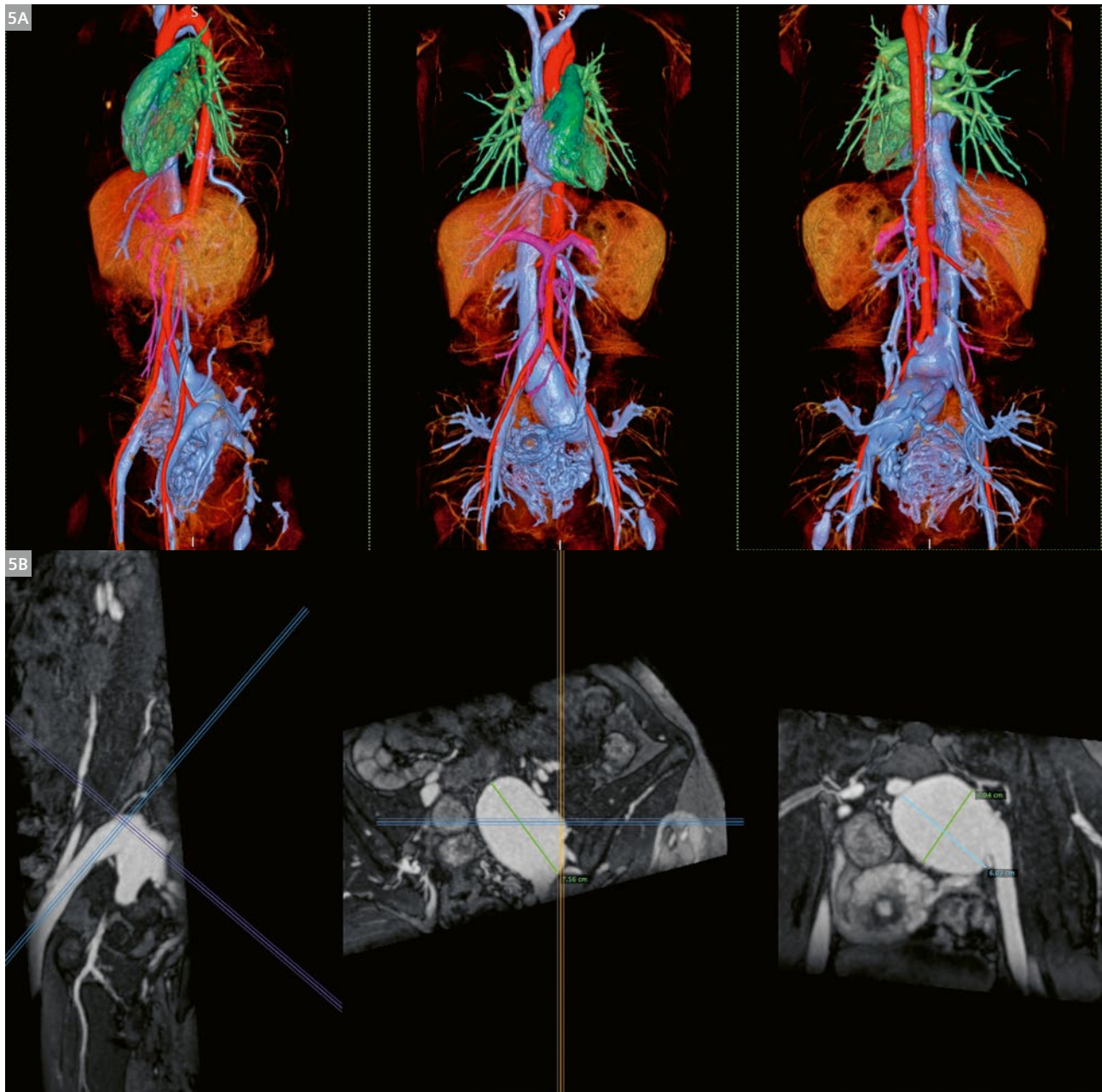


4 Ferumoxytol enhanced MRV (FEMRV) on a 1.5T in 47 year-old male with end-stage renal disease post renal transplantation presented with persistent right lower leg swelling 8 days after a filter placement in the inferior vena cava (IVC). Initial FEMRV source image (**4A**) and color 3D volume rendering (**4B**) show extensive occlusion extending from the IVC and bilateral common iliac veins to the right renal transplant vein and right common femoral vein (**4A** and **B**, green arrows). Following intervention (**4C**, **D**), the IVC and common iliac veins are largely recanalized (**4C** and **D**, purple arrows) and the IVC filter (**4C**, blue arrow) is in good position. Single breath-hold acquisition on both occasions. *Reproduced from [29] with permission.*

No degradation in vascular contrast occurs over the entire duration of an imaging study, so venography becomes as simple as infuse, wait a few minutes and scan (Figures 1–5).

Aortic disease

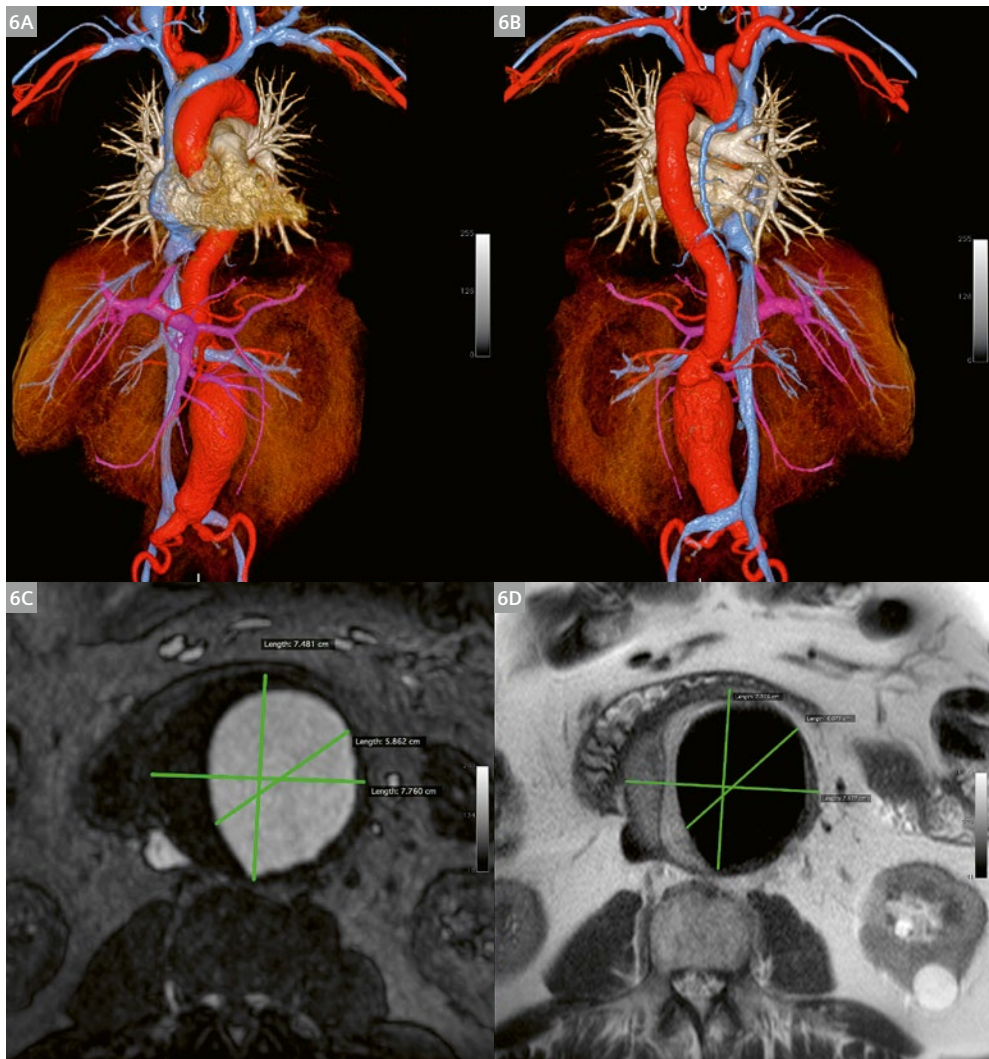
For the same reasons that ferumoxytol excels at imaging the venous system, it also excels at imaging aortic aneurysms, particularly in elderly patients with tortuous vessels and slow flow. In these circumstances, bolus timing for



5 Ferumoxytol enhanced MRA (FEMRA) on a 3T MAGNETOM Prisma^{fit} in a 23-year-old female with giant left iliac venous aneurysm. (5A) Color rendering from the single breath-held acquisition FEMRA shows the venous aneurysm and enlarged pelvic veins in blue. (5B) Multiplanar reformats show dimensions of the pelvic venous aneurysm and its narrow neck.

CEMRA and for CTA can be challenging, because distal segments of the aorta may fill long after more proximal

segments. With steady-state ferumoxytol, this is not an issue because contrast gains uniform access to every



6 Ferumoxytol enhanced MRA (FEMRA) in a 65-year-old male patient with renal failure and an infra-renal abdominal aortic aneurysm being evaluated for stent graft. Color rendered, composed FEMRA (**6A, B**) show the extent of the aneurysm and include the entire aorto-iliac system. Multiplanar reformats from FEMRA (**6C**) and non-breath held HASTE (**6D**) show the dimensions of the aneurysm. The HASTE image shows differential signal from aortic plaque and mural thrombus. Note how clearly the HASTE image differentiates perfused lumen (dark) from thrombus and plaque.



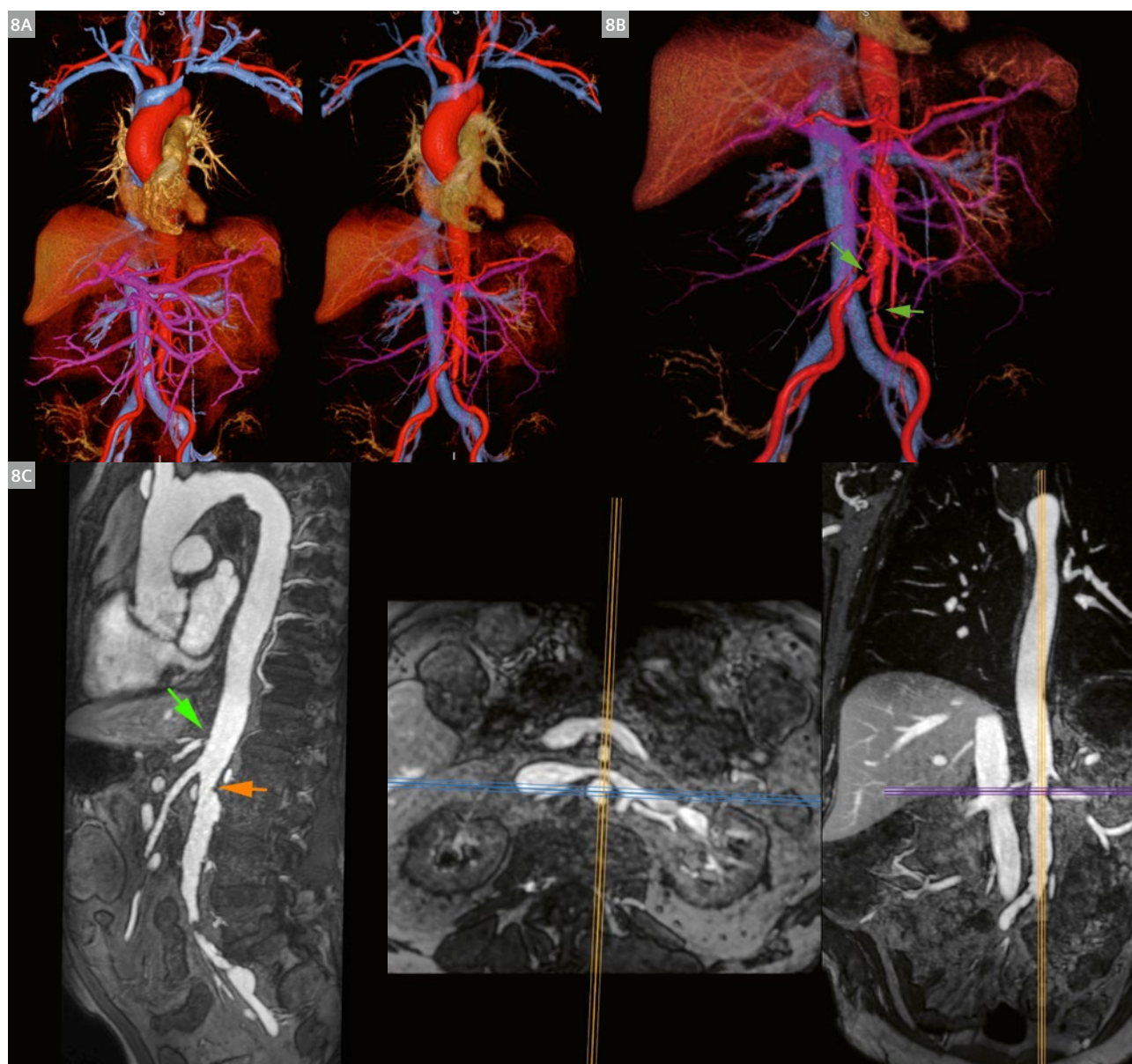
7 Ferumoxytol enhanced MRA (FEMRA) in an elderly male patient with renal failure, multi-focal, thoraco-abdominal aortic aneurysm, and prior aorto-iliac surgical graft. Color rendered, composed FEMRA (**7B**) show the extent of the aneurysm and include the entire aorto-iliac system. Multiplanar reformats from FEMRA (**7C**) and non-breath held HASTE (**7A**) show corresponding bright-blood and dark-blood images without mural thrombus.

crevice throughout the aorto-iliac system (Figures 4–8). Also, as with venous imaging, coverage can be extended with overlapping stations without loss of luminal contrast (Figures 5–8). Another advantage of ferumoxytol in aortic aneurysms is in defining mural thrombus and plaque with complementary black blood imaging (Fig. 6). This is as simple as running non-breath-held HASTE [22]. Because ferumoxytol decreases the T2 of the blood, there is no residual blood signal (or source of slow flow artifact) on HASTE, even at modest TE. Moreover, there is no requirement for black blood magnetization modules, such as

double inversion or dephasing gradients. Just as the blood signal is bright on T1-weighted MRA independently of flow, the blood signal is dark on T2-weighted sequences, independently of flow.

Lower extremity MRA

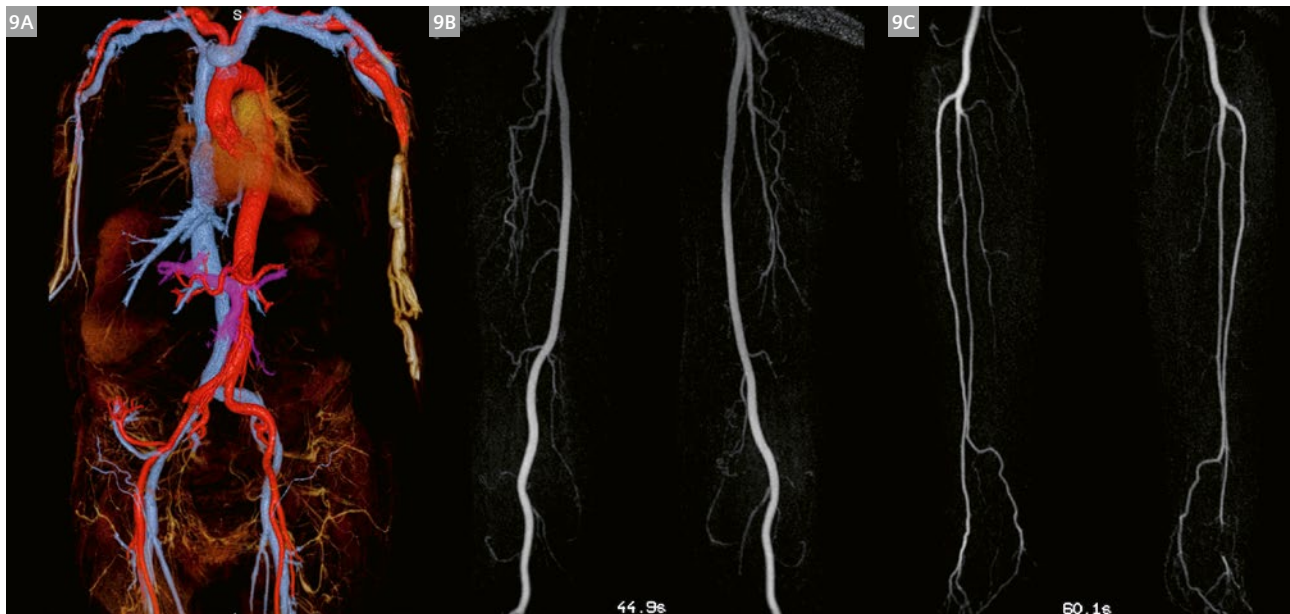
Whereas steady-state imaging is fully diagnostic in the chest, abdomen and pelvis, where arteries are easily distinguished from veins, in the calves, venous enhancement can make interpretation of abnormal arterial anatomy impossible. For this reason, we have found it helpful to



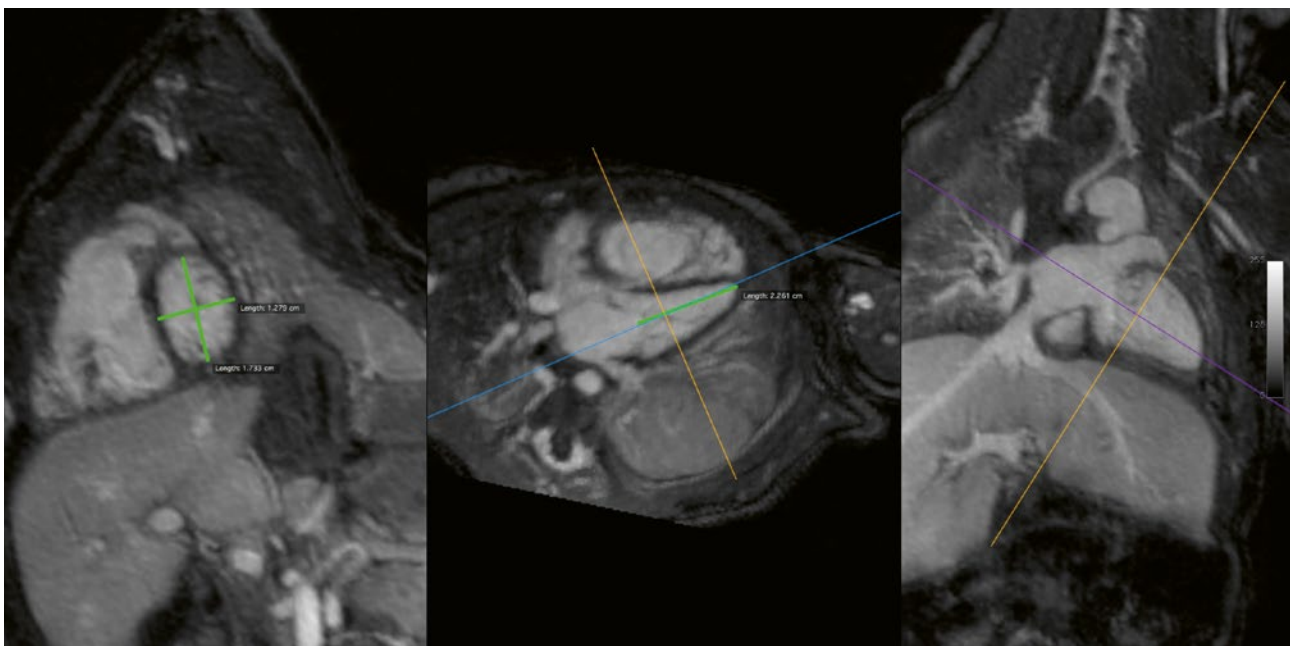
8 Ferumoxytol enhanced MRA (FEMRA) on a 3T MAGNETOM Prisma^{fit} in an 83-year-old male patient with renal failure and claudication. Panels (8A, B) show full field of view and focused iliac color renderings, with severe stenoses in the common iliac arteries (green arrows). Panel (8C) is a multiplanar reformat through the celiac artery, showing a tight stenosis at the origin (green arrow).

inject a small dose of dilute ferumoxytol over 10 seconds and acquire TWIST images (Fig. 9) in the calves and thighs. The remaining contrast can then be infused slowly and

steady state images of the chest, abdomen and pelvis acquired.



9 Ferumoxytol enhanced MRA (FEMRA) in a 75-year-old male patient with leg pain and chronic kidney disease. Low dose ferumoxytol was used for multi station dynamic TWIST imaging of the calf (**9C**) and thigh (**9B**). Subsequently, the remaining ferumoxytol dose was infused slowly and steady state imaging of the chest, abdomen and pelvis performed (**9A**, volume rendered image shows a transplant kidney in the right pelvis).



10 Ferumoxytol enhanced MRA (FEMRA) in a 2-day-old¹ neonate with suspected hypoplastic left heart syndrome. Single frame reformats from 4D MUSIC acquisition are shown. Uninterpolated voxel dimensions were $0.9 \times 0.9 \times 0.9$ mm³. Because of the volumetric, multi-phase acquisition, precise dimensional and volumetric measurements can be made for chamber and vessel sizes.

¹Siemens Healthineers Disclaimer: MR scanning has not been established as safe for imaging fetuses and infants less than two years of age. The responsible physician must evaluate the benefits of the MR examination compared to those of other imaging procedures. Note: This disclaimer does not represent the opinion of the authors.

Pediatric congenital heart disease

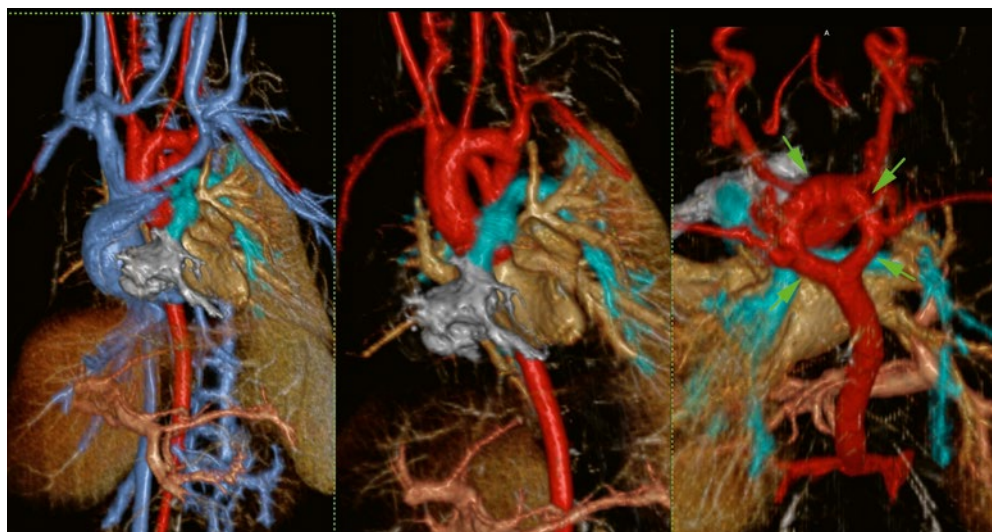
In children with congenital heart disease (CHD), ferumoxytol has ushered in a paradigm shift for MRI. Because of its long half-life in the blood, ferumoxytol supports high-resolution 4D (or 5D) imaging. When implemented with both cardiac and respiratory gating, high-dimensional techniques such as MUSIC (Multiphase, Steady-state Imaging with Contrast)² [35–39] and free-running 3D radial imaging³ [40] can produce images with uniformly high contrast throughout the cardiac chambers and blood vessels (Figures 10, 11). Data acquisition runs for several minutes (usually with continuous positive pressure ventilation) and images are immediately available for cine reconstruction in any plane and for comprehensive evaluation of vascular anatomy. MUSIC has proved reliable at multiple institutions and at both 1.5T and 3T [39]. The acquisition protocol is simple and reliable and is independent of the complexity of the underlying disease and anatomy.

²MUSIC is a prototype sequence developed at UCLA.

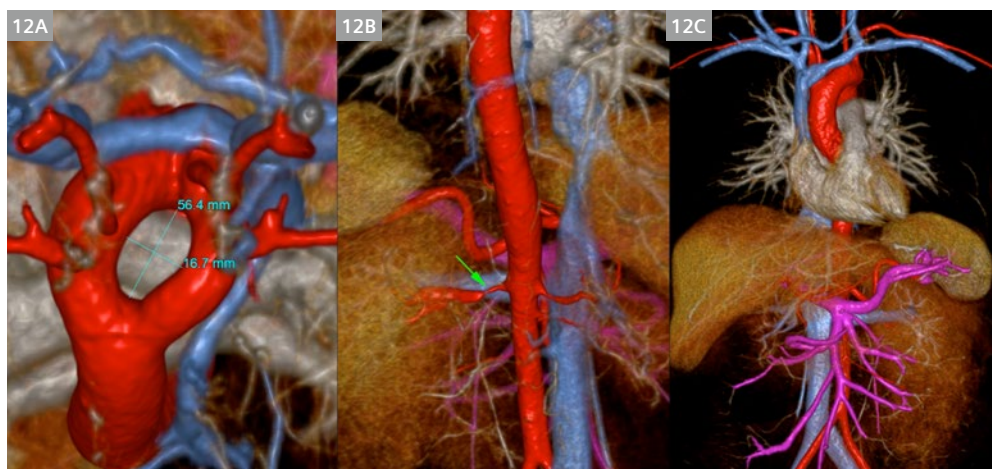
³Work in progress. The application is currently under development and is not for sale in the U.S. and in other countries. Its future availability cannot be ensured.

Adult congenital heart disease (ACHD)

In adult patients with CHD, timing of a contrast bolus for evaluation of shunts such as the Fontan and Glenn can be problematic and prone to misinterpretation. Again, because of its independence from bolus timing, MRA with ferumoxytol offers huge advantages over both CTA and CEMRA in the Fontan patient. Performing MRA with cardiac gating is desirable in patients with ACHD and abnormalities involving the great vessels (Fig. 12). First pass imaging of a GBCA bolus requires that the acquisition is timed accurately both with respect to the contrast bolus arrival and the phase of the cardiac cycle. This can be a complex procedure and if either gating or bolus timing fails, the first pass opportunity is lost. With ferumoxytol in steady state, there is no bolus timing and if gating or breath-holding is suboptimal the first time, the acquisition can be repeated at leisure.



11 Ferumoxytol enhanced MRA (FEMRA) in a 6-month-old¹ male with suspected vascular ring. Single frame volume-rendered images from 4D MUSIC acquisition are shown. Uninterpolated voxel dimensions were 1.0 x 1.0 x 1.0 mm³. Color volume rendered reconstructions comprehensively show all cardiac chambers and great vessel anatomy. The double aortic arch with complete vascular ring is well shown in the right panel (arrows).

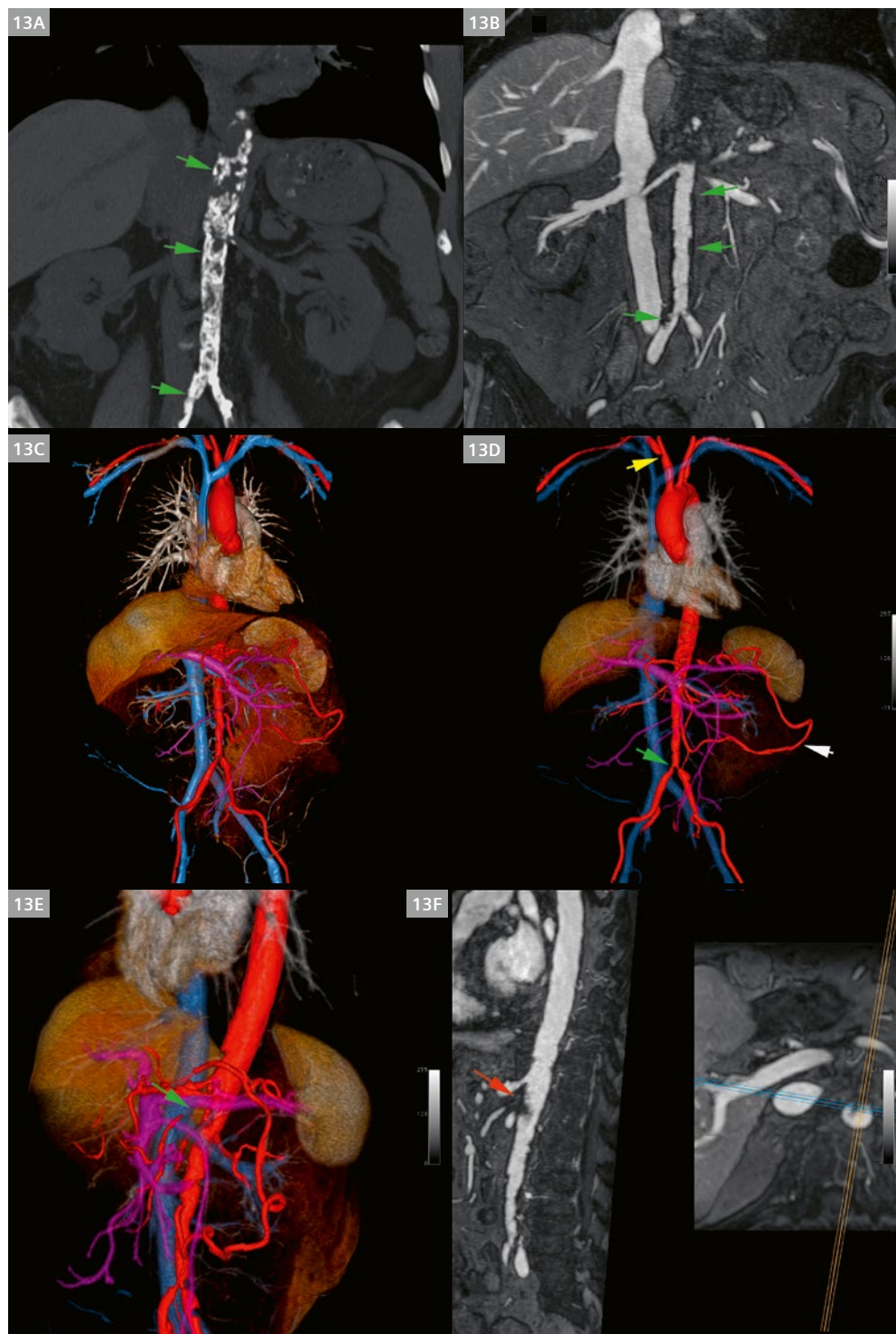


12 Ferumoxytol enhanced MRA (FEMRA) in a 48-year-old patient with double aortic arch and complete vascular ring. Color volume rendered images clearly depict a complete vascular ring and its relationship to other vessels (12A, viewed from above). Incidentally noted left renal artery stenosis (12B, arrow).

Claustrophobia

Claustrophobia of some degree is found in many patients who are otherwise suitable candidates for contrast-enhanced MR angiography (CEMRA). Conventional CEMRA examinations may exceed 30 minutes within the scanner bore and patients with claustrophobia may be unwilling

or unable to tolerate that. We have implemented a focused ferumoxytol-enhanced MRA (*f*-FEMRA) protocol in claustrophobic patients [41], whereby comprehensive vascular imaging can be completed in only a few minutes within the magnet bore (Fig. 13). For the *f*-FEMRA studies, where clinically appropriate, no pre-contrast imaging is performed



13 Ferumoxytol enhanced MRA (FEMRA) in a 79-year-old claustrophobic male patient with renal impairment and abdominal bruit. MIP of non-contrast CT (**13A**) and *f*-FEMRA (**13B**) show severe aortic calcification (green arrows). Note clear visualization of the perfused aortic lumen in panel 13B. *f*-FEMRA with color 3D volume rendering and an extended field of view (**13C, D**) confirm extensive distal aortic disease (13D, green arrow), stenosis of the right subclavian artery (13D, yellow arrow) and an enlarged inferior mesenteric artery forming an Arc of Riola (13D, white arrow). Occlusion of the proximal superior mesenteric artery is highlighted in (**13E, F**, arrows). Examination time for two-station *f*-FEMRA was 6 minutes and 46 seconds. Reproduced from [41] with permission.

and ferumoxytol is infused outside the scanner bore (or outside the MRI suite). Automated scanner tuning and coil adjustment, without patient-specific shimming, minimizes adjustment time. Following localizers, breath-held, high resolution 3D FEMRA is performed in one or more overlapping stations. Total time within the magnet bore for *f*-FEMRA may be as little as 3 minutes.

Conclusion

The use of ferumoxytol offers many distinct advantages over conventional approaches to vascular imaging with MRI. It can simplify procedures and protocols, shorten exam durations (sometimes profoundly), improve image quality, and open up clinical applications not otherwise possible. In the examples illustrated above, we only begin to explore the potential of this versatile agent. At the time of writing, the major barriers to the more widespread use of ferumoxytol are availability, cost and the lack of an approved diagnostic label. However, none of these obstacles is insurmountable and there is growing interest in removing all of them, much to the benefit of patient care.

References

- Napoli A, Anzidei M, Marincola BC, Zaccagna F, Geiger D, Di Paolo PL, et al. Optimisation of a high-resolution whole-body MR angiography protocol with parallel imaging and biphasic administration of a single bolus of Gd-BOPTA: preliminary experience in the systemic evaluation of atherosclerotic burden in patients referred for endovascular procedures. *Radiol Med*. 2009;114(4):538-52.
- Villablanca JP, Nael K, Habibi R, Nael A, Laub G, Finn JP. 3 T contrast-enhanced magnetic resonance angiography for evaluation of the intracranial arteries: comparison with time-of-flight magnetic resonance angiography and multislice computed tomography angiography. *Invest Radiol*. 2006;41(11):799-805.
- Guichet PL, Duszak R, Jr., Chaves Cerdas L, Hughes DR, Hindman N, Rosenkrantz AB. Changing National Medicare Utilization of Catheter, Computed Tomography, and Magnetic Resonance Extremity Angiography: A Specialty-focused 16-Year Analysis. *Curr Probl Diagn Radiol*. 2021;50(3):308-314.
- Dodd JD, Leipsic J. Cardiovascular CT and MRI in 2019: Review of Key Articles. *Radiology*. 2020;297(1):17-30.
- Mandell DM, Mossa-Basha M, Qiao Y, Hess CP, Hui F, Matouk C, et al. Intracranial Vessel Wall MRI: Principles and Expert Consensus Recommendations of the American Society of Neuroradiology. *AJNR*. 2017;38(2):218-229.
- Thomsen HS. Nephrogenic systemic fibrosis: a serious adverse reaction to gadolinium - 1997-2006-2016. Part 1. *Acta radiologica* (Stockholm, Sweden : 1987). 2016;57(5):515-20.
- Haneder S, Kucharczyk W, Schoenberg SO, Michaely HJ. Safety of magnetic resonance contrast media: a review with special focus on nephrogenic systemic fibrosis. *Topics in magnetic resonance imaging*: TMRI. 2015;24(1):57-65.
- Malayeri AA, Brooks KM, Bryant LH, Evers R, Kumar P, Reich DS, Bluemke DA. National Institutes of Health Perspective on Reports of Gadolinium Deposition in the Brain. *J Am Coll Radiol*. 2016;13(3):237-41.
- Radbruch A, Weberling LD, Kieslich PJ, Eidel O, Burth S, Kickingereder P, et al. Gadolinium retention in the dentate nucleus and globus pallidus is dependent on the class of contrast agent. *Radiology*. 2015;275(3):783-91.
- Woolen SA, Shankar PR, Gagnier JJ, MacEachern MP, Singer L, Davenport MS. Risk of Nephrogenic Systemic Fibrosis in Patients With Stage 4 or 5 Chronic Kidney Disease Receiving a Group II Gadolinium-Based Contrast Agent: A Systematic Review and Meta-analysis. *JAMA internal medicine*. 2020;180(2):223-230.
- Le Fur M, Caravan P. The biological fate of gadolinium-based MRI contrast agents: a call to action for bioinorganic chemists. *Metallomics: integrated biometal science*. 2019;20;11(2):240-254.
- Neuwelt EA, Hamilton BE, Varallyay CG, Rooney WR, Edelman RD, Jacobs PM, Watnick SG. Ultrasmall superparamagnetic iron oxides (USPIOs): a future alternative magnetic resonance (MR) contrast agent for patients at risk for nephrogenic systemic fibrosis (NSF)? *Kidney international*. 2009;75(5):465-74.
- Bashir MR, Bhatti L, Marin D, Nelson RC. Emerging applications for ferumoxytol as a contrast agent in MRI. *J Magn Reson Imaging*. 2015;41(4):884-98.
- Finn JP, Nguyen KL, Han F, Zhou Z, Salusky I, Ayad I, Hu P. Cardiovascular MRI with ferumoxytol. *Clin Radiol*. 2016;71(8):796-806.
- Toth GB, Varallyay CG, Horvath A, Bashir MR, Choyke PL, Daldrup-Link HE, et al. Current and potential imaging applications of ferumoxytol for magnetic resonance imaging. *Kidney International*. 2017;92(1):47-66.
- Daldrup-Link HE. Ten Things You Might Not Know about Iron Oxide Nanoparticles. *Radiology*. 2017;284(3):616-629.
- Prince MR, Zhang HL, Chabra SG, Jacobs P, Wang Y. A pilot investigation of new superparamagnetic iron oxide (ferumoxytol) as a contrast agent for cardiovascular MRI. *Journal of X-ray science and technology*. 2003;11(4):231-40.
- Food and Drug Administration. Feraheme Label. [cited 2018 February 5]; Available from: https://www.accessdata.fda.gov/drugsatfda_docs/label/2018/022180s009lbl.pdf
- Aime S, Caravan P. Biodistribution of gadolinium-based contrast agents, including gadolinium deposition. *J Magn Reson Imaging*. 2009;30(6):1259-67.
- Lopez A, Cacoub P, Macdougall IC, Peyrin-Biroulet L. Iron deficiency anaemia. *Lancet*. 2016;387(10021):907-16.
- Knobloch G, Colgan T, Wiens CN, Wang X, Schubert T, Hernando D, et al. Relaxivity of Ferumoxytol at 1.5 T and 3.0 T. *Invest Radiol*. 2018;53(5):257-263.
- Nguyen KL, Park EA, Yoshida T, Hu P, Finn JP. Ferumoxytol enhanced black-blood cardiovascular magnetic resonance imaging. *J Cardiovasc Magn Reson*. 2017;19(1):106.
- Buch S, Wang Y, Park MG, Jella PK, Hu J, Chen Y, et al. Subvoxel vascular imaging of the midbrain using USPIO-Enhanced MRI. *Neuroimage*. 2020;220:117106.
- Colbert CM, Thomas MA, Yan R, Radjenovic A, Finn JP, Hu P, Nguyen KL. Estimation of fractional myocardial blood volume and water exchange using ferumoxytol-enhanced magnetic resonance imaging. *Journal of Magnetic Resonance Imaging*. 2021;53(6):1699-1709.
- Nguyen KL YT, Hu P, Finn JP. Ferumoxytol-enhanced cardiac cine MRI in patients with implanted cardiac devices. 25th Annual ISMRM Scientific Sessions; 2017 April 22-27, 2017; Honolulu, HI, USA.
- van Zandwijk JK, Simonis FFJ, Heslinga FG, Hofmeijer EIS, Geelkerken RH, Ten Haken B. Comparing the signal enhancement of a gadolinium based and an iron-oxide based contrast agent in low-field MRI. *PloS one*. 2021;16(8):e0256252.

- 27 Food and Drug Administration. FDA Drug Safety Communication: FDA strengthens warnings and changes prescribing instructions to decrease the risk of serious allergic reactions with anemia drug Feraheme (ferumoxyl). 2015. Available from: <http://www.fda.gov/Drugs/DrugSafety/ucm440138.htm>.
- 28 Nguyen KL, Yoshida T, Kathuria-Prakash N, Zaki IH, Varallyay CG, Finn JP, et al. Multicenter Safety and Practice for Off-Label Diagnostic Use of Ferumoxyl in MRI. *Radiology*. 2019;293(3):554-564.
- 29 Shahrourki P, Moriarty JM, Khan SN, Bista B, Kee ST, DeRubertis BG, Yoshida T, Nguyen KL, Finn JP. High resolution, 3-dimensional Ferumoxyl-enhanced cardiovascular magnetic resonance venography in central venous occlusion. *J Cardiovasc Magn Reson*. 2019;21(1):17.
- 30 Shahrourki P, Khan SN, Yoshida T, Iskander PJ, Ghahremani S, Finn JP. High-resolution three-dimensional contrast-enhanced magnetic resonance venography in children: comparison of gadofosveset trisodium with ferumoxyl. *Pediatr Radiol*. 2022;52(3):501-512.
- 31 Cushman M. Epidemiology and risk factors for venous thrombosis. *Semin Hematol*. 2007;44(2):62-9.
- 32 Ghaye B, Szapiro D, Willems V, Dondelinger RF. Pitfalls in CT venography of lower limbs and abdominal veins. *AJR American journal of roentgenology*. 2002;178(6):1465-71.
- 33 Finn JP, Zisk JH, Edelman RR, Wallner BK, Hartnell GG, Stokes KR, Longmaid HE. Central venous occlusion: MR angiography. *Radiology*. 1993;187(1):245-51.
- 34 Miyazaki M, Akahane M. Non-contrast enhanced MR angiography: established techniques. *J Magn Reson Imaging*. 2012;35(1):1-19.
- 35 Han F, Rapacchi S, Khan S, Ayad I, Salusky I, Gabriel S, Plotnik A, Finn JP, Hu P. Four-dimensional, multiphase, steady-state imaging with contrast enhancement (MUSIC) in the heart: a feasibility study in children. *Magn Reson Med*. 2015;74(4):1042-9.
- 36 Nguyen KL, Han F, Zhou Z, Brunengraber DZ, Ayad I, Levi DS, Satou GM, Reemtsen BL, Hu P, Finn JP. 4D MUSIC CMR: value-based imaging of neonates and infants with congenital heart disease. *J Cardiovasc Magn Reson*. 2017;19(1):40.
- 37 Zhou Z, Han F, Rapacchi S, Nguyen KL, Brunengraber DZ, Kim GJ, Finn JP, Hu P. Accelerated ferumoxyl-enhanced 4D multiphase, steady-state imaging with contrast enhancement (MUSIC) cardiovascular MRI: validation in pediatric congenital heart disease. *NMR Biomed*. 2017;30(1).
- 38 Han F, Zhou Z, Han E, Gao Y, Nguyen KL, Finn JP, Hu P. Self-gated 4D multiphase, steady-state imaging with contrast enhancement (MUSIC) using rotating cartesian K-space (ROCK): Validation in children with congenital heart disease. *Magn Reson Med*. 2017;78(2):472-483.
- 39 Nguyen KL, Ghosh RM, Griffin LM, Yoshida T, Bedayat A, Rigsby CK, Fogel MA, Whitehead KK, Hu P, Finn JP. Four-dimensional Multiphase Steady-State MRI with Ferumoxyl Enhancement: Early Multicenter Feasibility in Pediatric Congenital Heart Disease. *Radiology*. 2021;300(1):162-173.
- 40 Di Sopra L, Piccini D, Coppo S, Stuber M, Yerly J. An automated approach to fully self-gated free-running cardiac and respiratory motion-resolved 5D whole-heart MRI. *Magn Reson Med*. 2019;82(6):2118-2132.
- 41 Shahrourki P, Nguyen KL, Moriarty JM, Plotnik AN, Yoshida T, Finn JP. Minimizing table time in patients with claustrophobia using focused ferumoxyl-enhanced MR angiography (f-FEMRA): a feasibility study. *Br J Radiology*. 2021;94(1125):20210430.



Contact

J. Paul Finn, M.D.
Department of Radiological Sciences
University of California Los Angeles
Peter V. Ueberroth Building, Suite 3371
10945 Le Conte Ave
Los Angeles, CA 90095-7206
USA
pfinn@mednet.ucla.edu

Advertisement

Learn more about Cardiovascular MRI

Multi-contrast, Multi-dimensional Imaging:

What's next in CMR?

Claudia Prieto Vasquez, PhD (King's College London, UK)

GOHeart including Cardiac Dot Engine

Johan Dehem, MD (Jan Yperman Ziekenhuis, Ieper, Belgium)

Novel Methods in Signal Generation and Reconstruction

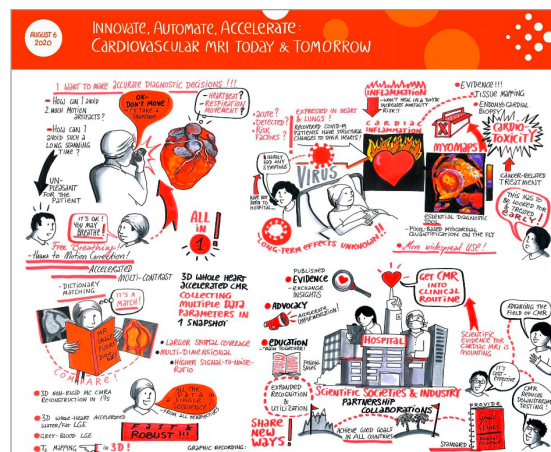
Rizwan Ahmad, PhD (Ohio State University, Chicago, IL, USA)

AI and Deep Learning. Where is CMRI heading to?

Vivek Muthurangu, MD (University College London, UK)

Don't miss this valuable source of information

[siemens-healthineers.com/MWS2020-recordings](https://www.siemens-healthineers.com/MWS2020-recordings)



Graphic Recording: [gabriele-heinzel.com](https://www.gabriele-heinzel.com)

3D Whole Heart Applications: Angiography and Delayed Enhancement

Jason Craft¹, Joshua Y. Cheng¹, Nancy Diaz¹, Karl P. Kunze², Michaela Schmidt³

¹St. Francis Heart Hospital, DeMatteis Research Center, Greenvale, NY, USA

²Siemens Healthcare Limited, Frimley, UK

³Siemens Healthineers, Erlangen, Germany

Introduction

It has become more important than ever before to diversify non-invasive imaging methods that involve contrast media administration. Compared to CT imaging, MRI does not involve nephrotoxic iodinated contrast or ionizing radiation. However, ungated first pass magnetic resonance angiography (MRA) cannot effectively freeze cardiac motion; and provides reduced quality of segmentation compared to CT pulmonary vein angiography [1]. Diaphragmatic navigator (dNAV) used for motion correction is associated with unpredictable scan times when respiration is irregular, and imperfect slab tracking ratio [2]. Furthermore, approximately 50–100 Hz off-resonance is frequently observed at the interface of the pulmonary veins and left atrium

due to susceptibility effects and inflow from the lungs [3]. Therefore, the use of balanced steady-state free precession (bSSFP) and fat saturation pulses, particularly at higher field strengths, can be technically unsatisfactory for this application. Thus, the unmet clinical need is to provide robust clinical angiographic methods that can effectively image complex patients with arrhythmias, while minimizing image artifacts.

Instead of tracking the diaphragmatic interface, image navigators (iNAV) track the blood pool contrast of the left ventricle [4]. 2D translational motion in the head-to-foot direction can be extracted and estimated on a per cardiac cycle basis and is used to bin data with

Imaging parameters for whole heart MRA and LGE			
Sequence	Inversion recovery GRE	Saturation recovery GRE	Inversion recovery Dixon GRE
FOV	320 mm (axial)	320 mm (axial)	320 mm (axial)
Spatial resolution	1.3 × 1.3 mm	1.3 × 1.3 mm	1.3 × 1.3 mm
Slice thickness	1.4 mm	1.4 mm	1.4 mm
Slice resolution	90%	90%	90%
Fat Sat	No	Yes	No
Acceleration Factor	2.9	2.9	2.8
Bandwidth	579 Hz/px	579 Hz/px	453 Hz/px
Flip angle	18°	18°	15°
TI/Saturation time	220–260 ms (systolic) 290 ms (diastolic)	150 ms	According to scout
TE/TR	1.42 ms/3.89 ms	1.42 ms/3.89 ms	2.38, 4.76 ms/6.97 ms
Data window duration	62–130 ms	62–130 ms	62–130 ms

Table 1: 3D whole heart sequence parameters.

respect to respiration. 3D image volumes are obtained using a non-rigid motion-compensated reconstruction of all binned data [5, 6], leading to 100% scan efficiency and predictable scan time. The sampling pattern consists of spiral-like interleaves acquired alternately based on the golden angle of rotation (variable-density golden-step Cartesian trajectory with spiral profile order sampling, or VD-CASPR)¹ [7].

As a result of scanning more efficiently, the predictable scan time translates into less gadolinium-based contrast agent (GBCA) use. Specifically, compared to dNAV based applications, we can use 33% less contrast [8, 9], and we can do it without the need for higher field strengths. Furthermore, we can acquire angiography and delayed enhancement at higher near isotropic spatial resolution. We acquire all 3D datasets at a true spatial resolution of $1.3 \times 1.3 \times 1.5 \text{ mm}^3$, with a reconstructed slice thickness of 1.4 mm (Table 1).

Pulmonary vein angiography and arterial delayed enhancement using iNAV

At our institution, we are asked to provide pulmonary vein anatomical imaging for segmentation and importation into the electro-anatomical mapping system. With MRI, not only is anatomical information obtained, but functional information such as atrial and ventricular volumetrics, left atrial delayed enhancement, and quantification of valvular heart disease. Obtaining one MRI examination is simply more logistically efficient than obtaining CT angiography plus echocardiography imaging. Our 3D MRA and late gadolinium enhancement (LGE) imaging is performed on a 1.5T MAGNETOM Sola, but our institution also has experience with the 3D inversion recovery Dixon multi-echo gradient recalled echo (GRE)¹ performed on the 3T MAGNETOM Skyra platform.

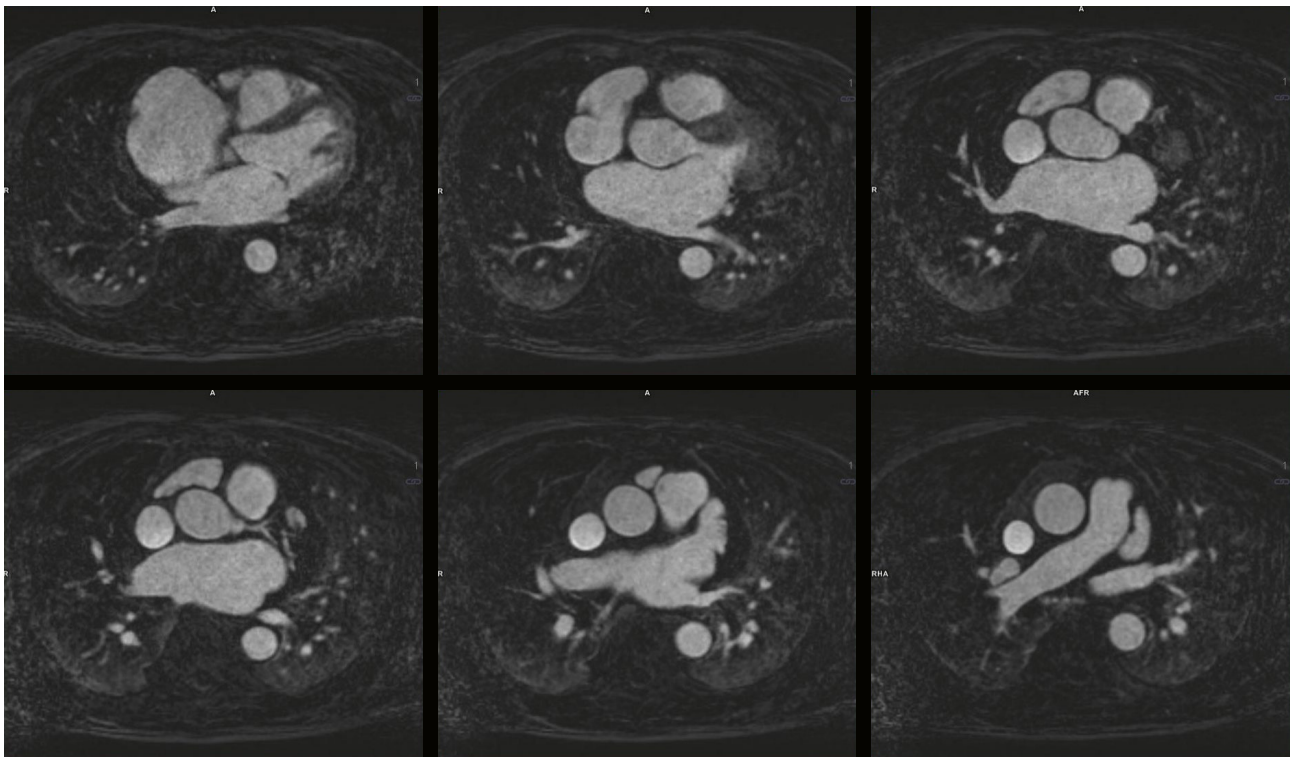
Concerning the MRA and LGE exam workflow, the image navigator and saturation band position can be automatically determined using free-breathing 3 plane localizers and the AI cardiac scan companion (AICSC)¹ prototype. The diastolic or systolic rest period of the left atrium can be determined using the included high temporal resolution free breathing 4-chamber (or HLA) cine [10]. The user can manually determine the data window duration, or this can be automatically determined based on the rest period of the right coronary artery by the AICSC. Given the diastolic rest period is longer at slower ventricular rates, we prefer diastolic imaging at regular heart rhythms < 80 BPM. When the ventricular rate is > 80 BPM or significant arrhythmia such as atrial fibrillation is present, systolic imaging is preferential.

In addition to the prototype sequence¹ for syngo XA20 featuring 3D inversion recovery Dixon multi-echo GRE, 3D

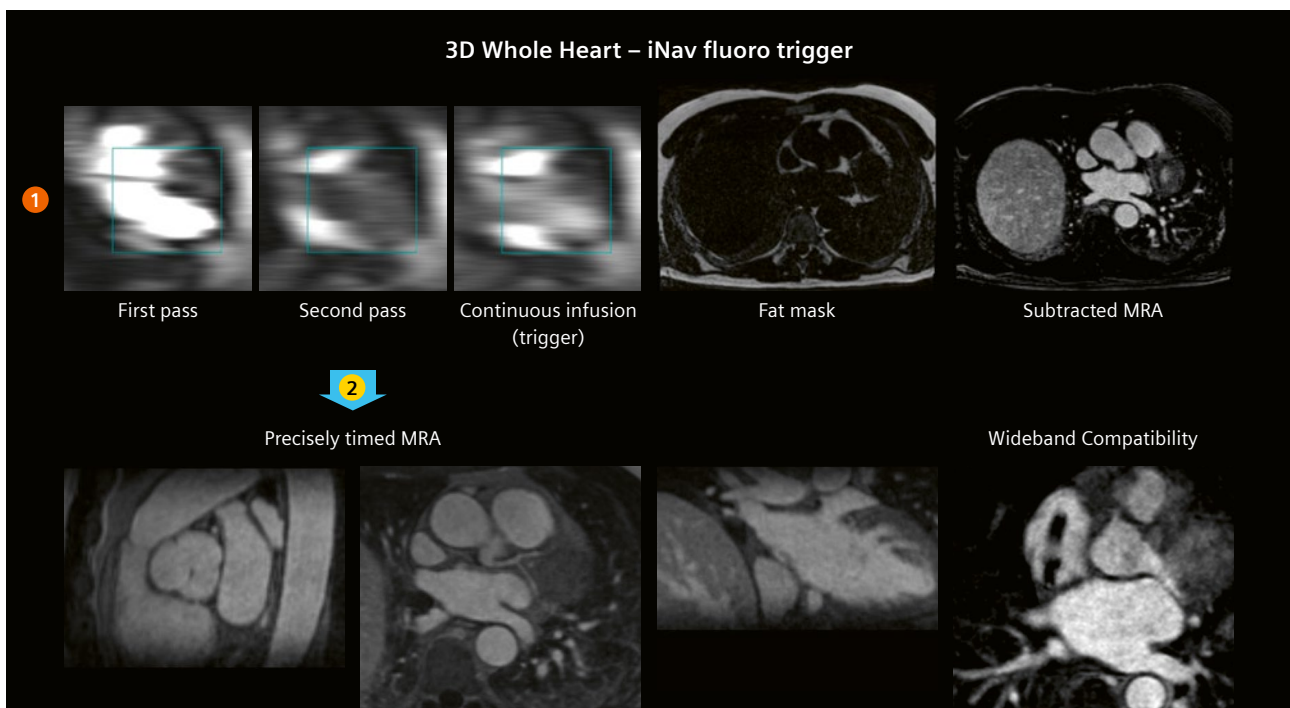
T2 prep bSSFP, and 3D T2 Prep Dixon multi-echo GRE, the user can configure different preparatory pulses to manipulate image contrast. We acquire pulmonary vein angiography using either inversion recovery GRE or saturation recovery GRE. Both methods have respective strengths and weaknesses. Inversion recovery maintains vessel sharpness and is compatible with the 1500 Hz wideband pulse which mitigates device artifacts. Furthermore, inversion recovery can be used without fat saturation, which makes this option especially attractive at higher field strengths. The inversion time parameter at 1.5T represents a balance between SNR and background suppression-values range from 220 ms to 300 ms at 1.5T [11–14]. Similar to previous literature [15], we have observed that image contrast is quite consistent even with irregular rhythms; iNAV tracking similarly remains quite robust despite the dependence of the beat-to-beat image contrast on the RR interval. Figure 1 depicts excellent image quality despite underlying atrial fibrillation, using inversion recovery GRE. Saturation recovery images have overall higher signal-to-noise, and can be used without manipulation of the inversion time parameter.

Simplifying the contrast injection scheme is important to reduce human error and to optimize workflow. Our contrast injection scheme does not involve the use of look-up tables, saline dilution, or manipulation of extra tubing and/or stop cocks. To provide adequate signal for iNAV tracking, 0.05 mmol/kg of 1 molar contrast agent is injected at 2 ml/sec, followed by 20 ml of saline at the same rate. Immediately after, the remaining 0.10 mmol/kg contrast is administered as a slow infusion, followed by saline at the same rate (0.2 ml/sec). The contrast is injected after starting the first 3D scan, and after observing satisfactory cardiac gating and appropriate iNAV placement prescription. This scan is solely run for the iNAV functionality in order to visualize contrast passage and arrival. The first, second pass, and continuous infusion dose is observed passing through the heart (Fig. 2). The first 3D scan is stopped as soon as the contrast peaks in the pulmonary artery. The exact same protocol is restarted by using STOP/CONTINUE on the inline display (which was linked by the copy reference “copy everything”). We target a maximum scan duration of 4 minutes given the length of the contrast administration and need to perform other imaging prior to delayed enhancement. 15 minutes after the initial injection of GBGA, we perform delayed enhancement of the left atrium using the inversion recovery Dixon multi-echo GRE whole heart sequence at identical spatial resolution. If desired, residual fat can be subtracted from the 3D MRA using the inversion recovery Dixon multi-echo.

¹Work in progress. The application is currently under development and is not for sale in the U.S. and in other countries. Its future availability cannot be ensured.



1 3D whole heart MRA inversion recovery subtracted images from a patient in atrial fibrillation.



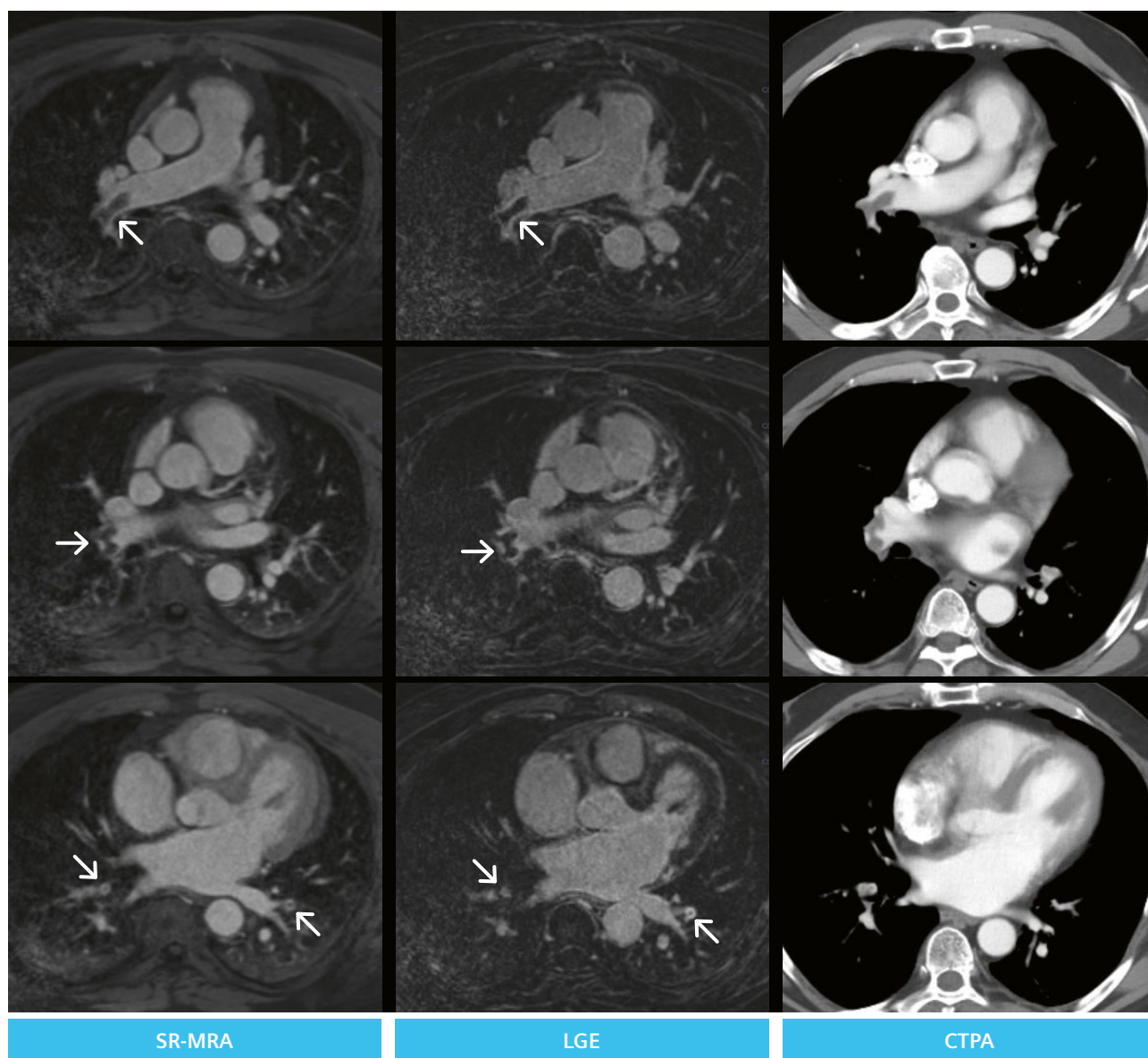
2 The iNAV fluoro trigger method for MR angiography. Two identical 3D whole heart program steps are created in the workflow. The first step (1) is used only for monitoring the passage of contrast with the iNAV. The second step (2), which will run to completion, is triggered at the peak of the continuous infusion in the pulmonary artery.

GRE fat image as a mask. As mentioned, because of the scan efficiency of the iNAV and precision timing of the contrast infusion, we are able to reduce contrast from 0.20 mmol/kg to 0.15 mmol/kg while still providing robust image quality whether patient is in sinus rhythm or has atrial fibrillation.

Case 1

A 59-year-old male was referred for evaluation of COVID-19 myocarditis and to evaluate the left atrial appendage. The patient contracted COVID-19 three weeks prior; one week prior to cardiac MRI imaging, the patient had new onset

atrial fibrillation and dyspnea on exertion. Ventricular function with bSSFP cine demonstrated enlargement of the right ventricle with mildly reduced systolic function. Revised Lake Louise criteria was not met for acute myocarditis; however the patient had bilateral pulmonary emboli involving the right middle, right upper, right lower, and left lower segmental branches, with thrombus extending into the right main pulmonary artery. There was no evidence of left atrial appendage thrombus. Figure 3 illustrates the findings on 3D whole heart saturation recovery angiography and inversion recovery Dixon multi-echo GRE. Subsequent CT pulmonary angiogram agreed with MRI findings, and ultrasound Doppler was positive for



3 Incidentally discovered bilateral pulmonary emboli (arrowheads). From left to right column: saturation recovery MRA, inversion recovery Dixon multi-echo GRE, and CT pulmonary angiography.

acute right popliteal deep venous thrombosis. It is important to understand that CT pulmonary venography is timed to opacification of the left atrium; therefore abnormalities involving the pulmonary arteries may be incompletely characterized. Imaging with 3D whole heart, however, does not suffer from this limitation.

3D left ventricular delayed enhancement

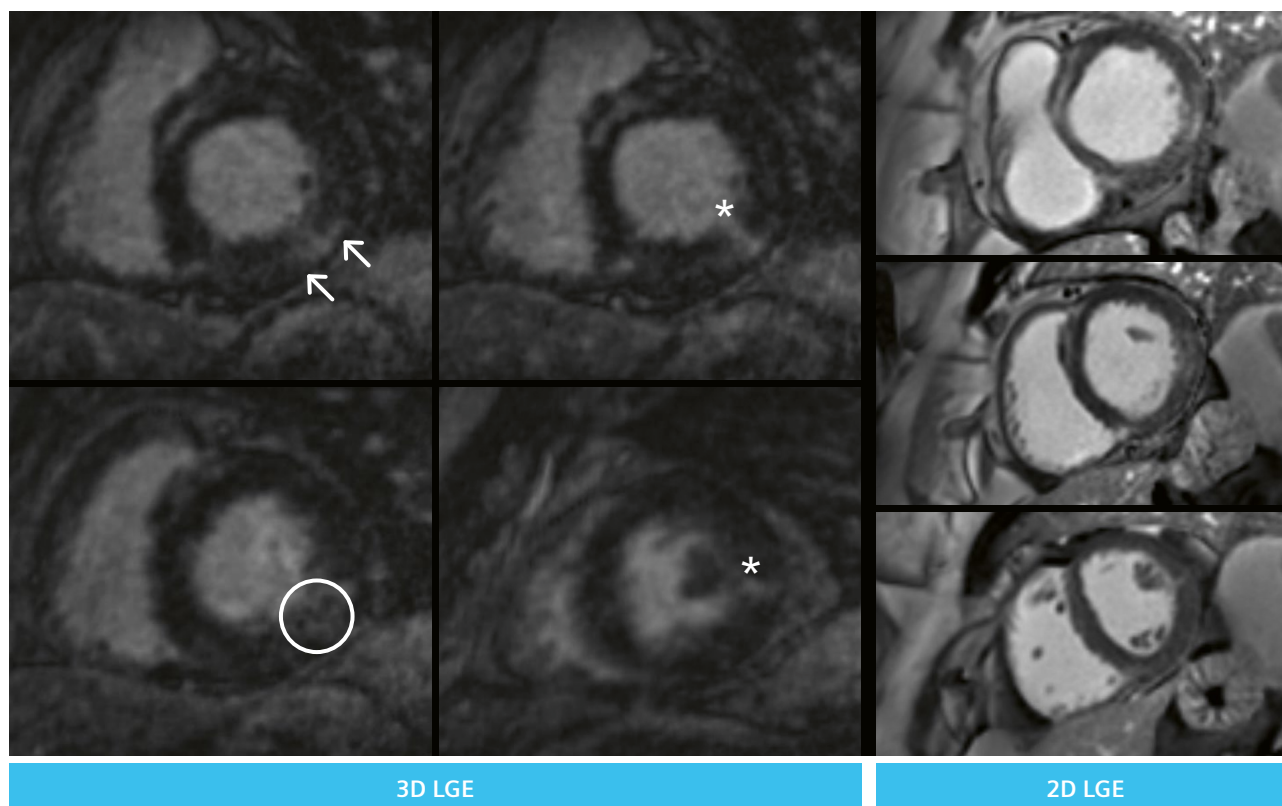
In most cases, 2D PSIR LGE can provide sufficient detail and quantification of left ventricular scar burden. However there are clinical scenarios where providing a 3D dataset is beneficial, such as pre-planning for electrophysiology procedures, or for improved visualization of the right ventricle [16]. Specifically, 3D high resolution LGE can identify substrate features that may be subtle or absent on 2D imaging. By acquiring these 3D datasets in high resolution and reduced partition thickness we can minimize partial volume effects, allow for visualization of heterogeneity within regions of enhancement, scar channels, and the presence of epicardial components. Here, the user has flexible options: the 3D inversion recovery Dixon multi-echo GRE which provides more robust fat separation and is most beneficial at 3T; whereas fat saturated inversion recovery GRE can be used for scan efficiency at 1.5T. Both methods are compatible with the 1500 Hz wideband pulse

which suppresses metallic artifacts caused by implanted devices such as ICDs or pacemakers.²

Case 2

A 67-year-old male referred for evaluation of non-sustained ventricular tachycardia (NSVT). The patient has frequent ventricular arrhythmia throughout the study, and ventricular function was only possible by using compressed sensing real time cine. Whole heart inversion recovery with fat sat LGE demonstrates heterogenous inferolateral scar with clear borders, scar channels, and epicardial component. A transmural segment of enhancement is also demonstrated in the mid anterolateral wall. 3D LGE with a restrictive temporal window is able to capture small and relevant details missing in the traditional 2D approach. This is only possible due to the 100% efficiency of the iNAV since we can trade acquisition efficiency for a smaller data acquisition window. In contrast, 2D PSIR LGE effectively freezes cardia

²The MRI restrictions (if any) of the metal implant must be considered prior to patient undergoing MRI exam. MR imaging of patients with metallic implants brings specific risks. However, certain implants are approved by the governing regulatory bodies to be MR conditionally safe. For such implants, the previously mentioned warning may not be applicable. Please contact the implant manufacturer for the specific conditional information. The conditions for MR safety are the responsibility of the implant manufacturer, not of Siemens Healthineers.



4 Comparison of 3D LGE vs 2D LGE. 3D LGE clearly demonstrates a heterogenous rim-like area of enhancement (circle), scar channels (asterisks), and epicardial component to scar (arrows). Features are ill-descript on 2D LGE.

motion, but incompletely characterizes respective areas of enhancement (Fig. 4).

Summary

In addition to what has already been described in this article, the potential for 3D whole heart to similarly accelerate coronary MRA has also been explored [17]. Submillimeter isotropic spatial resolution, with faithful representation of detail compared with the fully sampled reference can be obtained in a fraction of the time. Likewise, whole chest

non-contrast MRA can be acquired more efficiently with 3D T2 prep fat saturated bSSFP at 1.5T [18] or using 3D T2 prep Dixon GRE at 3T. In conclusion, 3D whole heart is a versatile and robust package that overcomes the limitations of traditional dNAV methods for motion correction, combining VD-CASPR and iNAVs for acquisition and SNR efficiency as well as predictable scan time. Furthermore, AI based automatic positioning features and rest period scout facilitate ease of use for new and experienced users alike.

References

- Dong J, Dickfeld T, Dalal D, Cheema A, Vasamreddy CR, Henrikson CA, Marine JE, Halperin HR, Berger RD, Lima JA, Bluemke DA, Calkins H. Initial experience in the use of integrated electroanatomic mapping with three-dimensional MR/CT images to guide catheter ablation of atrial fibrillation. *J Cardiovasc Electrophysiol.* 2006;17: 459-66.
- Moghari MH, Hu P, Kissinger KV, Goddu B, Goepfert L, Ngo L, Manning WJ, Nezafat R. Subject-specific estimation of respiratory navigator tracking factor for free-breathing cardiovascular MR. *Magn Reson Med.* 2012;67(6):1665-72.
- Hu P, Peters DC, Stoeck C, Kissinger KV, Goddu B, Goepfert L, Manning WJ, Nezafat R. Off-resonant pulmonary vein imaging. *J Cardiovasc Magn Reson.* 2009;11(Suppl 1):P185.
- Henningsson M, Koken P, Stehning C, Razavi R, Prieto C, Botnar RM. Whole-heart coronary MR angiography with 2D self-navigated image reconstruction. *Magn Reson Med.* 2012;67(2):437-45.
- Cruz G, Atkinson D, Henningsson M, Botnar RM, Prieto C. Highly efficient nonrigid motion-corrected 3D whole-heart coronary vessel wall imaging. *Magn Reson Med.* 2017;77(5):1894-1908.
- Zeilinger MG, Kunze KP, Munoz C, Neji R, Schmidt M, Croisille P, Heiss R, Wuest W, Uder M, Botnar RM, Treutlein C, Prieto C. Non-rigid motion-corrected free-breathing 3D myocardial Dixon LGE imaging in a clinical setting. *Eur Radiol.* 2022;32(7):4340-4351.
- Munoz C, Bustin A, Neji R, Kunze KP, Forman C, Schmidt M, Hajhosseiny R, Masci PG, Zeilinger M, Wuest W, Botnar RM, Prieto C. Motion-corrected 3D whole-heart water-fat high-resolution late gadolinium enhancement cardiovascular magnetic resonance imaging. *J Cardiovasc Magn Reson.* 2020;22(1):53.
- Bustin A, Sridi S, Gravinay P, Legghe B, Gosse P, Ouattara A, Rozé H, Coste P, Gerbaud E, Desclaux A, Boyer A, Prevel R, Gruson D, Bonnet F, Issa N, Montaudon M, Laurent F, Stuber M, Camou F, Cochet H. High-resolution Free-breathing late gadolinium enhancement Cardiovascular magnetic resonance to diagnose myocardial injuries following COVID-19 infection. *Eur J Radiol.* 2021;144:109960.
- Tandon A, James L, Henningsson M, Botnar RM, Potersnak A, Greil GF, Hussain T. A clinical combined gadobutrol bolus and slow infusion protocol enabling angiography, inversion recovery whole heart, and late gadolinium enhancement imaging in a single study. *J Cardiovasc Magn Reson.* 2016;18(1):66.
- Yoon SS, Hoppe E, Schmidt M, Forman C, Chitiboi T, Sharma P, Tillmanns C, Maier A, Wetzl JA. Robust Deep-Learning-based Automated Cardiac Resting Phase Detection: Validation in a Prospective Study. *Proc Intl Soc Mag Reson Med.* 2020;28:2210.
- Dabir D, Naehle CP, Clauberg R, Gieseke J, Schild HH, Thomas D. High-resolution motion compensated MRA in patients with congenital heart disease using extracellular contrast agent at 3 Tesla. *J Cardiovasc Magn Reson.* 2012;14:75.
- Lam CZ, Pagano JJ, Gill N, Vidarsson L, de la Mora R, Seed M, Grosse-Wortmann L, Yoo SJ. Dual phase infusion with bolus tracking: technical innovation for cardiac and respiratory navigated magnetic resonance angiography using extracellular contrast. *Pediatr Radiol.* 2019;49(3):399-406.
- Febbo JA, Galizia MS, Murphy IG, Popescu A, Bi X, Turin A, Collins J, Markl M, Edelman RR, Carr JC. Congenital heart disease in adults: Quantitative and qualitative evaluation of IR FLASH and IR SSFP MRA techniques using a blood pool contrast agent in the steady state and comparison to first pass MRA. *Eur J Radiol.* 2015;84(10):1921-1929.
- Zheng J, Bae KT, Woodard PK, Haacke EM, Li D. Efficacy of slow infusion of gadolinium contrast agent in three-dimensional MR coronary artery imaging. *J Magn Reson Imaging.* 1999;10(5):800-805.
- Groarke JD, Waller AH, Vita TS, Michaud GF, Di Carli MF, Blankstein R, Kwong RY, Steigner M. Feasibility study of electrocardiographic and respiratory gated, gadolinium enhanced magnetic resonance angiography of pulmonary veins and the impact of heart rate and rhythm on study quality. *J Cardiovasc Magn Reson.* 2014 ;16(1):43.
- Ghonim S, Ernst S, Keegan J, Giannakidis A, Spadotto V, Voges I, Smith GC, Boutsikou M, Montanaro C, Wong T, Ho SY, McCarthy KP, Shore DF, Dimopoulos K, Uebing A, Swan L, Li W, Pennell DJ, Gatzoulis MA, Babu-Narayan SV. Three-Dimensional Late Gadolinium Enhancement Cardiovascular Magnetic Resonance Predicts Inducibility of Ventricular Tachycardia in Adults With Repaired Tetralogy of Fallot. *Circ Arrhythm Electrophysiol.* 2020;13(11):e008321.
- Bustin A, Ginami G, Cruz G, Correia T, Ismail TF, Rashid I, Neji R, Botnar RM, Prieto C. Five-minute whole-heart coronary MRA with sub-millimeter isotropic resolution, 100% respiratory scan efficiency, and 3D-PROST reconstruction. *Magn Reson Med.* 2019;81(1):102-115.
- Hajhosseiny R, Rashid I, Bustin A, Munoz C, Cruz G, Nazir MS, Grigoryan K, Ismail TF, Preston R, Neji R, Kunze K, Razavi R, Chiribiri A, Masci PG, Rajani R, Prieto C, Botnar RM. Clinical comparison of sub-mm high-resolution non-contrast coronary CMR angiography against coronary CT angiography in patients with low-intermediate risk of coronary artery disease: a single center trial. *J Cardiovasc Magn Reson.* 2021;23(1):57.



Contact

Jason Craft, M.D.
Department of Cardiovascular Imaging
St. Francis Heart Hospital
DeMatteis Research Center
101 Northern Blvd
Greenvale NY, 11548
USA
Jason.craft@chsli.org

Addressing Flow and Pulsation-Associated Artifacts in TOF-MRA in Children

Ayaz Khan¹; Peter Kollasch²; Chris Goode¹; Asim Bag¹

¹St Jude Children's Research Hospital, Memphis, TN, USA

²Siemens Medical Solutions, Malvern, PA, USA

Introduction: MR angiography

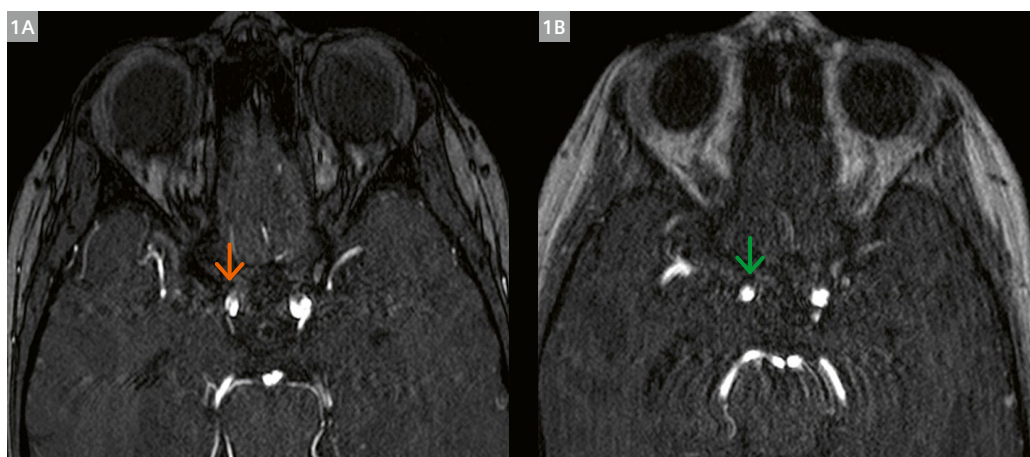
Time-of-flight [1] magnetic resonance angiography (TOF-MRA) images vascular structures without contrast [2, 3]. As its name suggests, TOF uses the phenomena of fresh blood flow into the imaging plane, which increases the signal intensity and causes blood to appear brighter than the surrounding tissue on the images [2, 3].

TOF-MRA utilizes multiple radio frequency (rf) pulses to saturate the magnetization of the spins in the imaging plane, while the moving spins in the blood vessel outside the imaging plane are not affected. Upon entering the imaging plane, these unsaturated spins result in higher signal than the stationary spins, which remain saturated. However, in-plane moving spins eventually also experience the saturation pulses and lose signal compared to the through-plane moving spins, which are always unaffected [4]. Additional in-plane spin signal loss arises from the fact that the phase of spin changes under the influence of the gradient field, although the gain and loss phases depend on the direction of the flow. In-plane flow and an area of vascular turbulence may cause signal loss [5].

To overcome the loss of signal in moving spins due to prolonged saturation RF bands, multiple thin slabs are acquired in 3D using a technique called multiple overlapping thin slab acquisition (MOTSA) [6]. This restricts the number of slices per slab and subsequently shortens saturation RF bands, which minimizes the saturation effect in the moving spin.

Using the current standard sequence in children

Standard MRA sequence: The standard TOF-MRA sequence that Siemens Healthineers provides on its scanners is optimized for adults. Some of the relevant parameters are shown in Table 1. For use with children, particularly those with sickle cell disease or those affected by radiation arthritis, the sequence will require some changes to compensate for the artifacts that may arise from turbulent flow caused by arterial stiffness or lumen narrowing [7]. Turbulent or slow flow reduced the T2 relaxation due to the spin dephasing [8]. To overcome the loss of signal caused by lower T2 relaxation, it is recom-



1 (1A) Orange arrow shows the pulsation artifact in the direction of phase encoding (right to left), which misregistered the vessel lumen. (1B) Green arrow shows the same vessel with no artifact.

mended to use shortest TE possible. To achieve that, we must also adjust other associated parameters (Table 1).

Common imaging practices: In MR imaging, choosing phase encoding (PE) direction is generally directed by the size of the region, to avoid any phase wrap. Unlike frequency encoding (FE), a higher number of data acquisitions in the PE direction costs extra time. Therefore, acquiring the PE in a shorter distance over the area of interest is common practice to keep the scan time lower. However, this strategy is not always ideal. For example, flow artifacts originating from eye movement could demand a change of PE direction to avoid propagation of the artifacts into the brain, resulting in a longer scan time. Pulsation artifacts arising from arteries is another example and could result in over- or underestimating the lumen in a segment of the vessels.

In this paper, we address turbulent flow and arterial pulsation-related artifacts in pediatric imaging and propose adaptations to improve MRA imaging quality in children.

Parameters	Standard sequence	Proposed pediatric sequence
TR	21 ms	25 ms
TE	3.42 ms	2.51 ms
Flip angle (FA)	18°	25°
Bandwidth (BW)	180 Hz/Px	448 Hz/Px

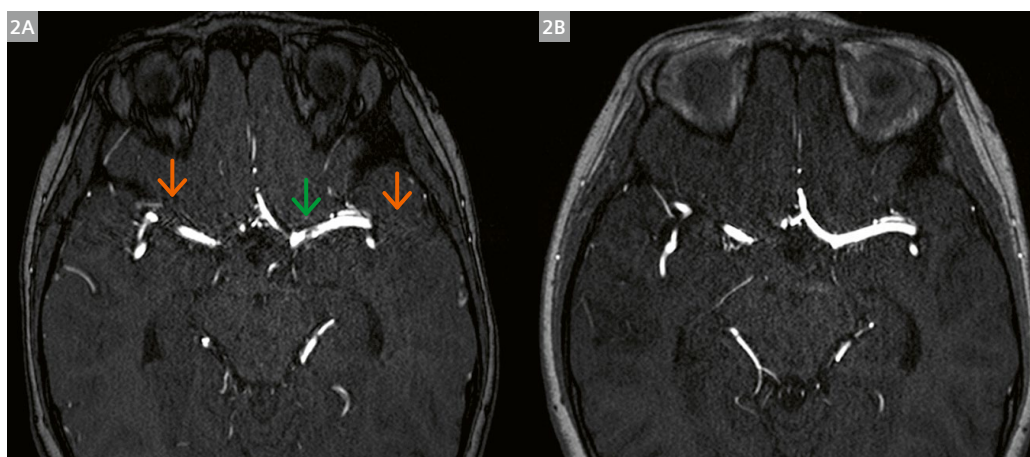
Table 1: Imaging parameters

Background

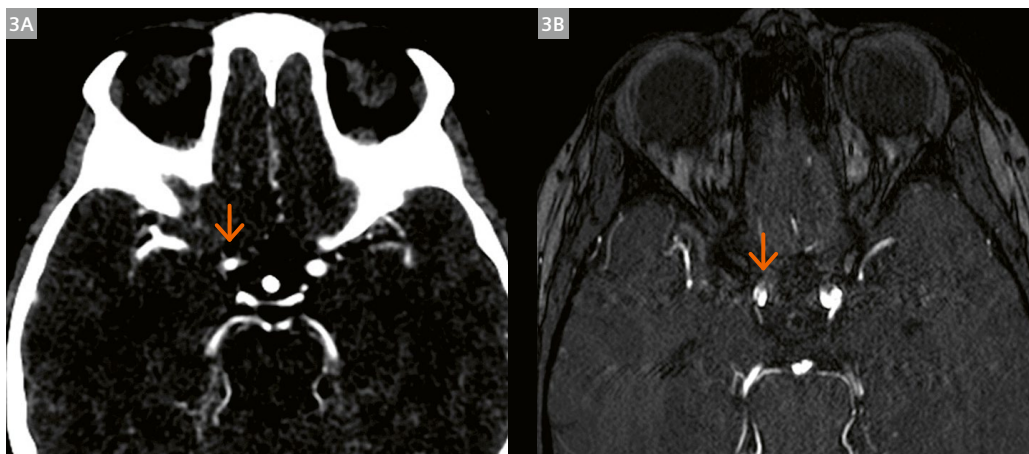
Acquiring TOF-MRA in the axial plane is common practice with right-to-left PE [9], avoiding artifacts from eye motion. However, pulsation artifacts arising from the middle cerebral artery (MCA) remain a challenge. Alongside any turbulent flow in the artery, running in-plane will create challenges in the form of signal loss that mimics vessel occlusion. In our case, we observed both phenomena in the form of occlusion in one segment of the MCA (Fig. 1A), and underestimation of the lumen at the bifurcation segments of the MCA (Fig. 2A). Occlusion-mimicking effects occurred consistently in one patient over several scans during the period, while a computed tomography angiogram (CTA) confirmed there was no occlusion, as shown in Figure 3. This finding triggered the discussion which led us to adapt the sequence to better serve pediatric patients by addressing the turbulent flow-related artifacts in sickle cell disease.

Sequence adaptation

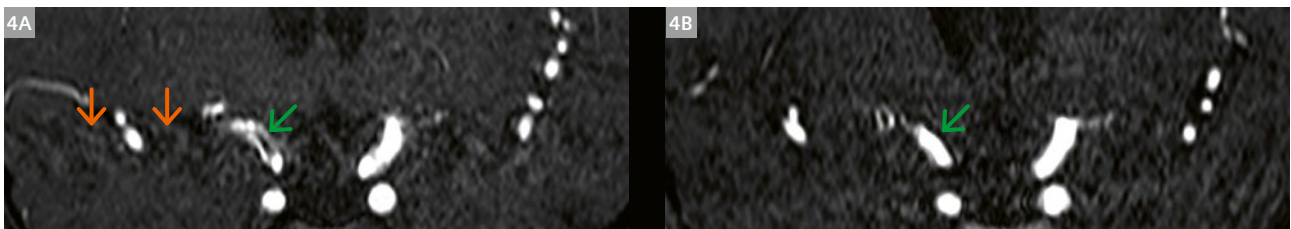
We made the following changes to the standard MRA sequence from Siemens Healthineers to minimize the phase dispersion by reducing TE and the associated parameters (Table 1): We increased the receiver bandwidth (BW) to 448 Hz/Px from 180 Hz/Px in the current sequence (thus increasing the sampling rate), which helped reduce the TE to 2.8 ms (original TE = 3.5 ms). We also changed the voxel size by reducing the resolution to 0.6 mm from 0.5 mm isotropic, which helped achieve a more suitable scan time and compensate for SNR. Increasing the TR to 25 ms helped with higher flow and therefore more signal. We increased the flip angle to 25°, which allows better background suppression.



2 (2A) Orange arrows show the pulsation artifact in the direction of phase encoding, and the green arrow shows the manifestation of possible turbulent flow. (2B) None of these artifacts are visible in the adapted sequence.



3 (3A) CTA shows normal flow as indicated by the arrow. (3B) MRA shows an occlusion-mimicking flow artifact due to a pulsation artifact.



4 Reformatted coronal images from (4A) the standard sequence and (4B) the adapted sequence. Orange arrows show the flow-related pulsation artifacts. The green arrow in (4A) shows the segment of the artery mimicking occlusion, while in image (4B) this artifact is not noticed.

Although these changes did not overcome the artifacts completely, they reduced them enough to provide much better images of the in-plane vessels. Figure 2 shows the images acquired using the standard sequence and the adapted sequence. The occlusion seen in the standard scans does not appear in the scans using the adapted sequence (Fig. 1B). Figure 4 shows coronal reformatted images from the standard and adapted sequences comparing the occlusion.

References

- Galldiks N, Rapp M, Stoffels G, Fink GR, Shah NJ, Coenen HH, et al. Response assessment of bevacizumab in patients with recurrent malignant glioma using [18F]Fluoroethyl-L-tyrosine PET in comparison to MRI. *Eur J Nucl Med Mol Imaging*. 2013;40(1):22–33.
- Edelman RR. Basic Principles of Magnetic Resonance Angiography. *Cardiovasc Intervent Radiol*. 1992;15(1):3–13.
- Laub G. [Basic principles of MR angiography. An introduction]. *Radiologe*. 1994;34(8):416–422.
- Haacke EM, Masaryk TJ, Wielopolski PA, Zypman FR, Tkach JA, Amatur S, et al. Optimizing blood vessel contrast in fast three-dimensional MRI. *Magn Reson Med*. 1990;14(2):202–221.
- Ozsarlak O, Van Goethem JW, Maes M, Parizel PM. MR angiography of the intracranial vessels: technical aspects and clinical applications. *Neuroradiology*. 2004;46(12):955–972.
- Blatter DD, Parker DL, Robison RO. Cerebral MR angiography with multiple overlapping thin slab acquisition. Part I. Quantitative analysis of vessel visibility. *Radiology*. 1991;179(3):805–811.
- Rivera CP, Veneziani A, Ware RE, Platt MO. Original Research: Sickle cell anemia and pediatric strokes: Computational fluid dynamics analysis in the middle cerebral artery. *Exp Biol Med (Maywood)*. 2016;241(7):755–765.
- Lenz GW, Haacke EM, Masaryk TJ, Laub G. In-plane vascular imaging: pulse sequence design and strategy. *Radiology*. 1988;166(3):875–882.
- Herholz K, Hölzer T, Bauer B, Schröder R, Voges J, Ernestus RI, et al. 11C-methionine PET for differential diagnosis of low-grade gliomas. *Neurology*. 1998;50(5):1316–1322.

Contact

Ayaz M. Khan, Ph.D.
Clinical MR Physicist / MR Safety Expert
St. Jude Children's Research Hospital
Department of Diagnostic Imaging
262 Danny Thomas Place, Mail Stop 220
Memphis, TN 38015
USA
Tel: +1 901-595-7336
ayaz.khan@stjude.org



Musculoskeletal MRI in Children: How We Do It

Małgorzata Grzywińska, M.Sc.^{1,2}; Dominik Świętoń, M.D.^{2,3}

¹Neuroinformatic and Artificial Intelligence Lab, Department of Human Physiology, Medical University of Gdansk, Poland

²Department of Radiology, University Clinical Centre in Gdansk, Poland

³2nd Department of Radiology, Medical University of Gdansk, Poland

Introduction

At the University Clinical Center in Gdansk, Poland, we offer dedicated magnetic resonance imaging (MRI) for children. This is due to the high demand for pediatric MR examinations from our pediatric departments. Diagnostics in our center focus on oncology, cardiology, hematology, nephrology, neurology, and orthopedic patients. Due to the patients' young ages¹, many examinations are carried out under general anesthesia. When patients weigh less than 5 kilograms, we perform the examination with a dedicated incubator (LMT Medical Systems GmbH, Lübeck, Germany), fed and swaddled.

To reassure children and encourage them to enter the MR room, we have a projector that displays cartoons and plays music videos. Our MR scanner is also decorated with pictures of underwater animals, and special lighting helps the children to feel at ease.

Examining pediatric patients presents a number of technical issues. The age range is large, covering newborns¹ to young adults. The challenge for the MR team is that we must always achieve a balance between acquisition time and the quality of the study. We have to consider various fields of view, as well as aspects such as slice thickness, matrices, coding directions, and appropriate fat saturation techniques. Imaging newborns and toddlers can also result in artifacts from diapers.

Equipment

Imaging is performed on a 1.5T MAGNETOM Sola (Siemens Healthcare, Erlangen, Germany) equipped with BioMatrix Technology. The protocols are optimized for image quality and acquisition time. For MSK examinations our center has the following coils: BM Head/Neck 20, Spine 32, Body 18, UltraFlex Large 18, TxRx Knee 18, Peripheral Angio 16, Special Purpose 4.

Protocols

We have a permanent pediatric imaging team consisting of five radiographers, one medical physicist, six radiologists, and four anesthesia nurses (not including the anesthesia personnel). Due to the variety of examinations, the diagnostic demand, and the variety of patients, there has been a call to create standard protocols that our team can change on an ongoing basis.

We have several standard protocols for musculoskeletal (MSK) imaging. For the joints, cartilage, and ligaments, we have three-plane proton-density turbo-spin-echo with fat saturation sequences, and turbo-spin-echo T1 and T2 sequences. For oncological or hematological problems with bones and soft tissue, our protocols include: T1 VIBE Dixon, diffusion-weighted imaging, T2 turbo-spin-echo Dixon, and T2 HASTE with and without fat saturation. When contrast is required, we can use dynamic sequences (T1 VIBE, TWIST) or we can first inject contrast and then scan the patient with T1 Dixon in three planes. While this is a very simplified picture of our protocols, it shows the basic sequences needed when examining MSK pathologies. However, as mentioned above, pediatric patients differ widely. This paper will therefore present a variety of cases and our approach to imaging them.

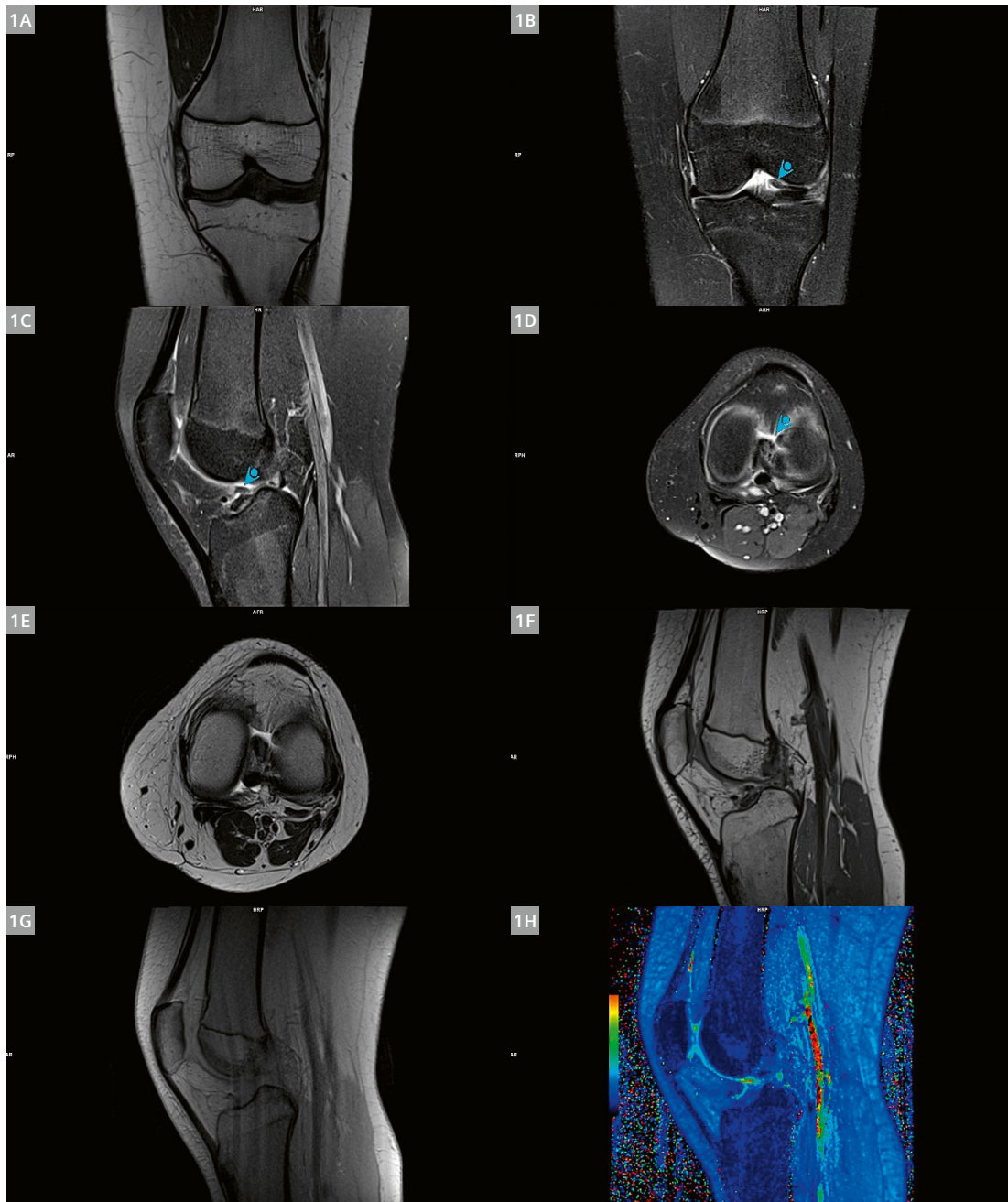
Conclusion

The demand for MSK imaging in children is growing. Pediatric patients vary widely in terms of height, weight, and the types of diseases. Therefore, it is worth developing basic protocols that can be supplemented by other sequences as needed. At the University Clinical Centre in Gdansk, the pediatric radiology team has developed and refined systems and basic sequences that can serve as a gold standard for diagnostic MR examinations in children. The sequences shown in this paper helped to improve, simplify, and accelerate MSK diagnoses for children.

¹MR scanning has not been established as safe for imaging fetuses and infants less than two years of age. The responsible physician must evaluate the benefits of the MR examination compared to those of other imaging procedures. Note: This disclaimer does not represent the opinion of the authors.

Case 1

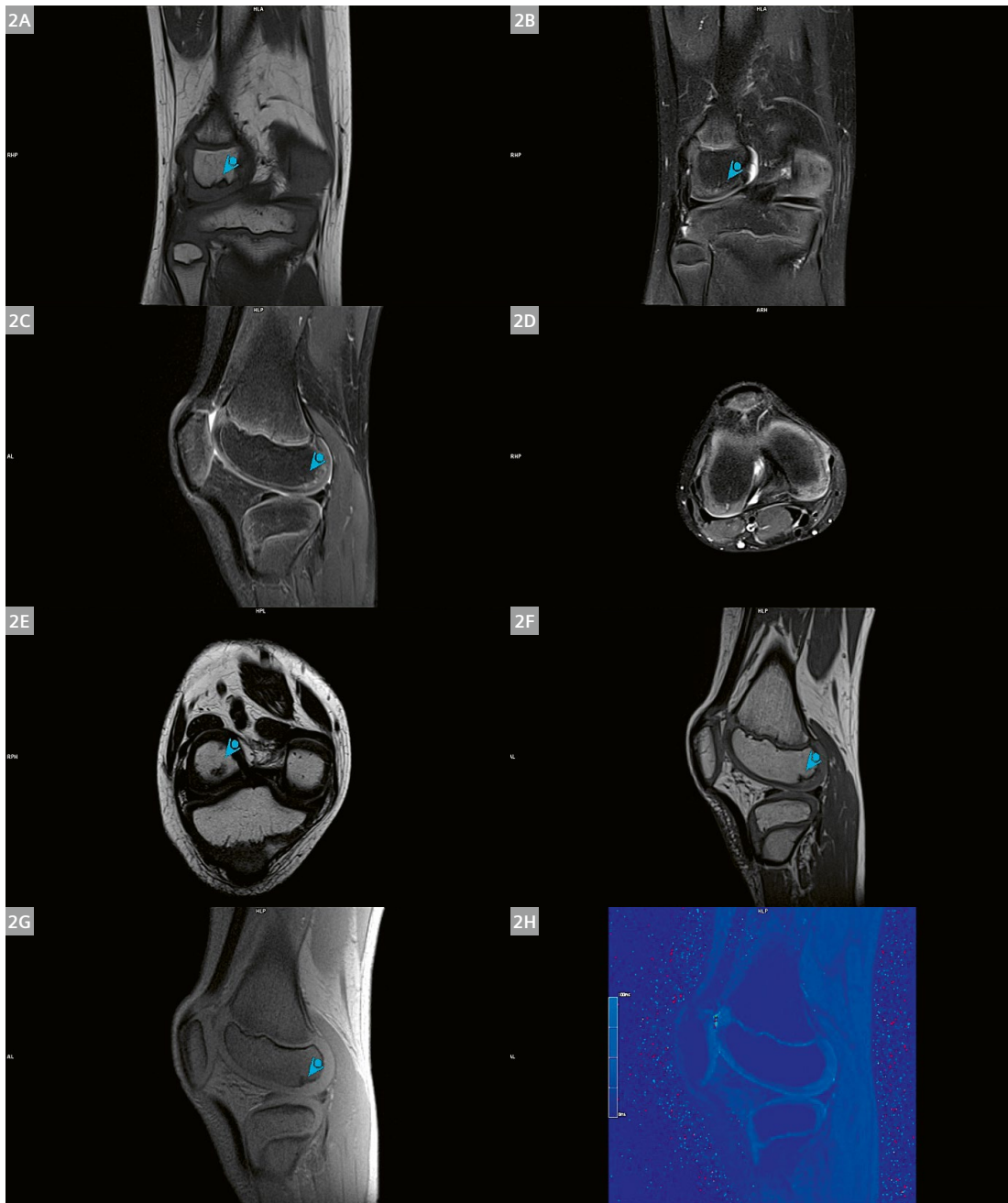
14-year-old female with a damaged meniscus. In terms of the shaft and the corner of the front-side meniscus: a horizontal gap, cracking with the movement of a fragment of the meniscus to the medial; flap damage; damage covering zone vascularization. For this case, we used our standard knee protocol and the TxRx Knee 18 coil.



1 Damaged meniscus. (1A) Coronal T1 TSE; (1B) coronal and (1C, D) sagittal PD TSE fatsat; (1E) transverse T2 TSE; (1F) sagittal isotropic PD SPACE; (1G) sagittal T2*; (1H) T2* map.

Case 2

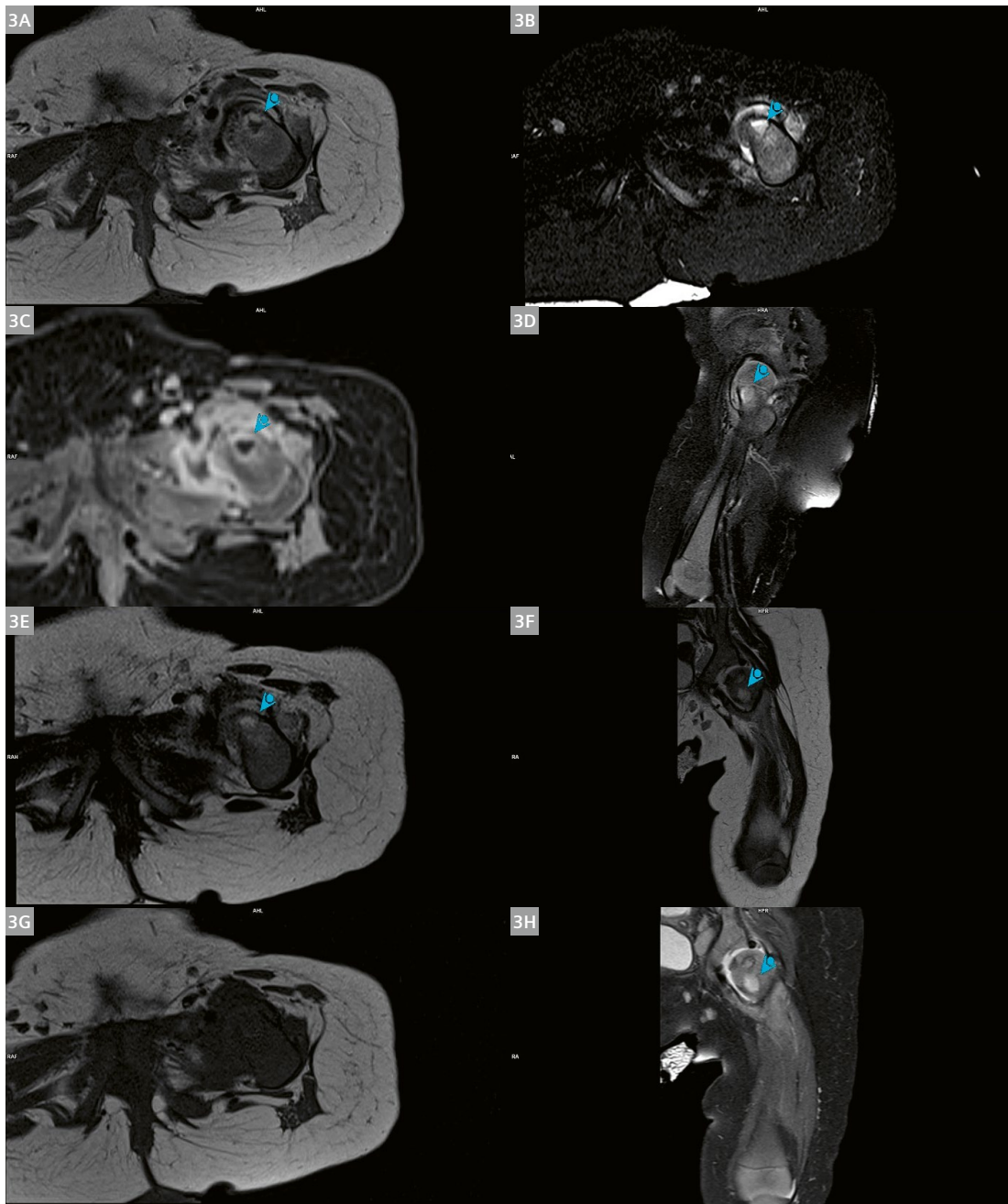
8-year-old patient with pathological post-traumatic damage in the femoral condyle.
Images acquired using the TxRx Knee 18 coil.



2 Pathological post-traumatic damage in the femoral condyle. **(2A)** Coronal T1 TSE; **(2B)** coronal PD TSE fatsat; **(2C)** sagittal PD TSE; **(2D)** transverse PD TSE fatsat; **(2E)** transverse T2 TSE; **(2F)** sagittal PD SPACE isotropic; **(2G)** sagittal T2*; **(2H)** T2* map.

Case 3

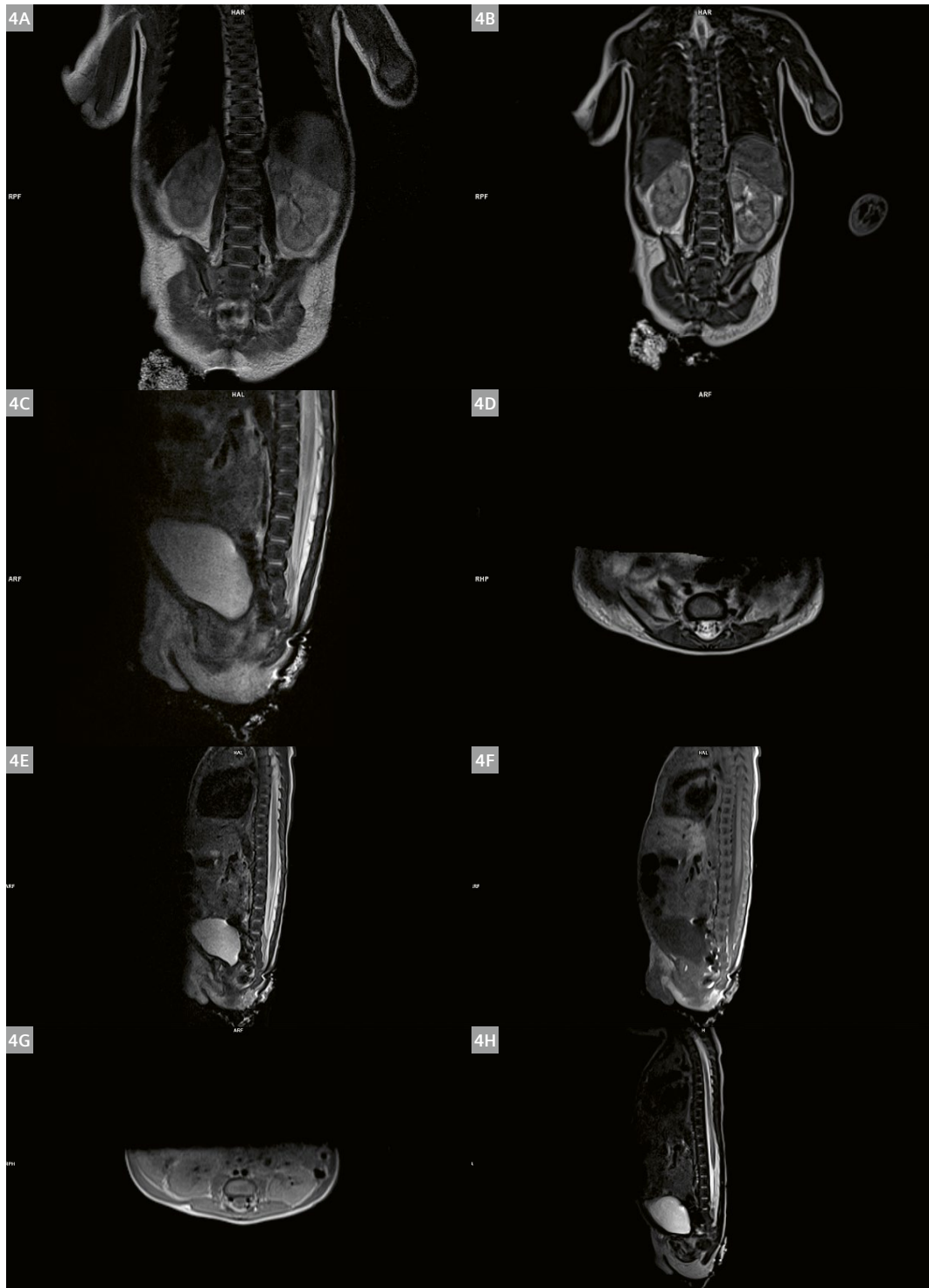
2-month-old¹ patient with inflammation of the femur. Visible intraosseous peripheral enhancement in the left femoral neck after contrast injection. A narrow channel connects the lesion with another inflammation located in the femoral head.



3 Inflammation is visualized using the following sequences: **(3A)** Transverse T2 TSE; **(3B)** coronal T2 TSE; **(3C)** transverse T1 TSE; **(3D)** coronal PD TSE fatsat; **(3E)** transverse T1 TSE post-contrast; **(3F)** coronal T2 TIRM; **(3G)** transverse T1 VIBE Dixon post-contrast; **(3H)** coronal PD TSE fatsat.

Case 4

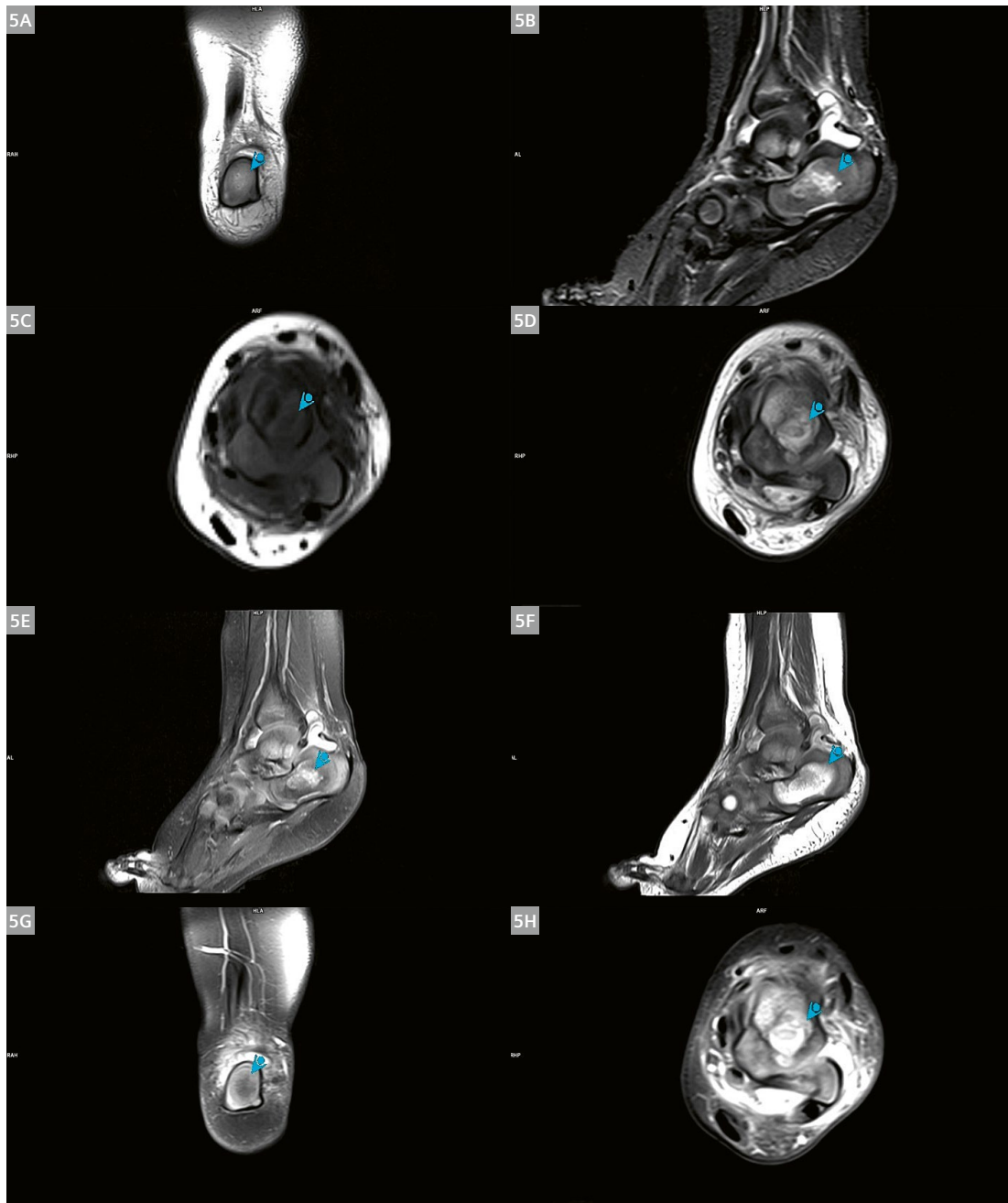
22-day-old¹ patient, lumbar spine examination without anesthesia, in MR incubator. Suspicion of caudal regression syndrome not confirmed by MR examination.



4 Suspected caudal regression syndrome. **(4A)** Coronal T2 TSE; **(4B)** T2 SPACE isotropic; **(4C)** sagittal high-resolution T2 TSE; **(4D)** transverse high resolution T2 TSE; **(4E)** sagittal T2 TSE Dixon water only; **(4F)** sagittal T2 TSE Dixon water only; **(4G)** T1 TSE Dixon water only; **(4H)** sagittal T2 SPACE.

Case 5

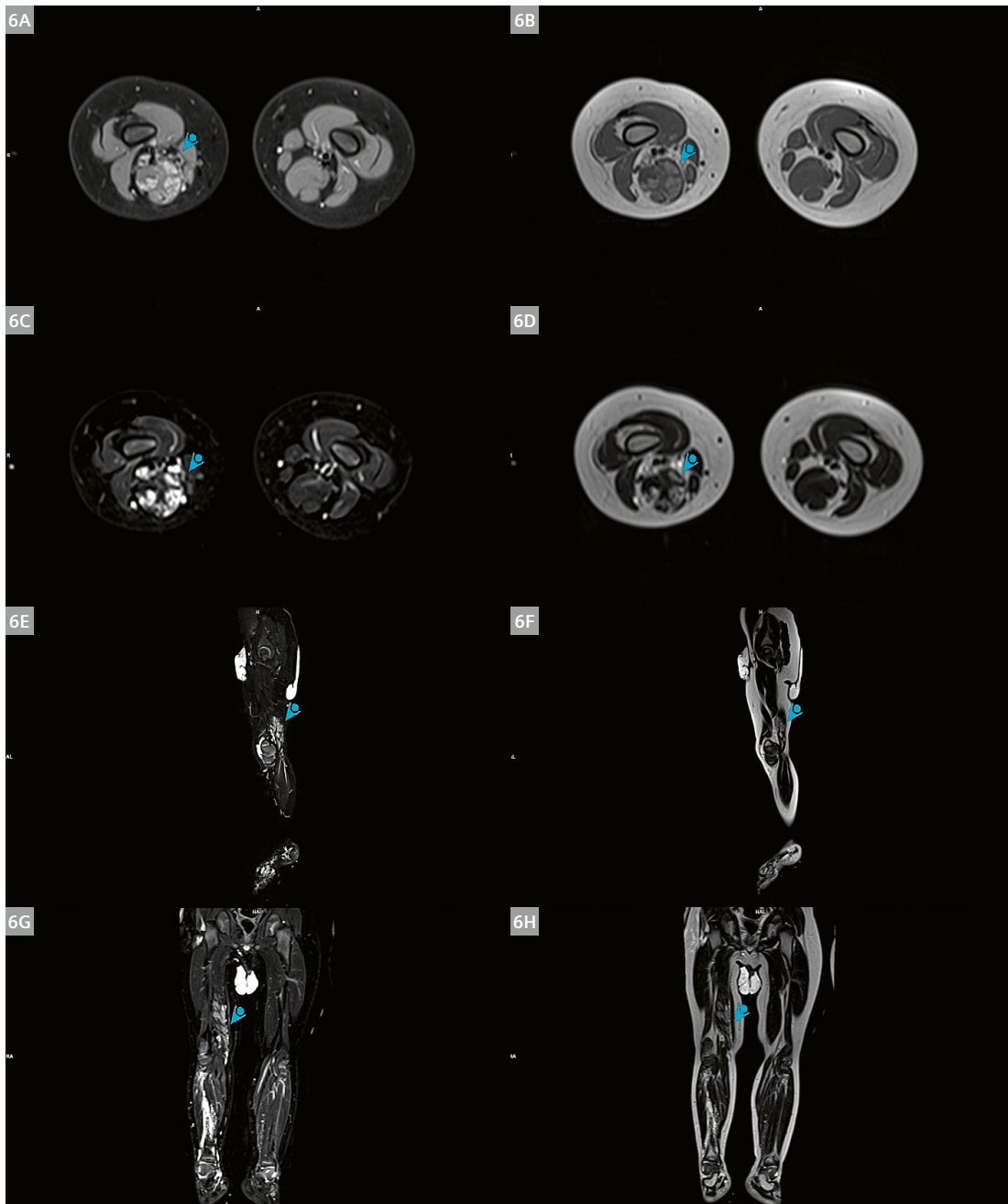
Ankle examination in a 12-month-old¹ patient. Suspicion of juvenile idiopathic arthritis (JIA); swelling of the joint from 6 weeks; high signal intensity in ossification nuclei.



5 Suspected juvenile idiopathic arthritis. (5A) Coronal T2 TSE; (5B) sagittal T2 TIRM; (5C) transverse T1 TSE; (5D) transverse T2 TSE; (5E) sagittal PD TSE fatsat; (5F) sagittal PD TSE; (5G) coronal PD TSE fatsat; (5H) transverse PD TSE fatsat.

Case 6

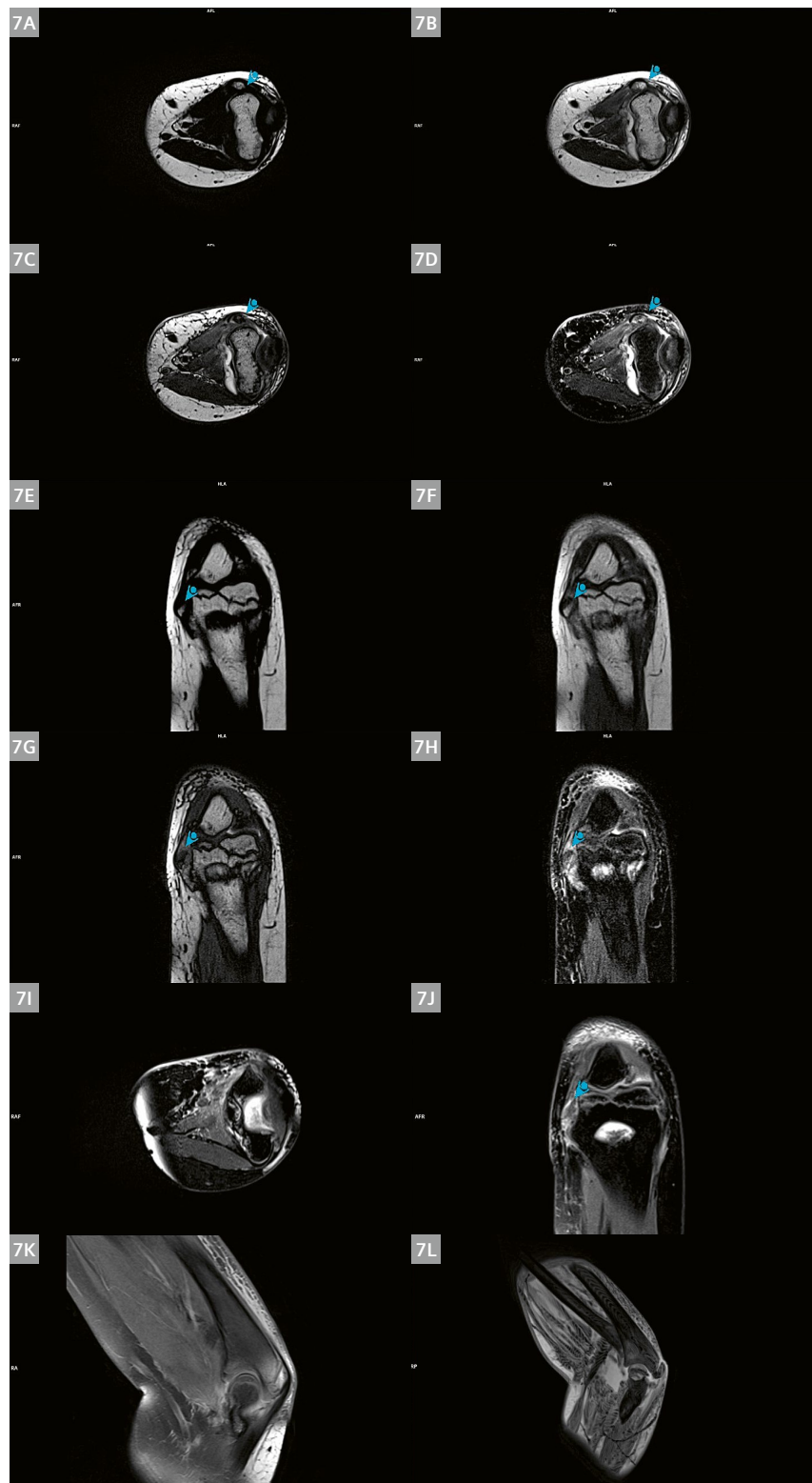
2-year-old patient with venous malformations of the lower extremity.



6 Venous malformations of the lower extremity. **(6A)** transverse T1 TSE Dixon water only; **(6B)** transverse T1 TSE Dixon in-phase; **(6C)** transverse T2 TSE Dixon water only; **(6D)** transverse T2 TSE Dixon in-phase; **(6E)** sagittal T2 TSE Dixon water only; **(6F)** sagittal T2 TSE Dixon in-phase; **(6G)** coronal T2 TSE Dixon water only; **(6H)** coronal T2 TSE Dixon in-phase.

Case 7

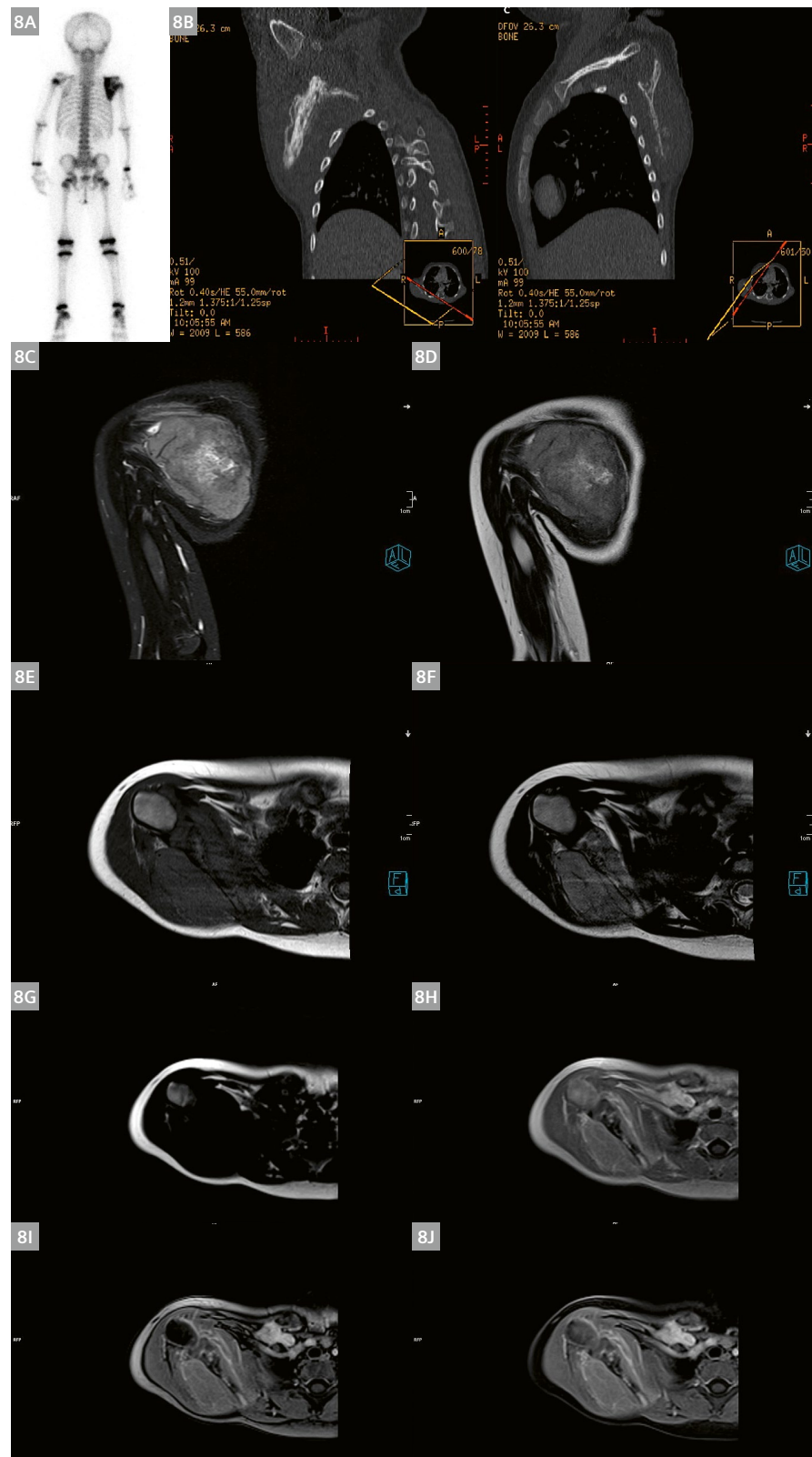
10-year-old patient, elbow examined in forced position (contracture), hand on the stomach facing upwards. Condition after fracture of the medial epicondyle of the left humerus with partial soft-tissue damage. Ligament damage, detachment of a bone fragment from the medial epicondyle of the left humerus.



7 Condition after fracture of the medial epicondyle of the left humerus with partial soft-tissue damage. Transverse T2 TSE Dixon, (7A) fat only; (7B) in-phase; (7C) opposed-phase; (7D) water only. Coronal T2 TSE Dixon (7E) fat only; (7F) in-phase; (7G) opposed-phase; (7H) water only. (7I) transverse PD TSE fatsat; (7J) coronal PD TSE fatsat; (7K) sagittal PD TSE fatsat; (7L) sagittal T1 VIBE black bone minIP.

Case 8

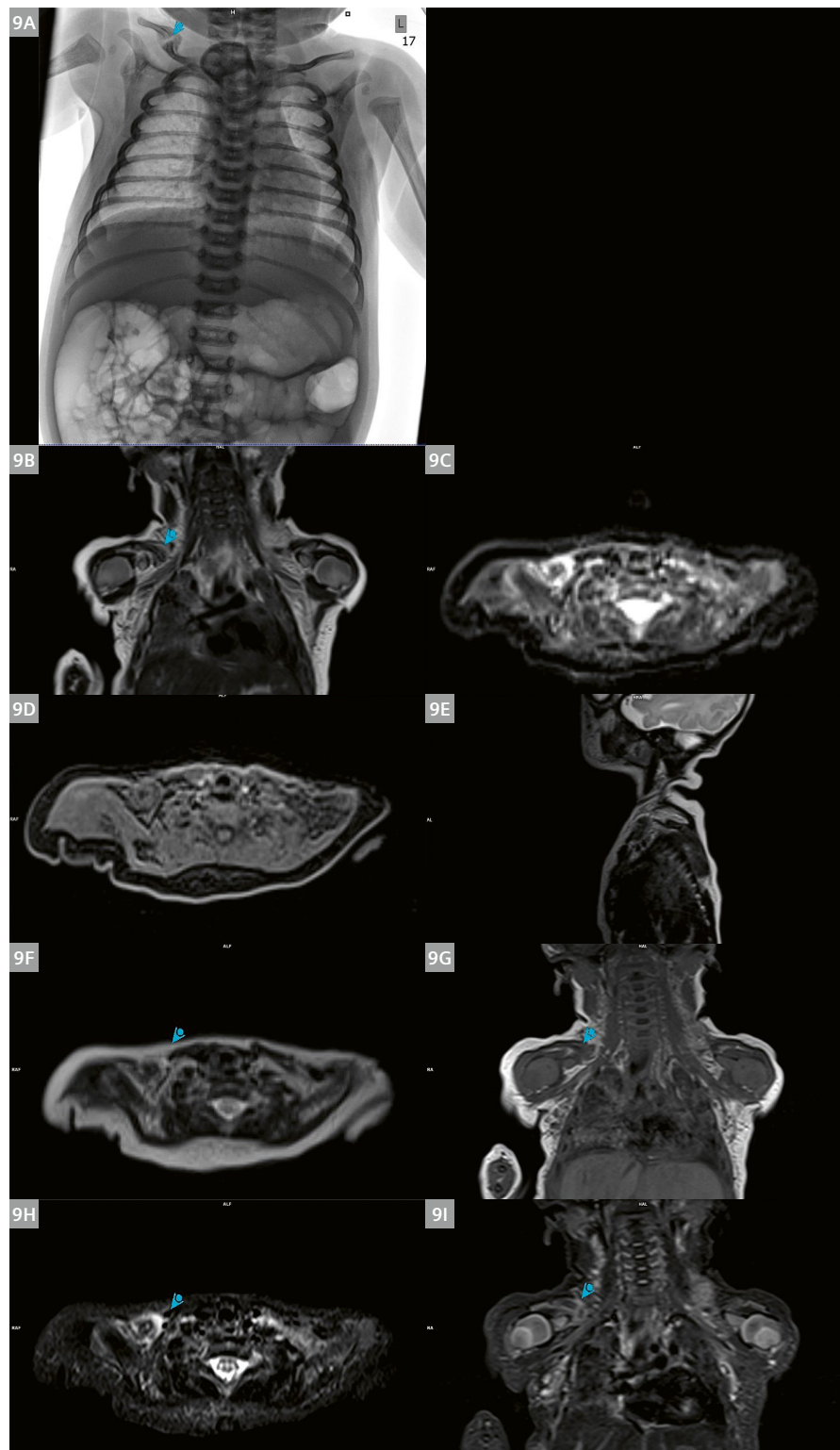
3-year-old patient with suspected Ewing's sarcoma. Pathological mass covering the right scapula, contrast enhancement, diffusion restriction.



8 Suspected Ewing's sarcoma. **(8A)** PET/CT; **(8B)** CT imaging. **(8C)** Coronal T2 TIRM; **(8D)** coronal T2 TSE; **(8E)** transverse T2 TSE; **(8F)** transverse T2 TSE. Transverse T1 VIBE Dixon post-contrast injection: **(8G)** fat only; **(8H)** in-phase; **(8I)** opposed-phase; **(8J)** water only.

Case 9

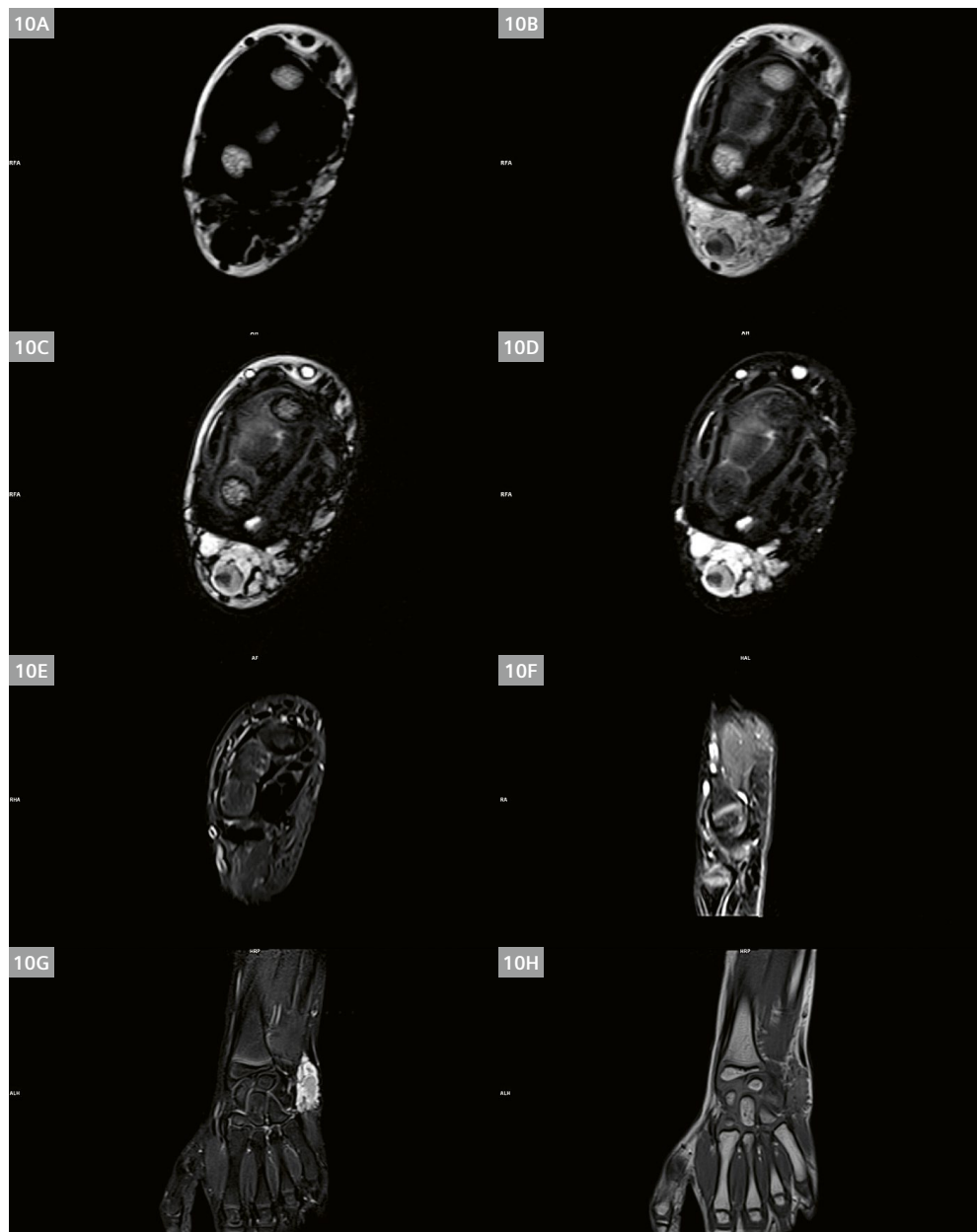
2-week-old patient¹ with fractured clavicle. Fracture in the outer third of the right clavicle with swelling of the soft tissue.



9 (9A) X-ray; (9B) coronal T2 TSE; (9C) transverse T2 Dixon water only; (9D) transverse T1 VIBE Dixon; (9E) sagittal T2 TSE; (9F) transverse T2 TSE Dixon; (9G) coronal T1 TSE; (9H) transverse T2 TIRM; (9I) coronal T2 TIRM.

Case 10

6-year-old patient with arteriovenous malformations (AVM) in the hand.



10 Arteriovenous malformation (AVM) in the hand. T2 TSE Dixon, **(10A)** fat only; **(10B)** in-phase; **(10C)** opposed-phase; **(10D)** water only. **(10E)** Transverse T2 TIRM; **(10F)** sagittal PD TSE fatsat; **(10G)** coronal T2 TSE STIR; **(10H)** coronal T1 TSE.

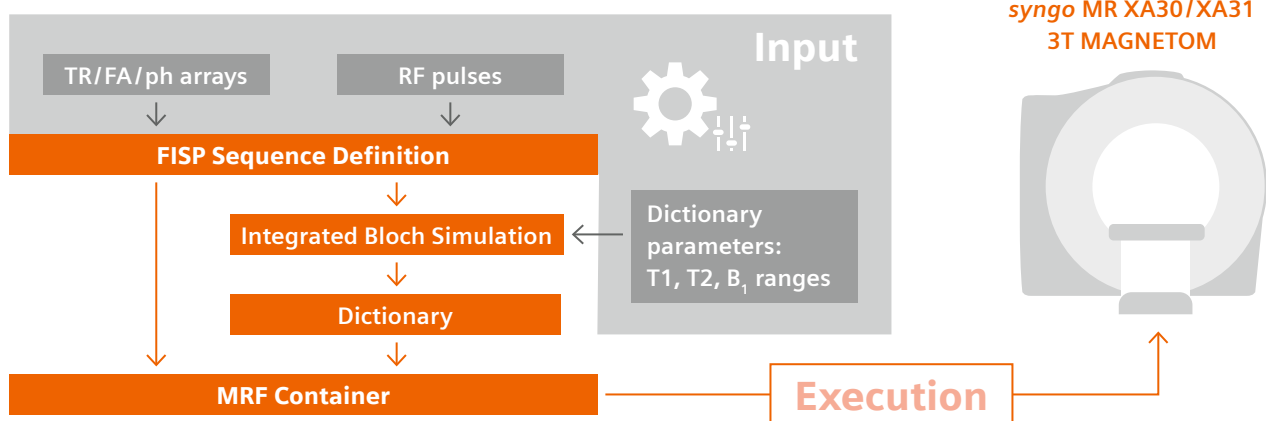


Contact

Dr Dominik Świętoń, M.D.
Uniwersyteckie Centrum Kliniczne GUMed
Dębinki 7
80-952 Gdańsk
Poland
dominik.swieton@gumed.edu.pl

MR Fingerprinting Development Kit

for Tailored Research Applications



The MR Fingerprinting Development Kit¹ takes files describing the input parameters T1, T2, RF- flip angles and pulse phases. This input generates a customized MR Fingerprinting¹ sequence. The input also serves as the basis for a Bloch simulation, which creates a MR Fingerprinting dictionary unique to its input parameters.

In a final step, the new MR Fingerprinting sequence and its unique dictionary are bundled in the so-called MR Fingerprinting container. This container can be transferred and executed on a qualified MAGNETOM 3T scanner from Siemens Healthineers² with a valid MR Fingerprinting license.

The sequence generation, the Bloch simulation, and the creation of the MR Fingerprinting container are performed by running a Windows command line tool³ provided with the MR Fingerprinting Development Kit.

The MR Fingerprinting Development Kit is available for download to all users of MR Fingerprinting at www.magnetomworld.siemens-healthineers.com/hot-topics/mr-fingerprinting/mrf-developer-kit

This unique MRF Development Kit empowers you to tailor the research application to your needs.

¹The product / feature is not for sale in the U.S. Its future availability cannot be guaranteed.

²syngo MR XA30: MAGNETOM Prisma, MAGNETOM Prisma Fit, MAGNETOM Skyra; syngo MR XA31: MAGNETOM Vida

³The user needs to install the MR Fingerprinting Development Kit on a standalone Windows 10 PC.

Installation on the host computer is not possible.

Clinical Benefits of MRF in Brain Tumors

Rui Zhang^{1,2}; Xianchang Zhang³; Yan Bai^{1,2}; Gregor Koerzdoerfer⁴; Meiyun Wang^{1,2}

¹Department of Medical Imaging, Henan Provincial People's Hospital & the People's Hospital of Zhengzhou University, Zhengzhou, China

²Henan Key Laboratory of Neurological Imaging, Zhengzhou, China

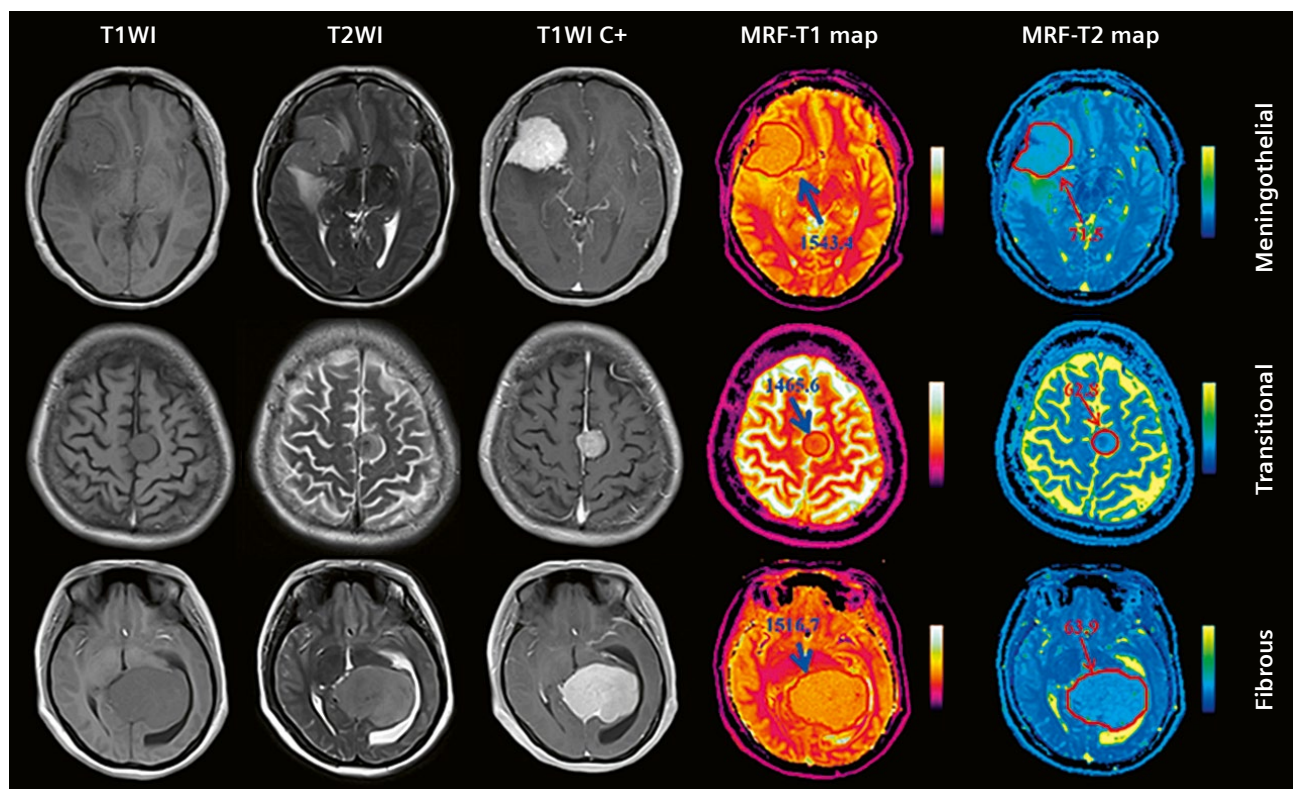
³MR Collaboration, Siemens Healthcare Ltd., Beijing, China

⁴Magnetic Resonance, Siemens Healthineers, Erlangen, Germany

Abstract

Preoperative differentiation between the subtypes of brain tumors could help to guide treatment. Conventional MRI cannot directly quantify the characteristics of brain tumors such as pituitary adenomas and meningiomas. Magnetic Resonance Fingerprinting (MRF) is an imaging technique that allows simultaneous quantification of T1 and T2 values. Quantitative T1 and T2 values yielded from MRF of gonadotroph pituitary macroadenomas were significantly higher than those of the non-gonadotroph pituitary mac-

roadenomas. Moreover, meningothelial meningiomas had significantly higher T1 and T2 values than transitional and fibrous meningiomas. Thus, MRF may help to pre-operatively differentiate between gonadotroph and non-gonadotroph pituitary macroadenomas and also to distinguish transitional and fibrous meningiomas from meningothelial meningiomas. MRF shows potential for guiding the treatment of pituitary macroadenomas and meningiomas.



1 Three representative patients with different meningioma subtypes. The T1 and T2 values in the solid tumor area of meningothelial patients appear slightly higher than those of transitional and fibrous patients.

Introduction

Radiology is essential for the initial evaluation of patients with primary brain tumors to characterize tumor types and determine treatment options [1]. The dominant modality is magnetic resonance imaging (MRI) because the multitude of image contrasts of conventional structural MRI allow for good localization of tumor-infiltrated areas. In addition, advanced image-based physiological and molecular biomarkers have been shown to offer comprehensive information about the biological characteristics of tumor types. However, conventional MRI is generally qualitative, providing relative intensity differences between tissues rather than absolute measurements from single tissues as the primary means for characterizing underlying pathology in tumor evaluation. This process may lead to interpretation discrepancies between different radiologists based on these qualitative MRI images and may therefore affect the objective comparison in the patients' follow-up [2].

Quantitative MRI techniques such as T1 and T2 relaxation time mapping could mitigate this problem by directly quantifying the tissue properties, providing a more accurate characterization of underlying changes at the cellular level than standard imaging. Several studies have used MR relaxometry for brain tumor diagnosis. Although most of these studies focus on T2 relaxometry, a recent study showed that T1 mapping might play an essential role in the earlier detection of recurrent tumors in patients on antiangiogenic therapy [2]. Nevertheless, because early conventional approaches for T1 and T2 mapping can only measure one parameter at a time, the reduced time efficiency of such conventional relaxometry techniques is one of the obstacles hindering their application in routine use.

Advanced multiparametric MRI schemes have been proposed to meet the clinical need for fast acquisition of quantitative MR biomarkers, allowing for reproducible and comprehensive measurement of clinically relevant tissue characteristics. Among these techniques, MR Fingerprinting (MRF) is a novel imaging framework that simultaneously estimates multiple quantitative biophysical parameters such as T1, T2, and proton density of different tissues in a clinically practicable acquisition time [3]. These quantitative tissue property measurements allow multiparametric analysis on perfectly co-registered maps, which have shown improved sensitivity and specificity in the characterization of pathological conditions, such as multiple sclerosis [4], epilepsy [5, 6], and brain tumors [7–9]. For example, recent studies found that MRF-derived T1 and T2 maps have shown specificity in identifying the quantitative difference in the solid tumor region and peritumoral regions in different brain tumor types [7].

Also, one study that used radiomic analysis of MRF found that texture analysis of MRF-derived maps can improve our ability to differentiate common adult brain tumors such as low-grade gliomas, glioblastomas, and metastases [9].

Here, we would like to demonstrate our initial experience with the clinical application of MRF in brain tumor diagnosis at our site, mainly focusing on meningiomas [10] and pituitary macroadenomas [11].

MRF sequence and protocol

MR Fingerprinting is a simple, fast, non-invasive quantitative MRI technique that enables measuring multiple physiological parameters simultaneously in a single, efficient acquisition [12, 13]. The MRF framework can be divided into a data acquisition and a pattern matching step. Firstly, MRF uses random excitation flip angles and repetition times (TRs) for data acquisition to obtain incoherent and distinguishable signal evolutions called “fingerprints”. Next, in the pattern matching stage, the unique “fingerprints” from each voxel are matched to a set of simulated fingerprints that constitute a dictionary which is generated by Bloch simulations of the same acquisition. Finally, the magnetic resonance parameters (e.g., T1 and T2) that produce the best match are used as definitive quantitative results.

A prototypical 2-dimensional, spiral, fast imaging with steady-state precession based MRF sequence was used to scan patients with brain tumors on a 3T MRI scanner (MAGNETOM Skyra, Siemens Healthcare, Erlangen, Germany). The protocol was as follows: transverse orientation, field of view (FOV) $256 \times 256 \text{ mm}^2$, matrix 256×256 , slice thickness 5 mm, flip angle variable $0\text{--}74^\circ$, TR variable between 12.1 and 15.0 ms, 3,000 measurements, and acquisition time 41 s/slice. Before the MRF acquisition, a B1 map [14] of the whole volume was acquired in 20 seconds and used during the MRF reconstruction.

For the inline MRF data processing, the quantitative T1 and T2 maps were simultaneously generated by matching the measured MRF signal time courses to the dictionary. In particular, the dictionary was calculated for a range of discrete T1, T2, and B_1 -field values based on Bloch simulations. The pre-calculated MRF dictionary comprised 691,497 entries of possible signal evolutions covering a wide range of discrete T1 (10 ~ 4500 ms), T2 (2 ~ 3000 ms), and B_1 -field values (factors 0.6–1.4 relative to the nominal B_1 -field). To improve the reconstruction speed, the dictionary was compressed to 50 main components in the time domain [15]. T1 and T2 maps were output for each section and used for the quantitative analysis.

In addition to the MRF sequence, the patients received conventional MRI scans, including T1w, T2w, FLAIR, DWI, and contrast-enhanced T1w imaging on meningioma, and T1w, T2w, and contrast-enhanced T1w imaging on pituitary macroadenoma.

MRF in meningioma

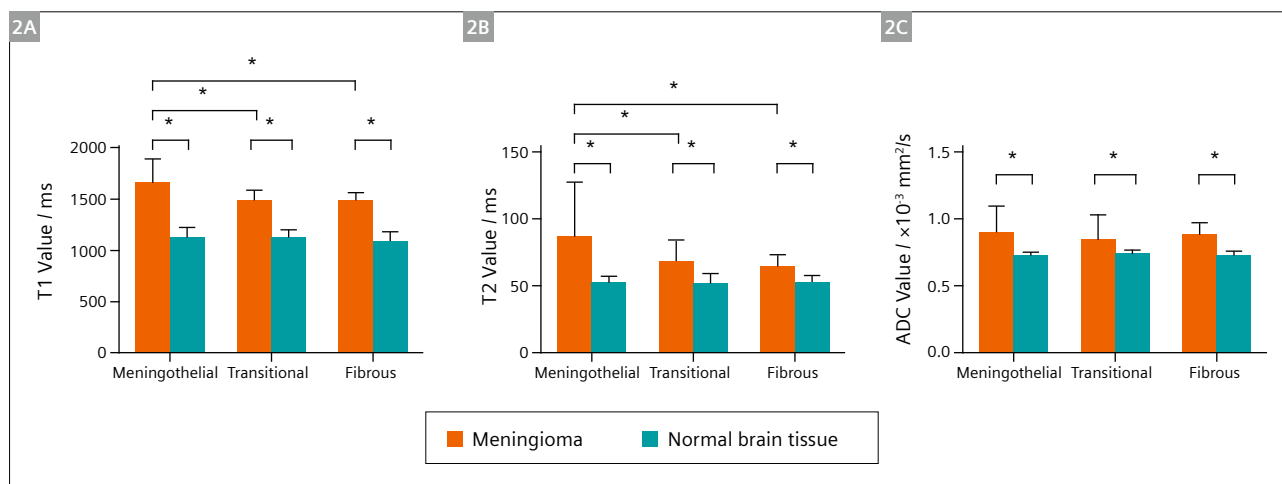
Meningiomas are the second most common central nervous system primary tumor [16]. Most meningiomas are World Health Organization (WHO) grade I, and the most common histological subtypes are meningothelial, transitional, and fibrous meningiomas. Although grade I meningiomas are benign, compared with the meningothelial subtype, transitional and fibrous meningiomas are associated with a higher bleeding risk during surgery and a worse outcome at follow-up [17]. Therefore, an accurate diagnosis of transitional and fibrous meningiomas before surgery is essential for selecting the most appropriate surgical procedure. However, conventional MRI can only reflect the gross morphological changes of tumors. The ability of conventional MRI such as T1w, T2w, and DWI-derived ADC values to differentiate WHO grade I transitional and fibrous meningiomas from meningothelial meningiomas is limited because of the overlap in imaging characteristics and ADC values among these subtypes. Therefore, we tried to use new MRI techniques such as MRF to improve the diagnostic accuracy in differentiating between meningioma subtypes [10].

MRF and conventional MRI data were acquired on 53 patients with suspected meningiomas before surgery. After surgery, 46 patients with pathologically confirmed meningothelial (n = 15), transitional (n = 18), and fibrous meningiomas (n = 13) were included for data analysis.

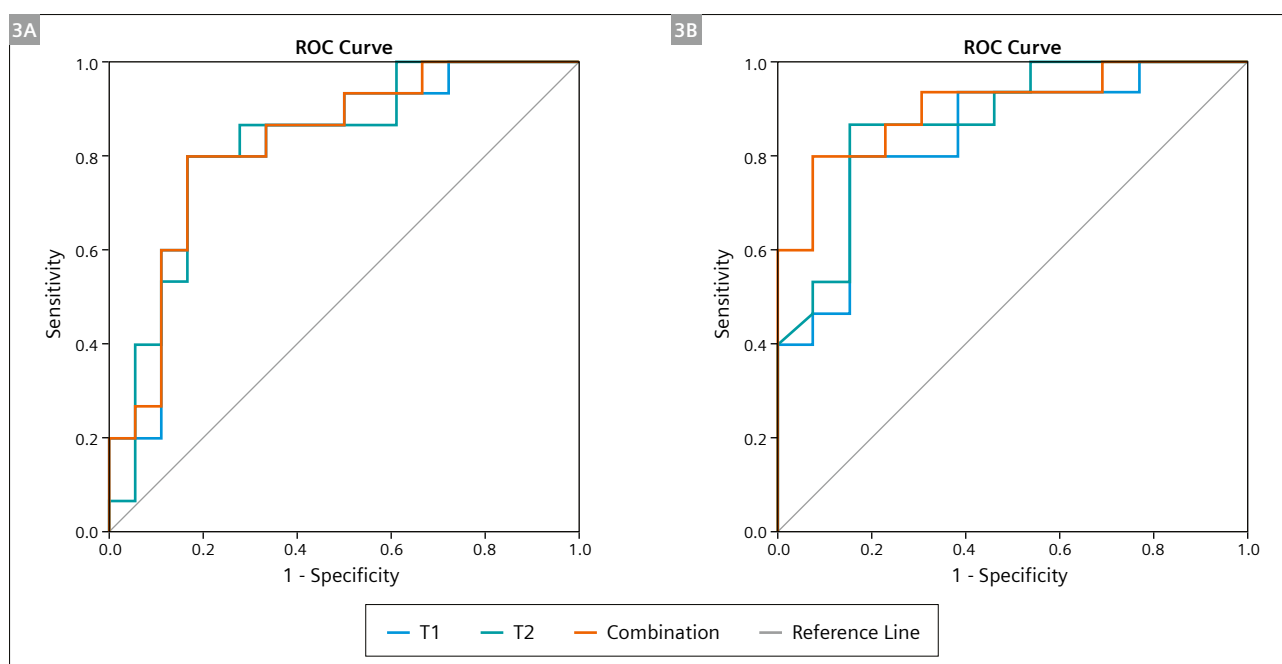
Data from three representative patients with different meningioma subtypes are shown in Figure 1. The T1WI and T2WI signals in the solid tumor areas of these patients were similar, and all showed noticeable enhancement. Therefore, there are still limitations in distinguishing between meningioma subtypes using conventional MRI. In the maps generated with MRF, the T1 and T2 values of the solid tumor areas of the meningothelial patients appeared to be slightly higher than those of the transitional and fibrous patients.

Further statistics found that the meningothelial subtype had significantly higher T1 and T2 values in the solid tumor area than transitional and fibrous meningiomas (Fig. 2A, B). No statistically significant difference was found in the T1 and T2 values between transitional and fibrous meningiomas. The ADC values of meningothelial, transitional, and fibrous meningiomas were not significantly different (Fig. 2C). Furthermore, the T1, T2, and ADC values of normal brain tissue were not significantly different between the three subtypes. The T1, T2, and ADC values of the three tumor subtypes differed significantly between the solid tumor area and the contralateral normal brain tissue. There were no statistically significant differences between the three meningioma groups in T1WI, T2WI, or contrast-enhanced T1WI.

Receiver operating characteristic (ROC) curve analysis was conducted, and the areas under the ROC curves (AUCs) were calculated between groups with statistically significant differences to evaluate the efficacy of T1 and T2 values in differentiating various subtypes of meningiomas. The combination of T1 and T2 values achieved the best diagnostic performance for differentiating transitional from meningothelial meningiomas (AUC = 0.826, sensitivity = 80%, and specificity = 83.33%) and differentiating



2 Quantitative MRI parameter comparison between three meningioma subtypes: (2A) MRF-derived T1 maps, (2B) MRF-derived T2 maps, and (2C) apparent diffusion coefficient (ADC) values. T1 and T2 values of meningothelial patients are significantly higher than those of transitional and fibrous meningioma patients. [10]



3 A receiver operating characteristic (ROC) curve of T1 and T2 values and the combination of the T1 and T2 values (combined variable) for the differential diagnosis of **(3A)** meningothelial and transitional meningiomas and **(3B)** meningothelial and fibrous meningiomas. [10]

fibrous from meningothelial meningiomas (AUC = 0.903, sensitivity = 80%, and specificity = 92.31%), as shown in Figure 3.

Our results suggested that transitional and fibrous meningiomas have significantly lower T1 and T2 values than meningothelial meningiomas. However, conventional MRI, including T1WI, T2WI, contrast-enhanced T1WI, and ADC values, indicated no statistically significant differences between transitional/fibrous meningiomas and meningothelial meningiomas. The ROC analyses showed that the T1 and T2 mapping generated by MRF might differentiate transitional and fibrous meningiomas from meningothelial meningiomas. These findings could benefit preoperative treatment plans for meningiomas and provide a more accurate prognosis.

MRF in pituitary macroadenoma

Pituitary adenomas account for 10–20% of all primary brain tumors. Macroadenomas represent about one-half of pituitary adenomas in the clinic [18]. The latest 2017 WHO classification of pituitary adenomas uses immunohistochemistry as the primary ancillary tool for diagnosis. Among them, gonadotroph adenomas are defined as tumors producing luteinizing hormone (β -LH) and follicle-stimulating hormone (β -FSH), which are secreted by the gonadotropic cells of the anterior pituitary gland [19]. In addition, there are several non-gonadotroph adenomas,

including somatotroph adenomas, lactotroph adenomas, corticotroph adenomas, and null cell adenomas (18). Somatostatin receptor type 3 (SSTR3) is expressed in 94% of gonadotroph pituitary adenomas, a putative target for drug therapy replacement for commonly used surgical treatment [20]. Therefore, preoperative differentiation between gonadotroph and non-gonadotroph pituitary macroadenomas could help to guide treatment. However, conventional MRI cannot directly quantify the characteristics of pituitary adenomas and therefore has limited capability to identify gonadotroph pituitary adenomas.

Our group aimed to use MRF to differentiate gonadotroph from non-gonadotroph pituitary macroadenomas according to the 2017 WHO classification of pituitary adenomas [11].

MRF and conventional MRI data from 57 patients with pituitary macroadenomas were included for analysis. Among them, 30 (52.6%) were categorized as gonadotroph pituitary macroadenomas; non-gonadotroph pituitary macroadenomas were diagnosed in 27 patients (47.4%).

Conventional MRI and MRF images of representative gonadotroph pituitary macroadenoma and non-functioning corticotroph pituitary macroadenoma are shown in Figure 4. The mean MRF-derived T1 and T2 values in the gonadotroph pituitary macroadenomas (T1 value, 1617 ± 274 ms; T2 value, 85 ± 26 ms) were significantly higher than those in the non-gonadotroph pituitary macroadenomas

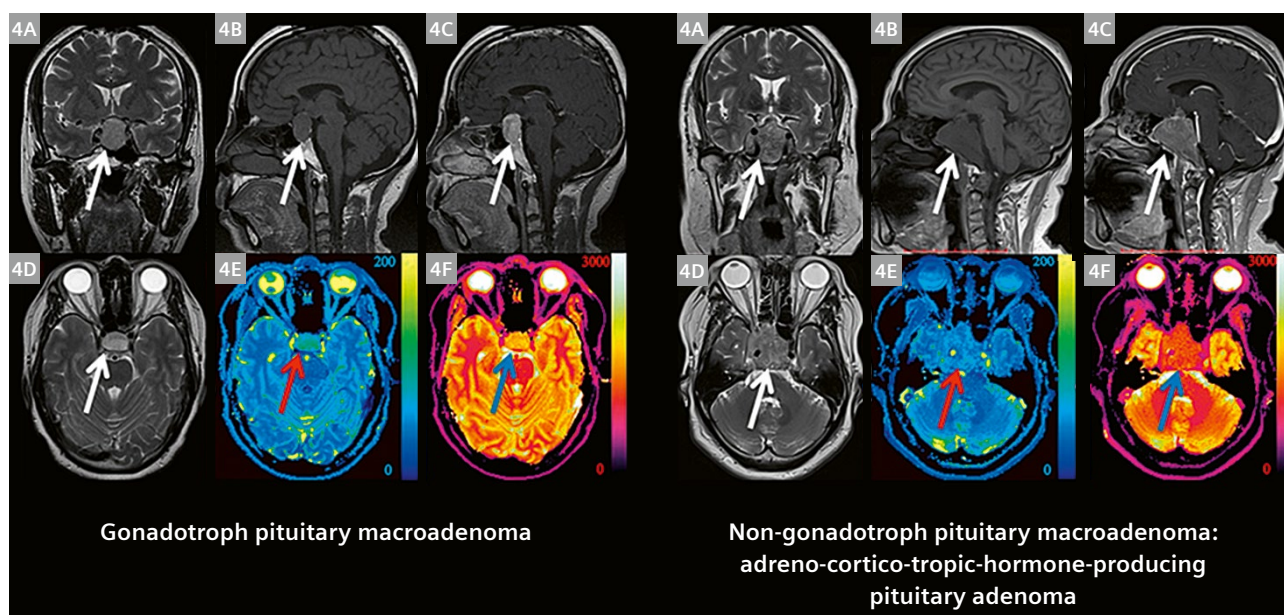
(T1 value, 1412 ± 180 ms; T2 value, 58 ± 13 ms), as shown in Figure 5.

Regarding the differentiation between gonadotroph and non-gonadotroph pituitary macroadenomas, the AUC for MRF-derived T2 values (0.888, 95% CI 0.776–0.956) was significantly greater than that for MRF-derived T1 values (0.742, 95% CI 0.609–0.849) ($p = 0.034$, Fig. 6).

This work showed that the quantitative T1 and T2 values derived from MRF were significantly higher in gonadotroph than in non-gonadotroph pituitary macroadenomas. These findings may be helpful in preoperatively differentiating these macroadenoma types, which will guide their treatment.

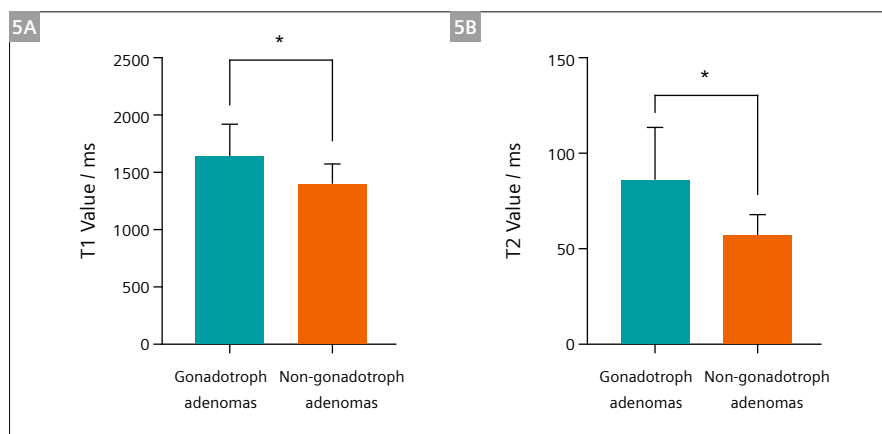
Conclusion

MRF shows greater potential than conventional qualitative MRI for brain tumor differential diagnosis. Quantitative T1 and T2 measurements can also be conducted using conventional MRI relaxometry mapping methods. However, this requires more scan time because the T1 and T2 measurements are acquired separately. MRF can simultaneously acquire T1 and T2 maps, thereby shortening the acquisition time and yielding perfectly aligned images that will benefit the data analysis. In addition to T1 and T2 relaxometry, the MRF framework allows for quantifying further tissue parameters such as diffusion or perfusion information based on its flexible sequence design

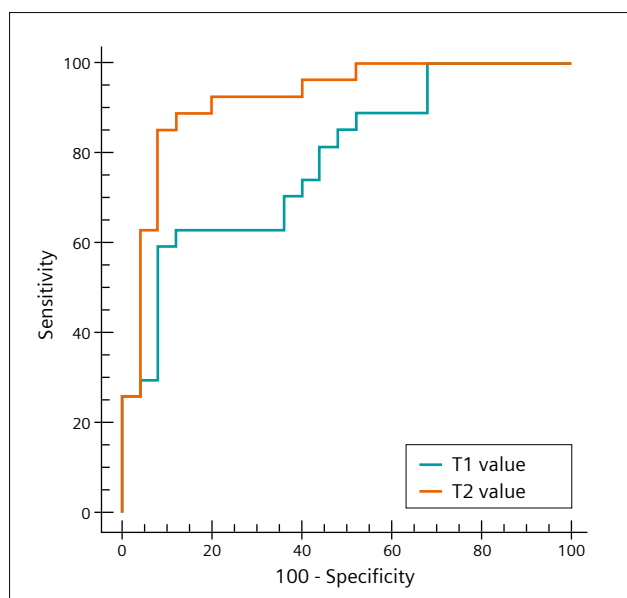


4 Representative gonadotroph pituitary macroadenoma and non-gonadotroph pituitary macroadenoma.

(4A) Coronal T2-weighted image, (4B) sagittal T1-weighted image, (4C) gadolinium-based contrast-enhanced sagittal T1-weighted image, and (4D) transverse T2-weighted image. (4E) MRF-derived T2 map shows increased T2 relaxation times in the tumor. (4F) MRF-derived T1 map shows increased T1 relaxation times in the tumor.



5 Average comparison of MRF-derived T1 values (5A) and T2 values and (5B) in ROIs in gonadotroph pituitary macroadenomas compared with non-gonadotroph pituitary macroadenomas. [11]



6 Comparison of receiver operating characteristic (ROC) curve analysis for differentiating gonadotroph and non-gonadotroph pituitary macroadenomas. The area under the ROC curve for MRF-derived T2 values was significantly greater than that for MRF-derived T1 values. [11]

characteristics [13]. This opens the door to a new approach to using imaging biomarkers in many applications of quantitative MRI, which will ultimately help the diagnosis and treatment of brain tumors.

References

- 1 Leung D, Han X, Mikkelsen T, Nabors LB. Role of MRI in primary brain tumor evaluation. *J Natl Compr Canc Netw*. 2014;12(11):1561-8.
- 2 Lescher, S., Jurcoane, A., Veit, A. et al. Quantitative T1 and T2 mapping in recurrent glioblastomas under bevacizumab: earlier detection of tumor progression compared to conventional MRI. *Neuroradiology*, 2015;57:11–20.
- 3 Ma D, Gulani V, Seiberlich N, Liu K, Sunshine JL, Duerk JL, Griswold MA. Magnetic resonance fingerprinting. *Nature*. 2013;95(7440):187-92.
- 4 Krauss W, Gunnarsson M, Nilsson M, Thunberg P. Conventional and synthetic MRI in multiple sclerosis: a comparative study. *Eur Radiol* 2018;28:1692–700.
- 5 Ma D, Jones S E, Deshmene A, et al. Development of high-resolution 3D MR fingerprinting for detection and characterization of epileptic lesions. *Journal of Magnetic Resonance Imaging*, 2019, 49(5):1333-46.
- 6 Liao C, Wang K, Cao X, et al. Detection of lesions in mesial temporal lobe epilepsy by using MR fingerprinting. *Radiology*, 2018;288(3):804-12.
- 7 Badve C, Yu A, Dastmalchian S, et al. MR fingerprinting of adult brain tumors: initial experience. *American Journal of Neuroradiology*, 2017;38(3):492-9.
- 8 Haubold J, Demircioglu A, Gratz M, et al. Non-invasive tumor decoding and phenotyping of cerebral gliomas utilizing multiparametric 18F-FET PET-MRI and MR Fingerprinting. *European Journal of Nuclear Medicine and Molecular Imaging*, 2020, 47(6):1435-45.
- 9 Dastmalchian S, Kilinc O, Onyewadume L, et al. Radiomic analysis of magnetic resonance fingerprinting in adult brain tumors. *European Journal of Nuclear Medicine and Molecular Imaging*, 2021;48(3): 683-93.
- 10 Zhang R, Shen Y, Bai Y, et al. Application of magnetic resonance fingerprinting to differentiate grade I transitional and fibrous meningiomas from meningothelial meningiomas. *Quantitative Imaging in Medicine and Surgery*, 2021;11(4):1447.
- 11 Bai Y, Shen Y, Chen R, et al. Magnetic resonance fingerprinting for preoperative differentiation between gonadotroph and non-gonadotroph pituitary macroadenomas. *European Radiology*, 2021;31(11): 8420-8.
- 12 Körzdörfer G, Kirsch R, Liu K, et al. Reproducibility and repeatability of MR fingerprinting relaxometry in the human brain. *Radiology*, 2019, 292(2): 429-437.
- 13 Panda A, Mehta B, Coppo S, et al. Magnetic resonance fingerprinting – an overview. *Current opinion in biomedical engineering*, 2017, 3: 56-66.
- 14 Chung S, Kim D, Breton E, Axel L. Rapid B1+ mapping using a preconditioning RF pulse with TurboFLASH readout. *Magnet Reson Med*. 2010;64:439–446.
- 15 McGivney D F, Pierre E, Ma D, et al. SVD compression for magnetic resonance fingerprinting in the time domain. *IEEE transactions on medical imaging*, 2014, 33(12): 2311-22.
- 16 O'leary S, Adams W M, Parrish R W, et al. Atypical imaging appearances of intracranial meningiomas. *Clinical radiology*, 2007, 62(1):10-7.
- 17 Gajbhiye S, Gosal J S, Pandey S, et al. Apoplexy inside a giant medial sphenoid wing meningothelial (Grade I) meningioma: An extremely rare but a potentially dangerous complication. *Asian Journal of Neurosurgery*, 2019, 14(3): 961.
- 18 Chen Y, De Wang C, Su Z P, et al. Natural history of postoperative non-functioning pituitary adenomas: a systematic review and meta-analysis. *Neuroendocrinology*, 2012, 96(4):333-42.
- 19 Mete O, Lopes M B. Overview of the 2017 WHO classification of pituitary tumors. *Endocrine Pathology*, 2017, 28(3):228-43.
- 20 Oystese KA, Casar-Borota O, Normann KR, et al. Estrogen receptor alpha, a sex-dependent predictor of aggressiveness in non-functioning pituitary adenomas: SSTR and sex hormone receptor distribution in NFPA. *J Clin Endocrinol Metab* 2017;102:3581-90

Contact

Dr. Meiyun Wang, M.D., Ph.D.
Department of Medical Imaging
Henan Provincial People's Hospital &
the People's Hospital of Zhengzhou University
7 Weiwu Road
Zhengzhou 450003
China
mywang@zzu.edu.cn



Arterial Spin Labeling as a Potential Biomarker in Imaging of Various Neurodegenerative Disorders: A PET-MR / PCASL Study in a Tertiary Neuropsychiatric Institute

Sandhya Mangalore; Kavish Kumar Chaurasia; Venkatesh Murthy

Department of Neuroimaging and Interventional Radiology, National Institute of Mental Health and Neurosciences, Bengaluru, India

Introduction

The term “neurodegenerative disorders” refers to a wide range of neurological conditions that develop slowly and steadily over time. These conditions can manifest as problems with cognitive disorders, motor abnormalities, or psychiatric disorders affecting activities of daily living [1]. Clinically, there is a lot of overlap in these domains and hence there is need for imaging biomarkers in the management of neurodegenerative disorders [2].

Varied character, overlapping clinical symptomatology, and the absence of precise clinical, pathological, and molecular diagnoses are major obstacles in the clinical management of neurodegenerative disorders. Confirming a suspected clinical diagnosis is frequently not straightforward and may at times require invasive neuropathological evidence [3]. Non-invasive imaging adjuncts have achieved great advancements in morphological, metabolic, and functional research in recent years.

The current study focuses on the alteration of perfusion patterns studied in 3D Pseudo-Continuous Arterial Spin Labeling (PCASL) MRI in key neurodegenerative disorders, and on the correlation with established molecular imaging techniques ^{18}F -FDG PET and ^{18}F -FDOPA PET. Our optimized protocol at 3T using a research 3D ASL GRASE sequence¹ is shared in the table on the right.

Objectives

1. To correlate the clinical profile, 3D-PCASL and PET-MRI findings in cases of neurodegenerative disorder.
2. To explore the role of 3D-PCASL as a reliable biomarker in the workup of neurodegenerative disorders.

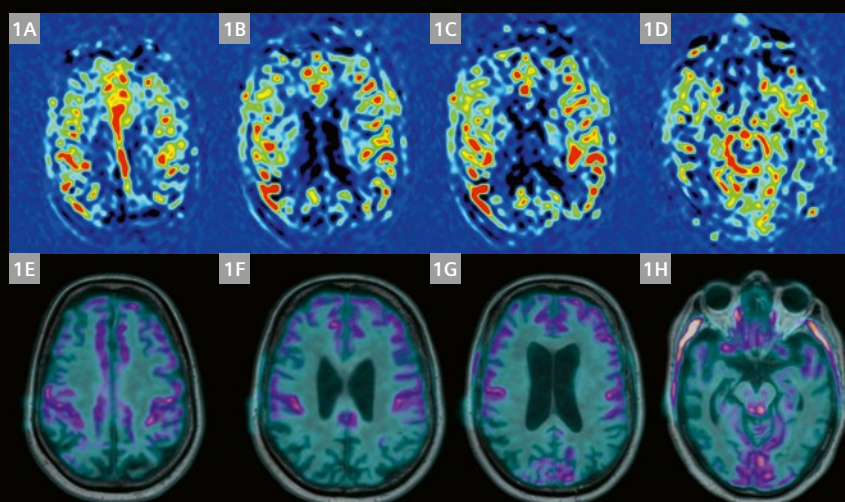
3D ASL protocol parameters	
TR	4600 ms
TE	22 ms
Flip angle	180°
Measurements	16
FOV read	250 mm
FOV phase	100.0%
Slice thickness	4.0 mm
Base resolution	64
Interpolation	On
Phase oversampling	0%
Slice oversampling	0.0%
Slices per slab	36
PAT mode	GRAPPA
Acceleration factor	PE 2
Prescan Normalize	On
AutoAlign	Head > Brain
Bandwidth	2442 Hz/Px
Echo spacing	0.5 ms
EPI factor	31
Turbo factor	12
Segments	3
Perfusion mode	PCASL
Label duration	1500 ms
Postlabel delay	1500 ms
Labeling gap	20.0 mm
PCASL flip angle	28.0°

¹Work in progress. The application is currently under development and is not for sale in the U.S. and in other countries. Its future availability cannot be ensured.

Part 1

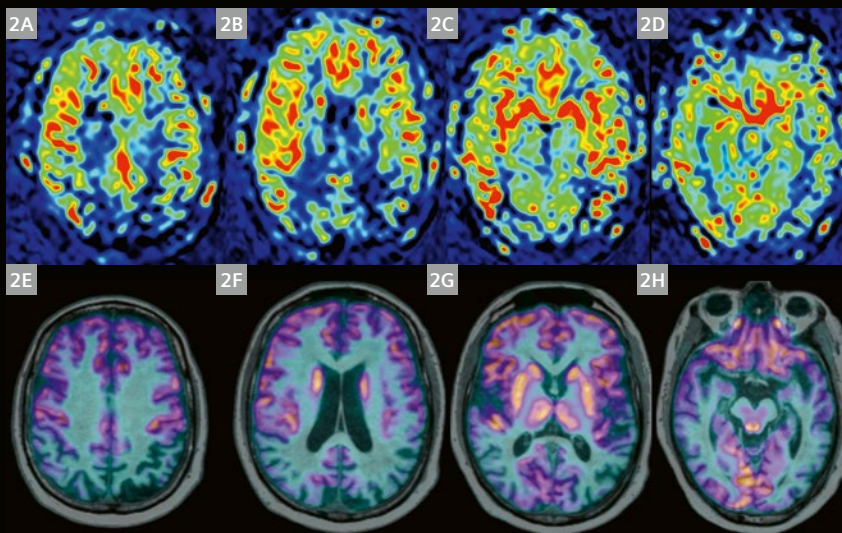
	Clinical presentation	PET-MRI and other investigations
Alzheimer's disease (AD) (Fig. 1)	Episodic memory affected early, progressively involved semantic memory, executive function and visuospatial function.	Hypoperfusion on PCASL and hypometabolism on FDG PET involving posterior cingulate gyri, precuneus, and posterior temporal and parietal cortices.
Posterior cortical atrophy variant of AD (Fig. 2)	Visual agnosia, apraxia, prosopagnosia, alexia, environmental disorientation, and Balint syndrome.	Predominant hypoperfusion and hypometabolism of posteromedial parietal and occipital lobes, with or without posterior cingulate hypometabolism.
Behavioral variant of frontotemporal dementia (FTD) (Fig. 3)	Cognitive dysfunction with changes in personality and social behavior. As the disease progresses involvement of language and memory may develop.	Hypoperfusion of dorsolateral prefrontal cortex, anterior cingulate cortex, with or without involvement of lateral and medial temporal lobes; pattern is unilateral and correlates with PET.
Semantic variant of FTD (Fig. 4)	Deficit in expressive and receptive language function, complaints of difficulty in remembering the names of places, people, or objects.	Hypoperfusion and hypometabolism is most marked in the left anterior temporal lobes, temporal pole, and anterior cingulate cortex.
Primary progressive aphasia variant of FTD (Fig. 5)	Agrammatism and effortful, halting speech with inconsistent speech (apraxia of speech).	Left posterior frontal lobe, including Broca's area hypoperfusion and hypometabolism with involvement of anterior cingulate cortex.
Dementia with Lewy bodies (Fig. 6)	Fluctuations in cognition especially in attention, executive function, and visuospatial orientation, visual hallucinations, REM sleep behavior disorder, bradykinesia / rest tremor / rigidity.	Hypoperfusion and hypometabolism in the primary visual cortex, cuneus, and the precuneus, with characteristic sparing of the posterior cingulate gyrus.
Corticobasal degeneration (Figs. 7 and 8)	Asymmetric movement abnormalities, myoclonus, cortical signs including ideomotor apraxia and alien limb phenomenon.	Disproportionate asymmetric cortical hypoperfusion and hypometabolism in the perirolandic posterior frontal (premotor, supplementary motor, primary motor) and superior parietal lobes, and also the basal ganglia.
Vascular dementia	Presenting signs and symptoms are dependent on the areas affected.	Perfusion patterns on PCASL suggesting internal / external watershed zones and normal metabolic uptake in neocortex. Areas of old infarcts in neocortex correspond on FDG PET with PCASL with an abrupt margin.

Table 1: Clinical details and FDG PET-MRI of dementia



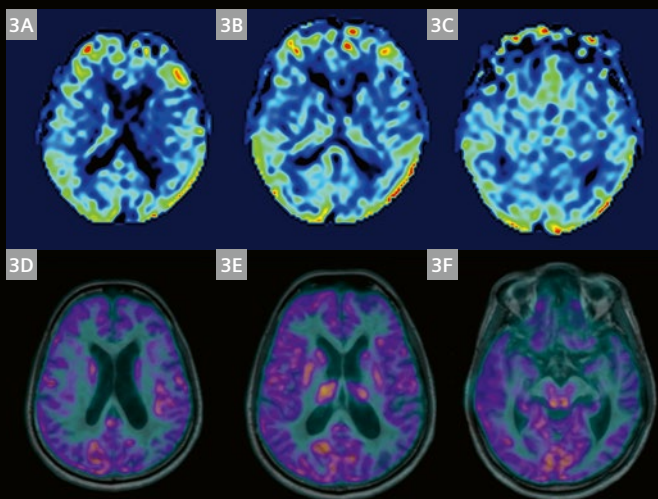
1 Alzheimer's disease (AD)

Patient presented with impaired memory and depression, there was also familial history of dementia in relatives. Upper row (1A–D) PCASL images, bottom row (1E–H) ^{18}F -FDG PET images demonstrating hypoperfusion on PCASL and hypometabolism on ^{18}F -FDG PET involving the posterior cingulate gyri, precuneus, and posterior temporal and parietal cortices.



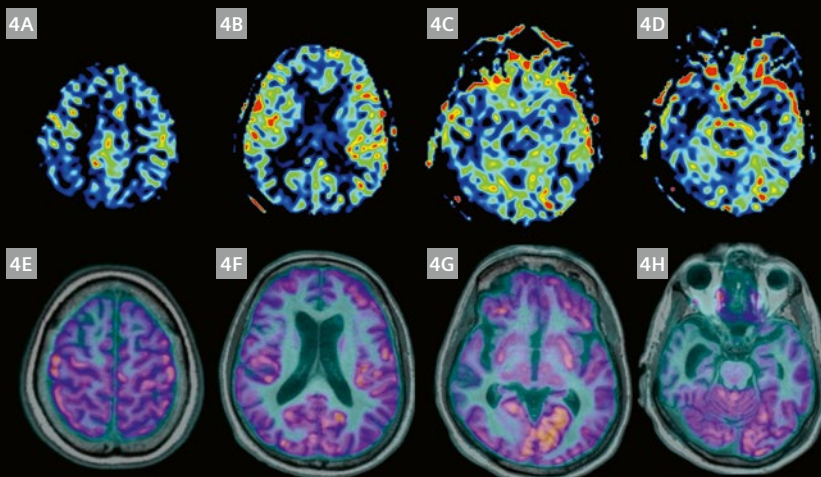
2 Posterior cortical atrophy variant of AD

Patient presented with difficulties in reading, getting dressed, identifying moving objects, identifying distance of objects, and differentiating left from right. Upper row (2A–D) PCASL images, bottom row (2E–H) ^{18}F -FDG PET images showing predominant hypoperfusion and hypometabolism of posteromedial parietal, and occipital lobes, with or without posterior cingulate hypometabolism.



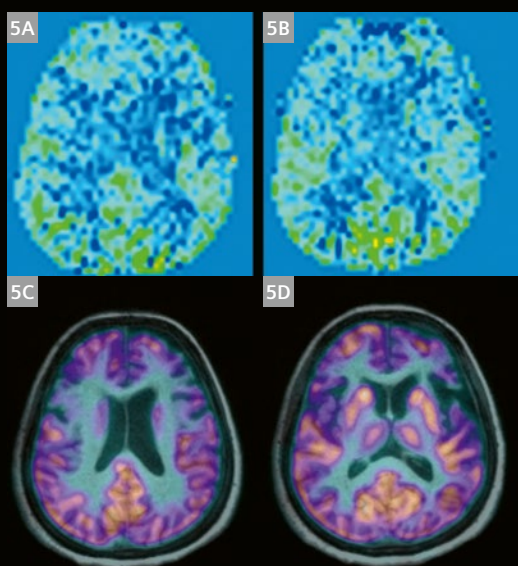
3 Behavioral variant of frontotemporal dementia (FTD)

Patient is chronic alcoholic and presented with impaired immediate and recent memory. Upper row (3A–C) PCASL images, bottom row (3D–F) ^{18}F -FDG PET images, demonstrating hypoperfusion and hypometabolism, respectively, in the dorsolateral prefrontal cortex, anterior cingulate cortex, and temporal lobes.



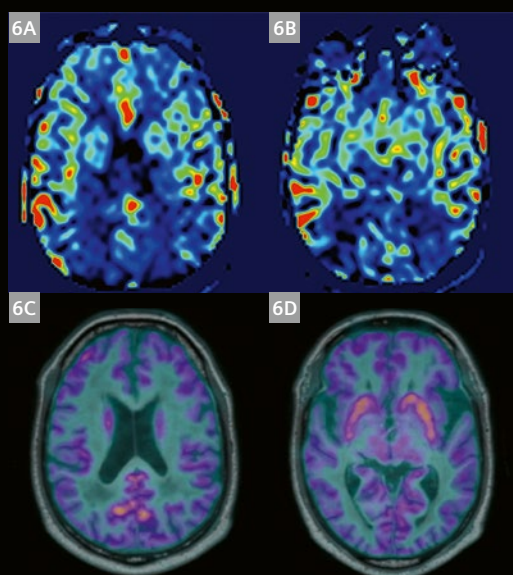
4 Semantic variant of FTD

Patient presented with complaints of decreased pace of movements, memory loss, not recognizing people, behavioral changes, and poor attention. Upper row (4A–D) PCASL images, lower row (4E–H) ^{18}F -FDG PET images, demonstrating that hypoperfusion and hypometabolism are particularly prominent in the left anterior temporal lobes, temporal pole, and anterior cingulate cortex.



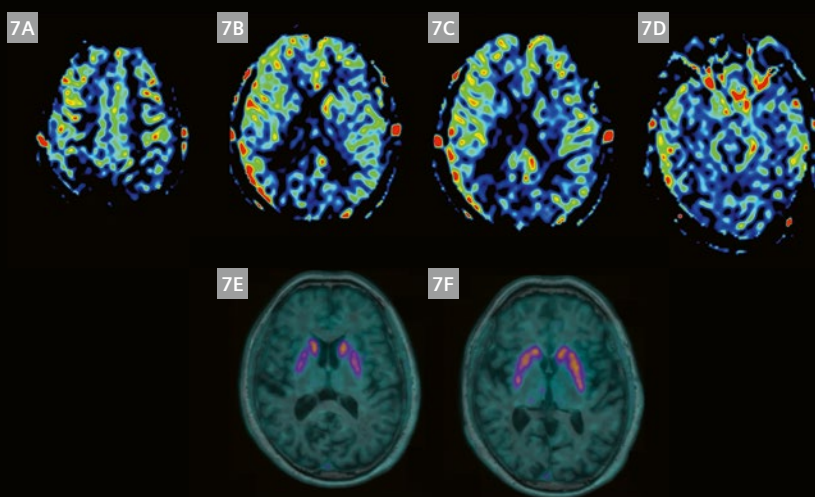
5 Primary progressive aphasia variant of FTD

Patient presented with memory disturbances, agrammatism, and effortful and halting speech for two years. Upper row (5A, B) PCASL images, lower row (5C, D) ^{18}F -FDG PET images demonstrating hypoperfusion and hypometabolism in the left posterior frontal lobe, including Broca's area, along with involvement of the anterior cingulate cortex.



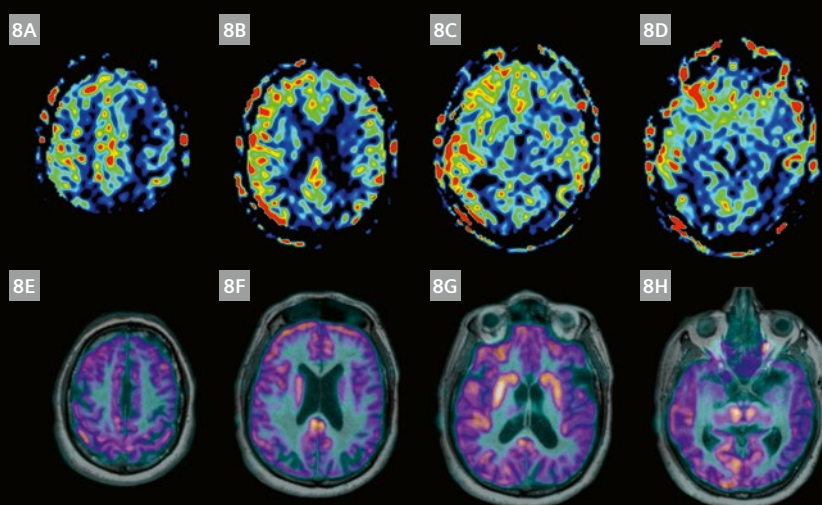
6 Dementia with Lewy bodies

Patient presented with two-year history of decreased pace of walking and cognitive decline, on further evaluation had attentional deficit, apathy, calculation difficulty, and REM sleep behavior disorder. Upper row (6A, B) PCASL images, lower row (6C, D) ^{18}F -FDG PET images, demonstrating hypoperfusion and hypometabolism in the primary visual cortex, cuneus, and the precuneus, with the characteristic sparing of the posterior cingulate gyrus.



7 Corticobasal degeneration

Patient presented with features of atypical PD (left upper limb tremors, unable to button shirt, and difficulty in walking). Upper row (7A–D) PCASL images, lower row (7E, F) ^{18}F -FDOPA PET images, demonstrating asymmetric cortical hypoperfusion in the right perirolandic posterior frontal-motor cortex (7A), parietal lobe (7A–C), and temporal lobe (7D), as well as right putamen (7B). Hypometabolism in right putamen (7E, F).



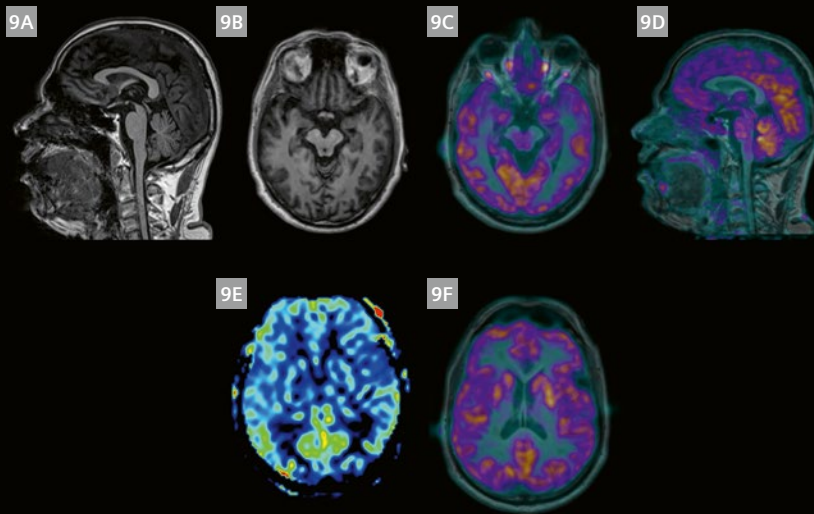
8 Corticobasal degeneration

Patient presented with gradual progressive recognition difficulty, visual spatial difficulty, calculation difficulty, decreased speech, and inability to recognize family members. Clinical examination revealed impaired cortical sensation, graphesthesia and apraxia. Upper row (8A–D) PCASL images; bottom row (8E–H) ^{18}F -FDG PET images showing disproportionate asymmetric cortical hypoperfusion and hypometabolism in the perirolandic posterior frontal (premotor, supplementary motor, primary motor) and superior parietal lobes, and also the basal ganglia.

Part 2

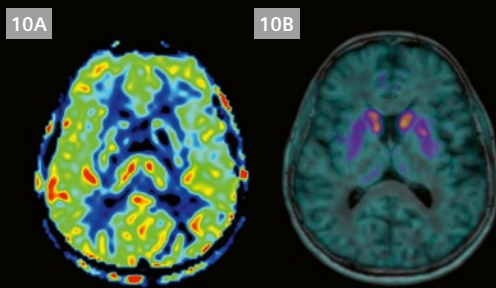
	Clinical presentation	PET-MRI and other investigations
Progressive supranuclear palsy (Fig. 9)	Early-onset postural and gait instability, dysfunction of vertical eye movements, ataxic or spastic dysarthria, dysphagia, levodopa non-responsive axial rigidity. In a subset of cases, frontal behavioral changes and subcortical dementia.	Hypoperfusion and hypometabolism noted in the bilateral putamen. Additionally, PCASL showed hypoperfusion in the bilateral frontal lobes and anterior cingulate cortex.
Idiopathic Parkinson's disease (Fig. 10)	Bradykinesia, rigidity, and resting tremor.	Hypoperfusion and hypometabolism in the uni-/bilateral posterior part of the putamen. Additionally, hypoperfusion was noted in the bilateral parietal lobe.
Drug-induced Parkinson's disease (Fig. 11)	Atypical tremors noted in background of functional and psychiatric disorders.	Normal perfusion and metabolism noted in the striatal structures. Additionally, normal perfusion noted in the neocortex.
Vascular Parkinson's disease	Diabetic / hypertensive presenting with tremors secondary to infarct / dopaminergic deficit.	Hypometabolism and hypoperfusion noted in the striatal infarcted areas. Additionally, infarcts in the neocortex and watershed zone, infarcts noted in PCASL.
Hypermanganese-induced tremors	Known case of exposure to manganese. MR showing T1 striatal hyperintensity.	Hypometabolism and hypoperfusion in the areas corresponding to T1 hyperintensity in the striatum.
MSA	Dysautonomia associated with either poorly levodopa-responsive parkinsonism (MSA-P), cerebellar ataxia (MSA-C), or both.	Hypometabolism and hypoperfusion in the putamen. Additionally, hypoperfusion noted in the cerebellum.

Table 2: Clinical details and FDOPA PET-MRI in movement disorders



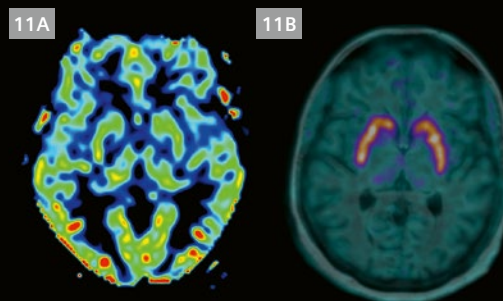
9 Progressive supranuclear palsy

Patient had visual hallucinations and was evaluated for drug-induced parkinsonism. Upper row: T1w sagittal and axial images (9A, B) showing significant midbrain atrophy; ^{18}F -FDG PET images (9C, D, F) and PCASL (9E) image showing hypoperfusion and hypometabolism in the bilateral putamen. Additionally, PCASL showed hypoperfusion in the bilateral frontal lobes, anterior cingulate cortex, and thalami.



10 Idiopathic Parkinson's disease

Patient presented with stiffness of right arm and right leg, tremors, and numbness. Clinical examination revealed rigidity and micrographia. PCASL image at level of basal ganglia (10A) and corresponding ^{18}F -FDOPA image (10B) demonstrating hypoperfusion and hypometabolism, respectively, in the bilateral posterior putamen.



11 Drug-induced Parkinson's disease, post-COVID-19 infection

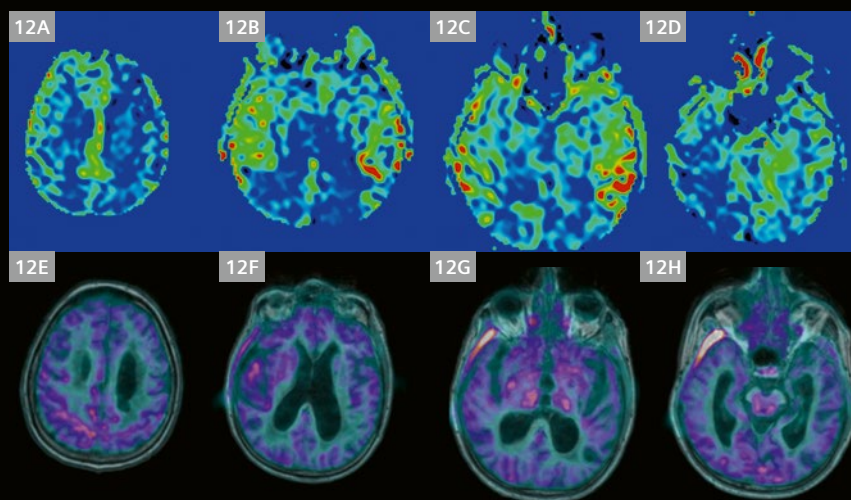
Patient had fearfulness, anxiety, autonomic hyperactivity, crying spells, symptoms of stress disorder, and had started on antipsychotic medications, after which developed parkinsonian features (rigidity, mask face, monotonous voice, and decreased hand movements). PCASL image at level of basal ganglia (11A) and corresponding ^{18}F -FDOPA image (11B) show normal perfusion in bilateral basal ganglia, thus demonstrating normal dopaminergic activities and suggesting secondary cause for parkinsonian symptoms.

Part 3

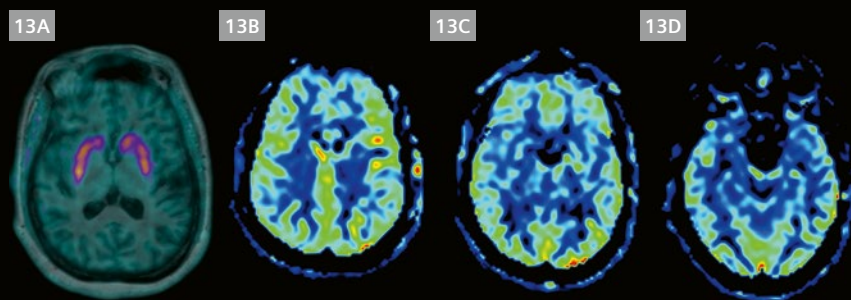
Clinical diagnosis	Clinical presentation
Parkinsonism	FTD-PSP
Parkinsonism	CBS then hemiparkinsonism
FTD	ASL suggestive of CBD-like pattern
	PET-MR findings suggestive of FTD-CBS phenotype
FTD	NPH with nonspecific global hypometabolism and hypoperfusion (Fig. 12)
	AD with CAA
FTD	FTD with vascular dementia
Atypical PD	CBS
FTD	CAA with atherosclerotic vessel disease
Huntington's chorea	FTD ALS / FTD-CBS
Young patient with tremors, anger outbursts, and depression suspected for functional / organic disease.	Structural MRI revealed no demonstrable abnormality. ¹⁸ F-FDOPA showed bilateral caudate hypometabolism. PCASL demonstrated hypoperfusion in bilateral caudate nuclei and fronto-temporal lobes, with hyperperfusion in occipital lobes similar to ¹⁸ F-FDG PET findings in Huntington's chorea. Case is under evaluation for Huntington's chorea / PSP / CBD (Fig. 13).

Table 3: Clinical details and FDG PET-MRI in complex neurodegenerative disorders

Abbreviations: AD, Alzheimer's disease; CAA, cerebral amyloid angiopathy; CBD, corticobasal degeneration; CBS, corticobasal syndrome; FTD, frontotemporal dementia; PSP, progressive supranuclear palsy; NPH, normal pressure hydrocephalus; PD, Parkinson's disease; MSA, multiple systemic atrophy.



12 Normal pressure hydrocephalus
Patient presented with difficulty in walking, memory loss (recent and in the past), and decreased self-care. Structural MRI showed disproportionate dilation of lateral ventricles to sulcal spaces. Upper row (12A–D) PCASL images followed by bottom row (12E–H) ¹⁸F-FDG PET images showing global hypometabolism in bilateral medial frontal lobes; anterior cingulate gyrus; bilateral parietal, temporal, and occipital lobes; and bilateral thalami.



13 Middle-aged patient presented with tremors, anger outbursts, and depression. Evaluated for suspected functional / organic disease. Structural MRI revealed no demonstrable abnormality. ^{18}F -FDOPA showed bilateral caudate hypometabolism. PCASL demonstrated hypoperfusion in bilateral caudate nuclei and frontal-temporal lobes, with hyperperfusion in occipital lobes similar to ^{18}F -FDG PET findings in Huntington's chorea. Case is under evaluation for Huntington's chorea / PSP / CBD.

Materials and methods

This is a prospective observational study that included 108 patients who were referred to our molecular imaging center for imaging between 2020 and today. The study has been divided into three sections. The first section discusses cases of dementia in which FDG PET was correlated with PCASL. The second section discusses cases of movement disorders in which PCASL and FDOPA PET were correlated. The third section discusses how disorders with overlapping clinical symptoms and PET imaging findings can be diagnosed with high sensitivity and specificity using the perfusion pattern of PCASL. Images were acquired using a Biograph mMR PET-MRI scanner and a 3T MAGNETOM Vida (Siemens Healthcare, Erlangen, Germany).

Results

The PCASL perfusion pattern is correlated with clinical symptoms and metabolic patterns as summarized in Tables 1–3.

Learning points

1. PCASL and FDG PET get similar information regarding perfusion and metabolism patterns (Table 1).
2. PCASL correlates with FDOPA for perfusion and metabolism in the striatal structures.
3. When additional FDG-like pattern analysis in movement disorders referred for FDOPA is done, it has been found helpful as discussed in the case-wise pattern in Table 2.
4. Rare cases explored on FDOPA, such as hypermanganesemia, can be better confirmed by FDOPA and PCASL.

5. Vascular dementia is the most common confounder in developing countries. PET is used to diagnose dementia, while PCASL is used for diagnosing the dementia pattern and the vascular perfusion abnormalities, thereby emphasizing the need for simultaneous PET-MRI in overlapping pathologies.
6. In conditions with dual neurodegenerative disorders, such as FTD-ALS and FTD-CBS, PET-MRI helps to confirm the diagnosis, using metabolism and the perfusion pattern (Table 3).

Discussion and conclusion

Neuroimaging findings in neurodegenerative disorders are widespread and difficult, as imaging findings in patients with modest signs and symptoms are frequently subtle and ambiguous. In many cases, by the time imaging findings are obvious, the patient has already manifested clinically, and the diagnosis is already established or at least highly suspected.

The radiation-free PCASL-MRI approach helps, based on the perfusion profile, to achieve an early and accurate diagnosis prior to gross morphological alterations when standardized with PET in simultaneous PET-MRI acquisitions. PCASL and PET changes preceded structural atrophy patterns and could aid in establishing early clinical diagnosis. The combination of PET and PCASL boosted the sensitivity of structural MRI and PET by synergistically diagnosing disease conditions. The synergistic effect of PCASL and FDOPA boosted the sensitivity and specificity in classifying disorders with dopaminergic deficit into IPD/APD phenotypes without the need for additional FDG PET or D2-receptor imaging.

Our study highlights the role of simultaneous PCASL PET-MRI in the workup of complex neurodegenerative conditions with FDG in centers that do not have a cyclotron facility for producing non-FDG tracers. In clear-cut clinical neurodegenerative disorders, where structural changes are equivocal, an additional PCASL sequence can help in early diagnosis without the need for expensive and radioactive PET studies.

Moreover, studies such as ours in a PET-MRI center with a cyclotron facility and referrals of various neuropsychiatric disorders have expanded our understanding of these disorders at a molecular level with functional imaging using PCASL, ^{18}F -FDG, and ^{18}F -FDOPA. Though not displayed in this study, whole-body FDG-PET with DWI MRI has also aided in workups of neurodegenerative disorders by excluding any underlying inflammatory or neoplastic etiology.

References

- 1 Saba L. Imaging in Neurodegenerative Disorders. Oxford: Oxford University Press; 2015.
- 2 Nagesh Babu G, Gupta M. Therapeutics in Neurodegenerative Disorders: Emerging Compounds of Interest. In: Ramasami P, Gupta Bhowon M, Jhaumeer Lallu S, Wah HLK. (eds) Emerging Trends in Chemical Sciences. Cham: Springer International Publishing; 2018, pp. 37–56.
- 3 Warren JD, Schott JM, Fox NC, Thom M, Revesz T, Holton JL, et al. Brain biopsy in dementia. Brain. 2005;128(Pt 9):2016–2025.
- 4 Benson DF, Davis RJ, Snyder BD. Posterior cortical atrophy. Arch Neurol. 1988;45(7):789–793.
- 5 Tripathi M, Tripathi M, Sharma R, Jaimini A, MD'Souza M, Saw S, et al. Functional neuroimaging using F-18 FDG PET/CT in amnesic mild cognitive impairment: A preliminary study. Indian J Nucl Med. 2013;28(3):129–133.
- 6 Tripathi M, Kumar A, Bal C. Neuroimaging in Parkinsonian disorders. Neurol India. 2018;66(7):68.



Contact

Sandhya Mangalore, M.D., DM
Additional Professor Neuro-Radiology
Molecular Imaging Centre
Division of Neuroradiology
Department of Neuroimaging
and Interventional Radiology
National Institute of Mental Health
and Neurosciences
Bengaluru 560029
India
Phone: 080 - 26995424/9480829866
sandhya@nimhans.ac.in

Advertisement

Learn more about ...

... ASL 2D, ASL 3D, and PCASL ...



Clinical Benefits of Multi-PLD PCASL in Pediatric Patients with Moyamoya Disease

Aya Tominaga et al., Miyagi Children's Hospital, Sendai, Japan

Read article (pdf) 2.57 MB



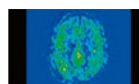
Perfusion Imaging in Pediatric Brain Tumors: Pseudo-continuous Arterial Spin Labeling at Work

Giovanna Stefania Colafati et al., Department of Imaging, Neuroradiology Unit, Bambino Gesù Children's Hospital, Rome, Italy

Read article (pdf) 0.73 MB

➔ Go to:
[magnetomworld.siemens-healthineers.com/
clinical-corner/case-studies/arterial-spin-labeling.html](https://magnetomworld.siemens-healthineers.com/clinical-corner/case-studies/arterial-spin-labeling.html)

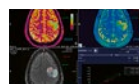
... or try it on your system with a free, 90-day trial license



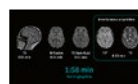
PCASL
Improved 2D or 3D brain perfusion imaging.



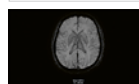
ASL 2D and ASL 3D
ASL is an MRI technique using the water in arterial blood as an endogenous contrast agent to evaluate perfusion.



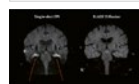
MR Fingerprinting
Quantitative tissue maps enabling improved tissue characterization.



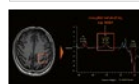
Deep Resolve Swift Brain
Deep Resolve Swift Brain is an ultra-fast brain protocol leveraging the fastest available imaging sequence together with a deep learning reconstruction.



Wave-CAPI SWI
Siemens-Healthineers unique Wave-CAPI SWI exploits coil sensitivity variations in all three dimensions.



BLADE Diffusion
Blade Diffusion is T2SE based diffusion technique.



Single-Voxel Spectroscopy Edit
Detection and relative quantification of J-coupled metabolites.



Deep Resolve Boost
Deep Resolve Boost uses raw-data-to-image deep learning reconstruction technology.

➔ For further details and general requirements visit us at:
[siemens-healthineers.com/magnetic-resonance-
imaging/options-and-upgrades/clinical-applications](https://siemens-healthineers.com/magnetic-resonance-imaging/options-and-upgrades/clinical-applications)

BLADE: Reducing Motion Artifacts in Uncooperative Patients with Acquired Brain Injury

Marta Cazzoli; Laura Pelizzari; Susanna Lipari

IRCCS Fondazione Don Carlo Gnocchi Onlus, Milan, Italy

Abstract

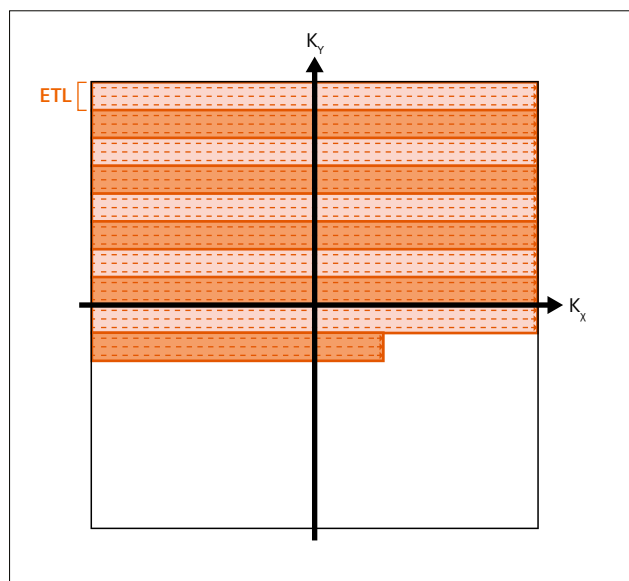
Obtaining good-quality MRI images in patients with acquired brain injury (ABI) is very challenging due to their uncontrolled movements during the acquisition. Motion artifacts can lead to partially or totally absent anatomical detail, which hampers the neuroradiologist's ability to perform an accurate examination.

The BLADE radial k -space filling technique from Siemens Healthineers is an excellent alternative to the conventional Turbo Spin Echo (TSE) T2-weighted sequence for scanning patients with ABI, as it reduces motion artifacts and therefore markedly improves image quality.

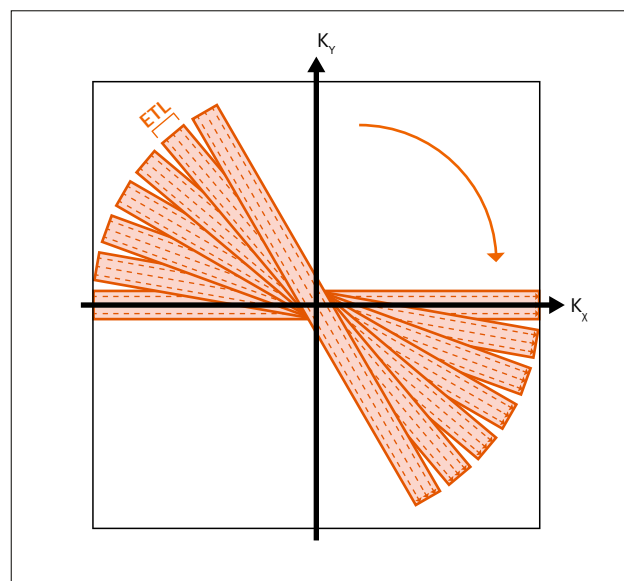
In the current paper, we present examples of ABI images obtained with the BLADE sequence, compare them with conventional TSE T2-weighted sequences, and highlight the advantages of BLADE for scanning patients with ABI.

Introduction

Acquired brain injury (ABI) is an overarching term generally describing insults to the brain that are neither congenital nor perinatal [1]. ABI can affect the brain's structural integrity, its functions, and its metabolic activity, and can result in long-term disability [2, 3]. Severe ABI can be classified into two sub-categories: traumatic brain injuries (TBI) and non-traumatic brain injuries. The former are defined as ABIs caused by external events such as falls, assaults, motor vehicle accidents, or sports injuries [4]; the latter are ABIs caused by internal factors such as stroke, near-drowning, aneurysms, tumors, infectious diseases, or lack of oxygen supply to the brain [5]. Although ABI diagnosis is still mainly clinical – namely, based on the medical history of the patient and on neurological and physical examinations – neuroimaging is a crucial instrument for ABI patient



1 Example of Cartesian k -space filling scheme. The echo train length (ETL) defines the number of data lines acquired for each TR period (orange box).



2 Example of radial k -space filling scheme (BLADE sequence). The echo train length (ETL) defines the number of data lines acquired for each TR period (orange box).

management [6, 7]. First, given the wide ABI spectrum, neuroimaging can provide useful additional information for patient characterization [7]. Second, it can be used to monitor the patient at follow-ups, aiding proper treatment management and prognosis [7, 8]. Among the available neuroimaging techniques, computed tomography (CT) imaging is widely used and is recognized as the mainstay for ABI imaging, as it is fast and accurate [9]. Magnetic resonance imaging (MRI) is slower, more motion sensitive, less accessible, and more expensive than CT imaging [10]. However, it is more sensitive than CT imaging when it comes to detecting certain intracranial injuries, such as axonal injuries. MRI is therefore still valuable for ABI evaluation in clinical practice [8, 11, 12].

MRI issues in ABI patients

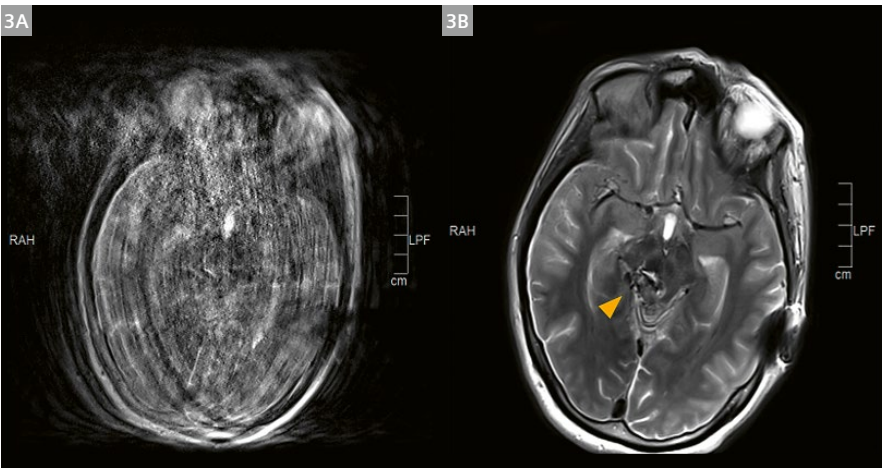
The key issue in MRI examinations of ABI patients is motion. Motion artifacts are caused both by the long scan times and the large movements of these patients, who are unable to lie still during the scan. If motion artifacts result in poor-quality images and lead to partially or totally absent morphological information, radiologists cannot accurately diagnose and characterize patients. Therefore, MRI diagnostic and prognostic value is totally lost. The high sensitivity of conventional MRI sequences to movement is in part caused by the Cartesian (or rectilinear) *k*-space filling scheme [13]. The Cartesian data acquisition technique consists of filling the *k*-space line by line, from top to bottom (Fig. 1). It provides good overall image quality. A number of data lines equal to the echo train length (ETL, Fig. 1) are acquired for each repetition time (TR) period. In a Cartesian acquisition, the *k*-space center, which contains the signal and contrast characteristics of the image, is acquired just once, unless multiple averages are used. Thus, patient movements have a moderate to severe effect on the resulting image when a linear *k*-space filling scheme is used [14].

BLADE

Multishot turbo spin echo (TSE) sequences with radial *k*-space trajectory were introduced with the aim of reducing motion artifacts [15]. With the TSE BLADE sequence (Siemens Healthcare, Erlangen, Germany), a set of radial data lines (“blades”) that are equal to the ETL and cross the center of the *k*-space is collected in order to fill the *k*-space (Fig. 2). The center of the *k*-space is sampled for each blade, providing excellent signal and contrast while reducing the sensitivity of the sequence to patient movement, as if multiple averages were made. A higher number of blades is associated with fewer motion artifacts, greater spatial resolution, but longer acquisition time [13]. In the framework of ABI imaging assessment, BLADE can dramatically improve the image quality when compared to T2 TSE sequences with traditional *k*-space Cartesian filling. In Figure 3, the brain of an ABI patient has been imaged using a T2 TSE sequence with traditional *k*-space Cartesian filling (Fig. 3A) and using a T2 TSE BLADE sequence (Fig. 3B) on the same 3T scanner (MAGNETOM Prisma, Siemens Healthcare, Erlangen, Germany), equipped with a 64-chan-

	T2 TSE	T2 TSE BLADE
Acquisition time (min:sec)	02:19	03:03
FOV (mm)	230 × 230	220 × 220
Matrix	512	320
In-plane resolution (mm)	0.4 × 0.4	0.7 × 0.7
Thickness (mm)	3	2
Slices	36	72
Distance Factor	30%	0%

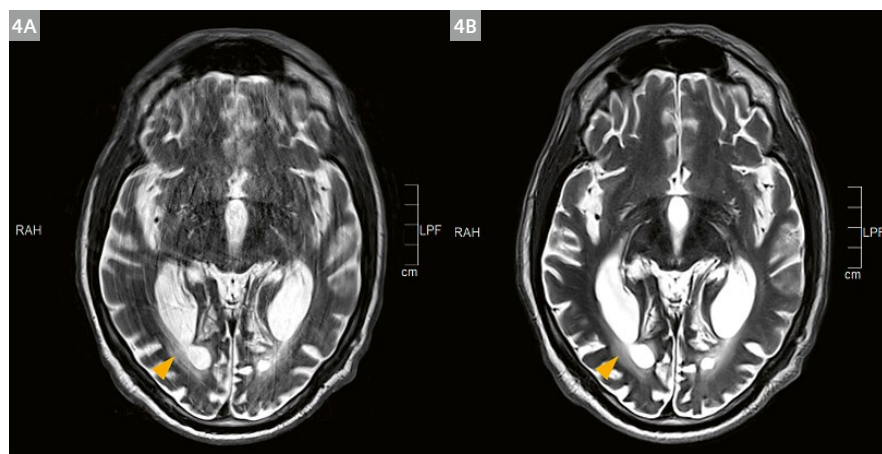
Table 1: Sequence parameters



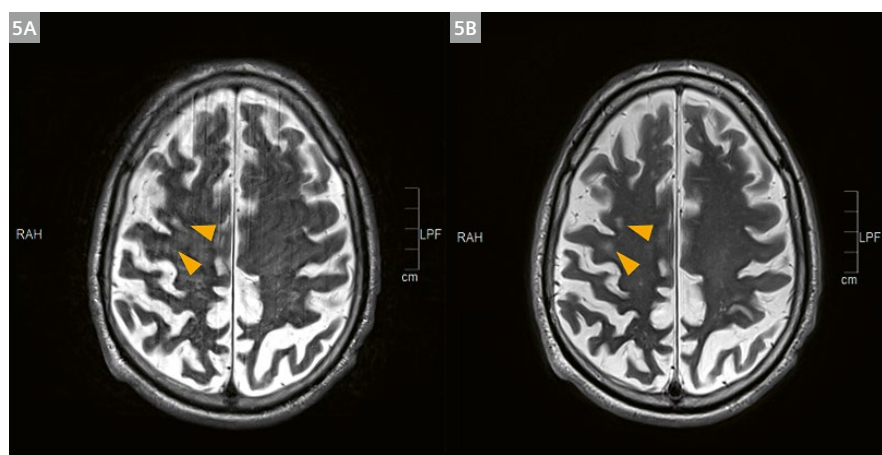
3 A conventional Cartesian T2 TSE (3A) and a T2 TSE BLADE (3B) in a moving ABI patient. The T2 TSE BLADE sequence dramatically improves image quality and provides clearer detail definition (yellow arrow).

nel head/neck coil, at IRCCS Fondazione Don Carlo Gnocchi Onlus. The image acquired with linear *k*-space filling does not provide any useful structural information, due to large motion artifacts. On the other hand, the T2 TSE BLADE sequence (Fig. 3B) yields an image with clear anatomy and injury information, allowing the radiologist to produce an accurate report. As previously mentioned, the acquisition of the image in Figure 3B took longer than the acquisition of the image in Figure 3A (acquisition

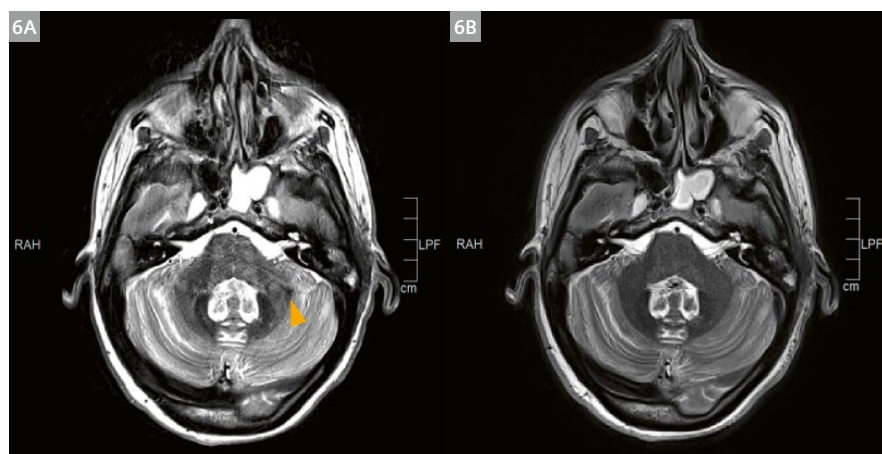
time (TA) = 03:03 min vs 02:19 min). The acquisition parameters of the two sequences are listed in Table 1. In addition, the oversampling of the *k*-space center comes at the expense of the peripheral area, thus yielding a lower spatial resolution of the acquired image (Fig. 2). The TSE BLADE parameters can be adjusted to compensate for this drawback by increasing the resolution parameters, such as matrix size, in-plane resolution, and slice thickness, and by augmenting the blade coverage.



4 Comparison between a conventional Cartesian T2 TSE (4A) and a T2 TSE BLADE (4B) in a moving ABI patient. The yellow arrow on the left image (4A) highlights a posterior periventricular hyperintensity that might be ascribed to external ghosting and erroneous signal spatial collocation. The T2 TSE BLADE image (4B) is sharper and confirms without doubt the presence of a posterior periventricular lesion.



5 A conventional Cartesian T2 TSE (5A) and a T2 TSE BLADE (5B) in a moving ABI patient. The comparison between the two images shows that an image affected by movement artifacts cannot be used to evaluate subcortical microvascular damage (yellow arrows).



6 A conventional Cartesian T2 TSE (6A) and a T2 TSE BLADE (6B) in an uncooperative ABI patient. The yellow arrow in (6A) shows an alleged hemosiderin deposit, which is then excluded by the T2 TSE BLADE acquisition.

Clinical impact

Besides the striking clinical advantages of the BLADE technique in ABI cases with extremely large movements (Fig. 3), the radial *k*-space trajectory might also be useful for solving ambiguities that may be present in ABI magnetic resonance images affected by a smaller number of motion artifacts. Figure 4A shows a traditional TSE scan of an ABI patient; the yellow arrow indicates a posterior periventricular hyperintensity that might be ascribed to external ghosting and erroneous signal spatial collocation, rather than to a periventricular lesion. Using a TSE BLADE sequence, a detailed and motion artifact-free image was obtained from the same subject (Fig. 4B). The improved image quality enabled the radiologist to confirm, with no doubt, the presence of a periventricular lesion (yellow arrow).

A further example is shown in Figure 5. Subcortical microvascular damage cannot be identified on the conventional TSE image because of motion-related artifacts (Fig. 5A). Conversely, the BLADE technique clearly shows the damage (Fig. 5B, yellow arrows).

Finally, Figure 6 compares Cartesian T2 TSE and T2 TSE BLADE acquisition techniques to show a case of false alteration detection caused by artifacts. The former sequence produces an image with hypointensity close to the medium cerebellar peduncles, which radiologists would interpret as hemosiderin deposits (Fig. 6A); the latter shows no abnormality in that anatomical region (Fig. 6B).

Conclusion

Despite some limitations, the BLADE radial *k*-space sampling technique is a valid alternative to conventional Cartesian T2 TSE in clinical assessment of ABI. Improved image steadiness, better image quality, higher signal-to-noise ratio (SNR), and enhanced lesion conspicuity enable correct and precise radiological evaluation of patients with ABI. Furthermore, increased acquisition time due to the radial filling scheme of the *k*-space should not to be considered a major defect. The sequence achieves a good acquisition in a single run; there is no need to repeat it several times until an adequate image quality is generated.

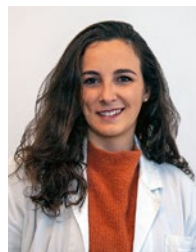
Although a Cartesian T2 TSE sequence should still be preferred when scanning cooperative subjects, as it provides superior overall image quality, TSE BLADE sequences may be a good alternative to conventional TSE in cases of uncooperative patients who are difficult to manage. In these specific cases, dramatically reducing the sensitivity to movement and providing clearer delineation of brain morphology justifies a longer TA.

Acknowledgments

We would like to thank Domenico Zacà from Siemens Healthineers Italy for assisting us with writing this article.

References

- 1 Najem D, Rennie K, Ribecco-Lutkiewicz M, Ly D, Haukenfrers J, Liu Q, et al. Traumatic brain injury: classification, models, and markers. *Biochem Cell Biol.* 2018;96(4):391–406.
- 2 Subbarao BS, Stokke J, Martin SJ. Telerehabilitation in Acquired Brain Injury. *Phys Med Rehabil Clin N Am.* 2021;32(2):223–238.
- 3 Magee WL, Clark I, Tamplin J, Bradt J. Music interventions for acquired brain injury. *Cochrane Database Syst Rev.* 2017;1(1):CD006787.
- 4 Capizzi A, Woo J, Verduzco-Gutierrez M. Traumatic Brain Injury: An Overview of Epidemiology, Pathophysiology, and Medical Management. *Med Clin North Am.* 2020;104(2):213–238.
- 5 Intercollegiate Stroke Working Party. National Clinical Guideline for Stroke, 4th edition [Internet]. London. Royal College of Physicians; 2012. Available from: <https://www.strokeaudit.org/Guideline/Historical-Guideline.aspx>
- 6 Smith LGF, Milliron E, Ho ML, Hu HH, Rusin J, Leonard J, et al. Advanced neuroimaging in traumatic brain injury: an overview. *Neurosurg Focus.* 2019;47(6):E17.
- 7 Mandeville ET, Ayata C, Zheng Y, Mandeville JB. Translational MR Neuroimaging of Stroke and Recovery. *Transl Stroke Res.* 2017;8(1):22–32.
- 8 Lagares A, Ramos A, Perez-Nunez A, Ballenilla F, Alday R, Gomez PA, et al. The role of MR imaging in assessing prognosis after severe and moderate head injury. *Acta Neurochir (Wien).* 2009;151(4):341–56.
- 9 Bodanapally UK, Sours C, Zhuo J, Shanmuganathan K. Imaging of Traumatic Brain Injury. *Radiol Clin North Am.* 2015;53(4):695–715, viii.
- 10 Chalela JA, Kidwell CS, Nentwich LM, Luby M, Butman JA, Demchuk AM, et al. Magnetic resonance imaging and computed tomography in emergency assessment of patients with suspected acute stroke: a prospective comparison. *Lancet.* 2007;369(9558):293–8.
- 11 Firsching R, Woischneck D, Diedrich M, Klein S, Ruckert A, Wittig H, et al. Early magnetic resonance imaging of brainstem lesions after severe head injury. *J Neurosurg.* 1998;89(5):707–12.
- 12 Paterakis K, Karantanas AH, Komnos A, Volikas Z. Outcome of patients with diffuse axonal injury: the significance and prognostic value of MRI in the acute phase. *J Trauma.* 2000;49(6):1071–5.
- 13 Ravanelli M, Farina D, Maroldi R. FREEZEit StarVIBE: Freezing the Moving Head and Neck at a Sub-millimetric Scale. *MAGNETOM Flash.* 2016;66(3):92–94.
- 14 Schmeets SH. *syngo* BLADE Motion Correction from Head to Toe. *MAGNETOM Flash.* 2006;3:24–25.
- 15 Koyama T, Fujimoto K, Togashi K. The Clinical Advantages of T2-weighted MRI Imaging in the Female Pelvis with *syngo* BLADE. *MAGNETOM Flash.* 2007;3:60–62.



Contact

Marta Cazzoli
IRCCS Fondazione Don Carlo Gnocchi ONLUS
Centro Avanzato di Diagnostica
e Terapia Riabilitativa
Via Capecelatro 66
Milan
Italy
mcazzoli@dongnocchi.it

Feasibility of 3D Sequences for Median Nerve Imaging Using UltraFlex Large Coils and CAIPIRINHA on a 3T System

Yatin Sharma

Siemens Healthineers, Gurugram, India

Introduction

Arm / forearm neurography can be a complex and time-consuming MRI scan. There are several sequences available for three-dimensional forearm nerve imaging. This article describes how using different T1 and T2 tissue times in the SPACE sequence and the application of CAIPIRINHA can improve MR neurography (MRN).

Technique

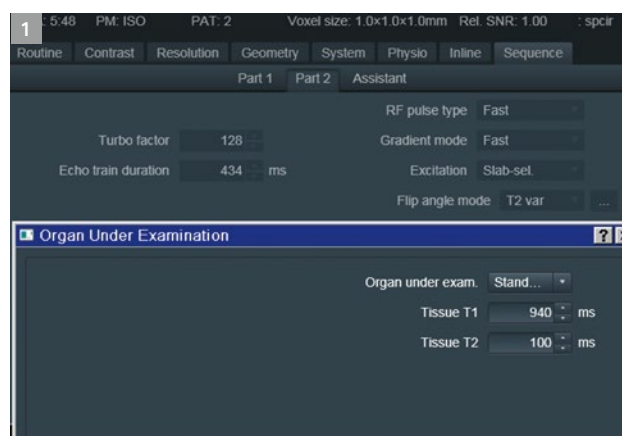
The SPACE (sampling perfection with application optimized contrast using different flip angle evolutions) sequence from Siemens Healthineers uses different flip angle evolutions: PD, T1, T2 and T2 var. T2 SPACE can be further combined with STIR and SPAIR fat suppression techniques. When using STIR SPACE and 3D SPAIR SPACE for forearm nerve imaging, two primary concerns arise: nerve signal visibility and decreased conspicuity of vessel signals.

The default T2 variation evolution of 3D STIR SPACE assumes a T1 tissue time of 940 ms and a T2 tissue time of 100 ms for the organ under examination (Fig. 1). However, this may not be optimal for forearm nerve imaging, in particular since the contrast is also dependent on patient age. This 3D sequence is primarily based on stimulated echos, the use of T1 tissue time in determining the amplitude of the stimulated echo, and the use of refocusing pulses to determine contrast behavior [1]. Using different T1 and T2 input times improved arm nerve signals and increased vessel conspicuity (Figs. 2A, B). (In both comparisons, the image on the left with the

default settings shows compromised nerve conspicuity, while the image on the right with optimized T1 and T2 input times and without the blood suppression pulse improves conspicuity.) When changing T1 and T2 input times, it is also helpful to consider the relaxation values for the median nerve [2].

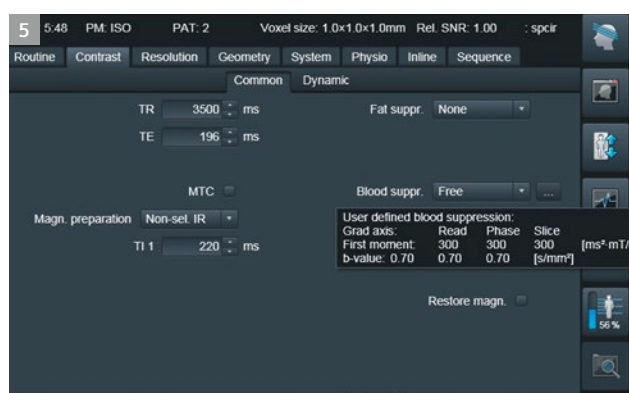
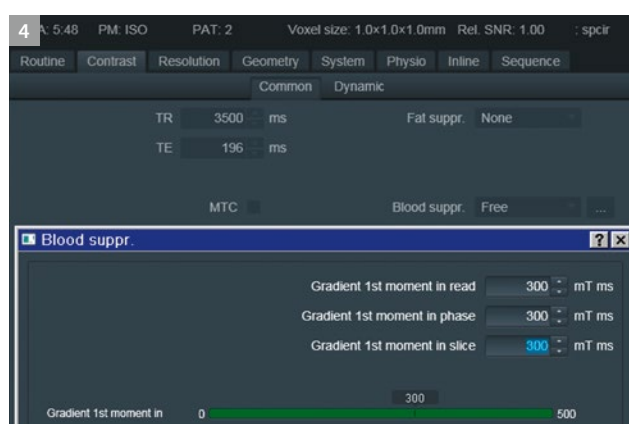
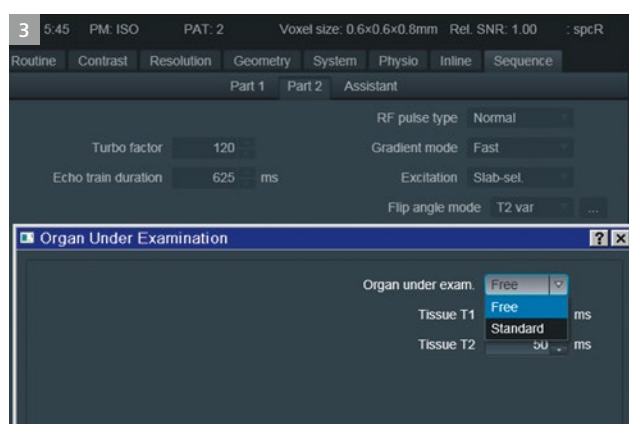
Working with the T2 SPACE sequence, the following equation helps to derive T1 and T2 input times suitable for improving forearm nerve signals in the majority of patient groups:

$$T1 \text{ input time} = 1450 - \text{Age} \times 10 \text{ ms}$$





- 2 Using different T1 and T2 input times to improve arm nerve signals and vessel conspicuity. The images on the left use the default settings, the images in the middle use optimized T1 and T2 tissue times (with higher resolution), while the images on the right use optimized T1 and T2 input times and the blood suppression pulse to improve conspicuity. Also, the resolution is higher.



In the context of this study, 1450 ms was defined as the average T1 relaxation time for forearm nerve signal, while 50 ms was selected for the T2 tissue time. For fat suppression, the SPAIR method was chosen because of its better signal-to-noise ratio and fat suppression efficacy, minimal shading effects, and insensitivity to B_1 inhomogeneity. See Figure 3 for the changes to these T1 and T2 times.

Next, a blood suppression pulse using a combination of three adiabatic RF pulses plus dephasing gradients was selected. We applied a gradient-first moment of $300 \text{ ms}^2 \cdot \text{mT/m}$ in all three directions to suppress signal from vessels (Figs. 4 and 5).

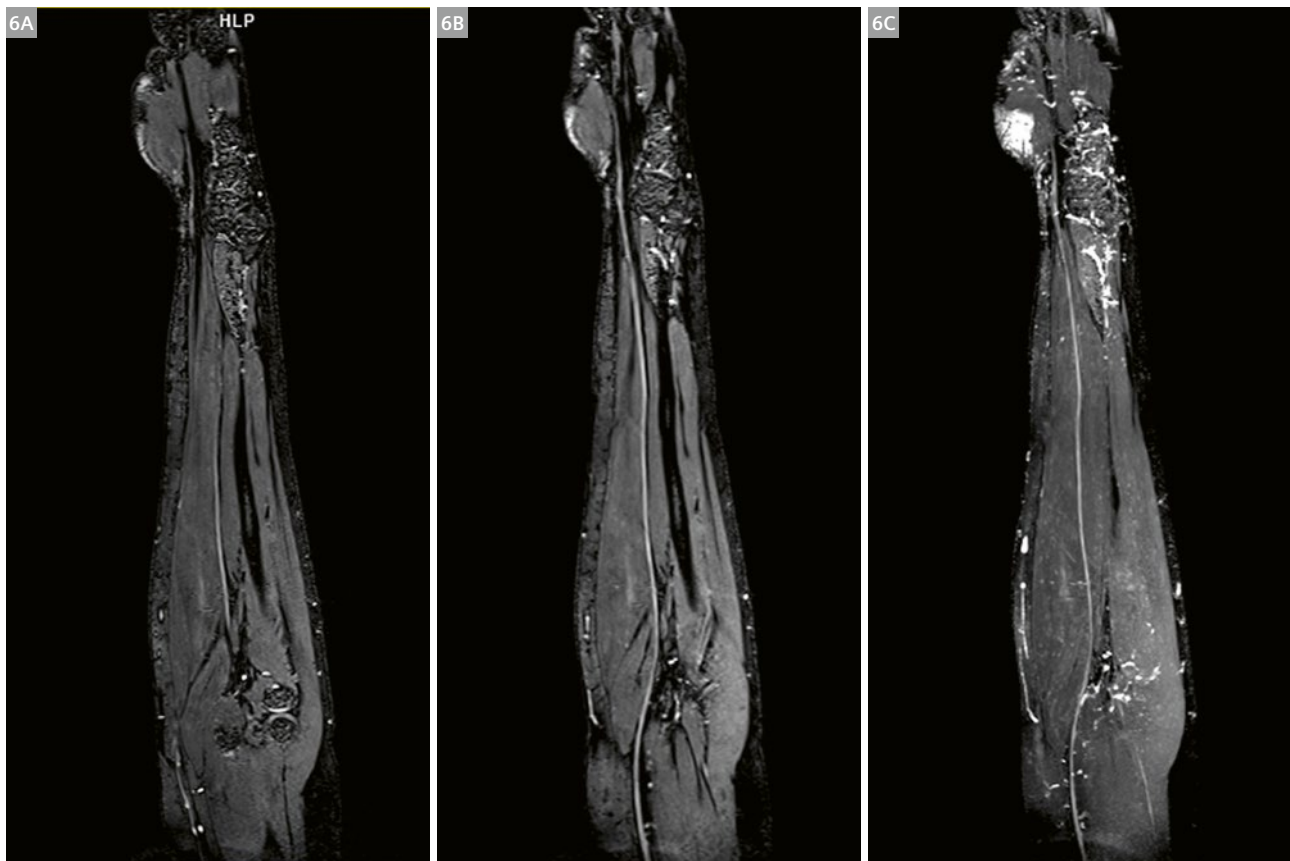
Using an 18-element UltraFlex Large high-density surface coil combined with the CAIPIRINHA sampling pattern enables higher acceleration factors, because it minimizes g-factor related SNR loss. This results in reduced scan time and allows this sequence to be added to routine protocols.

Protocol set-up

The T2 SPACE sagittal isotropic protocol from the lumbar spine program in the Siemens Healthineers library can act as a starting point. The following parameters should be adapted. In addition, the resolution can be adjusted to the local needs.

Parameter card	Parameter change
Routine	Slice thickness: 1 mm (thickness can be varied in order to achieve isotropic voxel size)
Routine	TR 2500 ms
Contrast → Common	SPAIR fat suppression → Strong
Contrast → Common	Blood suppression → Free → 300 in all three directions
Sequence → Part 2*	Turbo factor → 120 or higher
Sequence → Part 2*	Flip angle mode → T2 var → Click three dots → Organ under examination → Free (Fig. 3) Note: This may increase TR, go back to Routine card and set TR 2500 ms.
Sequence → Part 1	Optimize TE in order to achieve apparent TE of 110 ms or higher

*With software version syngo MR XA31 the T1 and T2 values can be found on the Contrast → Common parameter card.



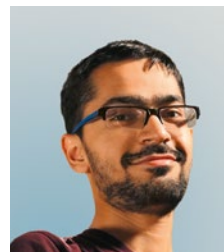
6 Curved multiplanar reconstructions provide better visualization of nerve anatomy and allow the course of the nerve to be traced. **(6A)** The image on the left is a single slice of the protocol with optimizations applied as explained in this article. **(6B)** A curved multiplanar reconstruction (MPR), and **(6C)** a curved maximum intensity projection (MIP).

Results

Compared to standard options, these modifications to the T2 variation of the SPACE sequence allow for faster 3D imaging of the median and other forearm nerves with reproducible results. (In Figure 6A, the image on the left displays a curved MPR, while the image on the right shows a curved MIP and Figure 6B shows a Curved MPR.)

References

- 1 Mugler JP III. Optimized Three-Dimensional Fast-Spin-Echo MRI. *J Magn Reson Imaging* 2014;39: 745–767.
- 2 Gambarota, Giulio; Mekle, Ralf; Mlynarik, Vladimir; Krueger, Gunnar; NMR Properties of Human Median Nerve at 3 T: Proton Density, T1, T2, and Magnetization Transfer. *J Magn Reson Imaging* 2009;29: 982–986.



Contact

Yatin Sharma
Application Services Engineer
Siemens Healthcare Private Limited
SHS AP IND CS EX-DI&AT&US NCR APPS
Plot No. 78, Sector 18
122015 Gurugram
India
yatin.sharma@siemens-healthineers.com

Meet Siemens Healthineers

Siemens Healthineers: Our brand name embodies the pioneering spirit and engineering expertise that is unique in the healthcare industry. The people working for Siemens Healthineers are totally committed to the company they work for, and are passionate about their technology. In this section we introduce you to colleagues from all over the world – people who put their hearts into what they do.

Eva Eberlein, Dipl.-Phys.

Eva comes from Baiersdorf, a small town in northern Bavaria. She studied physics at Friedrich-Alexander-Universität Erlangen, Germany, graduating in 1983 and taking a job as a research assistant in the Department of Applied Optics. After giving birth to her son in December 1984, Eva went on parental leave and returned to work in 1986. She spent 20 years as a developer in the Gradient Coil and Shim Team within the Magnetic Resonance Business Line at Siemens Medizintechnik. In 2006, she began leading the team, which was by then part of the Magnetic Resonance Business Line at Siemens Healthineers. She continues to lead the team today.



Erlangen, Germany



How did you first come into contact with MRI?

Part of my diploma examination involved giving a talk about the similarities and differences of CT, MRI, and ultrasound. For MRI, I interviewed some of my friends – like Franz Schmitt – who were already working in the field in 1983, and I became more and more interested in this technique. MRI was new back then, and even in the early 80s it was a really exciting technology.

Two years later, I got the opportunity to start working part time in the physics group within MR at Siemens Medizintechnik in Erlangen. The group focused mainly on gradient design and shim software. That was in 1986, and I've been working in this field of Research & Development (R&D) ever since. If you're curious and eager, you don't need to change roles every three years. In MRI, you can work on the same mission for years! The topics around gradient systems and shim grew over the time and became even more fascinating. Staying in the same field makes it easy to develop a deep relationship with your customers. It also let me really grow in my role.

What do you find motivating about your job?

Working in the field of gradient coil development involves not only drafting an electrical design that fulfills all performance parameters like gradient strength and slew rate, but also to translate that design into a buildable piece of hardware and to follow up by running the necessary tests with the gradient coil in the MRI system. This integration process is always full of challenges and surprises, but the

MR team always works together to solve these. Our ability to act as one team within R&D is one of the most motivational aspects of my job.

It was also really motivating to see how we could raise the gradient system's performance higher and higher, for instance with the Prisma gradient system or by using more than one gradient amplifier for one gradient coil (multi-GPA), as was the case with the Connectom¹ gradient system several years ago. And now we're translating this multi-GPA technique along with Liquid Cooling Technology into the new Gemini gradient coil¹ to create a clinical system, the MAGNETOM Cima.X² that reaches 200 mT/m³ at a slew rate of 200 T/m/s.

Feedback from customers, especially from researchers, about the new possibilities of using these gradient systems always makes us proud.

What are the biggest challenges in your job?

Providing gradient systems for the whole bandwidth – so for standard clinical systems, MRI systems with a focus on patient comfort like MAGNETOM Free.Max, and systems for the research community – is highly challenging. We focus on different aspects for different user groups, and superb image quality always goes without saying. Reliability is key for standard clinical systems, a large bore is important for patient comfort, and maximum performance is the main topic for the research group.

Figuring out which are the most important features for a special gradient system leads to heated debates at every

concept phase. But I think we've always found the best solution. Of course we're also thinking about an all-in-one solution that combines maximum performance with an open bore architecture – but my colleagues will solve that challenge after my time.

What would you do if you could spend a month doing whatever you wanted?

This is a very relevant question for me: I'm going to be retiring in a couple of months, so I'll have to find an answer for a lot more than four weeks! And I must confess that I don't yet have a clear idea. I always went to work in the morning with good grace; sometimes I wasn't in the best shape when I came home, but I really never questioned

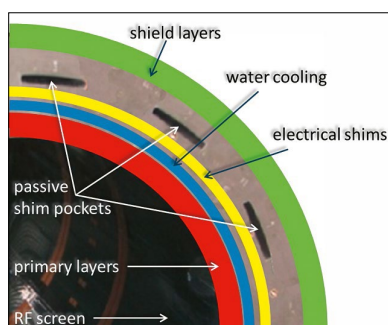
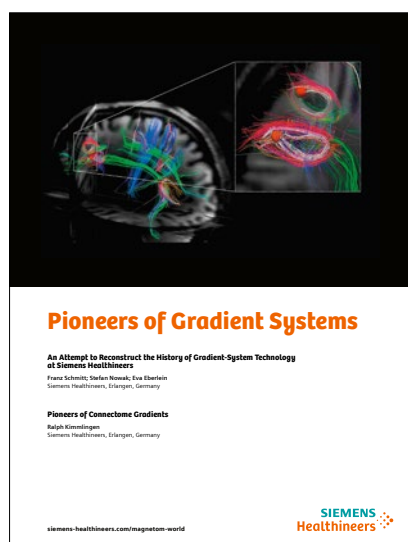
what we wanted to achieve. I enjoyed working closely with my colleagues in the gradient development team, and across MR as a whole. Our Business Line has an incredible drive – we work so hard to tackle challenges and solve them together. It's wonderful to have experienced so many successes together.

So maybe you can give me some suggestions for how to spend my retirement. Just no adult evening classes, cruises, or e-bikes, please!

Further Reading

Explore how Siemens Healthineers learned to make good gradients.

Read about the amazing technological advances from 1983, when Siemens Medizintechnik began to develop their first MRI product, the MAGNETOM; until today, when Siemens Healthineers provide MAGNETOM Prisma, MAGNETOM Terra.X², MAGNETOM Connectom¹, and MAGNETOM Cima.X² to the clinical and research community.



Please visit us at

www.magnetomworld.siemens-healthineers.com/publications/whitepapers

¹MAGNETOM Connectom is ongoing research. All data shown are acquired using a non-commercial system under institutional review board permission. Siemens Healthcare GmbH does not intend to commercialize the system.

²Work in progress. The system is currently under development and is not for sale in the U.S. and in other countries. Its future availability cannot be ensured.

³≥ 200 (±3% for design tolerances)

George Ferguson

After completing 10 years in the military where I had the opportunity to also specialize in MRI, I was fortunate enough to become an MR technologist at a fast-paced trauma facility. I gained experience in all forms of MR imaging exams and procedures. I then had the opportunity to become an applications specialist covering from Japan to New York where I continued my growth in the field or MRI assisting other users with our platforms that brought new features and hardware into their facilities. After several years as an applications specialist, I was accepted to become an applications developer for all field strengths up to 3T. This background gave me a good foundation to bring then all that gained knowledge to the ultra-high field (UHF) team as a UHF MSK applications developer. I enjoy making a positive difference in the lives of those in need, and in pain requiring medical care. It is my passion to be a part of ensuring that they receive the best care possible.



Erlangen, Germany



How did you first come into contact with MRI?

MRI was just something that landed into my lap by being in the right place at the right time. I was working as a lead sonographer, senior radiographer, and CT technologist, when the opportunity to learn MRI after normal working hours presented itself at a local imaging clinic. My first exams in MRI were on an open 0.3T magnet. I then relocated and ended up being a full time MRI technologist in a trauma hospital scanning the most critical and sick patients imaginable.

What do you find motivating about your job?

The idea of reshaping the entire landscape of medicine as we know it for a zero delay of diagnosis and treatment followed with the fastest recovery times possible are my motivation.

Here the value of collaboration comes into play: Making solutions robust enough for the future, by bringing professionals with different insights to the same problem, you can create more robust solutions which enable our patient care partners to provide the best care possible. This robustness is the only way we will keep our users believing in our products as they rely on them to work when they are depended on the most.

What are the biggest challenges in your job?

At the moment I consider creating products that are the perfect solution into the product line as the most challenging aspect. To explain why I say this we would need to evaluate what and to who defines the idea of the perfect solution. Is it a perfect solution for only the patient? The

technologist for ease of use? The radiologist with cost of purchase/ownership/throughput considerations? Is it for the administrator of the hospital with total patient care cost considerations? Sometimes these are not all in alignment and it can be quite challenging to find the right set of compromises to align all these different factors for a meaningful product while navigating the intricacies of project readiness and timelines.

The challenges of application development at 7T are due to the physics of 7T. As you increase the field strength you increase the chemical shift, and the B_1 effects in the image impression. Additionally, the specific absorption rate (SAR) becomes much more of a factor in measurement times compared to other field strengths. So, it can be tricky if the solutions to the image quality challenges increase the SAR challenge even more.

What are the most important developments in Healthcare?

The most important developments in healthcare are just now beginning and at a very early stage. Since the foundation is being laid down now for the most important advancements in healthcare, that foundation will need to be done with absolute robustness and in a rapid manner to secure our position in the market in the future.

What would you do if you could spend a month doing whatever you wanted?

I would go camping in a large camper parked as close to the ocean with the largest waves as possible. A large panoramic view of crashing waves surrounded by nature.

The entire editorial staff at Massachusetts General Hospital, Boston, MA, USA, at University Hospital Bonn, Germany and at Siemens Healthineers extends their appreciation to all the radiologists, technologists, physicists, experts, and scholars who donate their time and energy – without payment – in order to share their expertise with the readers of MAGNETOM Flash.

MAGNETOM Flash – Imprint

© 2022 by Siemens Healthcare GmbH,
All Rights Reserved

Publisher:

Siemens Healthcare GmbH
Magnetic Resonance,
Karl-Schall-Str. 6, D-91052 Erlangen, Germany

Editor-in-chief:

Antje Hellwich
(antje.hellwich@siemens-healthineers.com)

Guest Editors:

Susie Huang, M.D., Ph.D.
Associate Professor, Harvard Medical School Radiologist,
Massachusetts General Hospital, Boston, MA, USA;
Bruce Rosen, M.D., Ph.D.
Professor in Radiology, Harvard Medical School Director,
Athinoula A. Martinos Center for Biomedical Imaging,
Massachusetts General Hospital, Boston, MA, USA;
Daniel Paech, M.D., Ph.D.
Senior Physician, Neuroradiology, University Hospital
Bonn, Germany and Head of Clinical 7 Tesla MRI at DKFZ,
German Cancer Research Center, Heidelberg, Germany

Editorial Board:

Jane Kilkeny; Nadine Leclair, M.D.; Heiko Meyer, Ph.D.;
Rebecca Ramb, Ph.D.; Wellesley Were

Review Board:

Gaia Banks, Ph.D.; André Fischer, Ph.D.; Daniel Fischer;
Christian Geppert, Ph.D.; Christianne Leidecker, Ph.D.;
Felix Müller-Witt; Gregor Thörmer, Ph.D.

Copy Editing:

Sheila Regan, Jen Metcalf, UNIWORKS, www.uni-works.org
(with special thanks to Kylie Martin)

Layout:

Agentur Baumgärtner,
Friedrichstr. 4, D-90762 Fürth, Germany

PrePress and Image Editing, Production:

Clemens Ulrich, Paul Linssen, Siemens Healthcare GmbH

Printer:

Schmidl & Rotaplan Druck GmbH,
Hofer Str. 1, D-93057 Regensburg, Germany

Note in accordance with § 33 Para.1 of the German Federal Data Protection Law: Despatch is made using an address file which is maintained with the aid of an automated data processing system.

MAGNETOM Flash is sent free of charge to Siemens Healthineers MR customers, qualified physicians, technologists, physicists and radiology departments throughout the world. It includes reports in the English language on magnetic resonance: diagnostic and therapeutic methods and their application as well as results and experience gained with corresponding systems and solutions. It introduces from case to case new principles and procedures and discusses their clinical potential. The statements and views of the authors in the individual contributions do not necessarily reflect the opinion of the publisher.

The information presented in these articles and case reports is for illustration only and is not intended to be relied upon by the reader for instruction as to the practice of medicine. Any health care practitioner reading this information is reminded that they must use their own learning, training and expertise in dealing with their individual patients. This material does not substitute for that duty and is not intended by Siemens Healthcare to be used for any purpose in that regard. The drugs and doses mentioned herein are consistent with the approval labeling for uses and/or indications of the drug. The treating physician bears the sole responsibility for the diagnosis and treatment of patients, including drugs and doses prescribed in connection with such use. The Operating Instructions must always be strictly followed when operating the MR system. The sources for the technical data are the corresponding data sheets. Results may vary.

Partial reproduction in printed form of individual contributions is permitted, provided the customary bibliographical data such as author's name and title of the contribution as well as year, issue number and pages of MAGNETOM Flash are named, but the editors request that two copies be sent to them. The written consent of the authors and publisher is required for the complete reprinting of an article.

We welcome your questions and comments about the editorial content of MAGNETOM Flash. Please contact us at
magnetomworld.team@siemens-healthineers.com

Manuscripts as well as suggestions, proposals and information are always welcome; they are carefully examined and submitted to the editorial board for attention. MAGNETOM Flash is not responsible for loss, damage, or any other injury to unsolicited manuscripts or other materials. We reserve the right to edit for clarity, accuracy, and space. Include your name, address, and phone number and send to the editors, address above.

MAGNETOM Flash is also available online:

www.siemens-healthineers.com/magnetom-world

Not for distribution in the US

On account of certain regional limitations of sales rights and service availability, we cannot guarantee that all products included in this brochure are available through the Siemens Healthineers sales organization worldwide. Availability and packaging may vary by country and is subject to change without prior notice. Some/All of the features and products described herein may not be available in the United States.

The information in this document contains general technical descriptions of specifications and options as well as standard and optional features which do not always have to be present in individual cases, and which may not be commercially available in all countries.

Due to regulatory reasons their future availability cannot be guaranteed. Please contact your local Siemens Healthineers organization for further details.

Siemens Healthineers reserves the right to modify the design, packaging, specifications, and options described herein without prior notice. Please contact your local Siemens Healthineers sales representative for the most current information.

Note: Any technical data contained in this document may vary within defined tolerances. Original images always lose a certain amount of detail when reproduced.

Siemens Healthineers Headquarters

Siemens Healthcare GmbH
Henkestr. 127
91052 Erlangen, Germany
Phone: +49 9131 84-0
siemens-healthineers.com